Bridging Flows: Microfluidic EndUser Solutions

Sabourin, David; Dufva, Martin; Snakenborg, Detlef

Publication date:
2010

Document Version
Publisher's PDF, also known as Version of record

Bridging Flows: Microfluidic End-User Solutions

Ph.D. Thesis

David Sabourin

Fluidic Array Systems and Technology

DTU Nanotech,
Department of Micro- and Nanotechnology

Technical University of Denmark
(DTU)

June 2010

PREFACE

This thesis is presented to fulfil criteria for obtaining a Ph.D. degree from the Technical University of Denmark (DTU). The Ph.D. project was conducted at DTU Nanotech, Department of Micro- and Nanotechnology, from May 2007 until June 2010 and was funded by a DTU Ph.D. Stipend.

The project was supervised by Associate Professor Martin Dufva, leader of the Fluidic Arrays Systems and Technology (*FAST*) group, DTU Nanotech, and co-supervised by Assistant Professor Detlef Snakenborg of the ChemLabChip group, DTU Nanotech. Thesis contents are based on results described within peer-reviewed publications as well as unpublished material.

ACKNOWLEDGEMENTS

Thanks to family and friends for their encouragement to pursue further studies and for all the support received while in Denmark.

Maire – I hope I provide the support to you that you have given to me since we met. As one adventure ends another begins.

Sean MacDonald – Great friend, motivator. Thank you for bringing this wonderful opportunity to my attention. (P.S. I owe you one.)

Lars H. Pedersen – Your efforts made this possible. Thank you.

Martin Dufva – The guidance and input you provided during the project were the proper balance of supervision and freedom. Your inquisitive and attentive nature undoubtedly propelled the project forward. I look forward to our future and continued collaborations.

Detlef Snakenborg – Your knowledge, teaching and practical approach provided the strong base this project required for success. Myself, and countless others at DTU Nanotech are indebted to you for this.

FAST members - Thank you for constructive criticism, discussions, both humourous and serious, and for ideas and feedback. A special acknowledgement and thanks to Peder Skafte-Pedersen whose ideas and contributions were especially significant during my period of study.

Jesper Petersen – Fantastic colleague, good friend. The academic work we accomplished together was very motivating. Further pursuit of this path could be most rewarding. Outside of work, trips and times together will always be remembered with tremendous fondness. I hope that in future the hospitality you have extended to myself and Maire can be repaid.

LIST OF PUBLICATIONS

PAPERS:

Publication 1
Sabourin, D., Snakenborg, D. and Dufva, M. "*Interconnection blocks: a method for providing reusable, rapid, multiple, aligned and planar microfluidic interconnections*" Journal of Micromechanics and Microengineering. Volume 19, 035021 (9 pp), 2009. doi:10.1088/0960-1317/19/3/035021.

Publication 2
Sabourin, D., Snakenborg, D., and Dufva, M. "*Interconnection blocks with minimal dead volumes permitting planar interconnection to thin microfluidic devices*" Microfluidics and Nanofluidics. Volume 9, p. 87-93, 2010. doi:10.1007/s10404-009-0520-8.

Publication 3
Sabourin, D., Dufva, M., Jensen, T., Kutter, J., and Snakenborg, D. "*One-step fabrication of microfluidic chips with in-plane, adhesive-free interconnections*" Journal of Micromechanics and Microengineering. Volume 20, 037001 (7pp), 2010. doi: 10.1088/0960-1317/20/3/037001.

Publication 4
Skafte-Pedersen, P.[*], **Sabourin, D.**[*], Dufva, M., and Snakenborg, D. "*Multi-channel peristaltic pump for microfluidic applications featuring monolithic PDMS inlay*" Lab on a Chip. Volume 9 (20), p. 3003-3006, 2009.

Publication 5
Sabourin, D. [*], Petersen, J. [*], Snakenborg, D., Brivio, M., Gudnadson, H., Wolff, A. and Dufva, M. *"Microfluidic DNA microarrays in PMMA chips: streamlined fabrication via simultaneous DNA immobilization and bonding activation by brief UV exposure"*, Biomedical Microdevices. doi: 10.1007/s10544-010-9420-7

MANUSCRIPTS IN PREPARATION:

Dufva, M., and **Sabourin, D.**, *"Programming of cell cultures with microfluidics, biomaterials and nanostructures", submitted to Integrative Biology, June, 2010.*

Sabourin, D., Skafte-Pedersen, P., Coman, V., Alberti, M., Petersen, J., Hemmingsen, M., Kutter, J., Snakenborg, D. Dufva, M. "*SWAN:* Modular system for connecting and actuating parallel fluidic networks within polymeric microfluidic devices".

---

[*] Co-first authors

PEER-REVIEWED CONFERENCE PROCEEDINGS:

Sabourin, D., Snakenborg, D., Skafte-Pedersen, P., Kutter, J.P., and Dufva, M. "*Modular Microfluidic System with a Cast PDMS Pumping Bed and Planar PDMS Interconnection Blocks*", µTAS 2008, San Diego, California, USA. Kluwer Academic Publishers.

Sabourin, D., Snakenborg, D., Skafte-Pedersen, P., Kutter, J.P., and Dufva, M. *"Fast and Simple: Reconfigurable Elements and Solutions for Creating and Driving Fluidic Networks",* Accepted for oral presentation at µTAS 2010, Gronnigen, Netherlands.

Skafte-Pedersen, P., **Sabourin, D.**, Hemmingsen, M., Østergaard, P.F., Blaga, F.S., and and Dufva, M. *"A user-friendly, self-contained, programmable microfluidic cell culture system for high quality microscopy",* Accepted for µTAS 2010, Gronnigen, Netherlands.

CONFERENCE PROCEEDINGS:

Sabourin, D., Snakenborg, D., Kutter, J.P., and Dufva, M. "*Re-useable PDMS interconnect blocks allowing multiple rapid planar interconnections*", Poster Presentation, Lab On a Chip World Congress, Barcelona, 2008.

Sabourin, D. [*], Petersen, J. [*], Snakenborg, D., Brivio, M., Gudnadson, H., Wolff, A. and Dufva, M. "*Genotyping of Human β-Globin Mutations using capillary driven flows in PMMA microfluidic chips containing fully enclosed allele specific hybridization microarrays*", Poster Presentation, Molecular Diagnostics Europe, Stockholm, 2009.

Sabourin, D., Skafte-Pedersen, P., Snakenborg, D., Kutter, J.P., and Dufva, M. "*Peristaltic Micropump for microfluidic applications*", Oral Presentation, COMS, Copengagen, 2009.

Sabourin, D., Skafte-Pedersen, P., Snakenborg, D., Kutter, J.P., and Dufva, M. "*Modular system for connecting and actuating parallel microfluidic networks*", Poster Presentation, LabAutomation 2010, Palm Springs, USA, 2010.

[*] Co-first authors

ABSTRACT

Microfluidic applications hold promise for many different end-users both within and outside, and across many different research communities. Despite the benefits of microfluidic approaches, adoption and implementation thereof is often hindered by practical issues. Microfluidic components which are more reliable and robust, and which address practical issues are required to encourage and allow non-expert users, those not familiar with microfluidic fabrication methods, to adopt microfluidic approaches.

The first practical challenge encountered by users of microfluidics is the creation of interconnections between microfluidic devices and the outside world. This challenge results from the lack of standards for interconnecting components and the scale disparity between typical microfluidic channel dimensions, microns to hundreds of microns, and the "macro" methods required to address these channels. A second practical challenge users face stems from the peripheral equipment, e.g. pumps, required to drive microfluidic devices. This equipment is often costly and bulky and results in limitations and restrictions on microfluidic device operation, such as the number of channels or devices which can be actuated or microscopic observation.

To address the above issues interconnection and pumping solutions were developed. Methods for creating multiple, aligned, parallel and planar interconnections well suited to microscopy are described. Both reusable, non-integrated, and permanent, integrated interconnection solutions are presented. The construction of twelve and eight channel miniaturized, mechanically actuated peristaltic pumps is also described. The small footprint of the pumps allows their placement adjacent to microfluidic devices and on microscope stages.

The reusable, non-integrated interconnection and miniaturized peristaltic pump solutions were then combined into modular microfluidic systems. One system provides high interconnection numbers/density and allows many possible configurations. Additionally, and apart from many other accounts of modular microfluidic solutions, methods for control and actuation of microfluidic networks built from the modular components is described. Prototypes of the microfluidic system have begun to be distributed to external collaborators and researcher parties. These end-users will assist in the validation of the approach and ultimately fulfil the key driver for development of such a system: providing a practical method for collection of relevant and novel biochemical and biological data from microfluidic devices.

RESUME PÅ DANSK

For mange forskellige brugere både indenfor, udenfor og på tværs af mange forskellige forskningsmiljøer synes mikrofluide applikationer lovende. På trods af fordelene ved mikrofluide tilgange forhindres implementering heraf ofte af praktiske problemer. Det er nødvendigt med pålidelige og robuste mikrofluide komponenter, som kan fremme løsningen af de praktiske problemer. De skal blandt andet tillade nye brugere, der ikke er fortrolige med mikrofluide fabrikationsmetoder, at anvende mikrofluide tilgange.

Den første praktiske udfordring for brugerne af mikrofluide systemer er fremstilling og anvendelse af sammenkoblinger mellem mikrofluide og eksterne enheder. Denne udfordring skyldes generelt manglende standarder for dimensionering af sammenkoblingskomponenter og typiske mikrofluide kanaler, ofte bestående af størrelsesforskelle fra ganske få mikrometer og op til millimeter. En anden praktisk udfordring brugere ofte står overfor, stammer fra det perifere udstyr, f.eks. pumper, der kræves for at drive de mikrofluide enheder. Dette udstyr er ofte både dyrt og pladskrævende, og det resulterer i begrænsninger og restriktioner på driften af mikrofluide enheder, såsom antallet af kanaler eller anordninger, der kan anvendes. Desuden ses udfordringer og kompatibilitetsproblemer med mikroskopi.

For at løse ovennævnte udfordringer blev sammenkoblinger og pumpeløsninger udviklet og testet. Metoder til at oprette flere nøje afstemte, parallelle og plane sammenkoblinger, som er velegnet til mikroskopi, er beskrevet. Sammenkoblingsmetoderne består af to genanvendelige løsninger; en integreret samt en ikke-integreret sammenkobling. Herudover er fremstillingen af en otte- og tolv-kanals miniaturiseret og mekanisk aktueret peristaltisk pumpe beskrevet. Pumpens små dimensioner af pumpen resulterer i, at den let kan integreres i både mikroskopiopsætninger samt andre mikrofluide opsætninger.

Den genanvendelige, ikke-integrerede sammenkoblingsløsning og den miniaturiserede peristaltiske pumpeløsning er herefter blevet samlet i et modulopbygget mikrofluidsystem. Dette sammensatte system resulterer i en høj densitet af sammenkoblinger og tillader mange forskellige systemkonfigurationer. Herudover, og til forskel fra mange tidligere beskrevne modulbaserede mikrofluide systemer, er her beskrevet et modulbaseret system til aktuering og kontrol af mikrofluide netværk. Prototyper af dette system indgår allerede som en del af andre mikrofluide systemer blandt samarbejdspartnere. Disse brugere validerer og kontrollerer således systemet, og de vil i den sammenhæng være hovedansvarlige for feedback, som dermed kan drive udviklingen af disse systemer endnu videre. Hermed opfyldes hovedformålet med udviklingen af mikrofluide systemer, som især er målrettet mod indsamling af relevante og nyskabende biokemiske og biologiske data.

TABLE OF CONTENTS

LIST OF ABBREVIATIONS

ASH	Allele-specific hybridization
BJIB	Ball Joint Interconnection Block
BJIB-90	Ball Joint Interconnection Block with internal 90° channel bend
COC	Cyclic olefin co-polymer
COP	Cyclic olefin polymer
FAST	Fluidic Arrays Systems and Technology Group (DTU Nanotech)
HBB	Human beta-globin gene
HCS	High Content Screening
HUVEC	Human umbilical cord vein endothelial cell
HZ	Heterozygote
IB	Interconnection Block
ID	Inner diameter
IR	Infrared
mm	Millimetre, 10^{-3} m
MR	Multi-Roller, component of *µSlide* system mini-pump
MR-2	Multi-Roller, component of SWAN micropump
MSC	Mesenchymal stem cells
MT	Mutant type
OD	Outer diameter
PC	Polycarbonate
PDMS	Poly(dimethylsiloxane)
PI	Pumping Inlay, component of *µSlide* system mini-pump
PMMA	Poly(methyl methacrylate)
Q	Flow rate
RB	Rotor Bed, component of *µSlide* system mini-pump
RB-2	Rotor Bed, component of SWAN micropump
ssDNA	Single stranded deoxyribonucleic acid
SWAN	*S*ystem *W*ithout *A N*ame, modular microfluidic system
T_g	Glass transition temperature
TC	Tubing connector
UV	Ultraviolet
V_r	Rotational speed
WT	Wild type
µCCC	Micro cell culture chamber
µFR	Microfluidic ribbon
µL	Microliter, 10^{-6} L
µm	Micrometer, 10^{-6} m
% CV	Coefficient of variance

CHAPTER 1: INTRODUCTION

A. MICROFLUIDICS

Microfluidics is the science and technology allowing fluids to be handled and analyzed within channels with typical sizes between tens to hundreds of micrometers (µm) [1, 2]. Microfluidic applications hold great promise and offer many advantages to the chemical, biomedical and biological communities. Among these are decreased sample and reagent consumption, reaction and analysis time, and expected reduced space requirements for both experimental analysis equipment and device. Additionally, opportunities for parallelization, higher throughput and fine environmental control are also of interest [3, 4].

Some advantages of microfluidic approaches originate from the behaviour of fluids as they pass through channels and structures with dimensions in the µm range. The nature of the flows which result, termed laminar, can be useful in many applications. The presentation and description of physical concepts related to microfluidic flow presented below is sourced from the review of *Beebe et al* [1]. More comprehensive reviews of physics associated with both micro- and nanofluidics are available [5, 6].

The Reynolds number (Equation 1) is a dimensionless quantity allowing prediction of the flow regime of a fluid within a channel. The Reynolds number (R_e) is given by:

$$R_e = \frac{\rho \upsilon D_h}{\mu} \tag{1}$$

where ρ is the fluid density, υ the characteristic velocity of the fluid and μ the viscosity of the fluid. The term D_h is referred to as the hydraulic diameter and depends on the geometry of a channel's cross section. For Reynolds numbers < 2300, flow is described as laminar and for values > 2300 flow is described as turbulent. For dimensions typical of microfluidic structures, flow is usually laminar [1].

When two or more laminar streams are in contact with each other, their contents mix only by diffusion. As mixing occurs only by diffusion, the position of a molecule traversing from one stream into an adjacent stream is a function of time and can be estimated according to:

$$d = \sqrt{2Dt} \tag{2}$$

where d is the distance a particle has moved (in a single dimension), D is the diffusion coefficient of the molecule and t is time. The diffusion of particles from one laminar stream into an adjacent laminar stream is depicted in Figure 1.

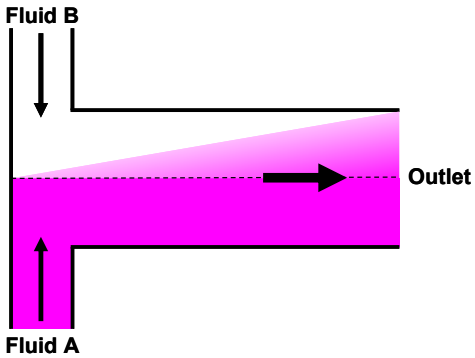

Figure 1. Schematic representation of diffusion between two laminar streams within a microfluidic channel. Fluid A, containing a diffusing molecule represented by the shading, and fluid B enter a microfluidic channel. As the streams are laminar mixing occurs only by diffusion. Mixing of the particles in fluid A into fluid B increasingly occurs as the fluids progress down the channel, as a function of time. The diffusion distance, or advancement, of the molecule in fluid A into fluid B, is a function of its diffusion coefficient and the residence times of the fluids within the channel (Equation 2). The dashed line indicates the fluid boundary between the two streams.

Typical diffusion coefficients, *D*, for different particles are listed in Table 1. The contents of Table 1 are reproduced from a review of microfluidic physics written by *Squires and Quake* [5].

Table 1. Diffusion Coefficient, *D*, for selected particles

Particle	*D* ($\mu m^2/s$)
Solute Ion	2000
Small Protein	40
Bacterium	0.2
Human Cell	0.02

Parameters including channel dimensions, the size of the particle found within the channel, and flow rates within the channel (as these dictate residence time) affect the degree of mixing of particles between adjacent streams. When designing microfluidic channels and networks, the above described parameters are important considerations. This point is nicely summarized by the example provided by *Beebe et al.* [1]: a haemoglobin particle takes approximately one million seconds to diffuse a distance of 1 cm, but only 1 second to diffuse 10 µm.

Both Equation 2 and Figure 1 describe "ideal" diffusion behaviour. Further studies of diffusion between adjacent laminar streams have shown that across a vertical cross-section of adjacent streams, this simple representation is not true [5]. Fluid near the top and bottom of the channels does not move as quickly as fluid in the middle of the channel. Residence times of particles at or near the top and bottom of the channels are therefore longer and as a result they diffuse further into adjacent streams [7, 8].

B. Microfluidic Cell Culture

Although initially not the focus of microfluidic research, microfluidic cell culture and reports thereof have become increasingly prevalent [9, 10]. Though the previously described benefits of a microfluidic approach, e.g. decreased sample and reagent

consumption, still apply to microfluidic cell culture, these advantages are not the key drivers. Miniaturization of assays alone is not what is important, but rather the ability to finely control the cellular environment [9, 11-13].

Microfluidic approaches and the previously described laminar flows allow the possibility of temporal stimulation, or said otherwise, the control of both timing and delivery of cues to cells such as growth factors or drugs. This is not something easily accomplished in traditional batch cell culture methods. As the physical scale of microfluidic channels is near that of cells, an environment which more closely approximates *in vivo* conditions, and is presumably more biologically relevant, can also be constructed [9] and used to monitor cellular response. Microfluidic methods also provide predictable shear stress conditions, an important consideration for many biological experiments [14]. Additionally, micro- and nanofabrication methods can be used to pattern and structure microfluidic channels so as to confer increased functionality [11, 14] and/or experimental inputs to cells under observation. As such, microfluidics provides the possibility to program cellular response and the opportunity to perform high content screening and extract increased information depth related to the kinetics of cellular processes and their regulation [11].

C. Project Basis

The intended start point of the Ph.D. project was a continuation of the work described within *Michael Stangegaard*'s Ph.D. thesis entitled "A biocompatible micro cell culture chamber (µCCC) for culturing and on-line monitoring of eukaryotic cells" [15]. The focus of his work was the construction of a miniaturized polymeric cell culture chamber allowing continuous perfusion studies of cells. The µCCC resulting from his research is shown in Figure 2.

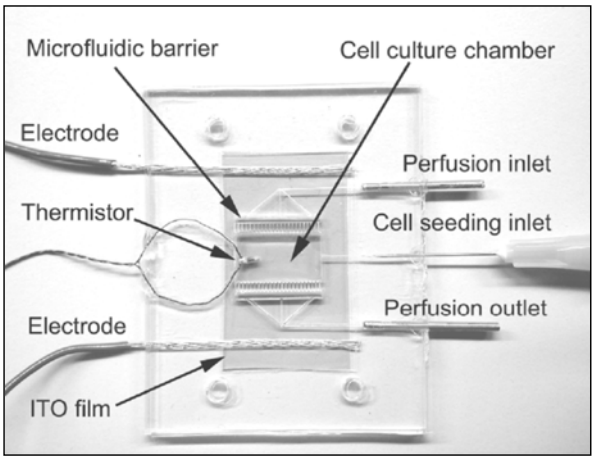

Figure 2. Micro cell culture chamber (µCCC). The µCCC produced by *Stangegaard* contained perfusion inlets and outlets, microfluidic barriers which equilibrated fluid flow through the cell culture chamber, a cell seeding inlet allowing direct injection of cells, and a transparent heating element covered with indium tin oxide (ITO). Overall dimensions of the device were approximately 40 mm *(w)* x 48 mm *(l)* x 5 mm *(h)*. Photo courtesy of M. Stangegaard and M. Dufva, *FAST*, DTU Nanotech.

The µCCC was assembled from several layers of poly(methyl methacrylate) (PMMA) (Figure 2) and permitted sustained culturing and monitoring of cancer and human embryonic stem cells for extended periods [15, 16]. Importantly it allowed direct

observation of cell culture on microscope stages and enabled recording of morphological and growth kinetics data. This is a great advantage over traditional, flask-based cell culture work. Through its miniaturization the µCCC profited from advantages associated with microfludics including lower consumption of reagents and fine environmental control, however it did not exploit further advantages of microfluidics.

The basis for this project was that parallel microfluidic, and hence laminar, flows result in adjacent streams for which molecules mix only by diffusion (Figure 1). Rather than perfuse a µCCC with a single fluid [15], *n* microfluidic streams could be used in two perpendicular directions to create an *n x n* experimental array within the µCCC (Figure 2). The experimental value of the µCCC would thus increase as it would afford both the possibility of higher content screening and increased throughput. An illustrative example is provided in Figure 3. Furthermore, if transient gradients of effector molecules were introduced into different streams and if coupled to time lapse microscopy, an experimental device capable of providing increased data depth related to cellular processes and kinetics thereof would be enabled.

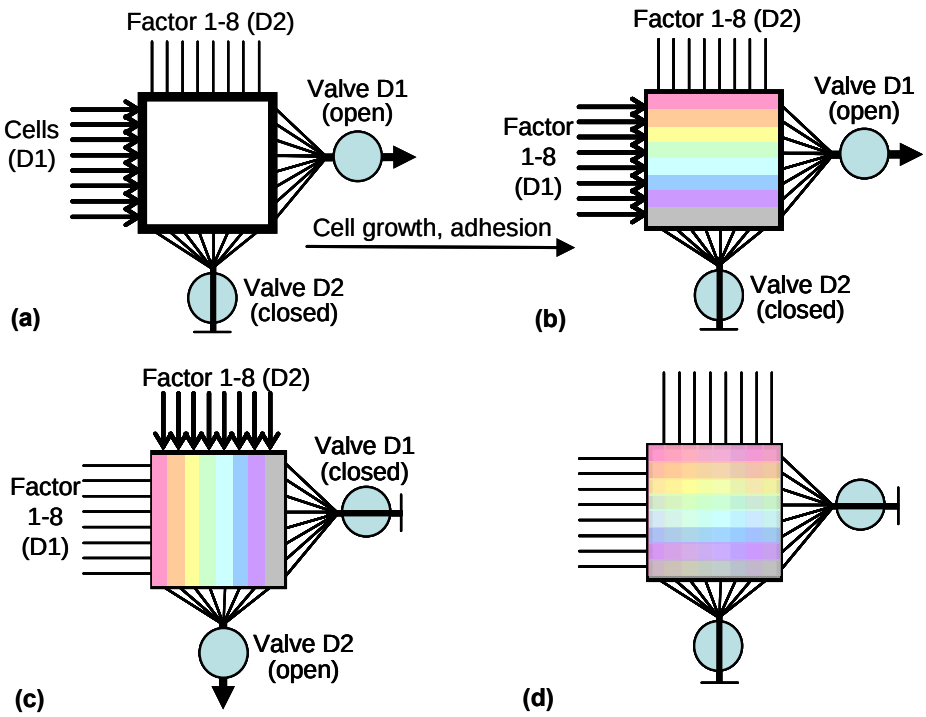

Figure 3. Schematic representation of bi-directional flows within a µCCC to generate a multiplexed, 64 condition experiment. (a) Adherent cells are introduced into the µCCC and are allowed to adhere and become confluent. (b) 8 microfluidic streams, each containing a different compound, are flowed across the cell culture area in direction D1. Each coloured band represents a different agent or compound. This exposes cells within the µCCC to 8 different agents or compounds. In doing so, 8 different experimental conditions have been established. For simplicity of presentation, diffusion of compounds into adjacent streams is not shown. (c) Flow in direction D1 is stopped and the direction of flow across the cell culture chamber is changed to D2. 8 additional agents or compounds then flow across the cell culture area in a direction perpendicular, D2, to the 8 streams shown in (b). As in (b), each coloured band represents a different agent and diffusion across streams is again not shown. This step subdivides each of the 8 experimental conditions generated in step (b) into a further 8 different experimental conditions. (d) As such, 64 experimental conditions would result. In this example, each of the 64 conditions represents a subpopulation of cells found in the microfluidic cell culture chip exposed to each combinations of streams from steps (b) and (c). Diagrams courtesy of M. Dufva, *FAST*, DTU Nanotech.

D. PROJECT OBJECTIVES

The original objective of the Ph.D. project was the construction of a µCCC permitting cell cultures to be treated with an 8 *x* 8 array of fluidic streams (Figure 3), thereby generating 64 experimental conditions within a µCCC.

During the initial phase of the project, microfluidic chips were fabricated from PMMA according to methods used for the previously reported µCCC (Figure 2). Though these methods were suitable for the previous project, the approach used to interface the microfluidic chip to the outside world, i.e. to pumps and/or fluids, was troublesome and triggered a review of project requirements and goals (see below). Connectivity concerns were not unique to this project and have been noted as problematic within the microfluidic community [14, 17-19].

The previous project interfaced the µCCC to the outside world by gluing blunted needles to fluidic ports within the PMMA layers. The approach of gluing needles to create interconnections was laborious, time consuming and prone to clogged channels and resulting yield loss. As the needle became integrated to the device, it was not only the fluidic port which was lost but the entire device could also be considered as "scrap". For microfluidic chips requiring only a few fluidic ports, the method may have been considered acceptable, however for devices such as that shown in Figure 3, potentially requiring high numbers or densities of interconnections, it was far from ideal. A method providing multiple parallel and reusable interconnections would be beneficial.

Furthermore, and apart from interconnections, consideration of methods to both deliver and control fluids to a microfluidic cell culture chip such as that shown in Figure 3 revealed that pumping strategies should also be considered. Introduction of media to the µCCC (Figure 2) required a single syringe pump. Fluidically addressing a device resembling that shown in Figure 3 with parallel and multiple streams could require multiple pumps and control mechanisms for these. This could pose a strain on laboratory resources and could also result in experimental setups not well suited to microscopy.

Consideration of the interconnection methods and peripheral equipment requirements led to a review, and expansion, of project objectives beyond the initial objective of fabrication of a microfluidic cell culture device.

Revised Project Objectives

For reasons described, the project's objectives were reviewed, redefined and broadened in scope. The revised project objectives became:

1. To propose and implement solutions which create multiple and reliable fluidic **interconnections** to polymeric microfluidic chips, and which are suited to microscopic observation,

2. To propose and implement solutions which increase **pumping** capacity, and which were suited to microscopic observation,

3. To combine the solutions developed above into a **microfluidic system,**

4. To demonstrate the utility and applicability of the system with respect to **microfluidic cell culture** using PMMA-based, microfluidic chips.

Several accounts describe that more reliable and robust microfluidic components and methods are required to encourage and allow "non-expert" users to adopt microfluidic approaches [2, 17, 19, 20]. Ideally, but not necessarily, the solutions and approaches developed were to be user-friendly and form a base which was transferable and applicable to other projects and collaborations within and outside of the *FAST* group. Said otherwise, the methods developed should be flexible, and not solely support the testing of "a" microfluidic cell culture chip, such as that shown in Figure 3, but also other microfluidic chip designs and applications.

E. Microfluidic Device Fabrication

Meeting project objectives required familiarization with fabrication methods associated with production of microfluidic devices and components. The following section describes considerations related to the construction of microfluidic devices. In general, construction of microfluidic devices requires consideration of materials, machining and bonding (lidding) methods. Specifications related to each of these three considerations were also provided and are highlighted within each respective passage. Material, machining and bonding specifications outlined were adopted to provide focus to the project with respect to microfluidic device construction. These were/are not meant to discount other approaches used in microfluidic research and products. As is described, these originate in part from observations and results collected by *Stangegaard* [15].

Materials

When initially considering microfluidic devices and systems, substrate selection is often the first consideration and selection thereof is heavily dependent on the intended application. The most commonly used materials for microfluidic device construction are silicon and polymers, including both elastomers and thermoplastics [21, 22].

From the early stages of microfluidic research to present, silicon-based fabrication approaches predominate [22]. This initially resulted from the belief that well characterized and established photolithographic processes from the semi-conductor industry could be leveraged and easily applied to production of microfluidic devices. Silicon is well suited for applications requiring high temperatures and strong solvents such as capillary electrophoresis [1, 22-24]. However, as a result of several disadvantages associated with silicon, emphasis has shifted to the use of other substrates [1, 2, 22-24]. These disadvantages include the cost of materials, labour, specialized equipment, and facilities required for silicon processing, limited geometries, limitations with normal optical detection methods as a result of its non-transparency, difficulty in component integration and it's not being well suited to many biological applications [1, 2, 22-24].

Following initial reports by *Xia et al.* [25] and *Quake et al*. [26] of the processing benefits and possibilities associated with "soft lithographic" approaches, use of elastomers, in particular poly(dimethylsiloxane) (PDMS), for microfluidic device construction has become increasingly widespread [22]. So much so, that it is considered the "workhorse" material for microfluidic research [27]. Soft lithography exploits the high replication fidelity of materials such as PDMS when these are cast over (typically) photolithographically patterned moulds [28]. Following curing of the elastomer and removal from the mould, a negative image of the photolithographic feature patterns are found on the elastomer. Submicron features can be reproduced with this method. Often cited advantages of PDMS are that it is inexpensive, optically transparent, unreactive to most reagents, gas permeable, biocompatible (see below), and is amenable to rapid fabrication methods [12, 29, 30].

Polymers, in particular thermoplastics, have also seen increasing use in microfluidic device fabrication and research [22, 23]. Thermoplastics are usually hard and transparent at room temperature. When warmed to a characteristic temperature, the glass transition temperature (T_g), thermoplastics soften. Upon cooling, they recover their original state and chemical properties. Many thermoplastics are available and offer favourable cost, mechanical, and optical characteristics, and are easily handled. As a result of the softening behaviour described above, they are suitable to processing via high volume replication and production methods. Additionally, as compared to silicon, thermoplastics are not as limited with respect to geometry and have been shown to be biocompatible [16] and/or well suited to biological applications [23, 24, 31]. The most commonly used thermoplastics are PMMA, polycarbonate (PC) and cyclic olefin polymers and co-polymers (COP and COC) [22].

Material Project Specification
PMMA was specified as substrate for µCCC construction in this project.

Benefits of PMMA include low cost, optical transparency, low hydrophobicity, amenability to fabrication and modification, and good biocompatibility [31]. Biocompatibility describes the property of a surface which is not found to promote or obstruct biological surfaces as compared to a given reference surface [32]. Importantly, *Stangegaard* used gene expression profiling to validate PMMA as being biocompatible for µCCC construction. In this case equivalence, beyond the typical morphological, phenotypic or growth kinetics-based assessment used to gauge biocompatibility, between culture conditions within the µCCC and conventional cell culture flasks was demonstrated [33, 34]. For cell-based studies, demonstration of equivalent environments is important for several reasons. To substantiate future biomedical or biological findings from the µCCC, one must show that the material is not responsible for imparting or effecting change. Traceability is thus provided and permits adoption of quality control activities related to the validation and monitoring of both different grades and vendor lots of PMMA, and more importantly, of new and old experimental results and findings.

Machining

Apart from substrate selection, microfluidic device construction requires consideration of machining methods. As PMMA was to be the base material for device construction, machining of thermoplastics is described below.

Microfluidic structures made in polymers are created *via* two primary methods: replication and direct writing. Replication involves use of a master to create multiple and identical copies of the same part [21]. Replication methods rely on the introduction of contact between the master and a softened or liquid polymer and subsequent hardening, by either thermal or chemical means, of the polymer while in contact with the master [21, 23, 24]. Examples of replication processes include hot embossing, injection moulding and casting. In general, replication methods are more suited to production runs, where many identical copies of a part are required. Due to the cost, labour and potentially long cycle times associated with master creation, replication methods are not usually suited to exploratory stages of projects; stages where prototyping and design changes are both required and dominate [21, 23].

In contrast to replication methods where polymer substrate is added or introduced to a master, direct writing methods remove material from the substrate to create structures [21]. These methods eliminate the requirement for master creation and usually permit same day design changes. Direct writing methods are well suited to projects at the prototyping stage, where design changes are expected and required. The disadvantage of these methods is that parts are usually made in a sequential manner, though this limitation applies more to mass production [21, 23].

The two most common direct writing methods are laser ablation and micromilling [21]. Structuring by laser ablation is based on either pulsed or continuous exposure to light [35]. Polymer is removed by either photodegradation (UV lasers) or thermal degradation (IR lasers) [35], or a combination thereof [24]. During laser ablation processes, substrates are placed on a stage and are either patterned by having the stage moved around below a stationary laser, or by having the laser aimed at different areas of the substrate. A moving stage is preferable in order to create more consistent features and feature profiles across the substrate [24]. Feature sizes depend on laser beam velocity, intensity (power) and the number of passes a laser completes over the area to be ablated [23]. In some cases laser ablation is used in combination with masks. When placed on top of the polymer, exposed areas on the mask define which areas will be patterned. Quality of patterning in this case also depends on mask quality [21, 24].

Micromilling removes material mechanically from substrates with assorted cutting tools [21, 36]. A tool is mounted above the substrate in a stationary housing which drives rotation of the cutting tool. The rotation permits cutting and patterning of the substrate. Usually, the cutting tool is held stationary over a stage onto which the substrate is affixed and the stage is moved around under the cutting tool to pattern the substrate. The profile and diameter of the cutting tool determine the shape written into the substrate.

Machining Project Specification

As they are more accessible, less costly and typically result in faster prototyping times than other methods [21, 23], direct writing methods such as laser ablation and micromilling were to be used.

Bonding

In almost all cases [1, 37, 38], regardless of the method or material used to fabricate a microfluidic device, the structured substrate must be lidded in order to fully encapsulate channels or define other fluidic features [22]. Selection of bonding methods requires consideration of required bond strengths and characteristics of the bond interface. For the latter, optical properties, material compatibility, homogeneity of the channel sidewalls and compatibility with working fluids (chemicals and solvents) are factors which must be considered [22]. For thermoplastics, there are two main bonding methods: indirect and direct bonding.

Indirect bonding involves use of an adhesive layer to seal two layers together. Indirect methods are simple and often rapidly implemented. Commonly adhesives, glues and epoxies are used to join layers of a device. Disadvantages of indirect approaches include the risk of channel clogging, and as a result of an intermediary layer, channel sidewalls of different composition, and hence mechanical and optical properties, from the bulk of the device. The sometimes unknown composition of adhesives and varied lot-to-lot properties can cause problems in fine chemical analysis applications, yields* and have been shown to be non-biocompatible [15].

Direct bonding methods mate thermoplastics without addition of materials to the interface. As additional agents are not used, sidewalls of the microchannels are homogenous and share identical surface properties with the rest of the device. The three most common direct bonding methods are thermal bonding, solvent bonding and bonding based on surface treatments and modifications [22].

Thermal bonding is the most common direct method of sealing thermoplastic microfluidic devices [22]. One or both of the surfaces to be joined is/are heated near, at or above the T_g of the material. Pressure is also applied to increase contact between the mating surfaces [21, 22]. Together, temperature and pressure result in polymer flow at the interface and interdiffusion of polymer chains between the two surfaces to generate a bond [21, 22]. The major challenge of thermal bonding is the prevention of channel distortion and collapse [22, 39, 40]. Non-optimized or inadequately controlled processes with respect to temperature, time and pressure can lead to channel distortion or collapse. In the case of PMMA, this can even occur at temperatures 10°C below T_g [40].

Placing a thermoplastic in contact with a solvent provides mobility to individual polymer chains. These are then free to diffuse across the solvated layer and chains from different layers can become entangled. Use of many solvents has been demonstrated and in some cases their use has been shown to limit or eliminate channel deformation [41, 42]. Solvents are not always considered user friendly and may not be compatible with process

* Based on personal work experience at *point-of-care* diagnostic manufacturer i-STAT, Abbott Laboratories

flows and negatively impact previous surface functionalization of the polymeric surface [36].

Treatments which break down molecules and produce highly reactive groups at the surface of the thermoplastic result in increased overall surface energy. Increased surface energy allows greater contact between pieces to be joined and greater diffusion of polymer across the layers. Treatments employing ions, electrons and UV photons can induce formation of these reactive groups [22]. Channel deformation can be avoided with these methods. As with solvent-based approaches, compatibility with process flows and previous functionalization of the polymeric surfaces is not guaranteed.

Bonding Project Specification

Direct bonding methods should be used and external agents such as adhesives and glues should be avoided. This specification results from previous observations concerning epoxy use and biocompatibility issues [15]. The unknown composition of such materials may introduce and unknown and/or untraceable experimental artefacts.

F. Fabrication Method Selection

Machining

Micromilling was the base machining method used for the thesis and was used to pattern the microfluidic chips, moulds, and parts for in-house developed peripheral component solutions (see Chapters 2, 3, 4 and 6). Micromilling, a direct writing method (machining project specification), features low running costs and typical cycle times of only a few hours [36]. A micromilling set-up at DTU Nanotech is shown in Figure 4.

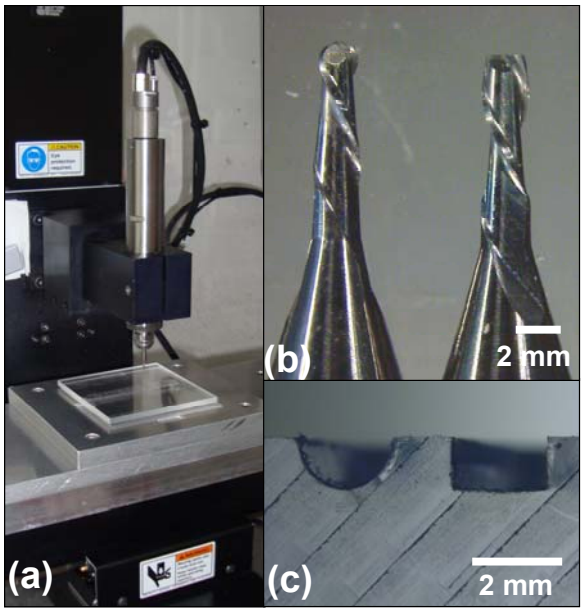

Figure 4. Micromilling. (a) Micromilling machine at DTU Nanotech. A vertically mounted spindle holds a cutting tool. The substrate is fastened to motorized plates below the spindle. To machine substrates, the spindle and cutting tool are held fixed while the plate holding the substrate is moved. The cutting tool height can be varied to control feature depth. (b) Example milling tools. Ball end mill (left) and end mill (right). These cutting tools result in channel profiles as shown in (c) Semi-spherical channel profiles resulting from ball end mill (left) and rectangular channel profile resulting from standard end mill (right).

Micromilling makes use of cutting tools which are readily available in a variety of sizes/diameters, between 50 µm to 3 mm, and which permit different channel profiles and geometries. Common tool types and resulting channel profiles are shown in Figure 4. Channel feature dimensions produced by micromilling are suitable for most microfluidic applications [43-45]. Assuming proper machine and substrate set-up, as the cutting tool is held perpendicular to the surface being patterned, micromilling results in consistent channel geometries, profiles and depths across the surface of the substrate. For example, when following proper procedures for the micromilling setup at DTU Nanotech (Figure 4) variance in channel depth over a 10 x 10 cm substrate is typically near 20 µm[*]. Another advantage of micromilling is that it can be used to shape a variety of substrates including plastics, metals and printed circuit boards. As project objectives included the realization of peripheral components, the option and ability to do so was important.

Owing to the reproducibility of micromilling, pieces and components produced by micromilling can be precisely aligned [46]. Multiple pieces formed by micromilling can thus be assembled to form moulds for either injection moulding and/or casting. This latter replication process was used extensively during the project, however it differed from the soft lithographic methods typically used for and associated with microfluidic device construction. Normally elastomers such as PDMS are poured and cured on top of a photolithographically patterned silicon wafer. For this project, PMMA pieces were patterned by micromilling and were assembled into three-dimensional moulds resembling those used for injection moulding. PDMS could be injected into and subsequently cured within the three-dimensional moulds. Following curing, the mould could be disassembled and the completed PDMS part removed. This casting approach is more completely described in Chapter 2 (Figure 8).

Bonding

With respect to PMMA bonding, indirect bonding methods were immediately discounted because these employ compounds of which composition is often unknown and which may have unwanted effects on cell culture or analytical investigations [33, 47]. *Truckenmuller et al.* [48] demonstrated a surface modification approach based on UV radiation. Exposure of PMMA to UV reduced the T_g of the polymer's surface layer, only to a depth of several microns. The T_g of the bulk polymer remained unchanged and as such structures could be bonded above the T_g of the surface layer but below that of the bulk PMMA layer. Sealing was permitted without a loss in structure quality or channel deformation [48]. PMMA chips produced during the Ph.D. thesis were bonded based on this method. The bonding procedures and conditions used to produce microfluidic chips are described either within corresponding publications or within chapters describing use of the PMMA chip.

[*] Personal communication from Per Thor Jonassen, Laboratory Technician and Machinist, DTU Nanotech.

G. Project Overview

The revised project objectives required development of solutions and approaches related to varied aspects of microfluidic research. Dependent on familiarity with microfluidics, the relationship between the solutions developed may not be obvious to all readers. As such a project roadmap (Figure 5) is provided to illustrate how delivered solutions relate both to each other and how these were combined in order to fulfil project objectives. Chapters describing content related to each objective are also indicated in Figure 5.

The project base was formed by becoming familiar with different fabrication methods. These were then used to develop microfluidic components and systems. Chapter 2 describes interconnection solutions developed (Objective 1) and Chapter 3 describes pumping solutions (Objective 2). Chapter 4 presents two approaches to combine the solutions developed in Chapters 2 and 3 to form a microfluidic system (Objective 3). Each chapter contains an introduction and review of relevant and published material. As project focus was shifted from cell culture to development of microfluidic components, cell culture (Objective 4) was used to establish applicability of the microfluidic systems and components developed (Chapter 4 and 5). Development of fabrication competencies allowed several side projects, not directly related to project objectives, to be undertaken during the period of study. These side projects are described in Chapter 6. In several cases work related to the objectives has been published either in journals or in peer-reviewed conference proceedings. Chapters corresponding to respective publications contain only an abridged version of material presented within the full publication. Complete publications are located in Appendices A and B.

Finally, realization of the broadened project objectives within the 3 year time period allotted for the Ph.D. implied that methods and solutions should be relatively simple and practical. With respect to solutions provided, focus should be placed on implementation and refrain from over characterization. Said otherwise, demonstrating validity, usability and applicability of solutions to the project and microfluidic community baselines or standards should be the goal, and not necessarily development of “best in class” solutions.

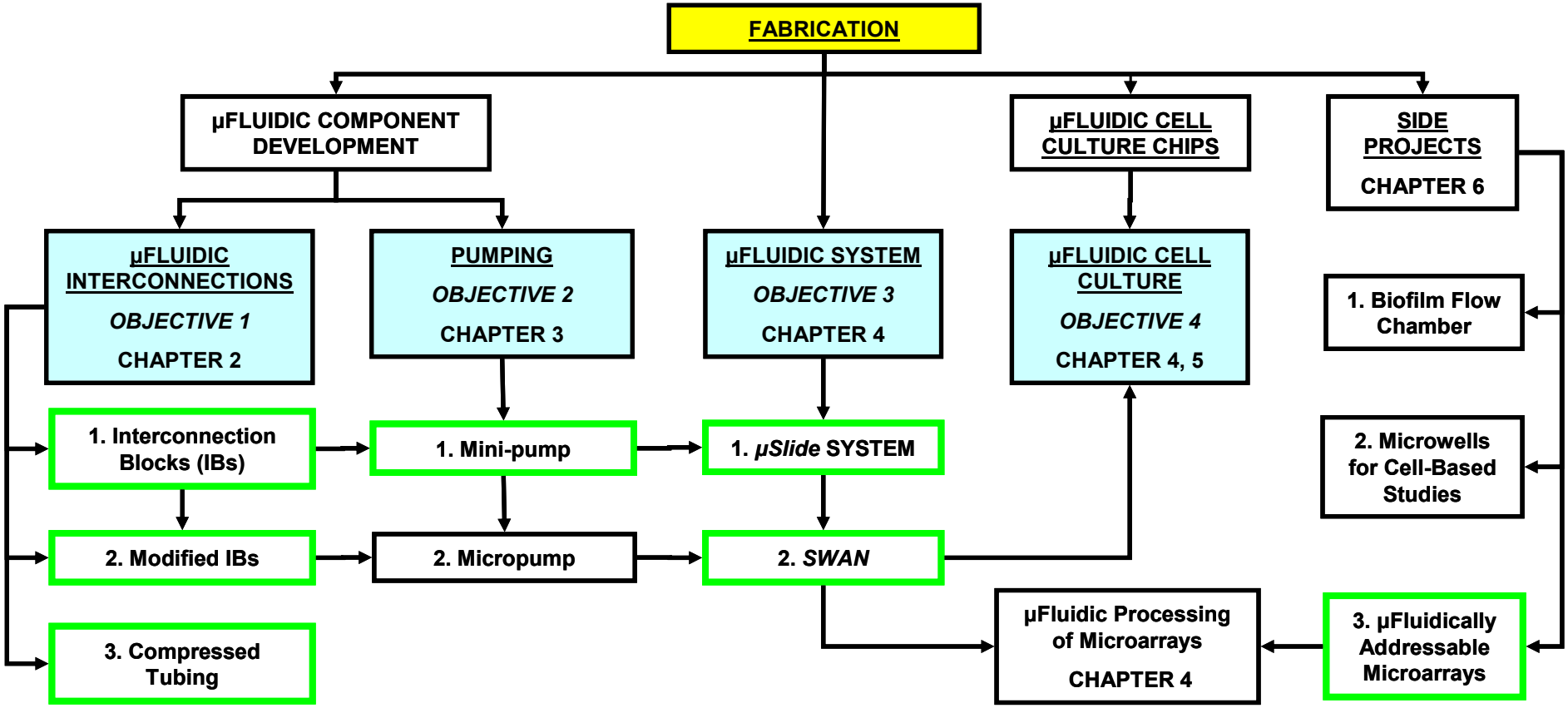

Figure 5. **Ph.D. project roadmap**. Blue boxes represent revised project objectives (Section D). Contents of boxes outlined in green indicate solutions proposed during the Ph.D. project which were published in either journals or peer-reviewed conference proceedings. Chapters describing box content are indicated. Fabrication knowledge (yellow box) formed the basis of the project. Fabrication competencies were first used to create microfluidic components satisfying the first two revised project objectives: interconnection and pumping solutions. Interconnection solution 1, IBs, and pumping solution 1, mini-pump, were then combined into a first modular microfluidic system, *µSlide*. Improvements to the IBs and the mini-pump resulted in the second interconnection solution, modified IBs, and a second pump, micropump. These were then combined and a second, improved modular microfluidic system resulted: *SWAN* (System Without A Name). *SWAN* satisfies the third project objective. Fabrication competencies were also leveraged to produce a third interconnection solutions, compressed tubing, microfluidic cell culture chips and for several side projects. Most important of these was the report of entirely polymeric microfluidically addressable, diagnostic microarrays. Both microfluidic cell culture and processing of the microarrays was performed using different configurations of *SWAN*.

REFERENCES

1. Beebe, D.J., G.A. Mensing, and G.M. Walker, *Physics and applications of microfluidics in biology.* Annual Review of Biomedical Engineering, 2002. **4**: p. 261-286.
2. Whitesides, G.M., *The origins and the future of microfluidics.* Nature, 2006. **442**(7101): p. 368-373.
3. Dittrich, P.S. and A. Manz, *Lab-on-a-chip: microfluidics in drug discovery.* Nature Reviews Drug Discovery, 2006. **5**(3): p. 210-218.
4. Wilding, P., et al., *Microtechnology in the Clinical Laboratory: Will It Solve Analytical Problems, and When Will It Make an Impact?* Clinical Chemistry, 2010. **56**(4): p. 508-514.
5. Squires, T.M. and S.R. Quake, *Microfluidics: Fluid physics at the nanoliter scale.* Reviews of Modern Physics, 2005. **77**(3): p. 977-1026.
6. Bruus, H., *Theoretical Microfluidics.* Oxford University Press, 2008.
7. Ismagilov, R.F., et al., *Experimental and theoretical scaling laws for transverse diffusive broadening in two-phase laminar flows in microchannels.* Applied Physics Letters, 2000. **76**(17): p. 2376-2378.
8. Kamholz, A.E. and P. Yager, *Molecular diffusive scaling laws in pressure-driven microfluidic channels: deviation from one-dimensional Einstein approximations.* Sensors and Actuators B-Chemical, 2002. **82**(1): p. 117-121.
9. Young, E.W.K. and D.J. Beebe, *Fundamentals of microfluidic cell culture in controlled microenvironments.* Chemical Society Reviews, 2010. **39**(3): p. 1036-1048.
10. Maerkl, S.J., *Integration column: Microfluidic high-throughput screening.* Integrative Biology, 2009. **1**(1): p. 19-29.
11. Dufva, M. and D. Sabourin, *A biologist's guide to programmable cell culture, manuscript submitted.* Integrated Biology, 2010.
12. El-Ali, J., P.K. Sorger, and K.F. Jensen, *Cells on chips.* Nature, 2006. **442**(7101): p. 403-411.
13. Jovic, A., B. Howell, and S. Takayama, *Timing is everything: using fluidics to understand the role of temporal dynamics in cellular systems.* Microfluidics and Nanofluidics, 2009. **6**(6): p. 717-729.
14. Young, E.W.K. and C.A. Simmons, *Macro- and microscale fluid flow systems for endothelial cell biology.* Lab on a Chip, 2010. **10**(2): p. 143-160.
15. Stangegaard, M., *A biocompaticle micro cell culture chamber (uCCC) for continuous on line perfusion.* Ph.D. Thesis, 2006.
16. Stangegaard, M., et al., *A biocompatible micro cell culture chamber (microCCC) for the culturing and on-line monitoring of eukaryote cells.* Lab Chip, 2006. **6**(8): p. 1045-51.
17. Fredrickson, C.K. and Z.H. Fan, *Macro-to-micro interfaces for microfluidic devices.* Lab on a Chip, 2004. **4**(6): p. 526-533.
18. Kim, L., et al., *A practical guide to microfluidic perfusion culture of adherent mammalian cells.* Lab on a Chip, 2007. **7**(6): p. 681-694.
19. Andersson, H. and A. van den Berg, *Where are the biologists? A series of mini-reviews covering new trends in fundamental and applied research, and potential applications of miniaturised technologies.* Lab on a Chip, 2006. **6**(4): p. 467-470.

20. Haeberle, S. and R. Zengerle, *Microfluidic platforms for lab-on-a-chip applications.* Lab on a Chip, 2007. **7**(9): p. 1094-1110.
21. Geschke, O., H. Klank, and P. Telleman, *Microsystem Engineering of Lab-on-a-chip Devices* Wiley-VCH, 2004: p. 270.
22. Tsao, C.W. and D.L. DeVoe, *Bonding of thermoplastic polymer microfluidics.* Microfluidics and Nanofluidics, 2009. **6**(1): p. 1-16.
23. Becker, H. and C. Gartner, *Polymer microfabrication technologies for microfluidic systems.* Analytical and Bioanalytical Chemistry, 2008. **390**(1): p. 89-111.
24. Becker, H. and L.E. Locascio, *Polymer microfluidic devices.* Talanta, 2002. **56**(2): p. 267-287.
25. Xia, Y.N. and G.M. Whitesides, *Soft lithography.* Annual Review of Materials Science, 1998. **28**: p. 153-184.
26. Unger, M.A., et al., *Monolithic microfabricated valves and pumps by multilayer soft lithography.* Science, 2000. **288**(5463): p. 113-116.
27. Klapperich, C.M., *Microfluidic diagnostics: time for industry standards.* Expert Review of Medical Devices, 2009. **6**(3): p. 211-213.
28. Li, N., A. Tourovskaia, and A. Folch, *Biology on a Chip: Microfabrication for Studying the Behaviour of Cultured Cells.* Critical Reviews in Biomedical Engineering, 2003. **31**(5&6): p. 423-488.
29. McDonald, J.C. and G.M. Whitesides, *Poly(dimethylsiloxane) as a material for fabricating microfluidic devices.* Accounts of Chemical Research, 2002. **35**(7): p. 491-499.
30. Tung, Y.C., et al., *Small volume low mechanical stress cytometry using computer-controlled Braille display microfluidics.* Lab on a Chip, 2007. **7**(11): p. 1497-1503.
31. Chen, Y., L. Zhang, and G. Chen, *Fabrication, modification, and application of poly(methyl methacrylate) microfluidic chips.* Electrophoresis, 2008. **29**(9): p. 1801-14.
32. Wang, Y.X., et al., *Effects of the chemical structure and the surface properties of polymeric biomaterials on their biocompatibility.* Pharmaceutical Research, 2004. **21**(8): p. 1362-1373.
33. Stangegaard, M., *A biocompaticle micro cell culture chamber (uCCC) for culturing and on-line monitoring of Eukaryotic cells, Ph.D. Thesis.* MIC - Department of Micro- and Nanotechnology, Technical University of Denmark, 2005.
34. Stangegaard, M., et al., *Whole genome expression profiling using DNA microarray for determining biocompatibility of polymeric surfaces.* Molecular Biosystems, 2006. **2**(9): p. 421-428.
35. Klank, H., J.P. Kutter, and O. Geschke, *CO2-laser micromachining and back-end processing for rapid production of PMMA-based microfluidic systems.* Lab on a Chip, 2002. **2**(4): p. 242-246.
36. Ogilvie, I.R.G., et al., *Reduction of surface roughness for optical quality microfluidic devices in PMMA and COC.* Journal of Micromechanics and Microengineering, 2010. **20**(6): p. 8.
37. Chiou, C.H. and G.B. Lee, *Minimal dead-volume connectors for microfluidics using PDMS casting techniques.* Journal of Micromechanics and Microengineering, 2004. **14**(11): p. 1484-1490.

38. Sabourin, D., D. Snakenborg, and M. Dufva, *Interconnection blocks: a method for providing reusable, rapid, multiple, aligned and planar microfluidic interconnections.* Journal of Micromechanics and Microengineering, 2009. **19**(3).
39. Shinohara, H., J. Mizuno, and S. Shoji, *Low-temperature direct bonding of poly(methyl methacrylate) for polymer microchips.* Ieej Transactions on Electrical and Electronic Engineering, 2007. **2**(3): p. 301-306.
40. Tsao, C.W., et al., *Low temperature bonding of PMMA and COC microfluidic substrates using UV/ozone surface treatment.* Lab Chip, 2007. **7**(4): p. 499-505.
41. Koesdjojo, M.T., C.R. Koch, and V.T. Remcho, *Technique for Microfabrication of Polymeric-Based Microchips from an SU-8 Master with Temperature-Assisted Vaporized Organic Solvent Bonding.* Analytical Chemistry, 2009. **81**(4): p. 1652-1659.
42. Lin, C.H., C.H. Chao, and C.W. Lan, *Low azeotropic solvent for bonding of PMMA microfluidic devices.* Sensors and Actuators B-Chemical, 2007. **121**(2): p. 698-705.
43. Bundgaard, F., et al., *Cyclic olefin copolymer (COC/Topas((R))) - An exceptional material for exceptional lab-on-a-chip systems*, in *Micro Total Analysis Systems 2004, Vol 2*, T. Laurell, et al., Editors. 2005. p. 372-374.
44. Friedrich, C.R. and M.J. Vasile, *Development of the micromilling process for high-aspect-ratio microstructures.* Journal of Microelectromechanical Systems, 1996. **5**(1): p. 33-38.
45. Yan, J., et al., *Fabrication of micro end mills by wire EDM and some micro cutting tests.* Journal of Micromechanics and Microengineering, 2009. **19**(2).
46. Perozziello, G., F. Bundgaard, and O. Geschke, *Fluidic interconnections for microfluidic systems: A new integrated fluidic interconnection allowing plug 'n' play functionality.* Sensors and Actuators B-Chemical, 2008. **130**(2): p. 947-953.
47. Saarela, V., et al., *Re-usable multi-inlet PDMS fluidic connector.* Sensors and Actuators B-Chemical, 2006. **114**(1): p. 552-557.
48. Truckenmuller, R., et al., *Bonding of polymer microstructures by UV irradiation and subsequent welding at low temperatures.* Microsystem Technologies-Micro-and Nanosystems-Information Storage and Processing Systems, 2004. **10**(5): p. 372-374.

CHAPTER 2: INTERCONNECTIONS

Proposal and implementation of solutions for reliable fluidic connections to polymeric microfluidic chips permitting unobstructed microscopic observation was the first of the revised project goals. During the Ph.D. project several solutions for creating fluidic interconnections were produced. These are described in the following publications:

Publication 1
Sabourin, D., Snakenborg, D. and Dufva, M. "*Interconnection blocks: a method for providing reusable, rapid, multiple, aligned and planar microfluidic interconnections*" Journal of Micromechanics and Microengineering. Volume 19, 035021 (9 pp), 2009. doi:10.1088/0960-1317/19/3/035021.

Publication 2
Sabourin, D., Snakenborg, D., and Dufva, M. "*Interconnection blocks with minimal dead volumes permitting planar interconnection to thin microfluidic devices*" Microfluidics and Nanofluidics. Volume 9, p. 87-93, 2010. doi:10.1007/s10404-009-0520-8.

Publication 3
Sabourin, D., Dufva, M., Jensen, T., Kutter, J., and Snakenborg, D. "*One-step fabrication of microfluidic chips with in-plane, adhesive-free interconnections*" Journal of Micromechanics and Microengineering. Volume 20, 037001 (7pp), 2010. doi: 10.1088/0960-1317/20/3/037001.

Contents from the above publications are condensed and presented in this chapter. Complete publications are found in Appendix A. The introduction to microfluidic interconnections is a condensed version of that found in publication 1.

A. INTRODUCTION

Though microfluidic approaches hold great promise, due to lack of reliability and ease of use and integration, they have not been adopted as widely as expected [1, 2]. Creating fluidic connections between microfluidic devices and the outside world represents a challenge, one (frustratingly) noted at the beginning of this project. Contributing to this challenge are a lack of standards for interconnecting components and a difference of scale [3]. Terms such as "macro-to-micro" and "world-to-chip" reflect the scale disparity between typical microfluidic channel dimensions, microns to hundreds of microns, and the tool and methods (often by hand) used to connect these to the outside world [4]. Additionally, the cost associated with packaging or interfacing devices can be prohibitive [5, 6].

Connections between microfluidic components and the devices which drive them, e.g. pumps, are generally classified as permanent or reversible (non-permanent). Permanent interconnection methods are often the easiest to implement and commonly involve directly attaching a needle, piece of tubing or fluidic reservoir to a corresponding inlet or

outlet port of a microfluidic device with adhesives such as epoxy [4, 7]. The disadvantages associated with permanent methods include the increased risk of clogged channels and larger dead volumes resulting from the required manual alignment of features over small areas. Several methods have been proposed to prevent clogging when making permanent interconnections however not all are applicable to polymeric processing [8-10]. Permanent methods can also be laborious and time consuming for devices requiring multiple connections. With time and device use, loss of sealing capabilities is often observed as device handling places stress on the connection. Additionally, biocompatibility problems with epoxy use have been observed [11].

Reversible interconnections are described as ideally being reliable, both in terms of high seal/pressure performance and repeatability thereof, re-useable, easy to fabricate and assemble, easy to use and handle, flexible, having minimal pressure drops, having low dead volumes, operating over a range of flow rates, being chemically and/or biologically compatible, of low-cost, and offering unobstructed observation [4, 12]. Commonly used methods to create reversible interconnections, not necessarily fulfilling all the criteria listed above, involve compression of an elastomeric microfluidic device [7], press-fit type connections (placing an "oversized" element into an "undersized" recess) [12-16], O-rings [12, 15, 17], deformation of soft tubing [5, 6, 18], or a combination thereof [12, 15]. Elastomeric layers can also be patterned to function as gaskets and create seals between layers of microfluidic devices [7, 16, 19]. These methods are depicted in Figure 6.

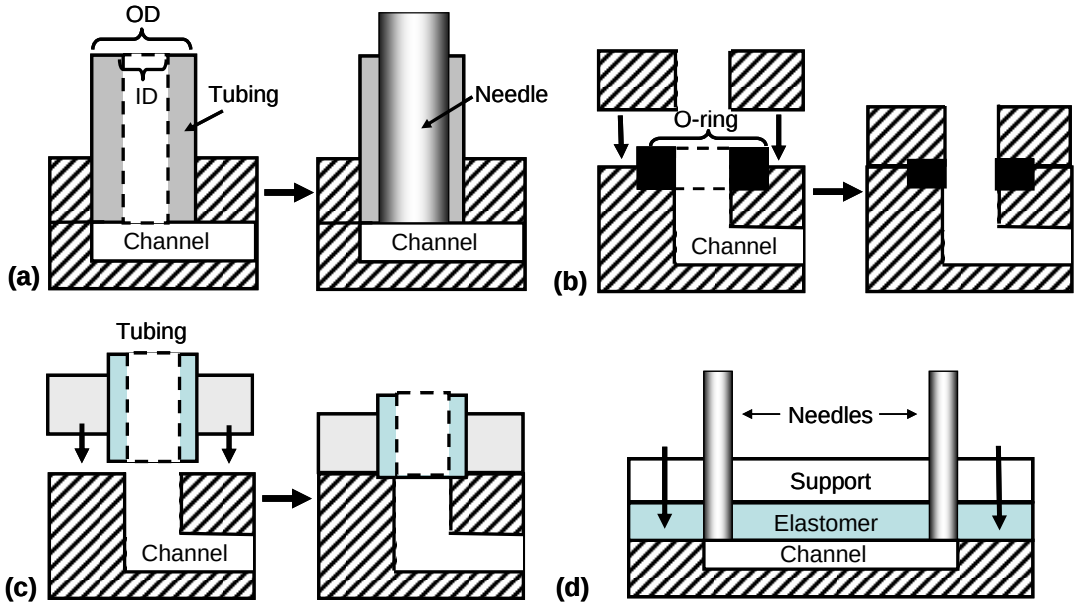

Figure 6. General interconnection methods. (a) Press-fit methods involve the insertion of an "oversized" element into an "undersized" recess. In this example, tubing with the same outer diameter (OD) as the circular port is inserted into the port directly above a microfluidic channel. A needle with a larger OD than the tubing's inner diameter (ID) is inserted into the tubing. The tubing is compressed against both the needle and side wall of the device and a seal is formed. (b) An O-ring is positioned on top of a microfluidic channel. A complementary layer, top, is brought in contact and compressed against the bottom layer. Compression of the O-ring results in a sealed interconnection between the two layers. (c) Deformation of extended soft tubing. As in the previous example, layers are compressed together. Deformation of the extended soft tubing portion causes it to behave as an O-ring and a seal is created. (d) An elastomeric layer is compressed between two layers to lid and seal the channel area. This example shows how methods can also be used in conjunction to seal and address microfluidic devices. Needles passing through the elastomeric layer are press-fit as in (a).

Reversible connections can be subdivided into integrated and non-integrated methods. Integrated methods contain an element which becomes part of the microfluidic component/device. Non-integrated connections can be wholly dissociated from the microfluidic device they address. Non-integrated approaches are favourable as they uncouple interconnection and microfluidic device yield, fabrication and design. Table 2 presents a summary of several reversible interconnection methods and their reported maximum leak pressures. The maximum values are not necessarily representative of expected performance and the noted reference should be consulted for a more complete description of test data collected.

Fluidic connections made to the PMMA µCCC reported by *Stangegaard* [11, 20] were made using permanent methods: blunted needles were directly epoxied into PMMA devices. When using this method, the disadvantages described for permanent methods, with the exception of dead volumes, were encountered. Yield loss from clogging occurred and as the PMMA device was permanently coupled it was also lost. For devices, such as the proposed cell culture chip (Figure 3, Chapter 1), requiring multiple interconnections, the prospect of using this time consuming and laborious approach did not seem acceptable.

For general applicability, microfluidic interconnections must withstand pressures of 2 bar [12]. The pressure, ΔP, which must be provided to generate a given flow rate, Q, within a microfluidic channel is related to the hydraulic resistance, R_{hyd}, according to:

$$\Delta P = R_{hyd}\, Q \tag{3}$$

Sealing elements must withstand this pressure in order to provide leak free operation at the same given flow rate. For microfluidic cell culture chips manufactured by micromilling (selected fabrication method, Chapter 1), channels of 100 µm in height and 100 µm in width are representative of practical minimum channel dimensions. The hydraulic resistance for such a square channel is calculated according to:

$$R_{hyd} = \left(\frac{12\eta L}{1-(0.917)(0.63)} \right) \left(\frac{1}{h^4} \right) \tag{4}$$

where η is the viscosity of the solution, h the height/width of the channel and L the length of the channel [21]. For a square channel with h = 100 µm, filled with water (η = 1mPa·s), with a length of 50 mm (an overestimate for many microfluidic devices) and a flow rate of 100 µL/min (an overestimate for many cell culture applications), the calculated pressure drop (Equation. 3) is approximately 0.25 bar. As such any method developed which meets the 2 bar threshold would be applicable for use in microfluidic cell culture applications developed in this project.

During the project three interconnection solutions were developed and descriptions of these follow. The first two, both reversible, solutions presented are related. The first of these introduced interconnection blocks (IBs), and the second modified the approach to increase functionality. The third method, a permanent solution, is free of epoxies and is of advantage as it avoids potential issues related to sensitivity and biocompatibility [29], but also because it uses readily available tubing. All methods provided seal capabilities well above the 2 bar threshold and as such are applicable to other applications, e.g. which use smaller channels and/or higher flow rates.

Table 2: Reversible Interconnection Method Summary

General Method	Description	Integrated	Planar	Number of Interconnections	Maximum Pressure (Bar)	Ref.
O-ring	O-rings heat annealed within PMMA microfluidic chip	Y	N	4	7.5	[15]
	O-ring compressed on top of microfluidic device/press-fit with tubing	N	Y[a]	3	15	[12]
	O-ring mounted in magnetic couplers	N	N	6	2.8	[22]
	O-ring pressed against chip by spring elements aligned in housings	N	N	6	20	[23]
Extended Soft Tubing	Silicone tube compressed to side of microfluidic device	N	Y	1	12.3	[18]
	Silicone tube compressed to top face of microfluidic device	N	N	20	2	[5]
	Silicone tube compressed to top face of microfluidic device	N	N	10	2	[6]
Gasket	PDMS on smooth surface – no compression	Y	N/A	N/A	0.3	[24]
	PDMS microfluidic chip compressed between acrylic plates	Y	N	2	5.6	[7]
	PDMS chip sealed against polymeric chip machined to contain vacuum lines	N	N	51	1	[19]
Press-fit	Cored PDMS bonded to 2nd PDMS layer via liquid PDMS	Y	N	2	4.9	[25]
	Cored PDMS O_2 bonded to PDMS and compressed	Y	N	1	7.0	[25]
	Cored PDMS O_2 bonded to PDMS	Y	N	1	5.1	[14]
	Cast PDMS compressed over matching surface relief silicon	N	N	3	2.2[b]	[16]
	Cast PDMS minimal dead volume interconnection	Y	Y	1	10.3	[26]
	Cast PDMS	Y	Y	1	2.7	[27]

[a]Tubings were bent to become effectively planar

[b]Maximum average value

B. INTERCONNECTION BLOCKS (IBS)

Contents presented are summarized from **Publication 1**:

Sabourin, D., Snakenborg, D. and Dufva, M. "*Interconnection blocks: a method for providing reusable, rapid, multiple, aligned and planar microfluidic interconnections*" Journal of Micromechanics and Microengineering. Volume 19, 035021 (9 pp), 2009. doi:10.1088/0960-1317/19/3/035021.

Interconnection blocks (IBs) are made from PDMS and allow rapid testing of microfluidic chips and unobstructed microfluidic observation. They represent a simple method and practical approach for creating re-usable, multiple, aligned, and planar interconnections. IBs are made from two materials/parts: a PMMA shell and a middle PDMS section. The PDMS portion of an IB is depicted schematically in Figure 7.

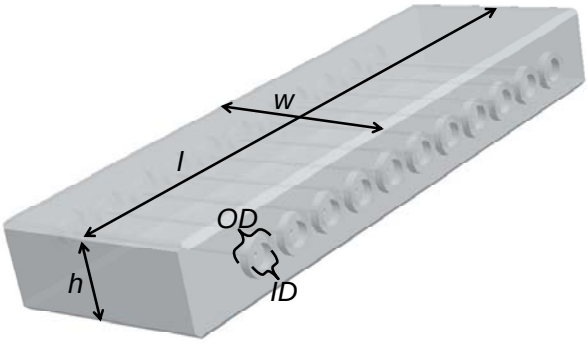

Figure 7. Schematic representation of PDMS portion of IB. The PDMS portion of the IB has a length (*l*) of 30 mm, a height (*h*) of 4 mm and a width (*w*) of 10 mm. O-ring-like structures are present on both sides of the IB. O-rings have inner diameters (*ID*) of 1.0 mm, outer diameters (*OD*) of 1.8 mm and protrude from the main PDMS body by 0.4 mm. The overall width of the IB is 10.8 mm. Integrated 240µm diameter channels are centered within the O-ring structures and are spaced 2.25 mm centre-to-centre. This channel spacing is identical to the standard published by SBS/ANSI for 1536 well microtiter plates.

IBs are monolithically cast by injecting PDMS into PMMA moulds made by micromilling (Figure 8). 240 µm diameter optical fibres were used during casting to create integrated channels. Moulds and finished IBs are shown in Figure 9.

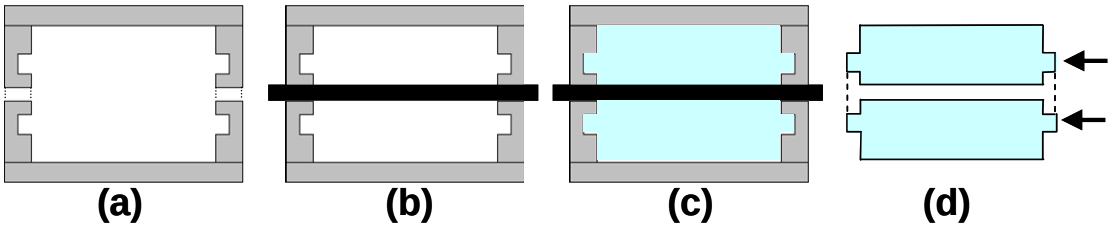

Figure 8. Schematic representation of IB fabrication. Drawings not to scale. (a) Cross-sectional view of mould used for casting IBs. Mould shapes defining O-rings are seen on left- and right-hand side of mould. Openings at end represent through holes through which fibre inserts are placed. (b) Fibre inserts resulting in integrated channels are placed through terminal mould pieces and are centred within structures forming O-rings. (c) PDMS is cast into mould and subsequently cured. Following PDMS curing, fibre inserts are removed and mould is disassembled. (d) Cross-section of completed IB. Arrows indicate O-ring sealing surface.

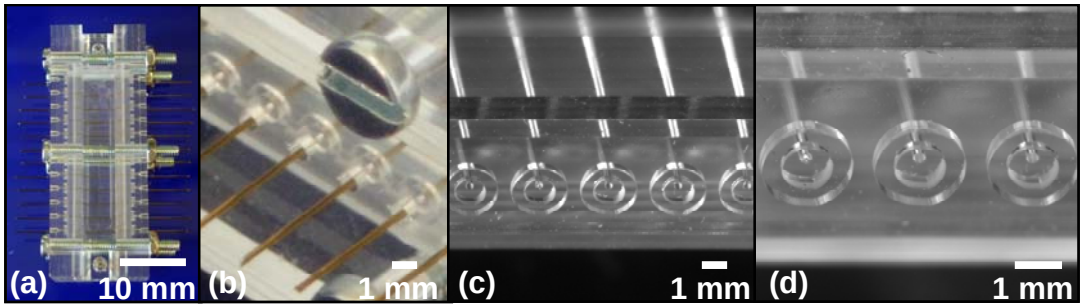

Figure 9. IB fabrication. (a) Mould used for casting IBs. Fibre inserts resulting in integrated channels pass through terminal mould pieces. (b) Close-up of terminal mould pieces which result in formation of O-ring like structures bookending integrated channels. (c) Section of cast IB. PMMA shell is visible on top of PDMS portion. Channels and O-rings are spaced 2.25 mm centre-to-centre. (d) Close-up of O-rings on completed IB.

When compressed between complementary microfluidic components (Figure 10), the IB's integrated O-rings are sealed and aligned to the fluidic channels in these structures. As shown in Figure 10, IBs can be used to allow different fluidic configurations through microfluidic devices. The PMMA portion of the IB facilitates placement and alignment of the IB to complementary microfluidic structures. The chip assembly shown in Figure 10 took only a few minutes to assemble and as such, IBs allowed rapid testing of microfluidic chips.

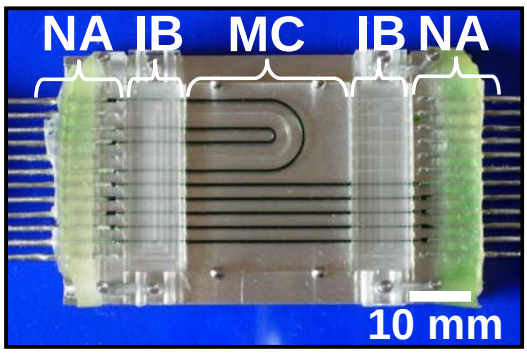

Figure 10. IB use. A PMMA microfluidic chip (MC) is placed between two IBs. Two needle assemblies (NA) constructed from PMMA and blunted needle tips for testing and demonstration purposes are shown at outer left and outer right. In the lower half of the chip fluid flows into the chip through one IB and out through a second IB. In the top half of the chip, fluid enters and leaves through the IB on the left hand side of the image.

The average pressure limit for the IB was near 5.5 bar, well above the 2 bar threshold considered applicable for most microfluidic applications [12]. The test data also indicated that IBs are re-usable and little degradation in overall performance occurred with repeated use. The 24 connections provided by a single IB are greater in number and packing density than most methods reported in Table 2. Additionally, the IB method presented many handling, processing and use advantages over either integrated, press-fit, or methods relying on O-rings and extended tubing.

C. BALL JOINT INTERCONNECTION BLOCKS (BJIBS)

Contents are summarized from **Publication 2**:

Sabourin, D., Snakenborg, D., and Dufva, M. "*Interconnection blocks with minimal dead volumes permitting planar interconnection to thin microfluidic devices*" Microfluidics and Nanofluidics. Volume 9, p. 87-93, 2010. doi:10.1007/s10404-009-0520-8.

The initial IB designs satisfied many of the "ideal" criteria of reversible interconnections, including being reliable and re-useable, [4, 12] but certain applications require interconnections that eliminate dead volumes [16] and/or interface with flat, thin side-walled microfluidic devices such as chips made of glass or silicon. The IB version described in Section B could not interface to flat or thin side-walled devices and had estimated dead volumes between 165 and 185 nL. By implementing changes to sealing feature geometries within the moulds used for casting of IBs and by creating curved channels through the IBs, two new IB designs were generated. The first, the Ball Joint Interconnection Block (BJIB) forms planar interconnections with zero dead volumes and the second, the BJIB-90, allows zero dead volume interconnections to flat or thin side walled microfluidic devices. The BJIB and BJIB-90 are described below.

The materials and methods used to fabricate BJIB and BJIB-90 were as described in section B with the exception that the BJIB and BJIB-90 incorporated a ball joint, instead of an O-ring sealing feature. The ball joint feature was made by machining mould pieces with a ball-end mill. A completed BJIB is shown in Figure 11. BJIBs interface to microfluidic chips in the same manner as IBs (Section B).

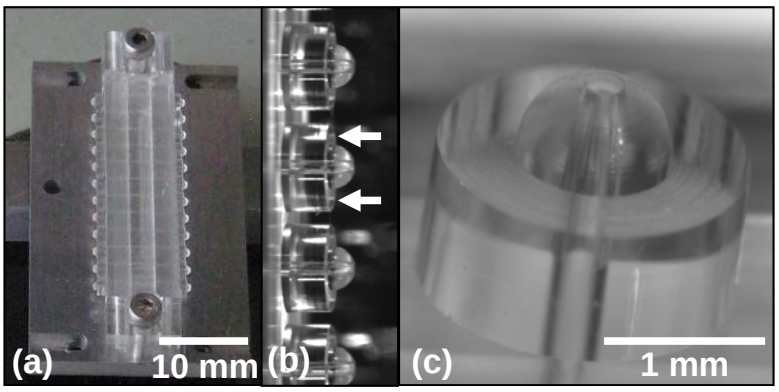

Figure 11. BJIB design and fabrication. (a) Completed BJIB (PDMS portion housed in PMMA shell) mounted on aluminium base plate used for testing. Ball joint features protrude from both sides. (b) Close-up of ball joint features. The sealing surfaces are indicated with arrows. (c) Close-up of single ball joint interconnection feature. The integrated channel can be seen in the middle of the ball joint feature.

The BJIB-90's integrated channels bend through 90° and terminate in a ball joint feature located on the bottom face (Figure 12). The 90° turns were made by bending fibres through the mould (Figure 12) prior to casting.

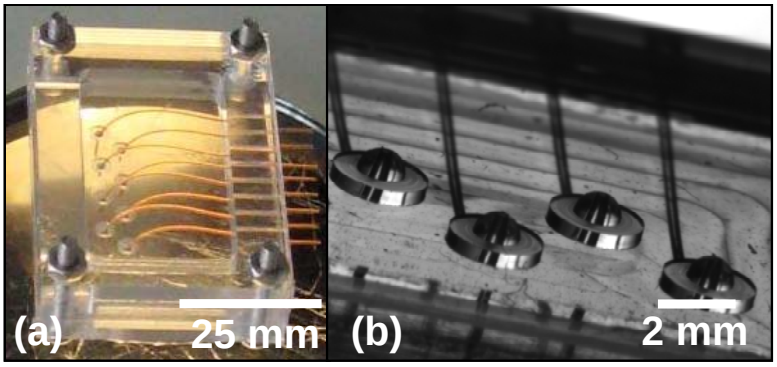

Figure 12. **BJIB-90 design and fabrication.** (a) Mould used BJIB-90 fabrication. Fibre inserts are bent through 90° within the mould (b) Close-up of array of ball joint interconnection features on the interfacing BJIB-90 surface. Integrated channels bend and exit through the top of the semi-spherical feature (not shown)

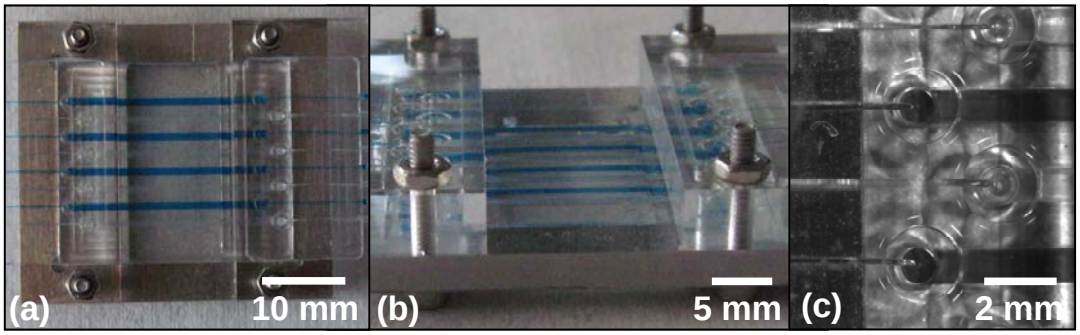

Figure 13. **BJIB-90 Interconnection.** (a) Top view of two BJIB-90s interfacing with a thin, 1.5 mm thick PMMA chip. Alternating channels filled with dye solution. (b) Side view of demonstration chip. (c) Close-up of BJIB-90 interconnection

All individual test pressures for the BJIB and BJIB-90 were above the 2 bar threshold. The new IB designs offered advantages compared to the O-ring based design detailed in Section B. The previous IB version had dead volumes estimated between 165 and 185 nL. As seen in Figure 14, effective dead volumes near zero can be realized with the BJIB versions. According to the analysis of *Puntambekar et al.* [9] dead volumes are expected to be near zero for the BJIB-90 when channel entries are properly designed and manufactured in the interfacing chip.

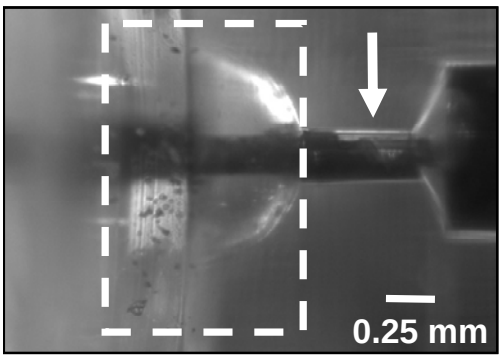

Figure 14. Close-up of BJIB and microfluidic chip interface in pressure test assembly. Dye solution is used to facilitate visualization. The BJIB interconnection feature is shown in the dashed white box. The arrow points to the inlet of the PMMA chip. Effective zero dead volumes result.

Both BJIB versions demonstrated self-aligning tendencies which simplified BJIB-chip junctions. The BJIB-90 increases the number of microfluidic device materials and designs with which the interconnection block approach can be used since the BJIB-90 interfaces with top or bottom, instead of side, surfaces of chips. For instance, thin-side walled devices made from polymers, glass or silicon can be addressed by the BJIB-90 whereas they cannot be by the BJIB or the IB. Though addressing the device from the top or bottom, the interconnections are effectively planar and still permit unobstructed microscopic observation (Figure 13).

D. COMPRESSED TUBING INTERCONNECTIONS

Contents are summarized from **Publication 3**:

Sabourin, D., Dufva, M., Jensen, T., Kutter, J., and Snakenborg, D. "*One-step fabrication of microfluidic chips with in-plane, adhesive-free interconnections*" Journal of Micromechanics and Microengineering. Volume 20, 037001 (7pp), 2010. doi: 10.1088/0960-1317/20/3/037001.

Though the IB approaches resulted in multiple, in-plane interconnections to polymeric devices, their implementation may be more involved than is desired. Like other interconnection solutions [5, 6, 12, 15, 19, 23, 28], the creation of additional components and assemblies apart from the microfluidic chip they address including holders, moulds and clamps, may prove too onerous in certain situations or for certain applications. In some cases, a rapid method for creating permanent interconnections is desired. For reasons previously described, methods which use adhesives, such as epoxy, to create permanent and integrated interconnections are not favoured. The third method developed created an adhesive free press-fit interconnection between readily available tubing and a PMMA microfluidic device during a UV-assisted bonding process. This is referred to as the compressed tubing interconnection. The compressed tubing fabrication process is shown in Figure 15 and resulting interconnections are shown in Figure 16.

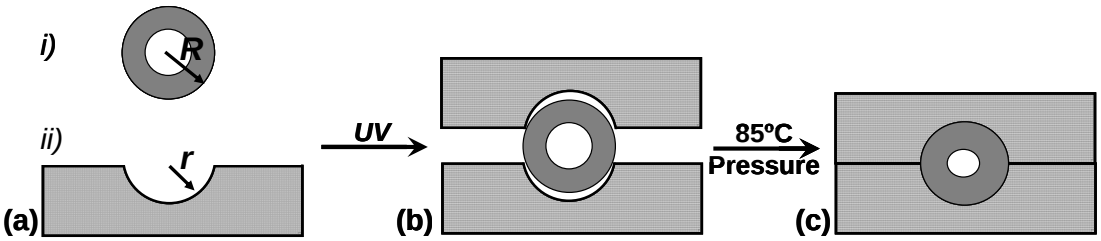

Figure 15. Schematic representation of the compressed tubing method. (a) (*i*) Cross-section of deformable tubing with outer radius *R* and (*ii*) cross-section of one of two PMMA layers milled with ball-end mill to yield nearly semi-circular half-ports with radius *r*. Note that *R* > *r*. (b) PMMA surfaces were UV exposed and aligned above and below the tubing. Parts were then placed in a bonding press under pressure and at 85°C for one hour. (c) Cross-section of completed interconnection. Due to compression, the ID of the tubing has decreased.

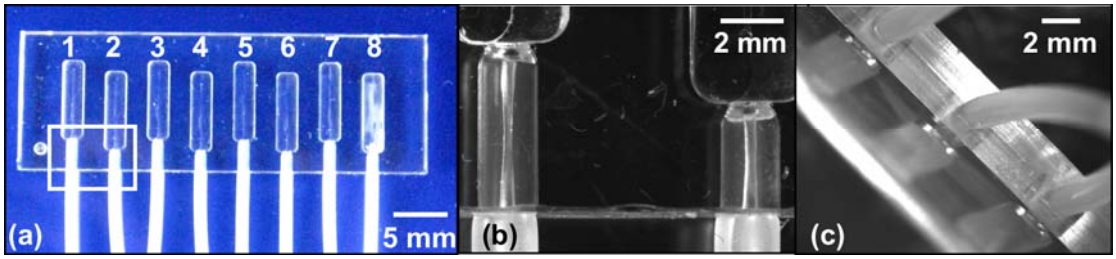

Figure 16. Compressed tubing interconnections. (a) PMMA chip used for pressure testing. Eight individual interconnections, assigned positions 1 through 8, were found on each chip. 2.1 mm OD tubing was inserted 5 mm into the PMMA device in positions 1, 3, 5 and 7, and 3 mm into the device in positions 2, 4, 6 and 8. Seal strengths for the different tubing length insertions were compared. A close-up of the area within the white box is shown in (b). (b) Top view of interconnection with 5 mm (left) and 3 mm (right) tubing inserts. (c) Side view of PMMA chip showing in-plane interconnections.

The compressed tubing method is an example of a permanent, integrated interconnection solution which eliminates additional processing steps while rapid, immediate testing is enabled resulting in in-plane interconnections suited to microscopic observation. The test condition which used 2.1 mm OD commercially available silicone tubing fit into a 1.9 mm diameter port feature (Figure 16) resulted in adhesive-free interconnections which tested to pressures near 6 bar. Finished PMMA chips and integrated in-plane interconnections simultaneously result from the bonding process (Figure 15 and 16). As UV radiation only reduces the T_g of polymer's surface layer to a depth of several microns, without changing the T_g of the bulk polymer [29, 30], structures can be bonded above the T_g of the surface layer but below that of the bulk PMMA layer. Loss in structure quality can thus be avoided.

The compressed tubing method is flexible with respect to chip size and interconnection location. Though solutions using holders and clamps facilitate rapid chip testing, the compressed tubing method negates this advantage as interconnections are formed with the chip and tubing, which could readily be connected to pumps, etc. For polymeric materials for which UV-assisted bonding is not possible, thermal or chemical bonding processes [30] could be used to implement the general approach. A method which does not incorporate adhesive use to form interconnections is of great advantage as it avoids potential issues related to sensitivity and biocompatibility [11].

REFERENCES

1. Andersson, H. and A. van den Berg, *Where are the biologists? A series of mini-reviews covering new trends in fundamental and applied research, and potential applications of miniaturised technologies.* Lab on a Chip, 2006. **6**(4): p. 467-470.
2. Blow, N., *Microfluidics: in search of a killer application.* Nature Methods, 2007. **4**(8): p. 665-668.
3. Pepper, M., et al. *Interconnecting fluidic packages and interfaces for micromachined sensors*. 2007.

4. Fredrickson, C.K. and Z.H. Fan, *Macro-to-micro interfaces for microfluidic devices.* Lab on a Chip, 2004. **4**(6): p. 526-533.
5. Yang, Z. and R. Maeda, *A world-to-chip socket for microfluidic prototype development.* Electrophoresis, 2002. **23**(20): p. 3474-3478.
6. Yang, Z. and R. Maeda. *Socket with built-in valves for the interconnection of microfluidic chips to macro constituents*. 2003.
7. Korivii, N.S.a.J., L, *A generic chip-to-world fluidic interconnect system for microfluidic devices.* IEEE 39th Southeastern Symposium on System Theory (Macon, GA March 04-06), 2007: p. 176-180.
8. Pattekar, A.V. and M.V. Kothare, *Novel microfluidic interconnectors for high temperature and pressure applications.* Journal of Micromechanics and Microengineering, 2003. **13**(2): p. 337-345.
9. Puntambekar, A. and C.H. Ahn, *Self-aligning microfluidic interconnects for glass- and plastic-based microfluidic systems.* Journal of Micromechanics and Microengineering, 2002. **12**(1): p. 35-40.
10. Tsai, J.H. and L.W. Lin, *Micro-to-macro fluidic interconnectors with an integrated polymer sealant.* Journal of Micromechanics and Microengineering, 2001. **11**(5): p. 577-581.
11. Stangegaard, M., et al., *A biocompatible micro cell culture chamber (microCCC) for the culturing and on-line monitoring of eukaryote cells.* Lab Chip, 2006. **6**(8): p. 1045-51.
12. Bhagat, A.A.S., et al., *Re-usable quick-release interconnect for characterization of microfluidic systems.* Journal of Micromechanics and Microengineering, 2007. **17**(1): p. 42-49.
13. Dalton, C. and K. Kaler, *A cost effective, re-configurable electrokinetic microfluidic chip platform.* Sensors and Actuators B-Chemical, 2007. **123**(1): p. 628-635.
14. Li, S.F. and S.C. Chen, *Polydimethylsioxane fluidic interconnects for microfluidic systems.* Ieee Transactions on Advanced Packaging, 2003. **26**(3): p. 242-247.
15. Perozziello, G., F. Bundgaard, and O. Geschke, *Fluidic interconnections for microfluidic systems: A new integrated fluidic interconnection allowing plug 'n' play functionality.* Sensors and Actuators B-Chemical, 2008. **130**(2): p. 947-953.
16. Saarela, V., et al., *Re-usable multi-inlet PDMS fluidic connector.* Sensors and Actuators B-Chemical, 2006. **114**(1): p. 552-557.
17. T., Y., et al., *Micromachined rubber O-rings microfluidic interconnectors.* IEEE 39th Southeastern Symposium on System Theory (Macon, GA March 04-06), 2000: p. 4.
18. Snakenborg, D., et al., *A fast and reliable way to establish fluidic connections to planar microchips.* Journal of Micromechanics and Microengineering, 2007. **17**(1): p. 98-103.
19. Cooksey, G.A., A.L. Plant, and J. Atencia, *A vacuum manifold for rapid world-to-chip connectivity of complex PDMS microdevices.* Lab on a Chip, 2009. **9**(9): p. 1298-1300.
20. Stangegaard, M., *A biocompaticle micro cell culture chamber (uCCC) for continuous on line perfusion.* Ph.D. Thesis, 2006.

21. Bruus, H., *Theoretical Microfluidics.* Oxford University Press, 2008.
22. Atencia, J., et al., *Magnetic connectors for microfluidic applications.* Lab on a Chip, 2010. **10**(2): p. 246-249.
23. Kortmann, H., L.M. Blank, and A. Schmid, *A rapid, reliable, and automatable lab-on-a-chip interfaced.* Lab on a Chip, 2009. **9**(10): p. 1455-1460.
24. McDonald, J.C. and G.M. Whitesides, *Poly(dimethylsiloxane) as a material for fabricating microfluidic devices.* Accounts of Chemical Research, 2002. **35**(7): p. 491-499.
25. Christensen, A.M., D.A. Chang-Yen, and B.K. Gale, *Characterization of interconnects used in PDMS microfluidic systems.* Journal of Micromechanics and Microengineering, 2005. **15**(5): p. 928-934.
26. Chiou, C.H. and G.B. Lee, *Minimal dead-volume connectors for microfluidics using PDMS casting techniques.* Journal of Micromechanics and Microengineering, 2004. **14**(11): p. 1484-1490.
27. Quaglio, M., et al., *Evaluation of different PDMS interconnection solutions for silicon, Pyrex and COC microfluidic chips.* Journal of Micromechanics and Microengineering, 2008. **18**(5).
28. Sabourin, D., D. Snakenborg, and M. Dufva, *Interconnection blocks: a method for providing reusable, rapid, multiple, aligned and planar microfluidic interconnections.* Journal of Micromechanics and Microengineering, 2009. **19**(3).
29. Truckenmuller, R., et al., *Bonding of polymer microstructures by UV irradiation and subsequent welding at low temperatures.* Microsystem Technologies-Micro-and Nanosystems-Information Storage and Processing Systems, 2004. **10**(5): p. 372-374.
30. Tsao, C.W. and D.L. DeVoe, *Bonding of thermoplastic polymer microfluidics.* Microfluidics and Nanofluidics, 2009. **6**(1): p. 1-16.

CHAPTER 3: PUMPING

Proposal and implementation of a pumping solution was the second objective of the project. A pumping solution was proposed and a solution was described in the following co-first authored publication:

Publication 4
Skafte-Pedersen, P*., **Sabourin, D.*,** Dufva, M., and Snakenborg, D. "*Multi-channel peristaltic pump for microfluidic applications featuring monolithic PDMS inlay*" Lab on a Chip. Volume 9 (20), p. 3003-3006, 2009.

The above publication's contents are condensed and presented below. The complete publication is found in Appendix A.

A. INTRODUCTION

As with interconnections, pumping can present a challenge and barrier to widespread adoption of microfluidic solutions [1]. Pump capacity, the number of channels available, and portability of pumps often hinder microfluidic experimental setups. Size of typical pumps, such as syringe pumps, does not permit their placement on instruments or stages used for observation, e.g. microscopes, of microfluidic systems and reactions. As a result, extended tubing is often required and complications related to this include its cumbersome nature (entanglements, tension placed on microfluidic device) and increased system dead volumes and compliance. Additionally, pump cost can place stress on research budgets. This project (and presumably others) would benefit from a simple pump with small footprint, that provided multi-channel capacity and which was able to fit on a microscope stage.

Peristaltic pumps employ a simple operating concept. Mechanical displacement of a diaphragm moves fluid by exerting a force on a solid-fluid or fluid-fluid boundary. Sequential opening and closing of a series of diaphragms result in fluid movement, usually in a pulsatile manner [2]. Peristaltic pumps (Figure 17) have been and continue to be employed for biological, amongst other, applications and studies. Advantages of peristaltic pumps include the ability to self-prime, to move theoretically infinite fluid volumes, to pump fluids bi-directionally by reversing diaphragm actuation order, and and easy maintenance [3, 4].

*Co-first authors

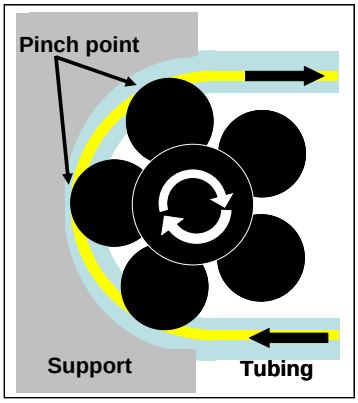

Figure 17. Roller type peristaltic pump. Tubing is placed between a roller and a rigid support. The roller is dimensioned and positioned so as to compress tubing against the rigid support. Occluded fluid volumes between different pinched points of tubing are created by the roller. As the roller rotates, shown as clockwise, the occluded fluid volumes are pumped through the tubing from the inlet (bottom) to the outlet (top).

For pump based applications, the elasticity of PDMS renders it suitable as a diaphragm material. PDMS-based peristaltic pumps which are actuated either pneumatically or mechanically have been described. Pneumatic PDMS micropumps have been made via soft lithographic methods [5]. Multiple patterned elastomeric layers are bonded together to form networks of fluid flow and control channels. Sequential activation of multiple control channels, by external valves, along a fluid flow channel results in peristaltic pumping. Though promising for highly multiplexed microfluidic applications due to scaling capabilities, construction and design is complicated by need of additional control channels and the cleanroom-based methods normally used [6]. Simple, mechanical-based approaches are well suited to established test platforms and assays which can benefit from fluidic activation [7].

Single channel PDMS-based micropumps have been reported by *Lim et al.* [8], *Yobas et al.* [6, 9] and *Du et al.* [10]. In each of these, a ball bearing was acutated either linearly [8] or magnetically [6, 9, 10] to pass on top of a PDMS channel in order to compress it. Fluid was pushed in the direction of ball bearing travel. *Koch et al.* [4] coupled a roller-type actuator to a motor and a microfluidic chip containing a circular PDMS-microchannel. This last approach most resembled a miniaturized version of a macroscale peristaltic pump. Mechanical methods which simultaneously and peristaltically pump multiple channels have also been described. Tactile pins of Braille displays have been programmed to move in a peristaltic actuation pattern. When the tactile pins are aligned underneath a PDMS channel and actuated, they push into the PDMS channels directly above them and cause fluid movement [11-13]. *Rhie et al.* [14] reported the coupling of a motor driven Archimedes screw insert to a sheathing elastomeric layer containing integrated channels. Fluids were pushed in the direction of screw rotation.

The PDMS casting methods used to create IBs (Figure 8, Chapter 2) yielded microfluidic components with integrated channels and terminal O-rings (Figure 9, Chapter 2). Viewed differently, this casting process created aligned banks of tubing with protruding flat ends (Figure 9) for which the “tubing” was cloaked in a central PDMS block. Using the same casting method and altered mould designs, a PDMS

piece was cast which contained 12 integrated channels and raised half-tubing features (Figure 19). When this PDMS piece was coupled to a miniaturized peristaltic roller, a 12 channel miniaturized peristaltic pump (mini-pump) resulted. Built from simple, low-cost materials and the aforementioned PDMS piece, the pump provided greater channel numbers than previous reports of mechanically actuated micropumps [4, 6, 8]. Measurement data for the mini-pump was collected and compiled by Ph.D. candidate Peder Skafte-Pedersen, co-author of the publication found in Appendix A.

B. MINI-PUMP

B.1 Mini-pump Design and Fabrication

The peristaltic mini-pump has three core components: a monolithically cast PDMS Pumping Inlay (PI), a PMMA Rotor Bed (RB), and a metal Multi-Roller (MR). A stepper motor was used to drive the pump. A schematic of pump assembly and an assembled mini-pump are shown in Figure 18.

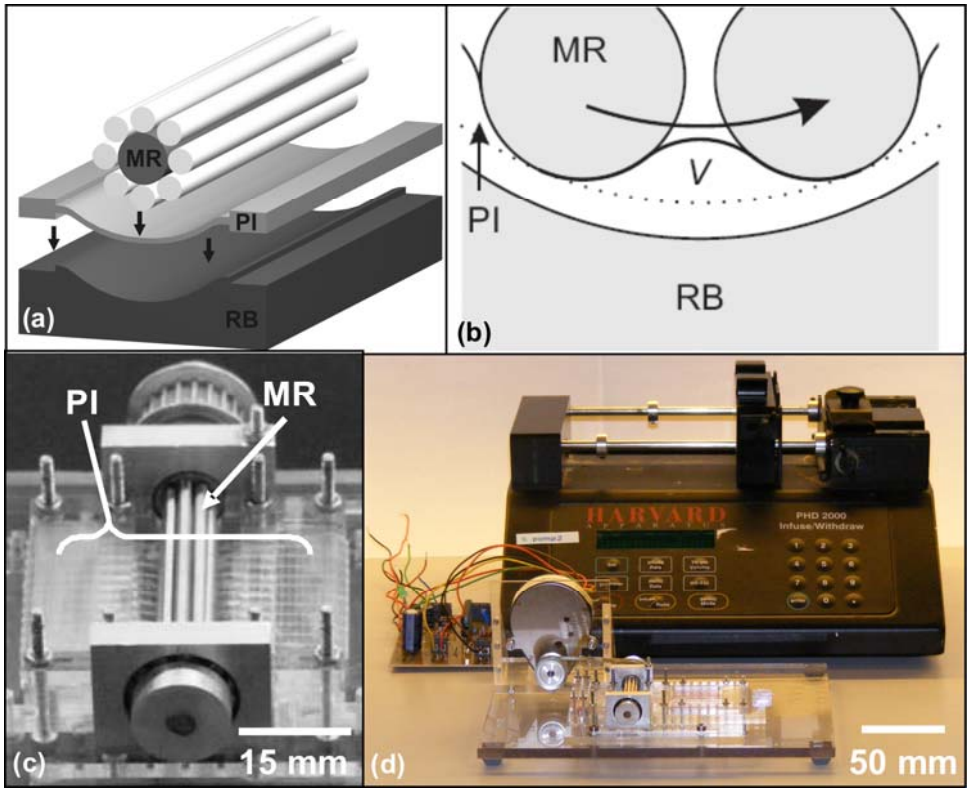

Figure 18. 12-channel micropump with monolithically cast PDMS pumping bed. (a) 3-D schematic of mini-pump assembly. The PDMS pumping inlay (PI), containing integrated channels is fit between a supporting PMMA rotor bed (RB) and a multi-roller (MR). When assembled, the PI is compressed between the multi-roller (MR) and RB. Photo courtesy of D. Snakenborg, ChemLabChip, DTU Nanotech. (b) Schematic representation of mini-pump operation. As the MR rotates over the PI, the channels within the PI(dashed line) are compressed by the pins of the MR. A fluid volume, *V*, is occluded between MR pins. As the MR rotates, *V* is pushed in the direction of rotation. (c) Assembled 12-channel micropump. The MR is mounted in ball bearings holders and the PI secured by PMMA brackets. The RB is not visible. Motor and controller not shown (d) Complete mini-pump showing stepper motor and controller attachments. The mini-pump is attached to a base plate for support. A typical 2-channel syringe pump is placed in the background for comparative purposes. Photos (b)-(d) courtesy of P. Skafte-Pedersen, *FAST*, DTU Nanotech.

The PI (Figure 19) contains twelve 240 µm integrated channels spaced 2.25 mm centre-to-centre (1536 well plate standards). The PI is monolithically cast from PDMS in a manner identical to the IB fabrication (Section B, Chapter 2). The PI contains terminal block and crossbeam features (Figure 19) which facilitate placement in the RB. The RB provides the PI with rigid support complementary to the curvature of the MR (Figure 18). The MR is made from eight 2 mm diameter brass rods placed equidistantly around a 4 mm brass drive shaft (Figure 18). When the MR rotates over and contacts the PI, the PI's integrated channels are compressed and fluid is pushed in the direction of rotation (Figure 18). The mini-pump, excluding motor, measures approximately 75 mm (*l*) by 25 mm (*w*) by 20 mm (*h*).

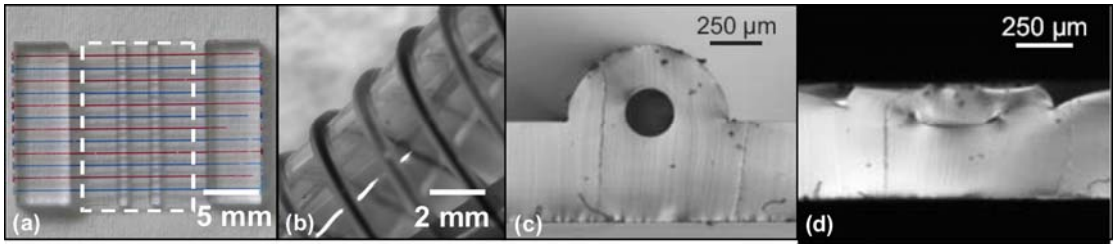

Figure 19. **Monolithically cast PDMS PI.** (a) The PI contains 12 integrated 240 µm channels. Channels filled with dye to facilitate visualization. The terminal blocks at either end of the PI and the crossbeam features found in the middle of the part facilitate alignment within the pump. A close-up of geometrical features found in the dashed box is shown (b). (b) The central portion of the PI contains raised half-tubing like features. Channels filled with dye to facilitate visualization. These elements are compressed, as shown in (d) during pump operation. (c) Cross section of an uncompressed PI channel (d) Cross section of the same channel when compressed as during pump operation. Photos (c) and (d) courtesy of P. Skafte-Pedersen, *FAST*, DTU Nanotech.

B.2 Mini-pump Operating Characteristics

As the pump operates peristaltically, a pulsatile flow pattern resulted (data not shown). Fixed volume displacement was expected and was obtained. A linear relationship between rotational speed, v_r, and average flow rate, *Q,* was observed over an order of magnitude increase in MR rotational speed (Figure 20). The mini-pump also demonstrated indifference to solution viscosity (data not shown).

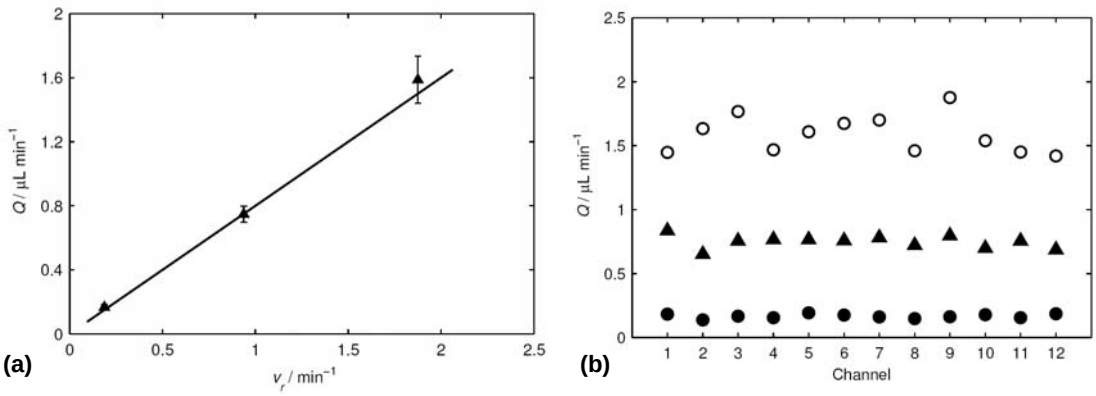

Figure 20. Mini-pump performance. (a) Theoretical (solid line) and average measured (triangles) individual channel flow rates, *Q,* at varying rotational speeds, v_r. Theoretical values are based on an estimate of the void volume between two roller pins. Measured flow rates are the average values from twelve individual channels. Error bars represent the standard deviation of the average flow rate of the 12 individual channels. (b) Individual channel flow rate data. Flow sensor data at v_r values of 0.19, 0.94 and 1.88 min^{-1} corresponding to average flow rates of 0.17, 0.75, and 1.59 µL min^{-1}.

The mini-pump demonstrated comparable performance to commercially available syringe pumps. At *Q* values of 0.17, 0.75, 1.59 µL min^{-1} (Figure 20) the channel-to-channel coefficient of variances (%CV) were 10, 7, and 9% respectively. As a comparison, channel-to-channel flow rate variability for a typical multi-channel microfluidic set-up at flow rates of Q = 0.24, 0.56, and 2.06 µL min^{-1}, % CVs were evaluated at 12, 6.9, and 0.6% respectively.

Although flow characteristics are not superior to commercially available syringe pumps, the mini-pump design provides many advantages. As the pump approaches dimensions of microfluidic devices, interfacing liquids to and from the pump can be completed without requiring excessive tubing and *via* simple methods such as press-fitting oversized needles into the PDMS channel inlet/outlets. This reduces pump dead volumes, estimated at only 2.1 µL, and likely compliance as compared to typical pump setups. As the mini-pump is smaller than typical syringe pumps (Figure 18) it can fit on microscope stages and the planar orientation of channel inlet and outlets helps provide unobstructed microscopic observation. The pulsatile flow resulting from the miniaturized peristaltic pump may not be suitable for all applications. However, peristaltic pumping is used in other microfluidic systems including those based on Braille displays and pneumatic deflection of elastomeric membranes [5, 11-13, 15, 16]. Cell culture and biochemical reactions have been demonstrated in these systems.

When outlet channels were blocked, the maximum pressure capability of the pump was 3.7 bar, well above the 2 bar threshold described as sufficient for most microfluidic applications [17]. Pump durability was assessed by running the pump continuously over a period of time. After 1875 MR revolutions a displacement of approximately 1.5 mL per channel, the test was voluntarily stopped. Inspection of channels no longer pumping at this point revealed wear did not occur at the raised half-tubing features (Figure 19) which contact the MR, but elsewhere on the component. The use of PDMS was thus not seen as limiting, however durability improvements were required. Improvements to other aspects of the pump were also required.

Pump assembly required the MR to be placed on top of the PI and RB (Figure 18). Dis- and reassembly of the mini-pump required to exchange PI components was tedious. Additionally, visual inspection of the PI feature during operation was limited. Though able to fit on microscope stages, the stepper motor and controller were relatively large compared to other micropump components (Figure 18). To increase portability and usability, smaller motors and drivers should be located. Finally, control of the micropump was not user friendly and relied on cumbersome equipment [18]. Methods to more easily actuate fluidic networks using the mini-pump should be located and implemented.

C. MICROPUMP

The aforementioned observations and requirements for improvement resulted in a redesign and further miniaturization of the mini-pump. The resulting peristaltic pump is referred to as the "micropump". As the micropump's design and operating characteristics have not yet been published, a detailed description is provided.

C.1 Micropump Design and Fabrication

The micropump operates in the same manner and utilizes the same three core components: a multi-roller (MR), a rotor bed (RB) and in this case, a Type II microfluidic ribbon (µFR) (see Chapter 4) instead of a PI (Figure 25). To distinguish micro- from mini-pump components, the micropump versions of the RB and MR are annotated with "-2".

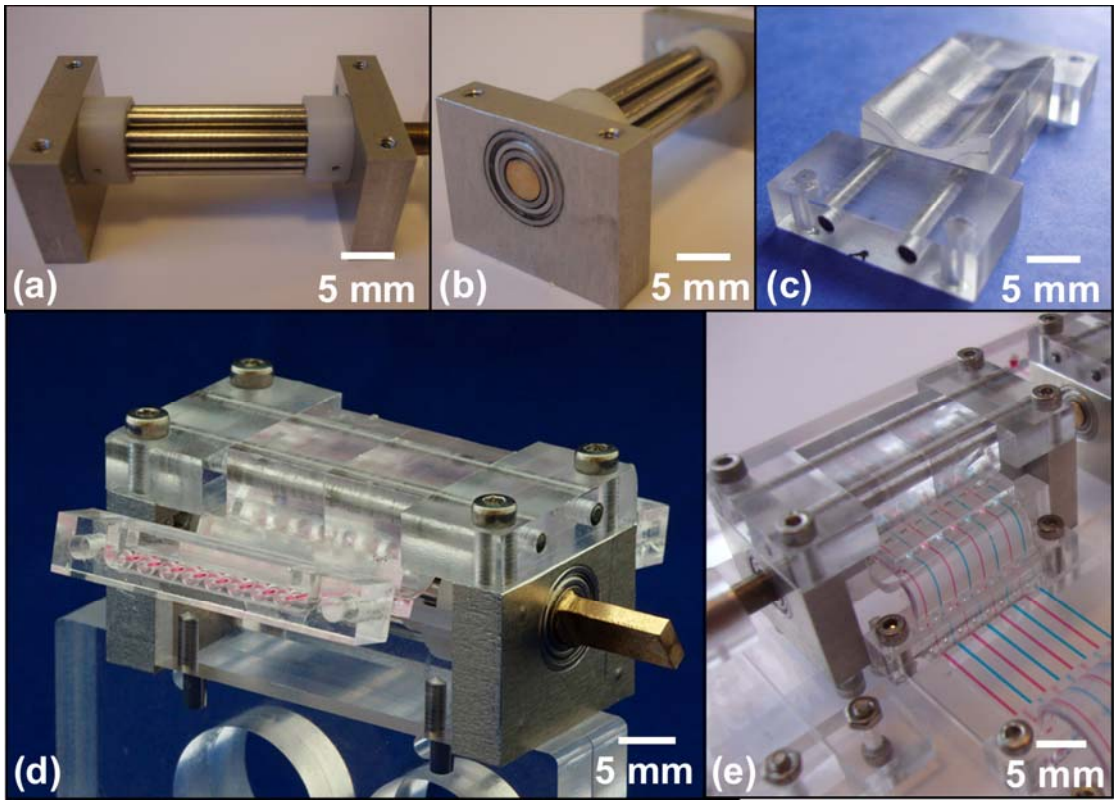

Figure 21: **8-channel peristaltic micropump.** (a) MR-2. Eight free-rolling 2 mm pins are housed in terminal nylon pieces. Nylon pieces are secured to a brass shaft that is aligned through two aluminium blocks. (b) Side view of MR-2. Ball bearings are housed in the aluminium blocks. (c) RB-2. The middle portion contains a curved shape complementary to the curvature of the MR-2 and which compresses the Type II uFR during operation to permit pumping. (d) Assembled micropump. The Type II uFR is seen protruding from between RB-2 and MR-2. Photo courtesy of V. Coman, Bioanalytics Group, DTU Nanotech. (e) Micropump addressing PMMA chip in *SWAN* system (see Chapter 4).

C.1.1 Type II µFRs

µFRs provide connectivity between components of microfluidic systems and are further described in Section C of Chapter 4. Type II µFRs (Figure 22 and 23) are analogous to the PI components described in Section B. They are cast from PDMS in micromilled moulds as previously described and contain eight integrated 240 µm wide circular channels spaced 2.25 mm centre-to-centre (1536 well-plate standards).

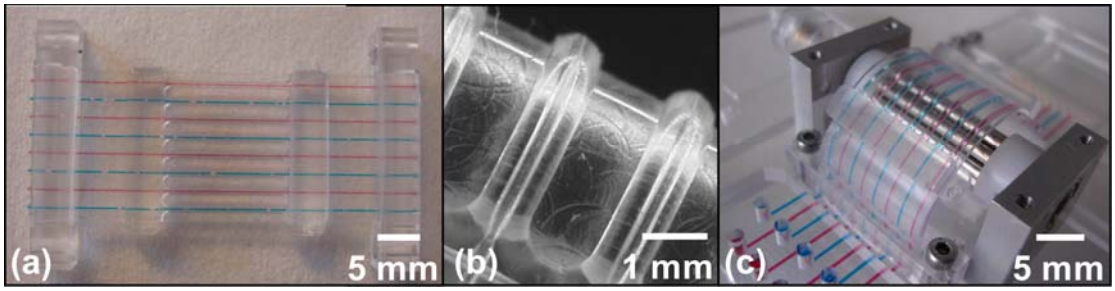

Figure 22. Type II µFRs. (a) Type II µFR. Channels filled with dye to facilitate visualization. Dashed box features shown in (b) (b) Raised tubing features of the Type II µFR. Webbed foot design visible at bottom of panel. (c) Type II µFR placed across a micropump. RB-2 not shown.

As with the PI (Section B), the Type II µFR contains tubing-like features raised above a supporting layer of PDMS (Figure 22). The tubing features are created using a 0.8 mm ball mill to pattern the mould. Tubing-features have a radius of 0.4 mm and height of 0.6 mm (Figure 23) and sit on a 0.7 mm thick PDMS supporting layer.

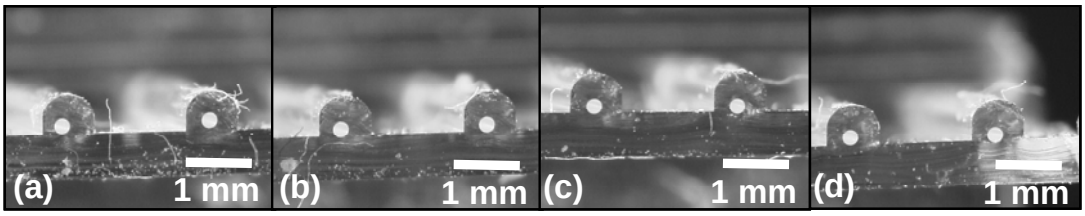

Figure 23. Type II µFR cross-section. Due to limitations with imaging equipment only 2 channels could be placed within the same frame. (a) Channels 1 and 2. (b) Channels 3 and 4. (c) Channels 5 and 6. (d) Channels 7 and 8.

To facilitate compression and reduce friction placed on motors, the position of the channels within the Type II µFRs were distanced approximately 125 µm further from the support layer (Figure 23) than in the PI (Figure 19). The PDMS blocks located outside of the tubing area of the Type II µFR prevent advancement of the Type II µFR through the pump during operation. To reinforce the portion of the Type II µFR where the tubing-like features meet the PDMS blocks, a webbed-foot design was used (Figure 22(b)). Overall length and width dimensions of the Type II µFRs are 48 and 30 mm respectively.

C.1.2 Multi-Roller-2 (MR-2)

The MR-2 is shown in Figure 21. Ball bearing housings located at both ends of the MR-2 are made from 5 mm thick aluminium and house 4 / 9 mm (ID/OD) ball bearings (VXB Bearing, Anaheim, California). 2 mm nuts are embedded within the MR-2 to permit attachment of the MR-2's to base plates and RB-2s (see below) with 2 mm screws. The rolling portion of the MR-2 is made from eight 2 mm x 24 mm stainless steel alignment pins spaced equidistantly around a 4 mm brass drive shaft (fabricated on a lathe). The reduction of pump channels was a result of difficulty in sourcing 2 mm alignment pins at lengths greater than 24 mm. The drive shaft is machined to interface to either a hand crank or LEGO® Mindstorms® servo motors (Figure 26). The alignment pins are inserted and held within 2.1 mm holes in nylon discs. The oversized holes allow the pins to freely rotate and prevent mechanical damage to the Type II µFR during pump operation. The nylon discs and alignment

pins are secured and aligned to the 4 mm diameter brass drive by 1 mm alignment pins. The drive shaft is then placed inside the aluminium ball bearings housings.

C.1.3 Rotor Bed-2 (RB-2)

A RB-2 is shown in Figure 21. The RB-2 is made from four 10 mm thick pieces of polycarbonate (PC) aligned by 2 mm alignment pins. The end pieces contain 2 mm alignment holes through which the RB-2 is aligned and fastened to the aluminium ball bearing housings of the MR-2 by 2 mm screws. The RB-2 provides rigid support complementary to the curvature of the rolling pins of the MR-2. When fastened to the MR-2, the RB-2 compresses the Type II µFR's tubing features and permits pumping.

C.1.4 Micropump Assembly

Contrary to the mini-pump described in section B, the Type II µFR is placed above the MR-2 (Figure 21). A RB-2 is then placed on top of the Type II µFR. The footprint of the micropump, excluding motors is 30 mm (*w*) x 40 mm (*l*) x 20 mm (*h*). This measurement includes the brackets of the Type II µFR which flank the MR-2 on either side. The brackets facilitate interconnections to microfluidic chips and/or components on either side of the pump are made (see *SWAN*, Section C, Chapter 4).

C.2 Micropump Control

The stepper motor and associated electronics used to drive the mini-pump were replaced by two separate actuation and control systems (Figure 24). The first is a hand-crank. The hand crank was made from milled PMMA. The second solution was the commercially available LEGO® Mindstorms® robotic system/kit. The LEGO® system provides multiple servo motors, an "Intelligent Brick" controller, software interface (LabView®) for programming of motors, and other required components such as connector cables.

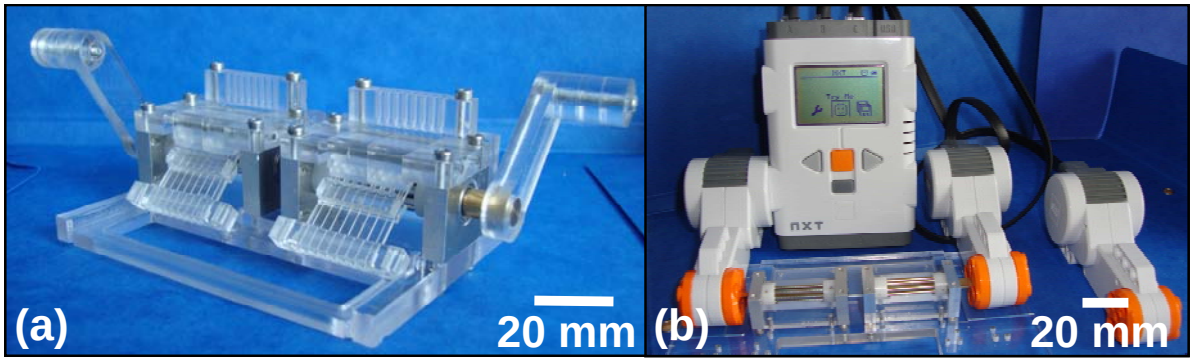

Figure 24. Micropump control. (a) A hand crank can be attached to the micropump to drive fluids through microfluidic chips and networks. (b) Components of the LEGO® Mindstorms® robotic system/kit attached to MR-2's of the micropump. Three motors can be connected to an "Intelligent Brick" controller. The controller houses a power source (battery). Programs written to control motors can be stored on the controller and accessed on demand.

C.3 Micropump Results and Characterization

Micropump assembly was simplified as compared to the mini-pump (Section B). Securing of the MR-2 and placement of the Type II µFR and RB-2 on top of the MR-2 led to easier interchange of the PDMS pumping insert (Type II µFR). Pump activation and fluid flow control was simplified by use of a hand crank mechanism and the LEGO® Mindstorms® kit. The hand crank is a very simple method of moving fluids through microfluidic networks. The LEGO® Mindstorms® kit system provides users without knowledge of electronics, motor construction and control, or programming to quickly control and activate the micropumps.

Two micropumps were tested at different LEGO® motor power settings (see below). Power settings are entered by the user in a field provided in the LEGO® Labview interface. Values for motor power can be set between 0 and 100%. A microfluidic chip was used which permitted measurement of displaced fluid volumes in all eight channels of each micropump after 25 pump rotations. The experimental setup is shown in Figure 25. Test results are shown in Table 3. Data in Table 3 was collected by Vasile Coman (Post-doctoral fellow, BioAnalytics Group, DTU Nanotech)

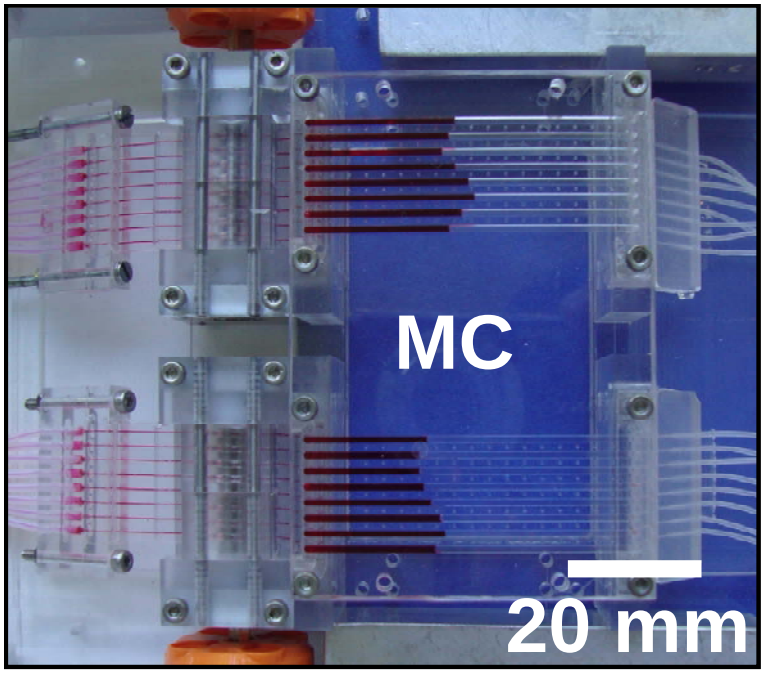

Figure 25. Experimental setup for displaced volume measurements. A microfluidic chip (MC) with 16 fluidic channels of known dimensions is connected to two miniaturized pumps in a *SWAN* (see Section C, Chapter 4) configuration. LEGO® motors can be seen above and below each pump. Motors were first run to introduce fluids into each channel. A "before" picture was then taken. The motors were then activated for 25 rotations. An "after" picture was taken at this point. Using the "before" and "after" pictures the amount of fluid displaced could be calculated. This was repeated for different LEGO® motor power settings.

Table 3: Displaced channel volumes at assorted LEGO® servo motor power settings

Pump	Power Setting (%)	Average Displaced Volume (µL)	Maximum Displaced Volume (µL)	Minimum Displaced Volume (µL)	% CV
1	25	0.71	0.76	0.67	5.1
	30	0.73	0.78	0.69	4.8
	35	0.74	0.78	0.70	4.5
	40	0.74	0.78	0.70	4.5
	45	0.73	0.76	0.70	3.7
	50	0.74	0.78	0.68	3.2
2	25	0.62	0.66	0.60	2.8
	30	0.64	0.69	0.60	3.9
	35	0.64	0.67	0.60	3.2
	40	0.64	0.68	0.62	2.9
	45	0.66	0.68	0.63	2.6
	50	0.65	0.68	0.62	2.8

Initial durability tests indicated significant improvements. In preliminary durability testing all eight channels of two Type II µFRs remained functional following 42000 pump rotations (data not shown, testing voluntarily aborted). This was a significant improvement over the mini-pump (section B) for which, after 1875 pump revolutions, several channels were no longer functional. To further characterize pump performance, displaced volume measurements were taken at intermittent points during a second durability test. Using the experimental setup shown in Figure 25 and an applied power of 30 % to the LEGO® motors, displaced volumes per pump rotation were determined. Results are shown in Figure 26. Durability testing was voluntarily stopped following 63000 rotations (see Discussion below). Inspection of the Type II µFRs used in this testing did not reveal damage.

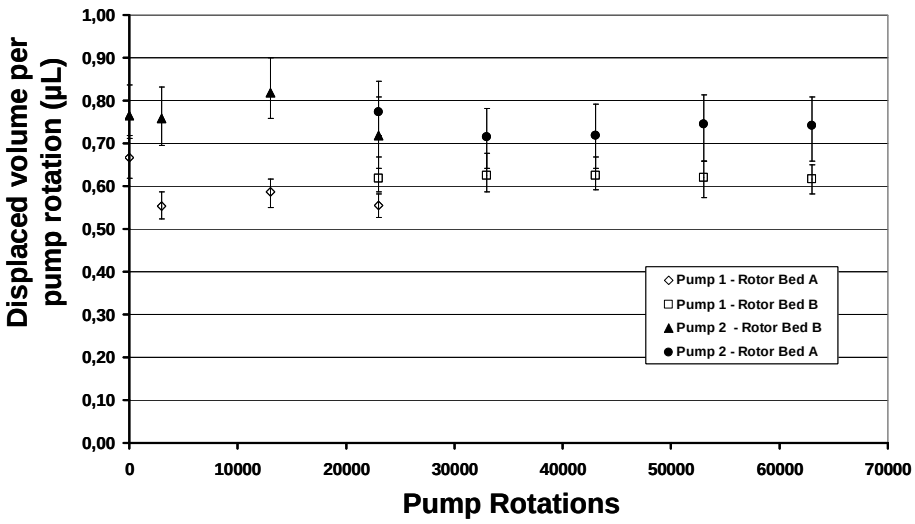

Figure 26. Average displaced volume per pump rotation at indicated cumulative pump rotations. Values shown represent the average displaced volume of all eight channels from a single micropump. Error bars represent observed maximum and minimum displaced volumes from individual channels. At 23000 rotations, the RB-2's from the two micropumps were switched. Testing was repeated at this point and for the duration of testing the RB-2's remained where they were. This exchange was performed to investigate assembly related influences on displaced volumes. For all test points, the average % CV value was 6%, with maximum and minimum % CVs of 8.7% and 4.2%.

LEGO® motors have provided average flow rates from sub- to 33/44 µL/min (dependent on displaced volumes as shown in Figure 26). This upper flow rate was obtained by applying 70% power to the LEGO® motors. Integrated optical controllers in the LEGO® motors also permit fluid metering as these can control pump rotation to within 1°. Based on rotational control of 1° and approximate average delivered volumes of 0.7 µL per pump rotation (Table 3 and Figure 26), fluid plugs of very small volumes can be delivered (theoretically 2 nL).

Use of LEGO® motors to drive the micropump does not currently permit selection or entry of desired flow rate. This is because rotation resistance, both pump-to-pump and within rotation of a single pump, varies as do displaced volumes (Table 3 and Figure 26). Though displaced volumes are constant from 25 to 50% motor power (Table 3), flow rate did not predictably increase (data not shown). Additionally, at 20% motor power or less, micropumps did not consistently turn over and fluids were not predictably delivered. To circumvent this issue and to achieve predictable flow rates the following procedure was implemented and should be used. Displaced volumes were first determined per micropump using a calibration chip (Figure 29). LEGO® motors were then programmed at a motor power at which micropumps consistently turn (i.e. 30% or higher) to *STEP and WAIT:* the motor *STEP*s a fixed number of degrees and *WAIT*s a fixed time between steps. *STEP and WAIT* is enabled by the motors' integrated optical controllers as well LabView® interface motor control tools. Knowing the time required to complete a series of *STEP and WAIT* operations, an average flow rate can be determined. The following example is provided for demonstrative purposes:

A. A displaced volume of 0.7 µL per pump rotation is assumed.
B. *STEP and WAIT* is set up such that the LEGO® motor advances in 5° steps and waits 0.05 seconds between steps.
C. The user programs the LEGO® motor to repeat the *STEP and WAIT* procedure 720 times, for a total of 3600° degrees of rotation, or 10 rotations. From A, the displaced volume per rotation is 0.7 µL and as such the total displaced volume will be 7.0 µL.
D. The program is started and the time required to complete the 10 rotations is recorded.
E. Dividing the volume delivered, 7.0 µL from C, and the time recorded to complete the test from D, an average flow rate can be determined.

An example *STEP and WAIT* programming block is shown in Figure 27.

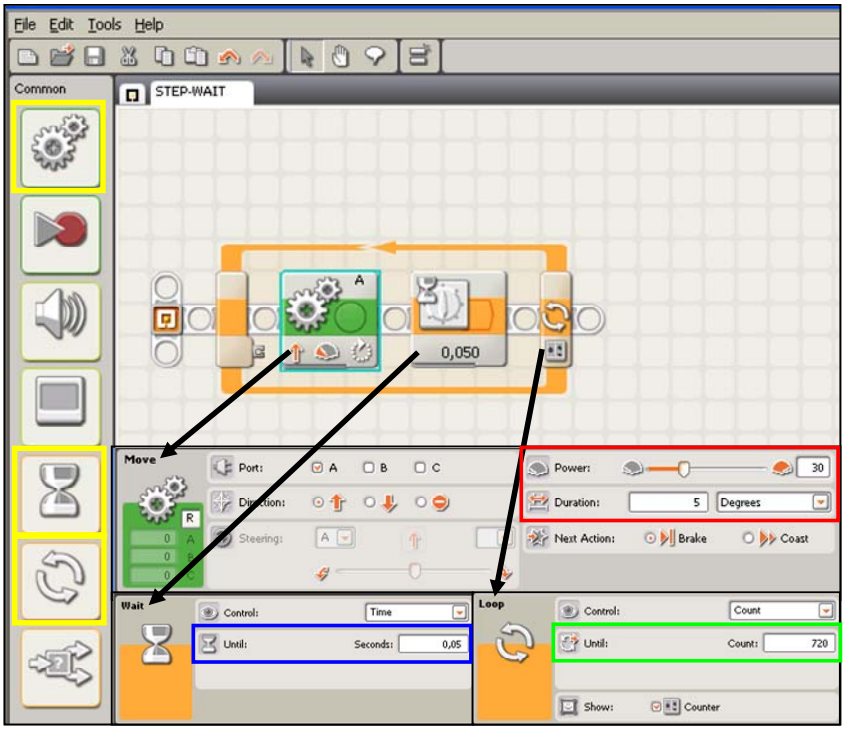

Figure 27. A *STEP and WAIT* programming loop. The default Mindstorms® LabView® Interface is shown. A *STEP and WAIT* program can be constructed using three buttons (yellow boxes) found within the column on the left-hand side: MOVE (meshed gears), WAIT (hourglass) and LOOP (circular arrows). Once added to the programming environment, (gridded area) parameters for each function can be set in the MOVE, WAIT and LOOP windows shown at the bottom of the figure. In this example, the MOVE function is set to activate through a 5° step at 30% power (red box). The WAIT function requests a 0.05 second wait (blue box) until the next operation. The LOOP function repeats the MOVE and WAIT functions a total of 720 times (green box), or a total of 720 x 5° = 3600° or 10 rotations. As such, 10 pump rotations are completed in 5° steps.

C.4 Discussion

Table 3 indicates that at different LEGO® motor power settings displaced volumes are equivalent. This is not unexpected given the rotational control of the LEGO® motors to within 1°. The intent of this test was to provide an initial assessment of channel-to-channel and pump-to-pump variability. Within pump, channel-to-channel %CVs for displaced volumes ranged between 2.8 and 8.7 % (Table 3 and Figure 26). Were the time required to displace the fluid volumes recorded the values in Table 3 and Figure 26 would be shown as flow rates rather than displaced volumes. As the time measurements for all eight channels would have been equivalent, the same variability values would result for flow rates. This allows comparison of the micropump to the mini-pump (Section B). In this respect, performance is similar as values of between 7 and 10% were obtained for the mini-pump for similar measurements (Section B). The data in Table 3 and Figure 26 indicate pump-to-pump differences in displaced fluid volumes at similar power settings. In the case of Figure 26, a larger disparity between displaced volumes is initially observed (prior to 23000 rotations), as compared to the test data collected at the same power setting, 30%, shown in Table 3. When the RB-2's were switched after 23000 rotations (Figure 26), the difference in displaced volumes collapses. This identifies the RB-2 and its

fastening to the MR-2 as a source of displaced volume variability. Further examination of the data used for Figure 30 indicates that RB-2's likely impart effects within and across a single micropump. The RB-2 is made from four individual sections (Section C.1.2.2). Two of these sections each compress four channels of a Type II µFR. These four channel groups tend to have different average displaced volumes (data not shown). Comparisons to reports of similar PDMS-based, mechanically actuated peristaltic pumps are not possible as these only present a single pump with a single channel [4, 6, 8, 10] or do not present such data [11, 14].

Further studies assessing pump variability, both within and across pumps, are planned as this must be addressed. To reduce pump variability, assembly of the micropump and the RB-2 will be re-examined. This will include RB-2 shapes, as well as trying to manufacture the RB-2 from a single piece. Type II µFR mould traceability will also be introduced. Currently Type II µFR mould components are not arranged into defined sets. This will be done for new moulds. The effect of a 4-pin vs. 8-pin MR-2's will also be investigated. It was observed during prototyping activities that over-compression of the Type II µFR completely occludes channels and eliminates fluid flow. Reducing the number of pins on the MR-2 may reduce the difference in occlusion volumes between pumps for given compression differences as a larger tubing portion remains uncompressed. Regardless of the results of these activities, pump calibration prior to system use is suggested. A calibration chip should be provided and used to allow displaced volume determination and flow rate programming (see below).

Encouragingly, both before and after the RB-2 switch, average displaced pump volumes were relatively stable (Figure 26). The cause of the initial decrease and subsequent stabilization in displacement volume from rotation 0 to rotation 3000 for pump 1 is not known. The stability of displaced volumes is different from results reported for a miniaturized pump which used commercially available tubing [4]. In this report, flow rates increased by 70% within the first hour of operation and thereafter remained stable. The stability of the flows provided by the micropump is an advantage as the user can assume that following initial calibration flows should remain relatively stable.

Improvements to durability render the pump suitable for extended experiments such as long term microfluidic cell culture. Using the minimum volume displaced for a pump rotation from Figure 26 of 0.52 µL per rotation and the cumulative 63000 rotations, the minimum estimate of total volume displaced per channel is 32.75 mL. Given the lack of damage to the Type II µFR following voluntary abortion of the durability testing this is an underestimate. Nevertheless, a 3-week microfluidic cell culture experiment running at 1 uL/min would consume 30.25 mL and as such the micropump and Type II µFR should meet requirements for such experiments. Durability will continue to be assessed as changes are made to the micropump components in order to reduce variability.

Two methods of driving fluids through microfluidic networks are provided. The hand crank is a very simple method to drive fluids through a microfluidic network. The

simplicity of the approach should not discount from its value. It is extremely economical and provides an easily implementable solution for introduction of fluids into multiple microchannels for which capillary flows may not be the most suitable option. For example, the hand crank can be used as a standalone station for priming chips, introducing coating or blocking solutions into microfluidic chips before their use in other, more complicated set-ups, or for static cell culture experiments. The hand crank is particularly well suited to resource limited or remote locations as no external power supply is required and/or for chips where capillary flows are not easily realized. Use of the hand crank in an application is demonstrated (see Section C.4.1, Chapter 5).

The LEGO® Mindstorms® kit is widely commercially available and economically priced. The LEGO® components shown in Figure 24, including 3 servo motors, controller unit and required accessories including rechargeable battery cost approximately 340 USD [19]. Off-the-shelf usability results in time and labour savings. The user friendly LabView® interface provided facilitates programming, by non-experts, of the servo motors used to actuate the peristaltic pump. Programming of flows in both forward and reverse directions, with respect to rate, duration, metering, and timing for multiple pumps can be done.

Efforts to simplify programming of flow rates will be undertaken. Whether the motors' integrated optical controller can vary motor power in real time, e.g. with a feedback loop, has not been investigated. Once programs for pump control are written, they can be stored on the control unit (NXT Intelligent Brick) (Figure 24). This controller operates by simple push button controls and controls up to three motors. Multiple programs can be stored on each Intelligent Brick unit and accessed on demand. The multichannel micropump and the ability of the LEGO® Intelligent Brick to control three servo motors, and hence three pumps or 24 fluidic inputs renders the approach most useful for multiplexed assays which benefit from or require fluidic activation. When greater fluidic inputs or pumps are required, multiple Bricks can be made to communicate with each other [19].

D. Next Steps

The mini- and micropump solutions fulfilled the second project objective. The next step in the project was to combine pumping and interconnection solutions in order to generate microfluidic systems. The development and presentation of two such systems is described in Chapter 4.

References

1. Laser, D.J. and J.G. Santiago, *A review of micropumps.* Journal of Micromechanics and Microengineering, 2004. **14**(6): p. R35-R64.

2. Inman, W., et al., *Design, modeling and fabrication of a constant flow pneumatic micropump.* Journal of Micromechanics and Microengineering, 2007. **17**(5): p. 891-899.
3. Iverson, B.D. and S.V. Garimella, *Recent advances in microscale pumping technologies: a review and evaluation.* Microfluidics and Nanofluidics, 2008. **5**(2): p. 145-174.
4. Koch, C., V. Remcho, and J. Ingle, *PDMS and tubing-based peristaltic micropumps with direct actuation.* Sensors and Actuators B-Chemical, 2009. **135**(2): p. 664-670.
5. Unger, M.A., et al., *Monolithic microfabricated valves and pumps by multilayer soft lithography.* Science, 2000. **288**(5463): p. 113-116.
6. Yobas, L., et al., *A disposable planar peristaltic pump for lab-on-a-chip.* Lab on a Chip, 2008. **8**(5): p. 660-662.
7. Situma, C., M. Hashimoto, and S.A. Soper, *Merging microfluidics with microarray-based bioassays.* Biomol Eng, 2006. **23**(5): p. 213-31.
8. Lim, K., S. Kim, and J.H. Hahn, *Roller-type squeezing pump with picoliter handling capability.* Sensors and Actuators B-Chemical, 2003. **92**(1-2): p. 208-214.
9. Yobas, L., et al., *A self-contained fully-enclosed microfluidic cartridge for lab on a chip.* Biomedical Microdevices, 2009. **11**(6): p. 1279-1288.
10. Du, M., et al., *A Peristaltic Micro Pump Driven by a Rotating Motor with Magnetically Attracted Steel Balls.* Sensors, 2009. **9**(4): p. 2611-2620.
11. Gu, W., et al., *Computerized microfluidic cell culture using elastomeric channels and Braille displays.* Proceedings of the National Academy of Sciences of the United States of America, 2004. **101**(45): p. 15861-15866.
12. Tung, Y.C., et al., *Small volume low mechanical stress cytometry using computer-controlled Braille display microfluidics.* Lab on a Chip, 2007. **7**(11): p. 1497-1503.
13. Futai, N., et al., *Handheld recirculation system and customized media for microfluidic cell culture.* Lab on a Chip, 2006. **6**(1): p. 149-154.
14. Rhie, W. and T. Higuchi. *Pen-Type Peristaltic Micropump for Portable Applications*. in *The 12th International Conference on Miniaturized Systems for Chemistry and Life Sciences (microTAS 2008)*. 2008.
15. Gomez-Sjoberg, R., et al., *Versatile, fully automated, microfluidic cell culture system.* Analytical Chemistry, 2007. **79**(22): p. 8557-8563.
16. Taylor, R.J., et al., *Dynamic analysis of MAPK signaling using a high-throughput microfluidic single-cell imaging platform.* Proceedings of the National Academy of Sciences of the United States of America, 2009. **106**(10): p. 3758-3763.
17. Bhagat, A.A.S., et al., *Re-usable quick-release interconnect for characterization of microfluidic systems.* Journal of Micromechanics and Microengineering, 2007. **17**(1): p. 42-49.
18. Skafte-Pedersen, P., et al., *Multi-channel peristaltic pump for microfluidic applications featuring monolithic PDMS inlay.* Lab on a Chip, 2009. **9**(20): p. 3003-3006.
19. www.LEGO.com.

CHAPTER 4: MICROFLUIDIC SYSTEMS

A. INTRODUCTION

Microfluidic approaches and applications promise reductions in the materials, including samples and reagents, labour, and time required to perform many different assays and investigations as compared to conventional and established methods [1, 2]. Additional benefits of microfluidics include reduced experimental footprints and increased parallelization and throughput. However, practical concerns including reliability ease of use and integration of microfluidic devices and components hinder mainstream use [2-6].

To facilitate usability and increase adoption of microfluidic devices, several groups have proposed modular microfluidic systems. Modular systems present self-aligning complementary elements and components designed with nominal repeating element spacing and overall dimension. Influenced by both LEGO® and electronic breadboards, these systems aim, at the very least, to allow non-experts to rapidly create sealed microfluidic connections and networks. Leak-free assembly of interconnections between individual modules is thought to be the major challenge of developing modular systems [7, 8]. Several reports describe methods of rapidly creating interconnections to microfluidic chips and the outside world. However not all of these solutions should be considered modular [9-12]. Apart from providing reliable interconnections, modular systems should present easily reconfigurable elements, ideally which can be assembled rapidly by non-expert users, that allow flexibility in design and construction of both serial and parallel fluidic networks [8, 13, 14].

This chapter describes modular systems intended for polymeric microfluidic chips which were developed during the Ph.D. project. Modular microfluidic systems using silicon, PDMS and polymeric-based microfluidic chips have been reported. As processing methods and applications for silicon-based chips differ from those related to polymeric chips these are not reviewed. In short, these systems use interlocking silicon-based fluidic circuit boards which have been machined to contain mechanically interlocking features [15-18].

Approaches allowing multiple polymeric chips or cartridges to be connected together have been presented. These allow the placement of different assay and processing functions on different chips. *Grodzinski et al.* vertically stacked multiple chips *via* connections made by interfacing either barbed or barrel-shaped connectors to O-rings housed in polymeric chips [19]. *Pepper et al.* demonstrated injection moulded cyclic olefin copolymer (COC) fluidic chips each containing a single inlet and outlet tubes [20]. The inlet/outlet tubings were sized such that an inlet/outlet pair could be snapped together to string chips one to another. A more comprehensive demonstration of this approach was provided by *Yuen et al* [7, 8]. The “plug-n-play” system’s microfluidic components, created by stereolithography, fit into a

motherboard and feature miniaturized luer fittings. These fittings mate components and allow the creation of planar and three-dimensional configurations. Modular systems based on PDMS have also been described. *Jiang et al.* demonstrated five modular PDMS elements intended for the generation of arbitrary gradient profiles [21]. Though flexibility in gradient generation was provided, the method was limited by its requirement for relatively large fluid volumes. *Rhee et al.* constructed assorted prefabricated individual PDMS microfluidic assembly blocks, each with different fluidic channel configurations and purpose [14]. Different block types could be attached together, using different methods, in order to assemble and construct devices with multiple configurations. Commercial systems are also available [22-25]. In general, these employ a breadboard or base plate approach into which fluidic chips are held and assorted elements linked.

While the above reports describe approaches and systems for connecting microfluidic chips together to form fluidic "networks", they do not always address concerns or provide solutions regarding connectivity to peripheral equipment and/or peripheral equipment requirements and integration. Fluidic actuation of the networks, i.e. fluid delivery and control thereof, are not always discussed in these reports. In previous chapters of the thesis, interconnection solutions (Chapter 2) and mechanically-actuated peristaltic mini- and micropumps (Chapter 3) were presented. The integration of these components into modular systems which provide interconnectivity and peripheral equipment solutions is described.

B. *µSLIDE* SYSTEM

The *µSlide* modular system was first described in the following peer-reviewed conference proceeding (Appendix B):

Sabourin, D., Snakenborg, D., Skafte-Pedersen, P., Kutter, J.P., and Dufva, M. "*Modular Microfluidic System with a Cast PDMS Pumping Bed and Planar PDMS Interconnection Blocks*" µTAS 2008, San Diego, California, USA. Kluwer Academic Publishers.

Content below is taken in part from this proceeding.

B.1 System Components

The main components of the *µSlide* system (Figure 28) are interconnections, microfluidic test chips, reservoir and sample outlet chips, and a base plate with guiding alignment rails.

B.1.1 Interconnections

The *µSlide* system used the interconnection blocks (IBs) described in Section B of Chapter 2.

B.1.2 Pump

The *µSlide* system used the mini-pump described in Section B of Chapter 3. Though not stated previously, each channel of the mini-pump's PI component (PDMS insert) was bookended by the same sealing O-ring features found on IBs.

B.1.3 Microfluidic Chips

Microfluidic chips (Figure 28) were made from micromilled PMMA and were bonded via a UV-assisted bonding process [26]. Fluidic inlets and outlets were found on the side faces of the chips.

B.1.4 Reservoir and Sample Outlet Chips

Reservoir chips (Figure 28) were made from micromilled PMMA and were bonded via a UV-assisted bonding process [26]. Outlet chips (Figure 28) were made from micromilled PMMA. Fluidic exits were made by press-fitting blunted needles into the micromilled througholes with a hammer. For both the reservoir and sample chips, fluidic channels were placed on the side faces of the chips.

B.1.5 Base Plate and Alignment Rails

The base plate and alignment rails (Figure 28) were made from micromilled PMMA. Both base plate and alignment rails contained alignment features (2 mm throughholes). The alignment rail featured an architecture which permitted system components to be slid along underneath an upper lip.

B.2 System Assembly

Figure 28 shows an assembled *µSlide* system.

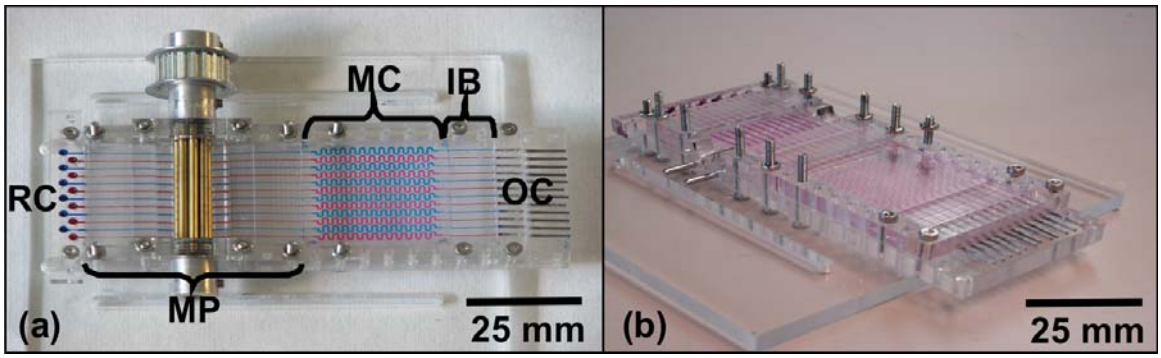

Figure 28. Assembled *µSlide* system. (a) Reservoir chip (RC), mini-pump (MP), microfluidic chip (MC), interconnection block (IB), and outlet chip (OC). Stepper motor not shown. Dye visible in chip corners results from incomplete bonding of chip. (b) System side profile with multi-roller removed. Planar features including microfluidic chip and IB are 4mm in height.

The *µSlide* system uses alternating placement of deformable PDMS-based and rigid (polymeric) components in order to create sealed fluidic networks between these. Over/undersizing of components to be placed adjacent to each other results in compression of the O-ring sealing features (Section B Chapter 2). Figure 28 can be used to understand the operating principal:

1. A reservoir chip is aligned and fastened by 2 mm screws next to one side of the PI, the PDMS-based and deformable, component of the mini-pump. The

alignment of the reservoir chip results in compression of the O-ring features found on that end of the PI, and sealed interconnections are formed between the reservoir chip and one side of the mini-pump. The mini-pump was previously fixed to the base plate.

2. On the other side of the mini-pump, a rigid and "oversized" PMMA microfluidic chip is slid along and underneath (hence the *µSlide* name) the alignment rails until it is adjacent to the PI of the mini-pump.
3. As with the PMMA chip, an IB is slid along and underneath the alignment rails until it is adjacent to the PMMA chip.
4. The outlet chip is aligned and fastened by 2 mm screws next to the IB. The placement of the sample outlet chip results in compression, due to the oversized PMMA chip, of the O-rings found on and between the PI and the PMMA chip, the PMMA chip and the IB, and the IB and the sample outlet chip. Sealed connections and networks result.

Exchange of microfluidic chips within the system was accomplished by unfastening the sample outlet chip and sliding out the IB and microfluidic test chip. A new test chip could then be slid along and under the alignment rails and the system reconnected as described above.

B3. Results and Discussion

The *µSlide* approach shown in Figure 28 allowed many interconnections to be quickly formed. A total of 48 fluidic interconnects are shown in Figure 28, and chips could be exchanged fairly rapidly. The proximal placement of the pump to microfluidic chips limits dead volumes to approximately 2.1 µL and likely compliance as compared to typical pump setups. For applications where only small sample volumes are required, such as DNA microarray hybridization and washing [27], the interfacing mechanism of the system (Figure 28) reduces the need for additional tubing and associated handling issues. Furthermore, the compact design of the micropump allowed for placement on microscope stages, and as a result of the in-plane orientation of the interconnections, unobstructed microscopic observation was possible.

Though the *µSlide* approach had several benefits, certain aspects were thought capable of improvement. These were mostly related to interconnections and component interfacing and in particular were:

- As described in section A of Chapter 2, use of IBs requires that interfacing microfluidic chips have polished side faces to help assure seals. This requires an additional processing step for microfluidic chip manufacture.
- Insertion of chips into *µSlide* configurations (not shown) meant to create fluidic interconnections in multiple, perpendicular directions proved difficult and could damage O-ring features of the PI and IBs.
- Solutions for facilitating interfacing of the system with sample volumes larger than that provided by the reservoir chip (Figure 28) was required.

These observations and the ensuing necessity for improvements resulted in a redesigned and improved system. A description of the revised system follows.

C. *SWAN* (SYSTEM WITHOUT A NAME)

Components of the *µSlide* system were redesigned to address the previously listed shortcomings. *SWAN* resulted from these efforts. As *SWAN* elements have not yet been published, detailed descriptions are provided. *SWAN* has been accepted for oral presentation at µTAS 2010, Groningen, Netherlands. The accepted, peer-reviewed abstract is found in Appendix B.

C.1 *SWAN* Component Design and Fabrication

C.1.1 Interconnections

SWAN interconnection components provide both chip-to-chip and chip-to-world connectivity. These components are *Microfluidic Ribbons (µFRs) and tubing connectors (TCs).*

C.1.1.1 Microfluidic Ribbons (µFRs)

Microfluidic ribbons (µFRs) interface system components to each other. There are three µFR versions: Type I, Type II and Type III (Figure 22). All µFR versions are cast from PDMS in micromilled moulds as previously described (Section B, Chapter 2). Each µFR contains eight integrated 240 µm wide circular channels spaced 2.25 mm centre-to-centre (1536 well-plate standards).

The Type I and Type II µFRs are bookended with eight ball joint interconnection features. Ball joint features are found on only on one end of the Type III µFR. The ball joint features contain a cylindrical portion of 1.8 mm OD, 0.5 mm in height and are topped by a 0.4 mm radius semi-spherical feature. Polymeric brackets are placed into the µFR moulds prior to injection and curing of PDMS and as such become integrated within the µFR. The brackets measure approximately 30 mm in length and 5 mm in both height and width. The brackets contain 2 mm alignment holes which simplify handling and alignment to other system components. The brackets also provide the compressive frame which results in sealed interconnections when µFRs are fastened to other system components by 2 mm screws (Figure 29 and 32).

Type I µFRs permit direct chip-to-chip or chip-to-reservoir connectivity (Figure 29). Overall length and width of the Type I µFR, inclusive of terminal brackets, are 25 and 30 mm respectively. The central PDMS portion of the Type I µFR is 1 mm thick. Type II µFRs connect microfluidic components through the micropump and were previously described (Section C, Chapter 3). Type III µFRs provide chip-to-waste connectivity (Figure 29). Type III µFRs components are made by integrating silicone tubing (0.3/0.7 mm ID/OD, Reichelt Chemietechnik, Germany) into the mould prior to casting of PDMS. Threading optical fibre through the mould and inside the silicone tubing channel prior to casting creates a single contiguous fluidic channel.

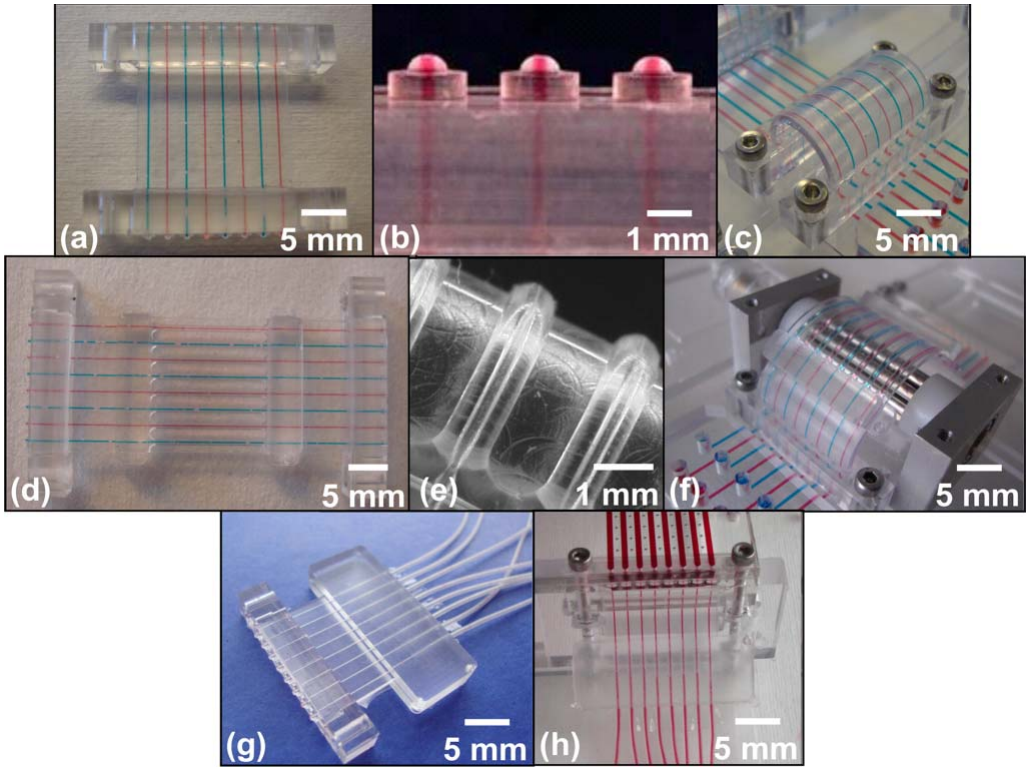

Figure 29. µFRs. (a) Type I µFR. Channels filled with dye to facilitate visualization. (b) Ball joint interconnection features found on all µFRs (Photo courtesy of V. Coman, Bioanalytics Group, DTU Nanotech). (c) Type I µFR connecting two PMMA microfluidic chips. (d) Type II µFR. Channels filled with dye to facilitate visualization. Dashed box features shown in (e). (e) Raised tubing features of Type II µFR. Webbed foot design can be seen at the bottom of the panel. (f) Type II µFR placed across a micropump. (g) Type III µFR. Integrated silicone tubings can be seen exiting from the right side of the piece. (h) Type III µFR at outlets of microfluidic chip and transporting fluid to waste.

C.1.1.2 Tubing Connectors (TCs)

The TCs (Figure 30) connect fluidic reservoirs, e.g. vials, to the micropump's (see below) Type II µFR. PTFE tubing (Bola, Germany) with 1.6 mm OD and 0.2 mm ID is used. The TCs are made of from two polymeric pieces. The first piece is made from a polymeric shell (PMMA or PC) which houses a custom-made PDMS gasket insert. The PDMS gasket contains eight 1.6 mm OD channels, each of which ends with a protruding 0.5 mm wide and 0.5 mm high O-ring like feature. The PDMS gasket was cast from micromilled moulds as previously described. In this case 1.6 mm OD tubing was used during the casting process to create 1.6 mm OD channels. The second piece is a polymeric (PMMA or PC) chip with eight througholes with diameters which transition from 1.6 mm to 0.8 mm. 0.8 mm corresponds to the diameter of the hemi-spherical ball joint interconnection features (Figure 29). When these two polymeric chips are interfaced to the Type II µFR, the O-rings of the custom made PDMS gasket are compressed and a seal is formed. Figure 30 describes how a seal is made between the PTFE tubing and the Type II µFR.

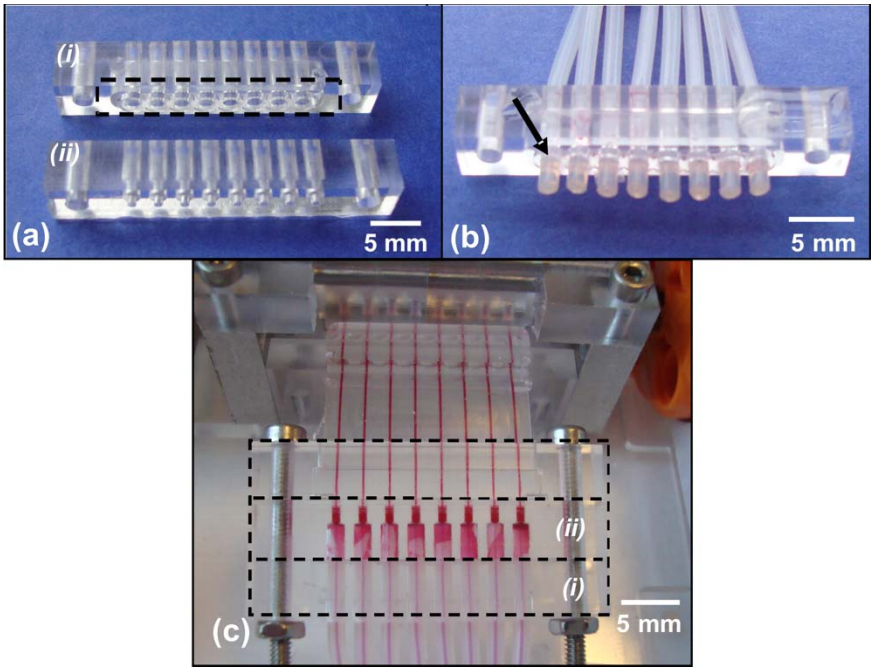

Figure 30. TCs. (a) TCs are made from two polymeric chips. (i) A polymeric shell (PMMA or PC) houses a custom-made PDMS gasket insert (dashed box). The PDMS gasket contains 1.6 mm diameter channels. At the end of each of these channels is a 0.5 mm wide O-ring protrudes by 0.5 mm. (ii) Polymeric chip (PMMA or PC) with througholes which transition from 1.6 and 0.8 mm diameters. (b) PTFE tubing of 1.6 mm OD is passed through the chip containing the PDMS gasket. Each protruding PTFE tube is thus collared by an O-ring feature. (c) Using 2 mm screws the TC is interfaced to one end of a Type II µFR. Dashed boxes correspond to individual components. The upper dashed box is the bracket of the Type II µFR. Parts (i) and (ii) are aligned such that the tubings enter the 1.6 mm portion of part (ii). Part (ii) is also aligned to the bracket of the Type II µFR. The Type II µFR ball joint features thus align with the 0.8 mm channel portion of part (ii). With compressive force, the gasket of part (i) forms a seal between part (i) and (ii) and the ball joint features form a seal between the Type II µFR and the part (ii). The lack of a seal between the 1.6 mm PTFE tubing and the 1.6 mm diameter channels for these in part (ii) is expected.

C.1.2 Pump

SWAN uses the micropump previously described. (Section C, Chapter 3). As mentioned, the micropump can be driven either by a hand crank or LEGO® components.

C.1.3 Microfluidic Chips

Microfluidic chips (Figure 32), including test chips and reservoir chips, were made from micromilled PMMA and were bonded via a UV-assisted bonding process. Bonding faces of the PMMA chips were exposed to UV (DYMAX EC 5000 with p/n 36970 bulb, Torrington, Connecticut) for 1 min. and were subsequently bonded between glass plates in a bonding press (P/O/Weber, Remshalden, Germany) at 85°C for 10 minutes at an initial applied pressure of approximately 8 kN for chips measuring 26 *(w)* x 76 mm *(l)* and 13.50 kN for chips measuring 52 *(w)* x 76 mm *(l)*. Fluidic inlets and outlets with 0.8 mm diameter were placed on either the top and bottom faces of the chips as required. The spacing and diameter thereof matched the 2.25 mm spacing of the channels/ball joint features of the µFRs.

C.1.3.1 Cell Loading chip

The cell loading chip was primarily designed to facilitate cell culture experiments, however it can also function as an outlet chip as it provides rapid attachment of multiple tubings to carry waste from microfluidic networks. The cell loading chip is made from a polymeric shell (PC) and a custom made PDMS insert (Figure 31).

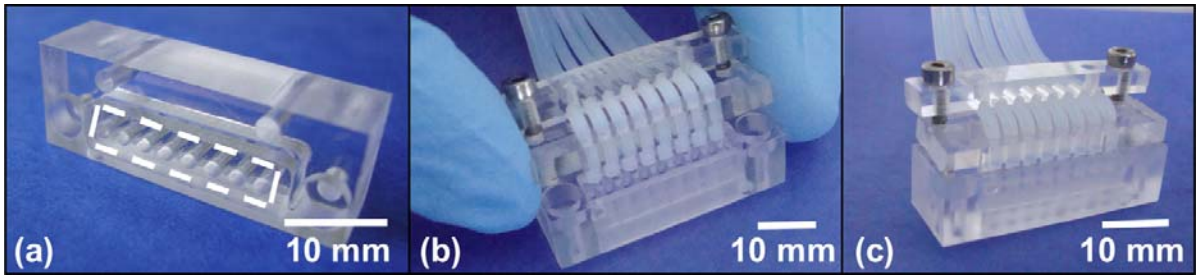

Figure 31. Cell Loading chip. (a) A polymeric shell surrounds a custom PDMS gasket insert (dashed white box). The PDMS gasket has eight 1.6 mm diameter wells of approximately 7 mm depth. The wells can be used for cell loading operations. The wells transition from 1.6 mm to 240 µm channels and terminate in ball joint interconnection features. When secured to a microfluidic chip (not shown), the ball joint features are compressed and a sealed interconnection results. (b) To connect the cell loading chip to the outside world, a pre-aligned bank of 1.75 mm OD PTFE tubing is first brought above the PDMS wells. (c) Pressing the aligned tubing bank into the PDMS gasket by hand results in press-fit type, sealed interconnections between tubings and each well.

The PDMS insert is made by casting PDMS within micromilled moulds. PTFE tubing (Bola, Germany) of 0.2/1.6 mm ID/OD and 240 µm fibres (Polymicro, USA) are placed within the mould before introduction of PDMS. The fibres are threaded through the mould and into the PTFE tubing. This creates eight 1.6 mm diameter reservoirs connected to 240 µm channels. The 240 µm channels lead to ball joint interconnection features. These interconnection features are found on the face of the PDMS insert which interfaces to the microfluidic chip (Figure 31). When fastened to microfluidic chips via 2 mm screws, the ball joint features seal the cell loading chip to the microfluidic chip. To seal the cell loading chip and connect it to the outside world, an aligned bank of 0.3/1.75 mm ID/OD PTFE tubing (Reichelt Chemietechnik, Germany) is used (Figure 31). Tubing spacing is complementary to the cell loading chip's reservoirs. When inserted into the cell loading chip, the oversized tubing creates a press-fit sealed interconnection (Figure 31). For cell loading operations, the tubing bank is removed and cells are loaded into each well of the PDMS insert. The micropump can then be activated to pull cells from the wells into microfluidic chips. The aligned tubing bank can then be put back in place. The cell loading chip was co-designed with Massimo Alberti (Post Doctoral fellow, *FAST*, DTU Nanotech).

C.1.4 Base Plates

Base plates were made from either micromilled PMMA or PC. In some cases 2 mm nuts were press-fit or epoxied into undersized recesses of the base plate to facilitate attachment of components.

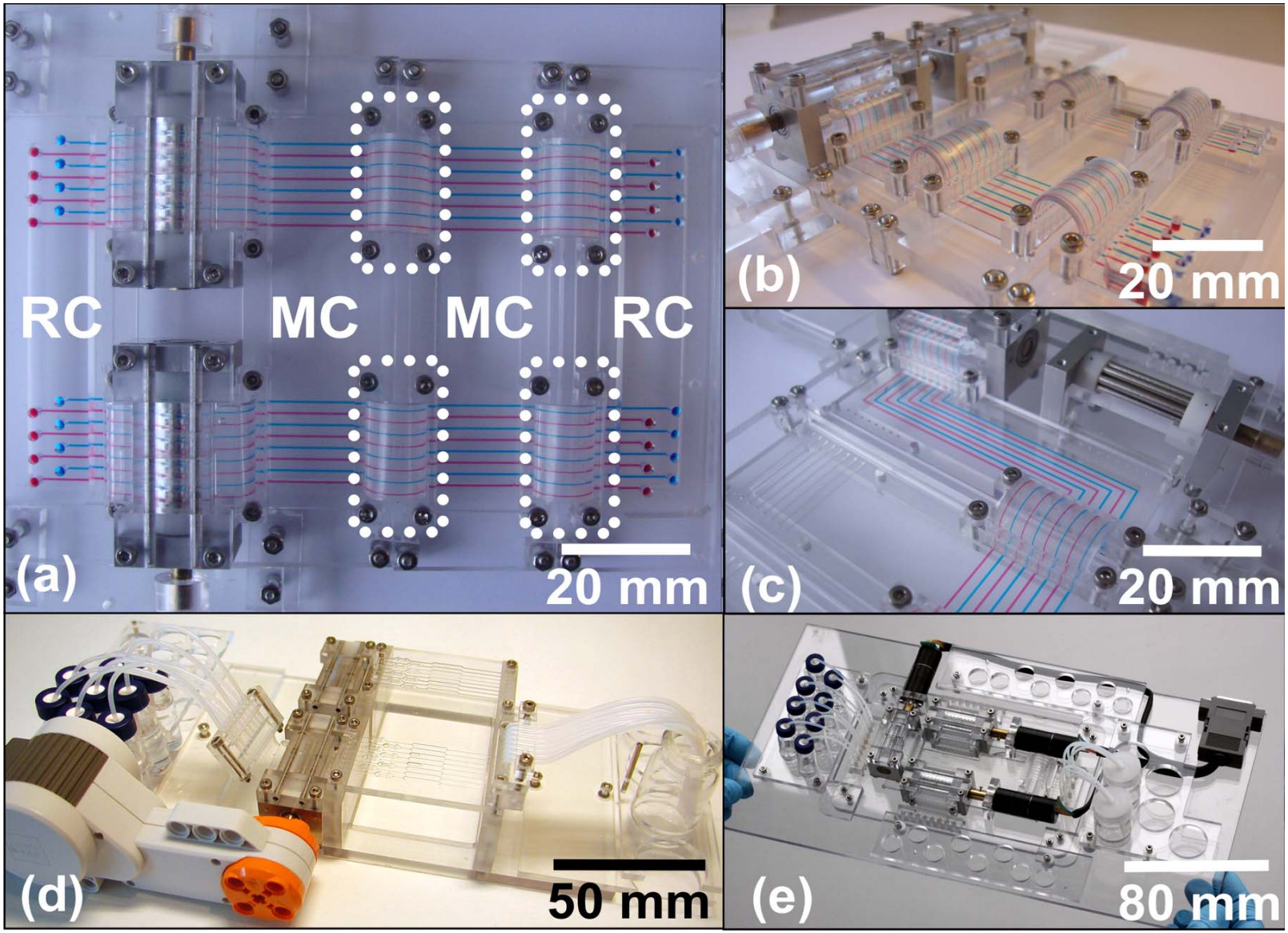

Figure 32. SWAN configurations. (a) Example *SWAN* configuration for inverted microscopy. Fluid travels from a sample reservoir chip (RC) through two micropumps and into a first 16 lane microfluidic chip (MC). Type I µFRs (dotted line boxes) connect the first microfluidic chip to a second chip, and the second chip to another reservoir chip. (b) Side view of the *SWAN* configuration shown in (a). (c) *SWAN* configuration using a microfluidic chip which routes fluids in a different flow path than shown in (a) and (b). (d) *SWAN* configuration for upright microscopy using TCs (left of pump) and cell loading chip (on top of microfluidic chip on right side) for system-to-world connectivity. (e) *SWAN* configuration used for PROCELL project. This configuration employs alternate motors. Further description of this project is provided in Chapter 5 and in Appendix B (peer-review conference proceeding 3).

C.2 *SWAN* Assembly

SWAN uses 2 mm screws to align and provide leak free interconnections between components by compressing the ball joint features of the interconnections in the Type I, II and III µFRs, and cell loading chip or the gasket feature of the TC. Multiple system configurations are possible (Figure 32). System configurations can be constructed which use single or multiple micropumps, which are suited to upright or inverted microscopy, and combinations thereof.

C.3 Results and Discussion

SWAN components are easily assembled and permit sealed fluidic networks of different configurations (Figure 28). Though not as sophisticated as other methods [8, 20, 25], use of screws to fasten components together is easy to implement and yields sealed connections. Other methods involving alignment frames have been employed but are not described (Figure 32(e)).

SWAN components addressed aspects of the *µSlide* system requiring improvement related to interconnections and component interfacing. The major point of difference compared to the *µSlide* approach is the vertical (Figure 32), instead of horizontal (Figure 28), interfacing of components. This eliminates the requirement for polishing side faces of polymeric chips following bonding processes [26]. The ball joint features of the µFRs allow interfacing to flat or thin side walled microfluidic devices. This increases the number of substrates which can be used for microfluidic chip construction, *e.g*. glass or silicon, as compared to *µSlide*. It also permits greater flexibility of microfluidic chip dimensions. Creating interconnections on multiple sides of microfluidic chips is simplified as is the construction of serial of parallel processing microfluidic networks (Figure 32).

Type I µFRs allow multiple chips to be linked together and can also provide, if required, a method for connecting fluidic lines across and within the same chip (not shown). Type I µFRs contain dead volumes of approximately 1µL between microfluidic chips. *Yang et al.* [28] demonstrate serially linked chips, but the minimal dead volume possible in this approach was estimated at 4 µL. Dead volumes between chips in other systems are difficult to estimate, but are likely larger for several of these [7, 8, 21, 25]. The Type II and III µFR, TC and cell loading chip simplify fluid delivery from and to containers such as sample and waste vials, and reduce handling, often cumbersome, of tubing. The interconnection pitch of 2.25 mm of all interconnection elements provides greater interconnection density than similar modular systems [8, 14, 22-25, 29]. As described previously (section C, Chapter 3), the Type II µFR limits pump dead volume to approximately 2.25 µL per channel and the small footprint of the micropump also permits proximal placement to microfluidic chips and likely reduces compliance.

The use of the hand crank and LEGO® kit reduced experimental and system footprint (Figure 33) as compared to *µSlide* system (Section B). While the LEGO® motor is still

large compared to the micropump, accessories such as the controller, power supply are compact and permit a highly portable setup. Assembled *SWANs* driven by LEGO® components, including motors and controller, are portable and suited for placement on microscope stages (Figure 32). Configurations compatible with upright or inverted microscopes can be assembled (Figure 32).

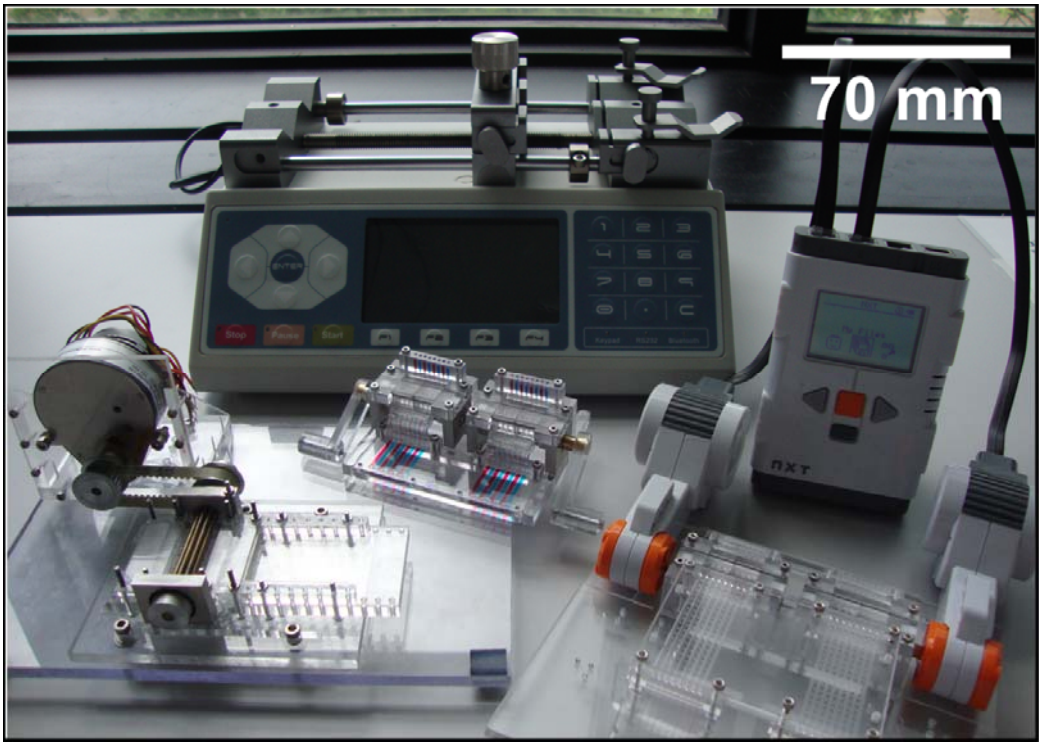

Figure 33. System comparisons. The *µSlide* system and its 12-channel peristaltic pump (section B, Chapter 3), including motor but without controller and power source are shown at front left. A *SWAN* configuration with two handcrank driven eight channel micropumps address a 16 lane microfluidic chip (middle). A *SWAN* configuration using two LEGO® driven micropumps address a 16 lane microfluidic chip (front right). The *SWAN* LEGO® configuration includes motors, controller and a power source. A typical two-channel syringe pump is shown in the background for comparative purposes.

C4. *SWAN* Applications

Wide micropump flow rate ranges (section C, Chapter 3), control options and compatibility of components with different lab instrumentation allow many potential applications. Two *SWAN* applications, one using the hand crank and the other using LEGO® parts for fluidic activation, are described below.

C.4.1 Hand Crank Application

A hand crank driven micropump was used to genotype patient samples for mutations in the human β-globin gene[27] (HBB) *via* an allele-specific hybridization (ASH) assay. Microfluidically-addressable microarrays were manufactured in PMMA chips (Figure 45, Chapter 6) as described in the following published report, further described in Chapter 6, prepared during the project:

Publication 5

Sabourin, D. *, Petersen, J. *, Snakenborg, D., Brivio, M., Gudnadson, H., Wolff, A. and Dufva, M. *"Microfluidic DNA microarrays in PMMA chips: streamlined fabrication via simultaneous DNA immobilization and bonding activation by brief UV exposure"*, Biomedical Microdevices, doi: 10.1007/s10544-010-9420-7

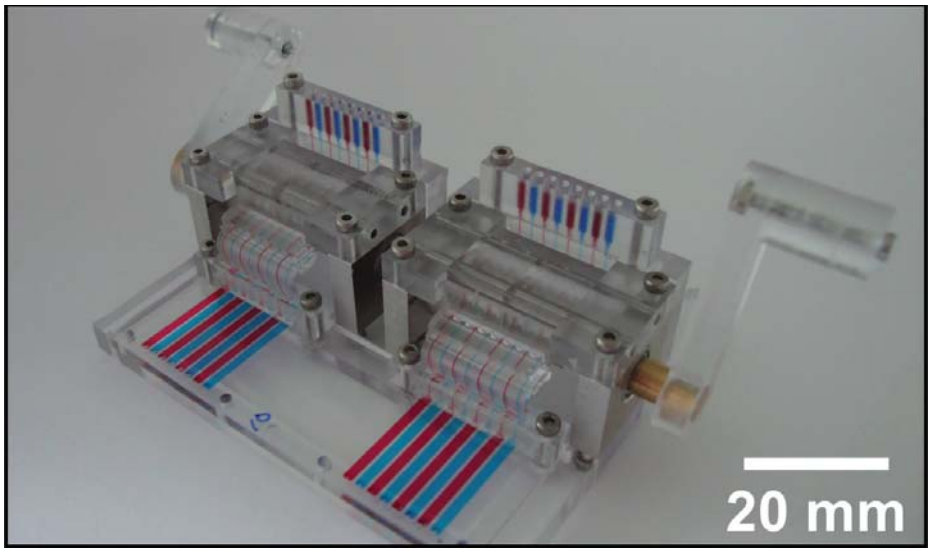

Figure 34. SWAN configuration employing hand crank driven micropumps interfaced to a PMMA genotyping chip. PMMA genotyping chips contained 16 lanes. Each lane contained an ASH diagnostic microarray for genotyping of HBB mutations. Alternating lanes are filled with blue and red dye to facilitate visualization. Loading chips are mounted to the top side of pumps and contain wells in which samples and reagents can be introduced.

The PMMA genotyping chip contains 16 microfluidic lanes (Figure 34). Each lane contained DNA arrays allowing ASH genotyping of mutations in the human β-globin (HBB) gene [27]. Four lanes are used to genotype each patient and as such four patients could be simultaneously genotyped per PMMA chip. Approximately 12 µL of each of the reaction solutions required [27] were transferred from a loading chip (Figure 34) through the pump and into the PMMA genotyping chip by turning the hand crank. Reaction solutions used, including a fluorescently cy3-labelled hybridization solution, and processing procedures (e.g. wait times and reaction temperatures) were similar to those described in Publication 5. Hybridization reactions were imaged using a ZEISS Axioscope microscope. Using the hand crank, four patients were simultaneously tested in the PMMA chip and were correctly genotyped for three mutations in the HBB gene (Figure 35).

* Co-first authors

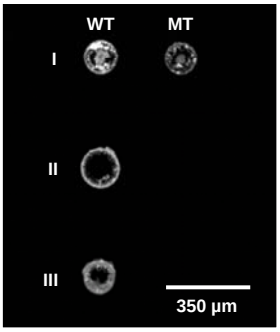

Figure 35. ASH genotyping. Image of microarray hybridization following processing with a hand crank driven *SWAN*. ASH microarrays contained Wild Type (WT) and Mutant Type (MT) probe spots for HBB mutation sites labelled above as I, II and III above. Hybridization of patient-derived target to only WT probes indicates the patient is homozygous unaffected. Similarly, hybridization to only MT probes indicates the patient is homozygous affected. Hybridization to both WT and MT probes indicates the patient is heterozygous for a mutation at a given site. In this case, the patient was heterozygous at mutation site I. Patient material was fluorescently labelled for detection purposes.

The genotyping application shown highlights that the hand crank is a simple method to introduce and drive fluids through multiple fluidic lanes simultaneously. The hand crank eliminates power requirements and allows the user to quickly introduce fluid into microfluidic chips. It is thus suited for use in remote locations but can also be of use in the laboratories of more developed settings (see above). That this application best demonstrates the utility of the hand crank in *SWAN* configurations is not claimed. Furthermore, efforts were not made to optimize assay parameters such as loading of reagents, microfluidic chip design, sample preparation and handling or detection methods. Potential solutions for these are addressed elsewhere [30, 31].

C.4.2 LEGO® system application

The original basis for this project was microfluidic cell culture (Chapter 1). *SWAN* is suitable for cell culture as its components allow unobstructed microscopic observation and lacks cytotoxic adhesives. PMMA microfluidic chips are used in such applications as these have been demonstrated to be biocompatible [32]. Cell culture experiments using *SWAN* and LEGO® Mindstorms® components have been undertaken. In these, all operations required for cell culture experiments including sterilization of the microfluidic chip, pre-treatment of the microfluidic chip with coating solutions, cell loading and perfusion were completed with a LEGO® driven *SWAN.* HeLa cells have been cultured for up to 6 days in SWAN system configurations.

A partnership between *FAST* and Bioneer A/S (Horsholm, Denmark) has been established. The goals of this partnership are further described in Section C, Chapter 5. Figure 36 shows the *SWAN* configuration used by Bioneer A/S. In this case, *SWAN* was used for culture of human umbilical vein endothelial cells (HUVEC) within a PMMA microfluidic chip.

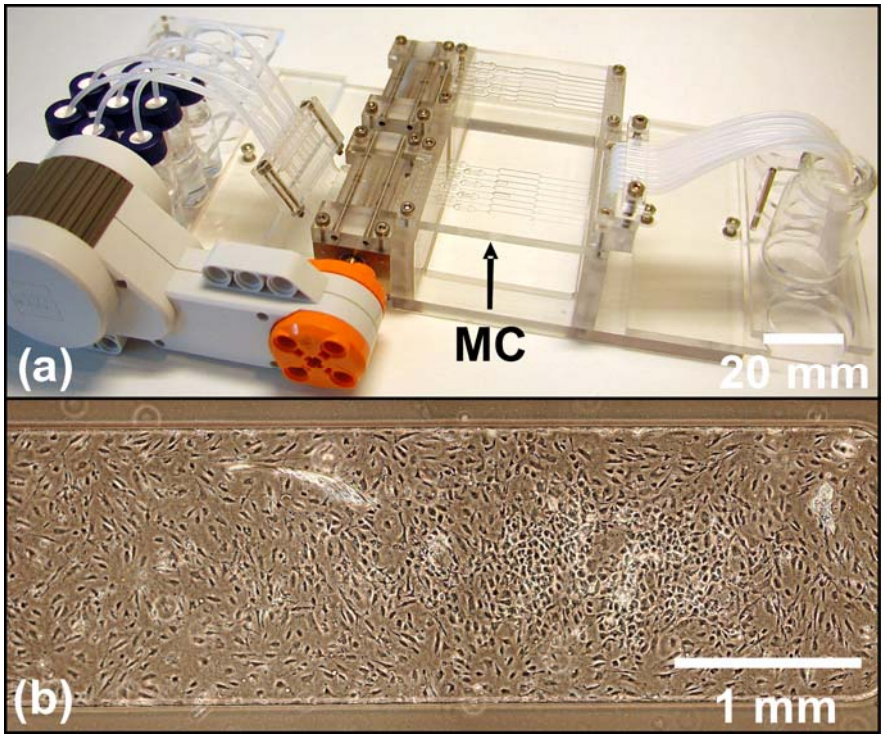

Figure 36. *SWAN* and microfluidic cell culture. (a) SWAN configuration used at Bioneer A/S. A PMMA microfluidic cell culture chip (MC) is interfaced to SWAN components. (b) Image of HUVEC cells following 24 hours of culturing. Photos courtesy of Flemming Jørgensen, Bioneer A/S.

REFERENCES

1. Beebe, D.J., G.A. Mensing, and G.M. Walker, *Physics and applications of microfluidics in biology.* Annual Review of Biomedical Engineering, 2002. **4**: p. 261-286.
2. Whitesides, G.M., *The origins and the future of microfluidics.* Nature, 2006. **442**(7101): p. 368-373.
3. Andersson, H. and A. van den Berg, *Where are the biologists? A series of mini-reviews covering new trends in fundamental and applied research, and potential applications of miniaturised technologies.* Lab on a Chip, 2006. **6**(4): p. 467-470.
4. Fredrickson, C.K. and Z.H. Fan, *Macro-to-micro interfaces for microfluidic devices.* Lab on a Chip, 2004. **4**(6): p. 526-533.
5. Young, E.W.K. and D.J. Beebe, *Fundamentals of microfluidic cell culture in controlled microenvironments.* Chemical Society Reviews, 2010. **39**(3): p. 1036-1048.
6. Young, E.W.K. and C.A. Simmons, *Macro- and microscale fluid flow systems for endothelial cell biology.* Lab on a Chip, 2010. **10**(2): p. 143-160.
7. Yuen, P.K., *SmartBuild - A truly plug-n-play modular microfluidic system.* Lab on a Chip, 2008. **8**(8): p. 1374-1378.
8. Yuen, P.K., et al., *Multidimensional modular microfluidic system.* Lab on a Chip, 2009. **9**(22): p. 3303-3305.

9. Bhagat, A.A.S., et al., *Re-usable quick-release interconnect for characterization of microfluidic systems.* Journal of Micromechanics and Microengineering, 2007. **17**(1): p. 42-49.
10. Cooksey, G.A., A.L. Plant, and J. Atencia, *A vacuum manifold for rapid world-to-chip connectivity of complex PDMS microdevices.* Lab on a Chip, 2009. **9**(9): p. 1298-1300.
11. Kortmann, H., L.M. Blank, and A. Schmid, *A rapid, reliable, and automatable lab-on-a-chip interfaced.* Lab on a Chip, 2009. **9**(10): p. 1455-1460.
12. Perozziello, G., F. Bundgaard, and O. Geschke, *Fluidic interconnections for microfluidic systems: A new integrated fluidic interconnection allowing plug 'n' play functionality.* Sensors and Actuators B-Chemical, 2008. **130**(2): p. 947-953.
13. Mark, D., et al., *Microfluidic lab-on-a-chip platforms: requirements, characteristics and applications.* Chemical Society Reviews, 2010. **39**(3): p. 1153-1182.
14. Rhee, M. and M.A. Burns, *Microfluidic assembly blocks.* Lab on a Chip, 2008. **8**(8): p. 1365-1373.
15. Gray, B.L., S.D. Collins, and R.L. Smith, *Interlocking mechanical and fluidic interconnections for microfluidic circuit boards.* Sensors and Actuators a-Physical, 2004. **112**(1): p. 18-24.
16. Gray, B.L., et al., *Novel interconnection technologies for integrated microfluidic systems.* Sensors and Actuators a-Physical, 1999. **77**(1): p. 57-65.
17. Schabmueller, C.G.J., et al., *Design and fabrication of a microfluidic circuitboard.* Journal of Micromechanics and Microengineering, 1999. **9**(2): p. 176-179.
18. Westwood, S.M., S. Jaffer, and B.L. Gray, *Enclosed SU-8 and PDMS microchannels with integrated interconnects for chip-to-chip and world-to-chip connections.* Journal of Micromechanics and Microengineering, 2008. **18**(6).
19. Grodzinski, P., et al., *A modular microfluidic system for cell pre-concentration and genetic sample preparation.* Biomedical Microdevices, 2003. **5**(4): p. 303-310.
20. Pepper, M., et al. *Interconnecting fluidic packages and interfaces for micromachined sensors*. 2007.
21. Sun, K., Z.X. Wang, and X.Y. Jiang, *Modular microfluidies for gradient generation.* Lab on a Chip, 2008. **8**(9): p. 1536-1543.
22. www.epigem.co.uk.
23. www.labsmith.com.
24. www.microliquid.com.
25. www.thinxxs.com.
26. Sabourin, D., D. Snakenborg, and M. Dufva, *Interconnection blocks: a method for providing reusable, rapid, multiple, aligned and planar microfluidic interconnections.* Journal of Micromechanics and Microengineering, 2009. **19**(3).
27. Sabourin, D., et al., *Microfluidic DNA microarrays in PMMA chips: streamlined fabrication via simultaneous DNA immobilization and bonding activation by brief UV exposure* Biomedical Microdevices, 2010: p. 9.

28. Yang, Z. and R. Maeda, *A world-to-chip socket for microfluidic prototype development.* Electrophoresis, 2002. **23**(20): p. 3474-3478.
29. Fujii, T., et al., *A plug and play microfluidic device.* Lab on a Chip, 2003. **3**(3): p. 193-197.
30. Linder, V., S.K. Sia, and G.M. Whitesides, *Reagent-loaded cartridges for valveless and automated fluid delivery in microfluidic devices.* Analytical Chemistry, 2005. **77**(1): p. 64-71.
31. Petersen, J., et al., *Detection of mutations in the beta-globin gene by colorimetric staining of DNA microarrays visualized by a flatbed scanner.* Anal Biochem, 2007. **360**(1): p. 169-71.
32. Stangegaard, M., et al., *A biocompatible micro cell culture chamber (microCCC) for the culturing and on-line monitoring of eukaryote cells.* Lab Chip, 2006. **6**(8): p. 1045-51.

CHAPTER 5: PROJECT REVIEW

The objectives of the Ph.D. project were to:

1. To propose and implement solutions which create multiple and reliable fluidic **interconnections** to polymeric microfluidic chips, and which are suited to microscopic observation,

2. To propose and implement solutions which increase **pumping** capacity, and which were suited to microscopic observation,

3. To combine the solutions developed above into a **microfluidic system,** and

4. To demonstrate the utility and applicability of the system with respect to **microfluidic cell culture** using PMMA-based, microfluidic chips.

The first three goals were met and were documented in either journal or peer-reviewed conference proceedings (a manuscript describing *SWAN* and the micropump is in preparation). The fourth goal is also considered to be complete. The *FAST* group has begun using the system for initial cell culture experiments and several research groups have adopted *SWAN*. Reviews, assessments, opportunities for improvement or future work, and general discussion with respect to each of these goals and the project in general are provided below.

A. OBJECTIVE 1: INTERCONNECTIONS

Three interconnection solutions were proposed (Figure 37) during the project.

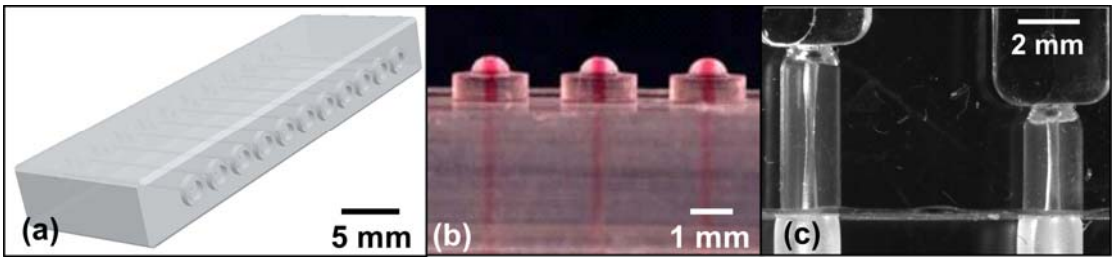

Figure 37: Interconnection solutions. (a) Interconnection block (IB). Photo courtesy of D. Snakenbord, ChemLabChip, DTU Nanotech. (b) Ball Joint Interconnection Block (BJIB). Photo courtesy of V. Coman, BioAnalytics, DTU Nanotech. (c) Compressed tubing.

The first two solutions introduced the IB concept: cast PDMS interconnection modules. PDMS was selected as it was commonly used in microfluidic research and because it was readily available. As *SWAN* also uses PDMS-based components, use of PDMS is further discussed in the microfluidic system objective section (see Section C).

Rather than use micromilled moulds and optical fibre inserts to create aligned banks of O-ring sealing features (Figure 9, Section B, Chapter 1), flat-cut soft tubing [1-3] could have been arrayed into PDMS blocks to create the first IB version [4]. From

experience, handling small tubing of approximately 10 mm length is cumbersome and more difficult than handling optical fibres. The use of fibres in conjunction with micromilled moulds also provides more flexibility. Spacing of interconnections, widths of O-ring features, etc. are more easily varied and created in this manner than with commercial tubing. The advantages of coupling optical fibres and custom moulds were more apparent in the BJIB approach as these created favourable geometries not provided by other methods or sources.

The IB approach is currently incorporated into SWAN (Section C, Chapter 4), *SWAN* addresses polymeric chips *via* the micro-peristaltic pumps. The sealing features of the IBs or BJIBs (Chapter 2) could also be placed on the terminal ends of pneumatically driven elastomeric channels. In this manner polymeric chips could be coupled to pneumatic networks. This approach is currently being investigated by other *FAST* members. Although described as an interconnection element, the IBs could also be used as microfluidic chips. Using similar moulds, circular channels could be cast within hydrogel materials and result in more *in vivo*-like three-dimensional architectures suited for study of vasculature networks.

The third interconnection method proposed compression of tubing during a UV-bonding procedure as an adhesive-free method of creating integrated interconnections. In retrospect, an alteration to the fabrication procedure may have benefits (Figure 38).

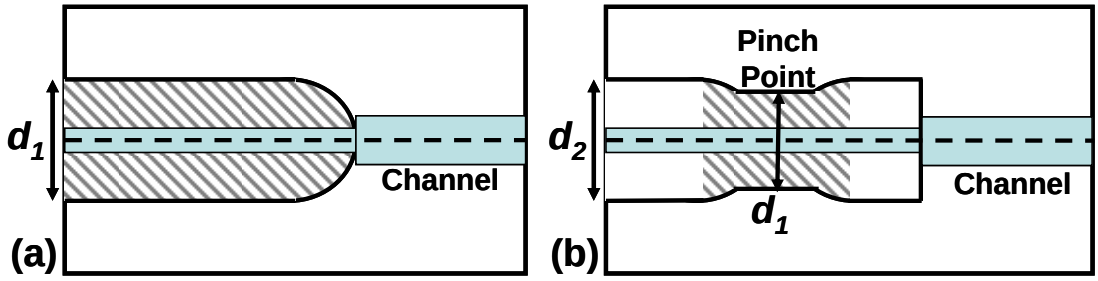

Figure 38. Compressed tubing interconnection method. (a) Schematic representation of side view of the PMMA device as published (Section D, Chapter 2). The dashed line represents the bonding plane of the PMMA device. The distance d_1 was made to be less than the OD of the tubing used. The hash marks indicate areas where the tubing is compressed or said otherwise, where the OD of the tubing is greater than the diameter of the milled circular port. (b) Schematic showing potential improvement to method. In this case features in the PMMA layers are milled such that tubing is placed in a circular channel with diameter d_2. d_2 is greater than or equal to the OD of the tubing used. In one section of the feature milled for placement of the tubing the diameter of the channel is decreased to d_1. This should result in compression of the tubing only at the pinch point and form a sealed interconnection.

The published method describes milling lengths of semi-circular channels of undersized diameter as compared to the diameter of the deformable tubing used. Instead, using the same tools, a single pinch point could have been used (Figure 38) rather than compressing the tubing along the whole channel length. A single pinch point has several potential advantages. It provides an architecture which may further protect against users pulling tubing out from devices. It would also decrease forces acting against bonding and increased connection density may thus be possible. Additionally fluidic resistance at device entrance and exit may be decreased as the tubing ID could be constricted over a shorter length. This proposed alteration to the

described method could readily be investigated and an update to the research community provided.

B. Objective 2: Pumping

During the course of the Ph.D. mini- and micro- peristaltic pumps were produced. A non-integrated approach was used as these tend to be simpler to fabricate [5], easier to troubleshoot and separate microfluidic device yield from pump yield [6]. As with interconnections, the suitability of PDMS as a material for manufacturing the disposable tubing component of the pump, the Type II µFR (section C, Chapter 3), is discussed later (see Section C).

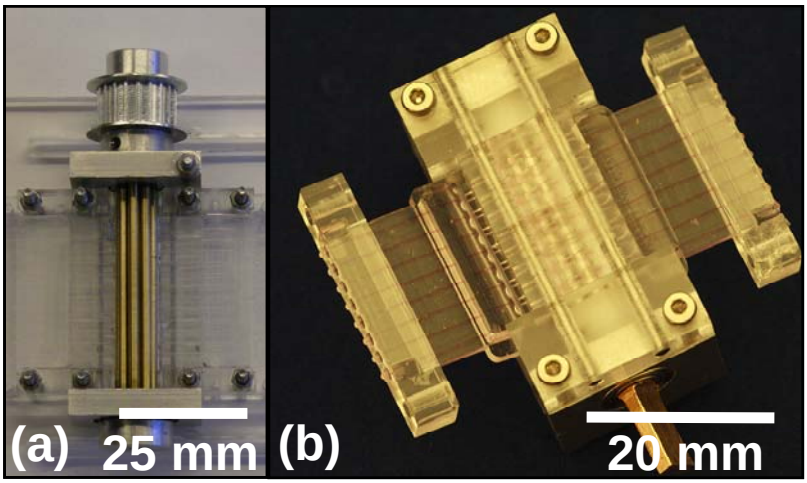

Figure 39. Pumping solutions.(a) Mini-pump. Photo courtesy of P. Skafte-Pedersen, *FAST,* DTU Nanotech. (b) Micropump. Photo courtesy of V. Coman, Bioanalytics Group, DTU Nanotech.

Recognizing that they were academically produced solutions, built from low-cost and inexpensive materials, the mini- and micropumps were internally described as adequate given that flow performance was comparable to commercially available solutions (Chapter 3). Investigations aimed at reducing variability of displacement volumes are required and have been initiated. To this point, partnerships with established manufacturers for production of pump components would likely lead to increased performance characteristics.

The second version of the micropump represents a portable pumping solution with many potential applications. Suitability of pulsatile flow is application dependent. For some studies pulsatile flow is physiologically relevant [7]. For applications requiring less pulsatile flow, apart from the method described in the minipump report (Appendix A) using adjacent channel pairs with offset flows, methods to reduce output pulsation from peristaltic pumps could be investigated [8, 9]. Outside of the micropump, use of flow rectification geometries within microfluidic chips could also be examined [10]. The latter was used in a Braille display-based flow cytometry applications [11] .

C. OBJECTIVE 3: MICROFLUIDIC SYSTEM

Components

SWAN components allow many potential microfluidic networks to be constructed. As with the micropump, the use of a non-integrated approach for system construction allowed components issues to be individually addressed and uncoupled yields thereof. For projects with compressed time frames and broad objectives such as this project (Chapter 1), this approach was believed to be favourable.

Use of micromilling as the base manufacturing method allowed realization of a microfluidic system and components thereof within the short project time frame. Development and construction of the components of the microfluidic system showcase the benefits and potential of micromilling as a base manufacturing method. Without the ability to quickly and economically prototype and machine in different materials the project would not have come as far. Why this direct writing method which is practical, inexpensive, suited to many material types, and capable of generating unique geometries, does not receive more attention in microfluidic investigations and reports is unknown.

PDMS-based components provide interconnectivity. Though PDMS has many reported benefits [5, 12-14], the suitability of the material for microfluidic applications has been reviewed. Absorption of hydrophobic molecules [15], adsorption of proteins [5], hydrophobicity, evaporation of water [16] and effects on cell culture [17] have been listed as disadvantages of PDMS. It is speculated that concerns related to absorption of molecules into PDMS may be lessened, not voided, in the microfluidic systems proposed as exposure to PDMS is limited to the components used to deliver fluids to polymeric (rigid) devices rather than for construction of the microfluidic device itself. Of course this should be investigated and where possible quantified for experiments where such behaviour may impact results [15, 18]. With respect to adsorption of proteins, several accounts describe that treatment of PDMS with Pluronic® limits protein adsorption [5, 19]. The channels found in the PDMS components of *SWAN* could easily be treated with Pluronic®. Of the concerns listed above, that which is of most concern is evaporation of water.

Initial cell culture experiments have been of limited (see below) duration as a result of bubble formation. Though the source of the bubbles has not been confirmed, and may not result from a single source, evaporation of water from the PDMS based Type II µFR is suspected. This is based on the observations that at lower flow rates (0.2 µL/min), and hence longer residence times within the Type II µFR, bubble formation within microfluidic cell culture chips seems to increase. Several approaches are being investigated in order to avoid this issue.

The first involves redesigning the Type I and II µFRs so as to make these shorter and to increase thickness of these in non-critical areas. Shortening of the components will limit residence times within the PDMS components and should reduce

evaporation effects. An added benefit of shortening these components is a reduction in system dead volumes. For example, in the presented Type II µFR the pump dead volume is approximately 2.25 µL. A redesigned component being investigated would reduce pump dead volume to approximately 1.5 µL. In their investigation on the effects of PDMS membrane thickness on osmolarity shifts within PDMS cell culture devices, *Heo et al.* [16] demonstrated that increasing PDMS membrane thicknesses from 100 to 200 µm and to 1 mm resulted in decreases in osmolarity shifts of approximately 55 and 85% respectively over a 96 hour time period at 37°C. Based on this data, the redesigned Type I and II µFRs are being made thicker where functionality of the part is not compromised.

The second approach involves replacing PDMS with commercially available tubings for fabrication of the Type I and II µFRs. The use of commercially available tubings may not be as cumbersome in this case as for fabrication of IBs as longer pieces of tubing would be required. This somewhat simplifies tubing handling. Use of tubing materials with lower permeabilities, such as PVC, may reduce evaporation. Initial investigations have been started (Figure 40) and, at the time of writing, do not indicate a significant advantage with respect to manufacture of the part

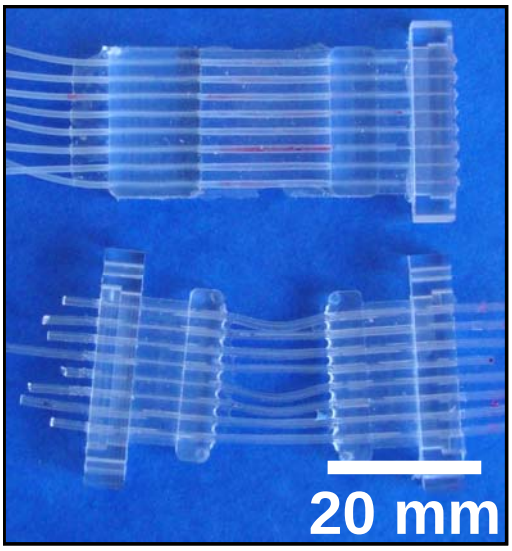

Figure 40. Prototype Type II µFR made with commercially available tubings. The top and bottom pieces incorporate silicone and PVC tubing respectively into the Type II µFR. Traces of red dye used for initial testing remain in some channels.

As with IBs, the use of fibres in conjunction with micromilled moulds likely provides more design flexibility as opposed to tubing. Creating methods to reproducibly cut tubing flat in order to reliably create interconnections, or incorporate tubings with terminal ball joint interconnection features will also be investigated.

Other potential solutions to limit evaporation involve use of parylene [16] treatments, soaking PDMS in water for 24 hours prior to the start of an experiment [20], and submerging microfluidic systems underwater [5]. Apart from the pre-soak, the practicality of these methods is questioned. Solutions which are both more practical and increase system value include the development of valving components, localized heating and reconsideration of cell culture chip designs and procedures.

The development of a valving component for the system would not only increase system utility but may also help reduce evaporation problems. When pumps addressing a fluidic network are not active their contents may evaporate and lead to bubble formations. By using a valve component to block channels after the pump and before the fluidic network and by keeping the pump running, an overpressure may result which will prevent the formation of bubbles by driving these through the gas permeable PDMS membrane. Local heating solutions should also be investigated. One such solution being considered is the use of flexible and transparent heating elements provided by Minco [21]. These heaters could be used to only heat the microfluidic chip and thus limit evaporation caused by bringing all system components to temperature. Local heating capability would also increase system portability and circumvent the need for heating control within or around observation equipment. If use of low flows results in formation of bubbles within the Type II µFR which are subsequently delivered into the chip, the simplest solution to avoid bubble build-ups within chips may be to design *SWAN* cell culture chips in which medium is pulled rather than pumped through the chip by the micropumps.

The suitability of PDMS will continue to be assessed and this analysis will be supplemented by feedback from research partnerships and collaborations (see below). Casting of components could be accomplished with other elastomers. Regardless of the elastomer selected it should be assessed for parameters described above and which could affect assay results, e.g. biocompatibility. As PDMS is the workhorse [22] of the microfluidic community, it is understandable that its use be further scrutinized. It is unknown whether researchers are also extending this scrutiny to materials apart from those used in microfluidic device construction. Effects from peripheral elements, e.g. commercially produced tubings and O-rings, and the similar effects these may have on experimental results should not be ignored and should be assessed when attempting to validate experimental data and approaches. Investigations within the *FAST* group have indicated biocompatibility issues with commercial O-rings (Joanna M. Lopacinska, *FAST*, unpublished results).

Modular Systems

Modular microfluidic systems attempt to increase usability and encourage adoption of microfluidic devices, presumably by non-experts, by facilitating the formation of interconnections between microfluidic elements and components. Like other systems [6, 23-28], *SWAN* provides a method for users to easily establish fluidic networks. However is doing so sufficient on its own? Does providing an interconnection method or standardized spacing of microfluidic chip elements alone significantly lower the barrier to use of microfluidic approaches?

Several reports describe “plug’n’play” approaches [6, 23-28]. Though these approaches provide methods for users to “plug” microfluidic chips together, they do not describe the methods and equipment users need in order to “play”. After placement of the chips and connecting the fluidic network together what is required or provided to drive, control and meter flows through the microfluidic chips? Consideration of the peripheral components and equipment, often costly and bulky,

required to drive microfluidic chips are often, for lack of better terms, discounted and ignored in reports describing modular systems. This is somewhat ironic, given that these components can eliminate many of the advantages of microfluidic approaches. For example, typical syringe and peristaltic pump sizes force placement some distance away from the microfluidic device and/or observation platforms. Extended tubings that then interface the pump to the device *i)* increase system dead volumes and result in loss of valuable reagent or sample, *ii)* can result in compliance, *iii)* place tension on the chip, and *iv)* can make unobstructed microscopic observation tricky. Furthermore, control and programming of the equipment required to drive microfluidic devices can be far from simple tasks (even for microfluidic "experts"). These points could dissuade non-experts from adopting microfluidic approaches and outweigh the novel experimental possibilities of microfluidics [29, 30].

In their report describing a PDMS-based modular microfluidic system, *Rhee and Burns* state that adoption of microfluidic approaches is hindered as the "high cost and expertise required for microfabrication deters non-expert users from using such systems". This statement is not agreed with. As an analogy, consider cell phones. These require high cost processes, facilities and levels of expertise to manufacture. However, as they are reliable and easy to use they are widely adopted by non-experts: those who know nothing and do not care about the manufacturing processes involved. Microfluidic approaches will be increasingly adopted if ease of use, reliability, and integration with existing laboratory equipment, especially that used for detection, observation and liquid handling, are demonstrated.

SWAN takes a step in this direction. Unlike many other modular microfluidic systems presented, solutions were proposed for both creating and driving entire microfluidic networks: interconnections between chips and to fluidic reservoirs, micropumps, and control of micropumps and flows are described. Companies such as Thin XXS, Dolomite Microfluidics and LabSmith provide microfluidic systems that can include pump components. However, the pumps offered with these systems deliver one (Dolomite Microfluidics and LabSmith®) or two (Thin XXS) channels per pump. This limits experimental throughput and possibilities. Activation of the fluidic networks in *SWAN* configurations by either the handcrank or the LEGO® control is fairly straightforward. With further development and investigation related to decreasing pump variability, use of the provided LabView® interface and motor characteristics, it is hoped that programming of flow rates will approach the simplicity of doing so with syringe pumps. Initial feedback from non-expert, end-users of microfluidics (biologists) has been favourable. Encouragingly and, to the knowledge of the author, unlike many other academically produced microfluidic systems, *SWAN* has been selected for use in multiple research collaborations. These include:

EXCELL:

EXCELL is an EU-FP7 project [31] which aims to integrate sensors arrays within microfludics systems in order to monitor cell mobility, morphology, gene expression and signalling activity simultaneously and in real time. The project will run multiple cell cultures per microfluidic chip. Four separate research groups and companies are currently receiving *SWANs* for electrochemical measurements in cells (Prof. Jenny

Emneus, Vasile Coman, DTU Nanotech.), optimisation of electrochemical reactions (Ulla Wollenberger, University of Potsdam), establishing neural stem cell differentiation protocols (Alberto Serrano, University of Madrid) and to characterize soluble oxygen and pH probes in cell culture systems (LUXELL, Ireland). Later stages of the project will involve deployment of *SWAN* to two additional laboratories, one in Lund, Sweden and another in Isreal. Use of *SWAN* in this project has produced promising preliminary results. Electrochemical measurements were used to simultaneously monitor the cellular redox environment of two different genotypes of *S. cerevisiae* using either glucose or fructose as substrates. In brief, *SWAN* allowed data to be captured which showed that NADPH was the preferred cofactor for menadione reduction [32].

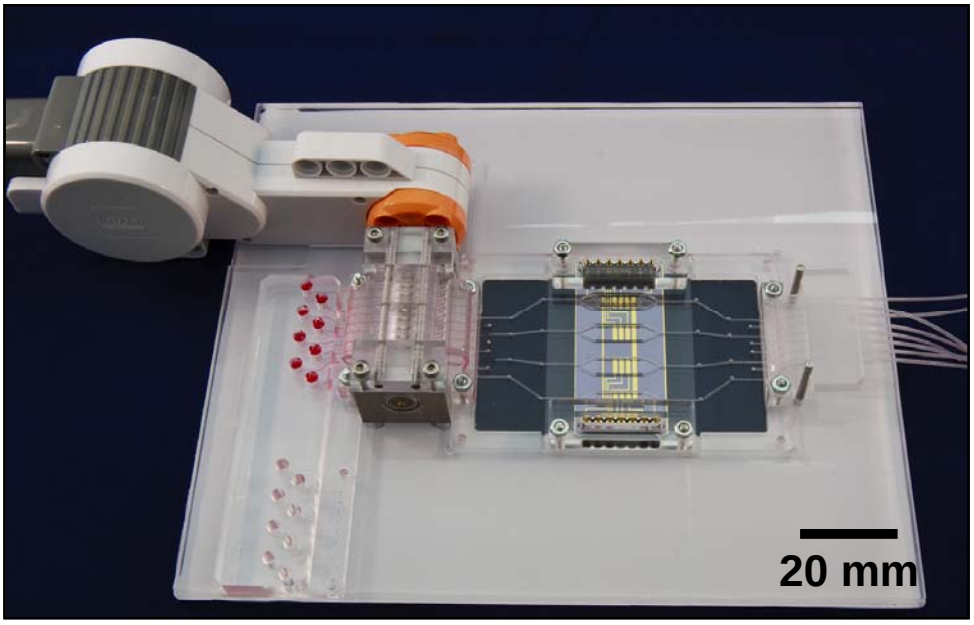

Figure 41. *SWAN* configuration used for initial EXCELL project work. *SWAN* components are shown addressing a hydrid silicon-PMMA based chip in which several yeast strains are cultured and electrochemically monitored within different cell culture chambers simultaneously. Photo courtesy of V. Coman, Bioanalytics Group, DTU Nanotech.

Bioneer A/S - Homing project:

The Homing Project has the goal of determining factors related to recruitment of stem cells to site of injuries, in particular bone fractures and stroke. Microfluidics plays an important role as chips containing bone fracture and stroke models will be developed. Chips will also be developed to house synthetic blood vessels allowing simulation of *in vivo* stem cell adhesion to, and migration through the endothelial layer. As many adhesion and migration factors need to be screened, the project required a highly parallel pumping system. *SWAN* was selected as it affords parallelization possibilities and simplicity. Currently Bioneer A/S is using a system for initial experiments (Section C.5.2, Chapter 4) but later *SWANs* will be sent to other project partners including Prof. Moustapha Kessems, University of Southern Denmark.

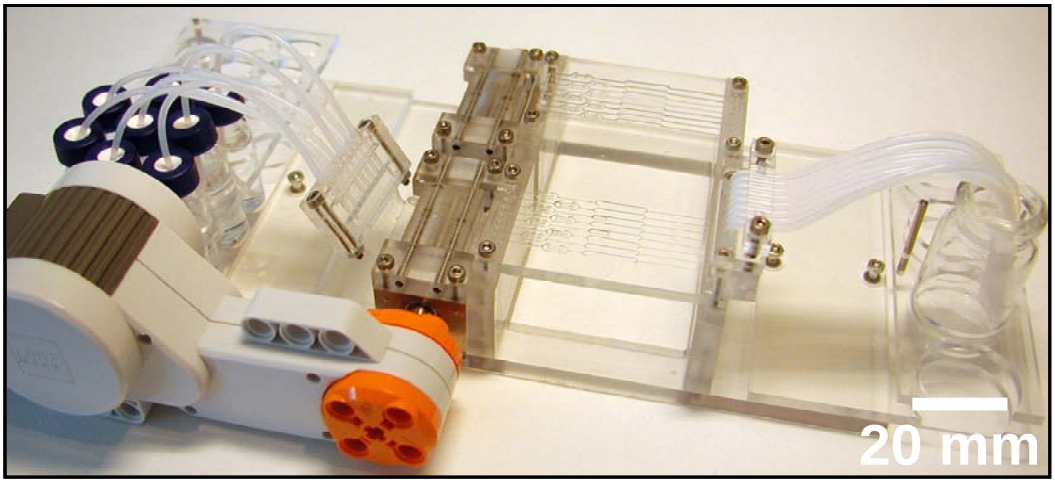

Figure 42. Bioneer A/S Homing project *SWAN* configuration. In this configuration, 16 parallel microfluidic cell culture chambers can be processed simultaneously. Photo courtesy of F. Jørgensen, Bioneer A/S, Denmark.

Bioneer A/S - *FAST*:
In this case *SWAN* will be used as the basis for construction of a highly automated *in situ* hybridization system allowing multiple, serial *in situ* hybridizations on a single tissue slice. Using a valving system (under development) *SWAN* should be easily scaled and programmed to flush the sample with up to 16 different buffer/reagents; sufficient for even highly complex *in situ* hybridizations.

PROCELL:
PROCELL will attempt to identify methods to control stem cell differentiation and to understand cancer cell behaviour. The compact design of *SWAN* components, pumps and interconnections, allows the entire required setup to be mounted on a microscope stage. This is crucial as PROCELL wishes to respond to cell characteristics or to molecular events occurring inside cells. Microscopy-based capture of events will be fed back to *SWAN* micropumps in order to control different medium influxes into chambers in order to guide stem cell differentiation. Three PROCELL partners will have access to the fluidic system.

The use of *SWAN* in these projects of varied scope and goals provides preliminary support that the system has wide applicability. Feedback from end-users in these projects should lead to improvements with respect to component design and usability. The use of the system in other projects also satisfied the project sub-goal (Chapter 1) that the solutions and approaches developed were to be user-friendly and form a base which was transferable and applicable to other projects and collaborations within and outside of the *FAST* group.

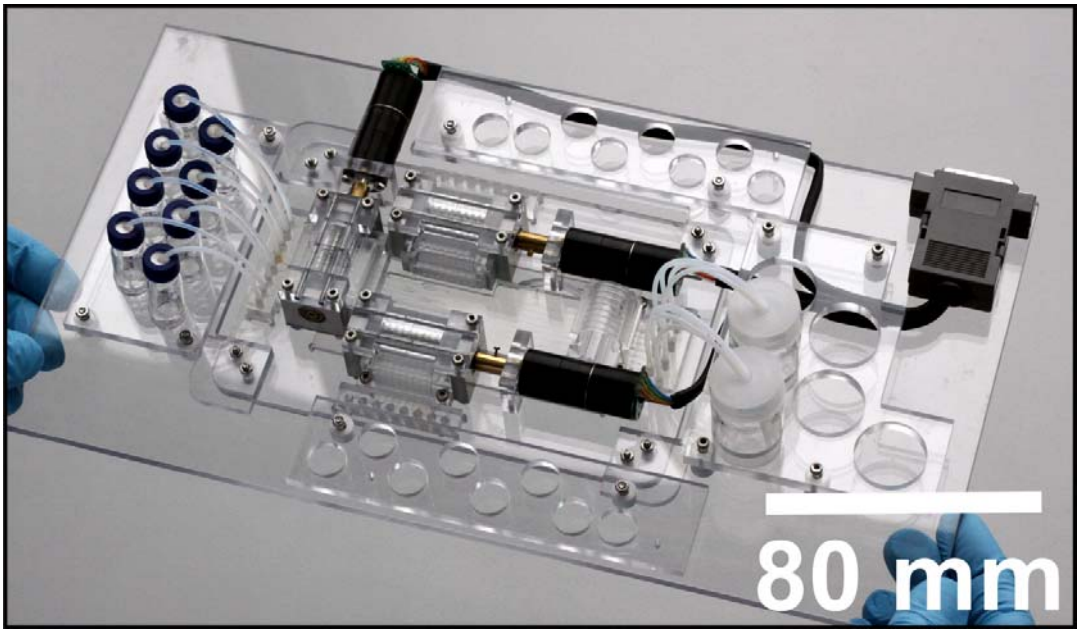

Figure 43. PROCELL SWAN configuration. Note use of different motor types. To further reduce system footprint and increase usability, loading reservoir and chips shown will be replaced by TC's and cell loading chips (section C, Chapter 4). Photo courtesy of J. Scheel, DTU Nanotech.

In their review article, *Mark et al.* [33] define a microfluidic **platform** as "an easily combinable set of microfluidic unit-operations that allows assay miniaturization with a consistent fabrication technology". They also state that different elements should ideally be connected "in a monolithic way by a well defined and ready-to-use interconnection and packaging technology". Unit operations which the platform should provide include fluid transport, fluid metering, fluid mixing, valving, reagent storage and release, and others, however not all of these must be provided. As such, it may be more appropriate to consider the *SWAN* and its components (Chapter 4) as a *platform* which can be configured into different and specific systems.

Several microfluidic platforms have been described [33, 34]. The elastomeric pneumatically driven systems (MLSI) pioneered by *Quake's* group demonstrate potential for serialization and higher experimental throughput [19, 35, 36]. However, the actuators required to drive these systems and elastomeric chips, solenoids and external pressure sources, limit the portability of the approach [33]. To this point, within the majority of articles related to PDMS-based devices the main body of the article presents pictures of only the microfluidic chip filled with dye and not of the entire experimental setup. Not explicitly presenting all auxiliary equipment required may hinder adoption by those not already familiar with these, i.e. non-experts, as these present key resource considerations related to the integration of such methods into research projects. Some also propose that the manufacturability of PDMS-based devices as compared to polymeric chips may represent a limitation for the approach [7, 12, 14, 22, 33, 37]. As *Mark et al.* state [33], further commercialization of the approach may reduce or end up solving this limitation and allow the platform to reach a wider audience. *Mark et al.* also state that use of Braille displays neatly attempted to bridge the gap between PDMS-based devices and end-users [33].

Tactile pins of Braille displays were programmed to mechanically actuate and peristaltically pump fluids through microfluidic chips made from PDMS [11, 38, 39]. Using this approach, rapid exchange of microfluidic chips within a hand-held, portable system has been demonstrated [11]. An advantage of the Braille display approach is the capability to independently valve channels. A valving component is under development and its realization will further increase value of and possible applications for the *SWAN*. Similarly to *SWAN* the Braille display approach also provides non-expert users with commercially available components to actuate fluidic network and therefore eliminates peripheral component need. However, uptake of the Braille system has been slow within research circles [37]. This is attributed to challenges associated with the complexity of the equipment and the unconventional nature of the platform [37]. By presenting users with components which are familiar, e.g. peristaltic pumps and LEGO® products, and by offering simplified interfacing and assembly, *SWAN* attempts to avoid such issues.

SWAN cannot match the multiplexing capabilities of the MLSI approach and throughput will not be as high. The micropump (Figure 39) allows multiple pumps to be connected to the same microfluidic chip without extensively increasing system footprint (Figure 41, 42 and 43). For system components as described, and using microfluidic chips measuring 52 mm (w) x 72 mm (l), 48 fluidic connections can readily be made. Further reduction of channel spacing is possible. Ten channels, rather than 8, could be placed in µFRs of the same dimensions, and increase the number of connections to 60. Nevertheless, for high content screening (HCS) applications the system should suffice. Currently capture and analysis of "deep" information from multiple kinetic processes (high content) is problematic [7, 30] and thorough analysis of greater number of processes is seen as a roadblock [7, 30]. Time lapse investigations are currently limited by detection speed. This parameter involves consideration of frame sampling rate, distance between detection sites, and the number of channels, i.e. types of light, that must be analyzed at each location [30].

Recently, an interesting platform has been described in which automated liquid handling machines are used to deliver fluids to PDMS-based microfluidic channels whose entrances and exits are positioned in accordance with 386 well plate spacing [40-42]. Deposition of fluidic drops on the entrances and exits of the fluidic channels results in passive, pressure-driven flows. This "tubeless" approach leverages both advantages of microfluidics and automated liquid handling. Scaling up tubeless systems requires only an increase in the number of automated pipetting operations. In contrast, for tube-based systems both tubes and connections must be scaled accordingly [37]. Importantly, recent reports using this system have presented protocols and data on repeatability of assays and cell seeding [41]. Another merit of this approach is that the reader, a potential future user, can understand and grasp all peripheral equipment requirements. For those who already own automated liquid handling machines it represents a method to seamlessly integrate microfluidic investigations into their laboratories. For those without liquid handling machines, the cost of acquiring these may be prohibitive.

Where possible, components of the *SWAN* were dimensioned to match current standard laboratory equipment. Spacing of fluidic channels in both *µSlide* and *SWAN* were set at 1536 well plate standards. This was done to permit coupling to fluidic handling robots. This would permit highly dynamic addition and subtraction of compounds and agents from test systems and would leverage many of the same advantages described in other reports [40-42]. For example, loading of 48 different cells lines into a perfusion based microfluidic system would be an onerous task for an operator. It is not improbable to picture that liquid handling robots could place multiple cell samples in defined locations on chips and that the micropumps could then be activated to place these cells within fluidic channels and perfuse them. Incorporation of *SWAN*'s micropump into microtiter plate format is planned. Microfluidic chips were also dimensioned to microscope or double microscope size standards. This facilitates use of these chips in processing and detection equipment [43].

Reports have stated that standards should be established for interconnections, materials, and for handling of cells in different systems [14, 22]. Though dimensions of common platforms were used to design system components, the call for standardization of materials and methods across microfluidics seems premature. For example, the myriad of possible combinations related to materials, processing methods and intended applications for microfluidics makes finding a single interconnection solution which satisfies these unlikely [4]. One of the great possibilities afforded by microfluidics is the capability to program cellular response. In such experiments cellular environments are both statically and dynamically influenced [30]. Standardization of protocols [14], e.g. flow rates, growth media, device fabrication, etc. will limit conditions, novel experiments and hence investigation of programmed cellular response [30]. Furthermore, why limit approaches when at present the influence of microenvironments on cellular function is just beginning to be established [44] and the correlation between microfluidic environments and *in vivo* conditions is unknown and difficult to quantify? Perturbations to "defined standards" are likely necessary to more finely resolve mechanisms and response. Whether or not this data is applicable or useful is an entirely different matter.

Rather than discuss standardization, it may be more fruitful for the research community to discuss methods for validation of results. Efforts to establish cellular baselines in microfluidic cultures and probe differences between these and macroscale cultures are a step in the right direction [44, 45]. It is perhaps time to push more resources towards the characterization of microfluidic environments rather than develop further novel devices. Biologists are more interested in generating novel data than concerned with the device or technological details [29]. However, in order to trust novel biological responses data generated by microfluidic systems, this data must first be validated. This validation procedure should likely involve sharing of data and microfluidic systems between laboratories so that assay reproducibility and effects related to factors such as operators can be investigated and quantified [30]. This lack of validation, or perhaps better put as establishment of baselines, is listed as a reason for lack of integration of microfluidic into cell biology

work [44]. To this point, biologists must remain open minded and should not expect microfluidic systems to yield data which is similar to that provided by current technologies and approaches (e.g batch culture, high throughput well plate based methods).

D. OBJECTIVE 4: MICROFLUIDIC CELL CULTURE

Microfluidic cell culture using the platform developed during the project and within microfluidic PMMA chips has been initiated. Cells have been cultured within devices for several days (Chapter 4), however the goal should be long-term cell culture (several weeks). Cell culture using *SWAN* will continue. For these studies, the effects of the UV treatment used for bonding of PMMA microfluidic chips on the PMMA surface should be interrogated, e.g. by gene expression profiling, to verify that this modified surface is not imparting experimental effects.

The majority of extended cell culture experiments were terminated as a result of bubble formation. This problem is not uncommon in microfluidics. Previously, strategies for reducing the introduction of air bubbles into the system from the micropumps were discussed. Strategies involving construction of the microfluidic chip should also be considered. Such strategies tend to aim to sequester bubbles. Simple steps include increasing bubble trap volume however given microfluidic chip surface areas this is not always easily implemented. Several reports describe architectures [46, 47] and surface treatments [48] which effectively trap and/or remove bubbles from microfluidic systems. A recent report describing the use of hemi-spherical shapes to trap bubbles [46] is of particular interest. Though described for PDMS-based devices, hemi-spherical geometries are readily made using ball-end mills when micromilling. The applicability of this approach to polymeric microfluidic chips should be examined. Whether milled and unmilled surfaces play different roles in bubble nucleation and/or trapping, and whether intentional surface defects [49] can be exploited to nucleate bubbles should also be investigated. Finally, use of either hydrophilic or hydrophobic membrane use in chip construction as a method for sequestering or venting bubbles could also be considered.

Chapter 1 described the project's initial basis as the fabrication of a µCCC which provided multiple experimental conditions (Figure 44). Priorities and objectives changed during the project.

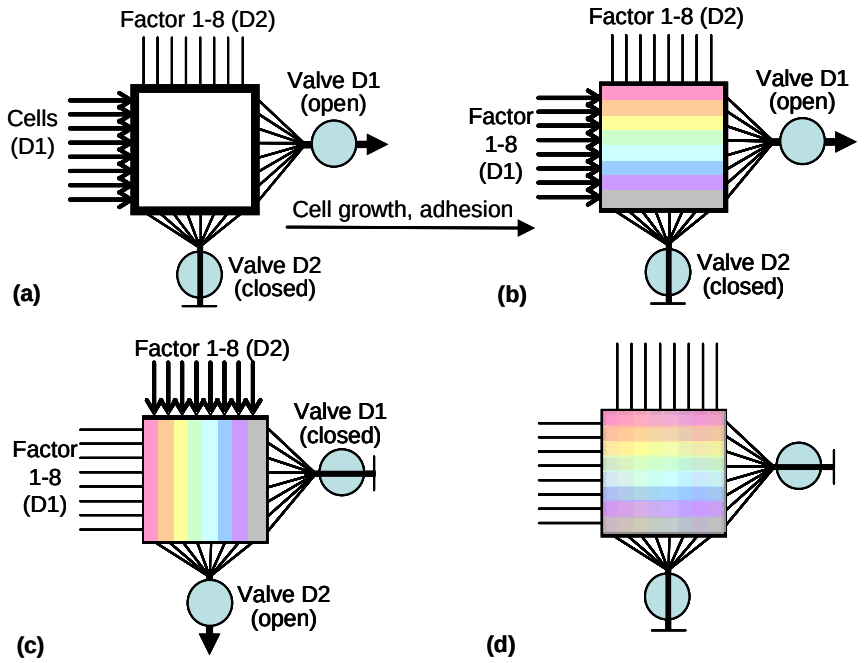

Figure 44. Original project basis. Following cell loading, (a), and use of perpendicular flows in two directions, (b) and (c), a multiplexed experimental microfluidic cell culture chip results. Refer to Chapter 1 for a more complete description.

Given both internal and community-wide concerns related to interfacing of microfluidic devices and setups, the development of a microfluidic system, inclusive of peripheral components, applicable to many projects, and which addresses end-user issues was thought more beneficial to the research community at large (not solely cell culture related) than production of a "single" microfluidic chip. Also, motivation for producing "a" microfluidic cell culture chip as shown in Figure 44 was reduced as microfluidic chips with similar designs and intentions were described [19, 35, 50-58].

The suitability of *SWAN* for microfluidic cell culture using chips with "large" open chambers (Figure 44) or individually addressable cell chambers will be investigated. Variabilities of flows between channels of the same micropump and across micropumps may limit such approaches as hydrodynamic focusing of such streams would be affected. In brief, adjacent streams merging within a single channel or chamber occupy widths proportional to their viscosity and flow rate. Assuming similar viscosities for solutions entering a test chip as shown in Figure 44, due to flow rate variability areas of the cell culture chamber exposed to various factors may be difficult to predict. Additionally, a report by *Cooksey et. al* [51] using open chambers measuring 5 mm x 7 mm x 0.1 mm indicated that flow rates near 4 µL/min are required to sustain parallel laminar flows in open chambers. These flow rates are likely not suited to perfusion experiments requiring expensive or limited volumes of compound. Furthermore, perturbations of flow within the system, e.g. caused by a blocked channel, can lead to erratic and uncontrollable focusing of parallel streams to unwanted regions and a "lost" experiment. This suggests that approaches such as the "microfluidic palette" [50] or the use of individually addressable cell culture chambers may be more successful [53-55]. The "palette" approach is of particular interest. By uncoupling convective flow from delivery channels from diffusion within

an open chamber, it reduces fabrication complexity and can create multiple and dynamic gradients [50]. In either case, both approaches could benefit from the high interconnection capacity of the *SWAN* and the possibility to generate multiplexed experiments.

Involvement of end-users at an earlier stage of the project should have occurred and would likely have brought the project further along with respect to cell culture. However, end-user involvement is not a guarantee of success [59] and can in some cases lead to systems focused on single types of assays and experiments. For the latter, the preliminary list of research partners and their intended use indicate that this is not the case for *SWAN*. *Young et al.* [14] end their review of macro- and microfluidic systems for endothelial cell biology by stating that the revolution, or transition, from macro-to microfluidic experiments will be facilitated by engineers who design with the biologist in mind. This is not enough as it proposes and implies a distant relationship between engineer and biologist where they are not working closely together. Prominent adoption of microfluidic devices will occur as more biologists and engineers are embedded within the same project and are made to work alongside each other to achieve project goals. Project leaders must also recognize that this necessitates recruitment of proper personnel, competencies and resources and co-ordination of project activities.

REFERENCES

1. Snakenborg, D., et al., *A fast and reliable way to establish fluidic connections to planar microchips.* Journal of Micromechanics and Microengineering, 2007. **17**(1): p. 98-103.
2. Yang, Z. and R. Maeda, *A world-to-chip socket for microfluidic prototype development.* Electrophoresis, 2002. **23**(20): p. 3474-3478.
3. Yang, Z. and R. Maeda. *Socket with built-in valves for the interconnection of microfluidic chips to macro constituents*. 2003.
4. Sabourin, D., D. Snakenborg, and M. Dufva, *Interconnection blocks: a method for providing reusable, rapid, multiple, aligned and planar microfluidic interconnections.* Journal of Micromechanics and Microengineering, 2009. **19**(3).
5. Wu, M.H., S.B. Huang, and G.B. Lee, *Microfluidic cell culture systems for drug research.* Lab on a Chip, 2010. **10**(8): p. 939-956.
6. Yuen, P.K., et al., *Multidimensional modular microfluidic system.* Lab on a Chip, 2009. **9**(22): p. 3303-3305.
7. Jovic, A., B. Howell, and S. Takayama, *Timing is everything: using fluidics to understand the role of temporal dynamics in cellular systems.* Microfluidics and Nanofluidics, 2009. **6**(6): p. 717-729.
8. Inman, W., et al., *Design, modeling and fabrication of a constant flow pneumatic micropump.* Journal of Micromechanics and Microengineering, 2007. **17**(5): p. 891-899.

9. Lewis, D., *Nano Flow Precision with a Peristaltic Pump! Exceeding Conventional Flow Limits Using Electronic Feedback.* Oral Presentation, Labautomation 2010, Palm Springs, CA, 2010.
10. Fadl, A., et al., *The effect of the microfluidic diodicity on the efficiency of valve-less rectification micropumps using Lattice Boltzmann Method.* Microsystem Technologies-Micro-and Nanosystems-Information Storage and Processing Systems, 2009. **15**(9): p. 1379-1387.
11. Tung, Y.C., et al., *Small volume low mechanical stress cytometry using computer-controlled Braille display microfluidics.* Lab on a Chip, 2007. **7**(11): p. 1497-1503.
12. Mukhopadhyay, R., *When PDMS isn't the best.* Analytical Chemistry, 2007. **79**(9): p. 3249-3253.
13. Whitesides, G.M., *The origins and the future of microfluidics.* Nature, 2006. **442**(7101): p. 368-373.
14. Young, E.W.K. and C.A. Simmons, *Macro- and microscale fluid flow systems for endothelial cell biology.* Lab on a Chip, 2010. **10**(2): p. 143-160.
15. Toepke, M.W. and D.J. Beebe, *PDMS absorption of small molecules and consequences in microfluidic applications.* Lab on a Chip, 2006. **6**(12): p. 1484-1486.
16. Heo, Y.S., et al., *Characterization and resolution of evaporation-mediated osmolality shifts that constrain microfluidic cell culture in poly(dimethylsiloxane) devices.* Analytical Chemistry, 2007. **79**(3): p. 1126-1134.
17. Regehr, K.J., et al., *Biological implications of polydimethylsiloxane-based microfluidic cell culture.* Lab on a Chip, 2009. **9**(15): p. 2132-2139.
18. Saarela, V., et al., *Re-usable multi-inlet PDMS fluidic connector.* Sensors and Actuators B-Chemical, 2006. **114**(1): p. 552-557.
19. Gomez-Sjoberg, R., et al., *Versatile, fully automated, microfluidic cell culture system.* Analytical Chemistry, 2007. **79**(22): p. 8557-8563.
20. Randall, G.C. and P.S. Doyle, *Permeation-driven flow in poly(dimethylsiloxane) microfluidic devices.* Proceedings of the National Academy of Sciences of the United States of America, 2005. **102**(31): p. 10813-10818.
21. www.minco.com.
22. Klapperich, C.M., *Microfluidic diagnostics: time for industry standards.* Expert Review of Medical Devices, 2009. **6**(3): p. 211-213.
23. Fujii, T., et al., *A plug and play microfluidic device.* Lab on a Chip, 2003. **3**(3): p. 193-197.
24. Perozziello, G., F. Bundgaard, and O. Geschke, *Fluidic interconnections for microfluidic systems: A new integrated fluidic interconnection allowing plug 'n' play functionality.* Sensors and Actuators B-Chemical, 2008. **130**(2): p. 947-953.
25. Rhee, M. and M.A. Burns, *Microfluidic assembly blocks.* Lab on a Chip, 2008. **8**(8): p. 1365-1373.
26. www.epigem.co.uk.
27. www.labsmith.com.
28. www.thinxxs.com.

29. Andersson, H. and A. van den Berg, *Where are the biologists? A series of mini-reviews covering new trends in fundamental and applied research, and potential applications of miniaturised technologies.* Lab on a Chip, 2006. **6**(4): p. 467-470.
30. Dufva, M. and D. Sabourin, *A biologist's guide to programmable cell culture, manuscript submitted.* Integrated Biology, 2010.
31. www.excell.nu.
32. Coman, V., et al., *Bioelectrochemical probing of intracellular redox processes in living yeast cells using a microfluidic electrochemical sensor array, Oral presentation, Biosensors Europe 2010, Glasgow, Scotland.* 2010.
33. Mark, D., et al., *Microfluidic lab-on-a-chip platforms: requirements, characteristics and applications.* Chemical Society Reviews, 2010. **39**(3): p. 1153-1182.
34. Haeberle, S. and R. Zengerle, *Microfluidic platforms for lab-on-a-chip applications.* Lab on a Chip, 2007. **7**(9): p. 1094-1110.
35. Taylor, R.J., et al., *Dynamic analysis of MAPK signaling using a high-throughput microfluidic single-cell imaging platform.* Proceedings of the National Academy of Sciences of the United States of America, 2009. **106**(10): p. 3758-3763.
36. Unger, M.A., et al., *Monolithic microfabricated valves and pumps by multilayer soft lithography.* Science, 2000. **288**(5463): p. 113-116.
37. Young, E.W.K. and D.J. Beebe, *Fundamentals of microfluidic cell culture in controlled microenvironments.* Chemical Society Reviews, 2010. **39**(3): p. 1036-1048.
38. Futai, N., et al., *Handheld recirculation system and customized media for microfluidic cell culture.* Lab on a Chip, 2006. **6**(1): p. 149-154.
39. Gu, W., et al., *Computerized microfluidic cell culture using elastomeric channels and Braille displays.* Proceedings of the National Academy of Sciences of the United States of America, 2004. **101**(45): p. 15861-15866.
40. Meyvantsson, I., et al., *Automated cell culture in high density tubeless microfluidic device arrays.* Lab on a Chip, 2008. **8**(5): p. 717-724.
41. Puccinelli, J.P., X. Su, and D.J. Beebe, *Automated High-Throughput Microchannel Assays for Cell Biology: Operational Optimization and Characterization.* Journal of the Association for Laboratory Automation, 2010. **15**(1): p. 25-32.
42. Yu, H.M., C.M. Alexander, and D.J. Beebe, *A plate reader-compatible microchannel array for cell biology assays.* Lab on a Chip, 2007. **7**(3): p. 388-391.
43. Sabourin, D., et al., *Microfluidic DNA microarrays in PMMA chips: streamlined fabrication via simultaneous DNA immobilization and bonding activation by brief UV exposure* Biomedical Microdevices, 2010: p. 9.
44. Paguirigan, A.L. and D.J. Beebe, *From the cellular perspective: exploring differences in the cellular baseline in macroscale and microfluidic cultures.* Integrative Biology, 2009. **1**(2): p. 182-195.
45. Stangegaard, M., et al., *Whole genome expression profiling using DNA microarray for determining biocompatibility of polymeric surfaces.* Molecular Biosystems, 2006. **2**(9): p. 421-428.

46. Kang, E., et al., *A hemispherical microfluidic channel for the trapping and passive dissipation of microbubbles.* Journal of Micromechanics and Microengineering, 2010. **20**(4).
47. Sung, J.H. and M.L. Shuler, *Prevention of air bubble formation in a microfluidic perfusion cell culture system using a microscale bubble trap.* Biomedical Microdevices, 2009. **11**(4): p. 731-738.
48. Hibara, A., et al., *Surface modification method of microchannels for gas-liquid two-phase flow in microchips.* Analytical Chemistry, 2005. **77**(3): p. 943-947.
49. Kim, L., et al., *A practical guide to microfluidic perfusion culture of adherent mammalian cells.* Lab on a Chip, 2007. **7**(6): p. 681-694.
50. Atencia, J., J. Morrow, and L.E. Locascio, *The microfluidic palette: A diffusive gradient generator with spatio-temporal control.* Lab on a Chip, 2009. **9**(18): p. 2707-2714.
51. Cooksey, G.A., C.G. Sip, and A. Folch, *A multi-purpose microfluidic perfusion system with combinatorial choice of inputs, mixtures, gradient patterns, and flow rates.* Lab on a Chip, 2009. **9**(3): p. 417-426.
52. Greve, F., et al., *A hybrid microsystem for parallel perfusion experiments on living cells.* Journal of Micromechanics and Microengineering, 2007. **17**(8): p. 1721-1730.
53. Hung, P.J., et al., *A novel high aspect ratio microfluidic design to provide a stable and uniform microenvironment for cell growth in a high throughput mammalian cell culture array.* Lab on a Chip, 2005. **5**(1): p. 44-48.
54. Hung, P.J., et al., *Continuous perfusion microfluidic cell culture array for high-throughput cell-based assays.* Biotechnology and Bioengineering, 2005. **89**(1): p. 1-8.
55. Lee, P.J., et al., *Nanoliter scale microbioreactor array for quantitative cell biology.* Biotechnology and Bioengineering, 2006. **94**(1): p. 5-14.
56. Park, E.S., et al., *Continuously perfused, non-cross-contaminating microfluidic chamber array for studying cellular responses to orthogonal combinations of matrix and soluble signals.* Lab on a Chip, 2010. **10**(5): p. 571-580.
57. Sugiura, S., et al., *Pressure-driven perfusion culture microchamber array for a parallel drug cytotoxicity assay.* Biotechnology and Bioengineering, 2008. **100**(6): p. 1156-1165.
58. Tourovskaia, A., X. Figueroa-Masot, and A. Folch, *Differentiation-on-a-chip: A microfluidic platform for long-term cell culture studies.* Lab on a Chip, 2005. **5**(1): p. 14-19.
59. Wilding, P., et al., *Microtechnology in the Clinical Laboratory: Will It Solve Analytical Problems, and When Will It Make an Impact?* Clinical Chemistry, 2010. **56**(4): p. 508-514.

CHAPTER 6: SIDE PROJECTS

A. INTRODUCTION

Development of fabrication competencies allowed several side projects, not directly related to project objectives, to be undertaken during the period of study. Three such side projects are described in this chapter. The first of these merged the fabrication competencies with microarray development and processing knowledge of the *FAST* group. This project aimed to create a method to facilitate cell localization within wholly polymeric microfluidic cell culture chips. The two other projects involved manufacture of devices for groups outside of DTU Nanotech. In both cases, the devices were made by casting PDMS within micromilled moulds. These devices further demonstrate that micromilling, a simple and practical machining method, can be used to generate devices which are of use to, and can address applications of interest to the research community.

B. TOWARDS CELL LOCALIZATION

Reproducible placement, immobilization and compartmentalization of cells within defined areas or regions of microfluidic cell culture devices remain a challenge. The ability to control cell placement within microfluidic devices directly impacts the ability to reliably deliver spatial and temporal cues to cells, and hence also impacts programming and recording of cellular response [1]. Resolution of this obstruction should lead to assays which are more reproducible, demonstrate increased functionality and benefit applications related to cellular analyses, cell-based sensing and tissue engineering. For example, increased sensitivity is expected for cell-based sensing as cells could be placed closer to sensors, e.g. electrochemical sensors and with respect to tissue engineering, arrangement of different cell types into cellular mosaics and architectures resembling those found *in vivo* may result in more meaningful *in vitro* experimental results [2, 3].

With respect to the original project objective of creating a multiplexed cell culture chamber (Figure 44, Chapter 5), cellular patterning represents another method to increasing the multiplexing capacity of cell culture chambers. These methods could provide means to more finely control and establish cue delivery to cells. There are three general methods used to control cellular location within microfluidic devices. These are: i) chemical patterning of surfaces, ii) use of topographical features to trap cells, and iii) directed delivery of cells to discrete locations [2-4].

Chemical treatments of surfaces can influence parameters known to affect cellular adhesion including surface charge, wettability, and chemistry [3, 5]. Photolithographic and soft lithography approaches are commonly used to chemically pattern cell culture surface areas. In brief, photolithography patterns light-sensitive materials onto substrates by means of irradiation through a photomask. Soft

lithographic approaches use a master which has been topographically patterned by photolithographic methods to create an elastomeric, e.g. PDMS, stamp by casting methods [6, 7]. The resulting stamp is a negative image of the master. In microcontact printing, raised features of the elastomeric stamp are inked with various chemicals. When the stamp is pressed against a substrate, micropatterns of chemical that enhance or block cellular adhesion are transferred to the surface of the substrate [4]. Microfluidic patterning can also use stamps which contain fluidic channels and networks. Pressing the stamp to the substrate seals the stamp's channels. Fluids containing chemicals of interest can be injected into the stamp's channels and thus pattern the substrate [4].

The use of topographical features, patterns of microstructures, such as wells and weirs, within microfluidic devices have also been used to pattern cells. Various microstructures have been reported which allow physical isolation of single cells or groups of cells [3, 8, 9]. PDMS stencils have also been used to pattern cells [10]. In this approach, a stencil containing througholes is placed on top of the substrate to be patterned. Coating the stencil with cells allows cells to only contact the substrate in the location of the throughholes. The stencil is subsequently peeled off and cells only remain in the area of the throughholes.

Directing cells to discrete locations or regions of a substrate include direct arraying of cells via typical microspotting and arraying equipment [11] and the use of membrane containing devices to hydrodynamically pattern cells [12]. Recently a method for localizing cells using DNA-barcoding has been described [13, 14]. The first step of the process involves chemical treatment of cells to covalently attach a specific single stranded DNA (ssDNA) to a cell surface receptor. The ssDNA serves as a bar code for a specific cell type and each cell type can be assigned a distinct bar-coding DNA sequence. The surface to which the cells are to be attached is then patterned with ssDNAs complementary to particular cell types. This can be accomplished with standard microarraying equipment. When barcoded cells are flowed over areas of the microfluidic device patterned with ssDNAs complementary to the cells ssDNA, a DNA hybridization reaction occurs and the cells are localized/immobilized. This method demonstrated control of placement of both adherent and non-adherent cell types. As one of the core competencies of the *FAST* group (DTU Nanotech) is microarray processing and DNA hybridization research, this method was of particular interest.

A disadvantage of the previously described approach was the long incubation times, greater than 3 days, required to covalently attach the DNA bar code to cells. Work within *FAST* attempts, when and where possible, to limit exposure of cells to unnatural environments such as the chemical treatment required to bar-code cells. To circumvent this extended incubation step and to take a more natural approach, it was thought that a cell localization approach based on aptamers may be possible.

Aptamers are short artificial ligand-binding nucleic acid sequences [15, 16]. Aptamers demonstrate affinity for many different types of target including peptides, proteins, drugs, organic and inorganic molecules and whole cells [16]. Classically,

aptamers are identified by a process called Systematic Evaluation of Ligands by Exponential enrichment (SELEX). A comprehensive description of SELEX is provided elsewhere [16]. For several, and very practial reasons, aptamers have become of increasing interest [17]. In many cases the affinity of aptamers for their ligands is equal to or surpasses the affinity of monoclonal antibodies [15, 16]. Furthermore, aptamers show increased promise for analytical applications because they are easily synthesized, readily functionalized with reporter molecules, and demonstrate robustness [15, 16].

Recently *FAST* has demonstrated the direct and rapid immobilization of DNA probes containing a poly(T)poly(C) tag to various substrates *via* UV exposure [18, 19]. Direct attachment of DNA probes containing this tag to different substrates including agarose, bare glass and unmodified PMMA was demonstrated. A cost-efficient microarray based method for detection of human beta-globin gene (HBB) related mutations which used the poly(T)poly(C) tag to attach DNA probes to agarose-covered slides was also validated by *FAST* members [20, 21]. At this same time, exposure to UV was being used during the project as a method of bonding PMMA devices (Chapter 1). It was hypothesized that it may be possible to combine the immobilization of TC-tagged aptamers onto unmodified PMMA and simultaneously activate the surface of unmodified PMMA for bonding below the bulk *Tg* of PMMA. If so, enclosed, microfluidically addressable arrays of aptamers could be constructed within entirely PMMA (the material specified for research in this thesis) devices, without use of chemical or adhesive agents, and a potential method for controlling cellular location therein could result.

As UV treatment results in DNA damage, the central concern at the onset of investigations was whether a UV exposure could be found which would facilitate low temperature bonding without rendering the DNA unselective and non-functional. Using the UV source previously reported for TC-tag immobilization on PMMA, UV exposure beyond points known to irreversibly damage DNA [22] (H. Gudnason, DTU Nanotech, unpublished data) did not sufficiently activate PMMA to permit bonding (unpublished results). As a different and stronger UV exposure (DYMAX EC 5000 with p/n 36970 bulb, Torrington, Connecticut) was being used for PMMA bonding initial investigations should focus on the effects of this light source on DNA probes. Rather than use new DNA probes, i.e. those containing aptameric sequences, and for which the group had no prior knowledge with respect to expected behaviour, the probes used for HBB diagnostic array validation [20, 21] mentioned above would be used as the model system. More specifically, as probe immobilization alone does not validate probe functionality post-UV treatment, the functionality and selectivity of the microarrays containing the immobilized probes would be tested via an allele specific hybridization (ASH) to segments of the HBB containing mutations. For this ASH assay, patient samples were used. The hypothesis was that if ASH worked, probe function was retained to a high degree and the method would be suitable for immobilization of aptamers.

Although initially meant as a study to investigate potential applicability of the TC-tag approach to cell localization within PMMA microfluidic devices, the study provided a

streamlined fabrication method suited to production of low-cost microfluidic microarray-based diagnostic devices equally applicable to the development of diagnostics for both resource rich and resource limited settings. This work was described in the following article published during the project:

Publication 5

Sabourin, D. *, Petersen, J. *, Snakenborg, D., Brivio, M., Gudnadson, H., Wolff, A. and Dufva, M. *"Microfluidic DNA microarrays in PMMA chips: streamlined fabrication via simultaneous DNA immobilization and bonding activation by brief UV exposure"*, Biomedical Microdevices, doi: 10.1007/s10544-010-9420-7

Detailed descriptions of hybridization methods and materials, analysis methods and further discussion of fabrication, genotyping and implication of the method to diagnostics in general are found in the full article located in Appendix A. Descriptions below focus on manufacture of the arrays as this is most relevant to cell localization.

B.1 First Steps

Microarrays enable parallel analysis of biological variation, via DNA, RNA or protein that are spotted and attached to a solid support. Microarrays hold great promise for, and can significantly impact, global health as they can be used for biosafety, diagnostic and preventative care applications. The suitability of PMMA as a microarray support has been investigated by several groups [23-32]. Chemical modification [23-26, 31, 32] and UV exposure [27-30] have been used to attach nucleic acids to the surface of PMMA. Though there are many advantages of merging microarrays with microfluidic approaches [33], including significant increases in ease-of-use and handling, and polymeric processes present an opportunity to do so, there are limited reports describing arrays integrated within fluidically addressable channels of entirely polymeric devices [31].

Fabrication of the enclosed microarrays is described in Figure 45. Two 0.5 mm thick PMMA layers were milled to be i) a featureless microscope slide and ii) a microscope slide containing eight 250 µm deep channels bookended with 1 mm diameter througholes (fluidic inlets and outlets). Allele-specific DNA probes, with a poly(T)10–poly(C)10 tag (TC tag) in the 5' end, were designed for genotyping small genetic variations in the HBB. For each of the 8 HBB mutagenic sites investigated, the probe set contains a wild-type (WT) and a mutant (MT) probe. WT refers to the non-disease causing nucleic acid sequence present in the majority of the population. The DNA probes were spotted onto the featureless PMMA layer using a commercially available spotter (GeSim, Germany). Both the featureless and channel-containing PMMA piece were then exposed to UV light and subsequently bonded.

* Co-first authors

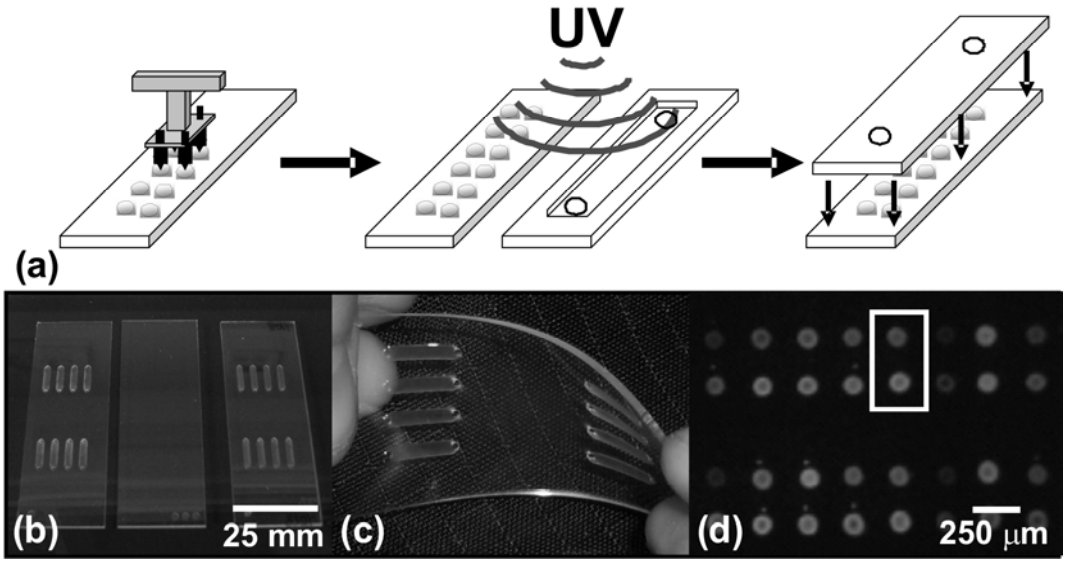

Figure 45. PMMA microfluidic microarray construction. (a) Schematic representation of PMMA microfluidic array manufacture. A featureless 0.5 mm thick PMMA layer, sized identically to a microscope, slide is spotted with poly(T)-poly(C)-tagged DNA probes. The spotted layer and a second 0.5 mm thick PMMA layer, containing channels and througholes for sample introduction and removal, are then placed with bonding surfaces facing a UV source. Channels in the second PMMA layer are spaced according to 384 well plate standards. Both layers are exposed to UV for 30 sec. and are subsequently bonded in a bonding press at 85°C for 1 hr. (b) The two 0.5 mm PMMA layers used to create the enclosed microarray device are shown on the left and in the centre. A bonded and completed enclosed PMMA microarray structure is shown to the right. (c) Twisting of the completed device did not result in delamination. (d) Two of four replicate subarrays found within each channel of the fluidic array made in PMMA. MT probes are found in the 1st and 3rd rows from the top, WT in the 2nd and 4th. Probe pairs for each mutagenic site were grouped as shown by the example rectangle.

18 patients were tested via the multi-salinity gradient method [20, 34]. For the 8 mutagenic sites investigated, use of a PMMA array together with the multi-salinity gradient method correctly identified the genotypes of all 18 patients for each mutagenic site. The original diagnosis of the patients used in the study was made by measuring the level of HbA2 by high-performance liquid chromatography (HPLC) and genotyping by automated DNA sequencing. The ASH assay's correct genotyping of all patients confirmed functionality of the microarrays and probe specificity retention following UV exposure.

As compared to chemical methods [23-26, 31, 32], the use of UV to directly immobilize TC tagged probes to unmodified PMMA surface is more rapid and streamlined method as it removes the processing step(s) required to prepare the PMMA surface for subsequent probe immobilization. Potentially harsh and/or toxic chemicals are avoided. *Kimura* and *Soper et al*. previously reported the use of UV exposure to immobilize DNA arrays on PMMA [27, 30]. *Soper et al.* used an initial UV treatment of 5 to 30 minutes to carboxylate PMMA [30]. This UV treatment is longer and, in contrast to our method whereby UV treatment directly immobilizes DNA to unmodified surface, is used to create a scaffold onto which probes in an EDC solution are spotted. *Kimura* attached DNA probes containing a poly(T) and undisclosed spacer sequence to the surface of unmodified PMMA [27] while we use a known, fully described and easily incorporated probe tag.

Glues and/or adhesive films (e.g. double-sided tape) could also have been used to assemble the enclosed microarray. As with chemical treatments, these add steps, materials and/or labour to the fabrication process and their use can lead to manufacturing defects resulting from, for example, tape ooze. Additionally, the composition of these materials may not be well defined and may result in sensitivity and detection problems by either absorption of reacting species and/or general biocompatibility [35]. In the case of reactions carried out at more elevated temperature, the release of volatiles from such materials may be especially problematic. The use of UV-assisted bonding avoids these potential issues and a streamlined, scalable process for the mass production of functional microarrays enclosed within PMMA microstructures results. As described in Chapter 1 UV-assisted bonding [36] has advantages over both solvent and thermal bonding of PMMA and permits sealing without loss in structure quality. The manufacture of arrays within very small channels, potentially required due to small sample volume requirements, is enabled while minimizing device yield loss.

B.2 Next Steps

The conservation of probe function within the PMMA-based microarrays described above indicated that use of UV to immobilize TC-tagged aptameric sequences within PMMA devices and subsequently localize cells remained a possibility. One of the most studied and characterized aptameric sequence is the 15-mer, GGTTGGTGTGGTTGG, which binds to thrombin and inhibits its role in the blood clotting cascade [37-39]. As required thrombin reagents were readily available, and as work with cells is more involved, TC-tagged thrombin aptameric sequence were used for initial studies involving recognition by intended target molecules (i.e. thrombin). Such a study could also provide insights into the effects of the same UV treatment on DNA-protein based interactions as these may differ from wholly nucleotide based reactions previously investigated. In short, due to problems with the spotting machine and time constraints associated with the Ph.D., the study was not completed and only initial results were obtained. As such, a brief description of the experimental device produced, preliminary results and applicability of the approach/device to aptamer research is provided.

B.2.1 Device Manufacture

PMMA layers were milled to the size of microscope slides and to contain channels identical to those described in Section B.1. In this case UV bonded PMMA devices sized identically to microscope slides contained 25 individual channels and spaced according to 384-well plate standards were created. Figure 46 shows a completed, and bonded device.

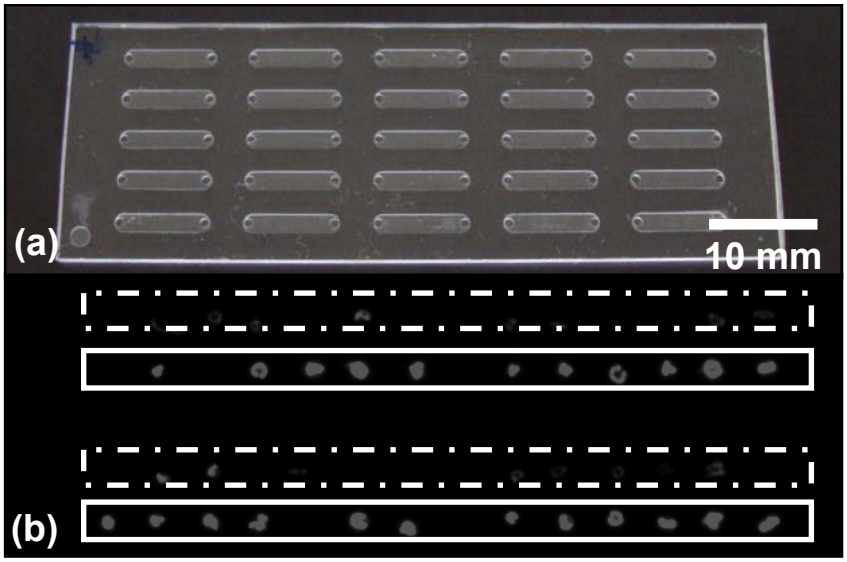

Figure 46. PMMA device used for initial aptamer based studies. (a) Bonded PMMA device with 25 channels spaced at 384 well plate standards. Microarrays of TC-tagged aptameric and scrambled sequences are found within each channel. (b) Sample hybridization result. Microarrays found within each channel of the device contained spots for aptameric (solid line box) and scrambled sequences (dashed line box). Spot sizes are approximately 250 µm. Visualization of hybridization of biotyinlated thrombin was enabled by use of strep-cy3. The results shown are from an experimental condition in which PMMA components were UV irradiated for 60 sec. and where a solution containing 2 µm thrombin in 1 X PBS was hybridized within a channel that was previously blocked with a 1% BSA in 1 X SSC solution.

Within each of the individual channels, 12 different oligonucleotide sequences (Appendix D) were spotted in four replicates. Oligonucleotide sequences were ordered which belonged to two general classes: aptamer and scrambled. The aptamer class had the proper thrombin recognition sequence whereas the scrambled sequences contained no particular sequence. The aptamer and scrambled sequences were also ordered in permutations containing different TC-tag and spacer sequences in order to investigate the effects thereof. Spacer sequence length has previously been shown to influence hybridization efficiency [34].

Figure 46 shows an image taken following hybridization of the aptameric sequence containing microarrays. 2 µM biotinylated thrombin (HCT-BFPRCK, Haemotologic Technologies Inc, Vermont) in 1 X PBS solution was incubated in the chamber for 1 hour at 37°C. Channels were then rinsed with 1 X PBS. In order to visualize and quantify thrombin reactions, strepavidin-cy3 (Sigma Aldrich) was diluted in a 1:50 ratio in 1 X PBS and allowed placed in the channel for 1 hour at 37°C. Channels to which the strepavidin-cy3 solutions were added were then rinsed twice with one system volume of 1 X PBS at RT. Hybridization reactions were imaged on a microscope (ZEISS Axioscope).

The hybridization reaction image shown in Figure 46 shows some thrombin specificity towards sequences containing the thrombin aptamer sequence as opposed to the scrambled thrombin aptamer sequence. This preliminary result provides motivation for continuation of this work with respect to both aptameric research and cell localization.

Reports describe that aptamer research is currently limited with respect to the investigation of effects related to temperature and buffer composition, e.g. ion concentration [15, 17]. As similarly occurred with transfer of oligonucleotide hybridization reactions from solution states to solid supports [20, 34], surface effects may result in discrepancies and deviations from expected binding capacity and specificity of aptamers.

The device shown in Figure 46, containing 25 individually addressable aptamer microarrays, provides a method to simultaneously screen and investigate many experimental parameters simultaneously related to aptamer performance. Factors affecting hybridization efficiency which are likely most easily investigated include the effect of i) blocking solutions and ii) ionic concentration [15]. Reduction of non-specific binding would aid to determine processing conditions which reduce background to noise ratios and thus increase assay sensitivity. Ionic concentration investigations, a direct parallel of those reported by *FAST* in previous publications [20, 34] and in the ASH assay described in Section B, could be repeated in order to determine ionic conditions at which individual aptamers function best. Simultaneous processing of aptamer array panels and analysis thereof based on multi-salinity gradients could lead to devices which simultaneously detect multiple analytes. It is important to note the caveat that such data would be relevant only to PMMA-based devices. These are however amenable to mass production and deployment.

Samples were introduced into the channels of the device shown in Figure 46 by capillary force. While this may be onerous for manual introduction and removal of samples, it is certainly feasible with automated fluidic handling equipment. Additionally, as PMMA samples can be shaped and dimensioned at will, larger devices containing even greater number of microfluidically addressable microarrays could be easily fabricated.

With respect to cell localization, if not an aptameric approach, then at the least use of TC-tagged probes and UV exposure to create immobilized DNA probes within enclosed fluidic devices which could “locate” and bind cells according to the previously described DNA bar-coding method [13, 14] should be pursued. Additionally, studies which investigate the use of aptameric sequences reported to recognize whole cell types should be considered. A suggested starting point is investigation of whether the aptamer sequences reported as recognizing differentiated and undifferentiated PC12 cells [40] can recognize these same cell types within PMMA microfluidic devices according to the method proposed above.

C. Rapid Fabrication of Microwells for Cell-Based Studies

The Department of Biochemistry, Institute of Medical Biochemistry, University of Oslo, Norway, a partner in the ProCell project (Section C, Chapter 5), requested aid in fabricating arrayed microwells in PDMS. The microwells were to be used to monitor differentiation in adult mesenchymal stem cells (MSC) isolated from human adipose tissue and induced to differentiate into adipocytes.

The microwells were to have a footprint of approximately 100 µm x 100 µm, and a minimum depth of 20 µm. The PDMS parts containing the microwells were to then be affixed to glass-bottomed Petri dishes (Mattek, Maryland, USA). In order to conserve optical quality, the bottom of the microwells should be free of PDMS. The finished device was intended for static cell culture. Cells would be placed within the Petri dish, above the PDMS part and allowed to settle into microwells. This method of use thus required that microwells have an open structure: that both top, for introduction of cells, and bottom, for visualization and imaging of the cells, of the microwells be free of PDMS.

Feature dimensions such as those requested are usually made by casting PDMS over silicon wafers which contain photolithographically patterned SU-8 features (Figure 47 a-c). When using this casting approach, normally one of either the top or bottom faces of the channel or well is made from PDMS.

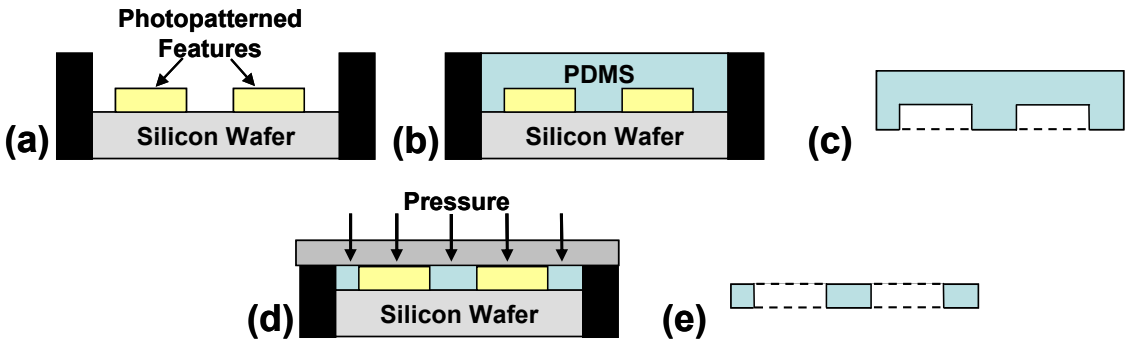

Figure 47. **PDMS casting procedures.** (a) A silicon wafer (master) is photolithographically patterned. Topographical features result. (b) PDMS is poured over the wafer and cured. (c) Following demoulding the PDMS part is removed and a negative image of the master results. In this case, the top surface of "void" features is made of PDMS. (d) In order to create open structures, thin films (not shown) can be placed on top of the photopatterned features of the master. When PDMS is poured over and pressure applied, open structures can result as shown in (e).

The use of microfluidic stencils to create open well structures has been reported. This method (Figure 46d and e) also uses a silicon wafer with photolithographically patterned SU-8 features. After PDMS is poured over the wafer, a thin film is placed on top of the wafer and pressure is applied by a top plate during the curing process. *Cho et al.* [10] used this approach to create a stencil containing arrays of 500 µm diameter wells. The stencil was used to pattern hepatocyte and fibroblast co-cultures. A variation of this method was used to create the requested microwells, however a micromilled aluminium mould was used in lieu of a photopatterned silicon wafer.

Aluminium moulds were patterned to feature two-tiered pillars with top sections measuring 100 µm (*w*) x 100 µm (*l*) x 75 µm (*h*) placed on top of 250 µm (*w*) x 250 µm (*l*) x 250 µm (*h*) sections (Figure 48). The two-tiered pillar structure results in a two-stage microwell when PDMS is cast (Figure 48).

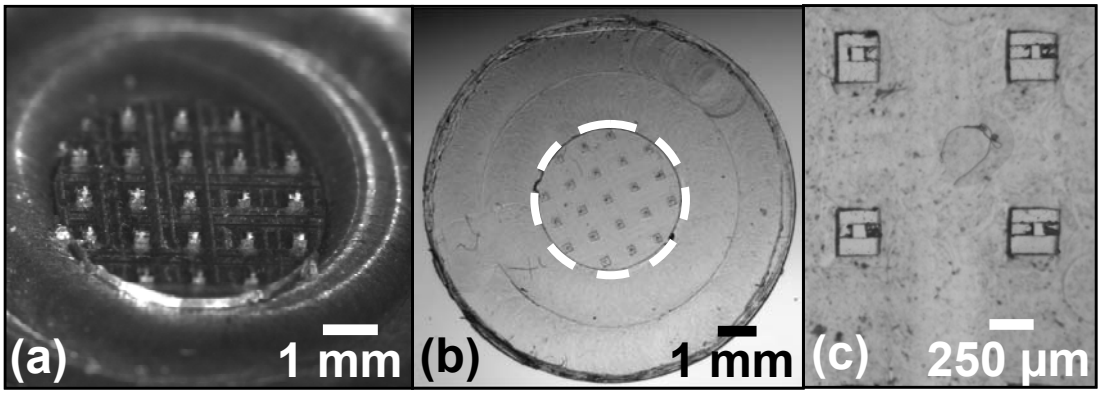

Figure 48. Arrayed microwells in PDMS. (a) Micromilled aluminium mould. (b) PDMS part containing arrayed microwells. (c) Close-up of microwell features. Note two-stage design with smaller inner well within larger outer well.

The aluminium moulds contained 2 mm alignment holes. To provide open structure microwells, a PMMA lid was fastened to the top of the mould with 2 mm screws. The PMMA lid also contained 2 mm holes allowing the injection of PDMS. Aluminium foil was intercalated between the PMMA lid and the mould and the screws were tightened until the foil could be seen to be marked by the top of the features defining the microwells. This ensures that PDMS is not found on the bottom of the well features. PDMS was injected and cured. The PDMS parts were bonded to glass-bottomed Petri dishes using a hand-held corona treatment [41].

For validation purposes, an immortal human epithelial cell line stably carrying a fluorescently tagged Histone 2B construct (HeLa $^{H2B\text{-}GFP}$) [42] was used. Growth medium was first added to the Petri dish and a tip sonicator was used to remove air bubbles trapped inside the microwells. Cell suspensions were added to the top of the PDMS part and cells were allowed to settle into the microwells for 5 minutes. An image of the HeLa $^{H2B\text{-}GFP}$ cells within a microwell is shown in Figure 49. The description of the use of intercalated aluminium foil and of procedures following casting of the PDMS component were provided courtesy of Qamar Ali and Thomas Kuntzinger from Philippe Collas' group at the University of Oslo, Norway.

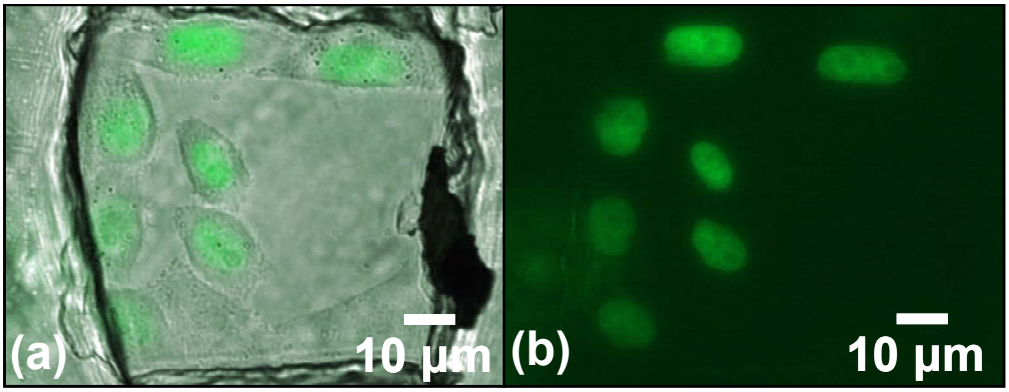

Figure 49. Cell imaging within microwells. Imaged HeLa $^{H2B\text{-}GFP}$ shown in merge of transmitted light and EGFP fluorescence (a), and EGFP fluorescence (b). Photo courtesy of T. Kuntzinger, Department of Biochemistry, Institute of Medical Biochemistry, University of Oslo, Norway.

As Figure 49 shows, the edges of the microwells are not crisply defined. This results from use of micromilling to create the master moulds. This process was not optimized as the goal was to provide the research group in Oslo with a starting point: a functional component which compartmentalizes cells. The imaging of the cells, as shown in Figure 49, by users for periods of up to five days satisfies this objective. Photolithographic processes and/or methods and materials which result in better micromilled moulds may be used in future.

D. Adhesive-Free Biofilm Flow Chamber

The third side project involved work related to biofilm analysis. Flow systems commonly used for biofilm analysis use a polymeric part which has been machined to contained open flow chambers [43]. A typical example is shown in Figure 50.

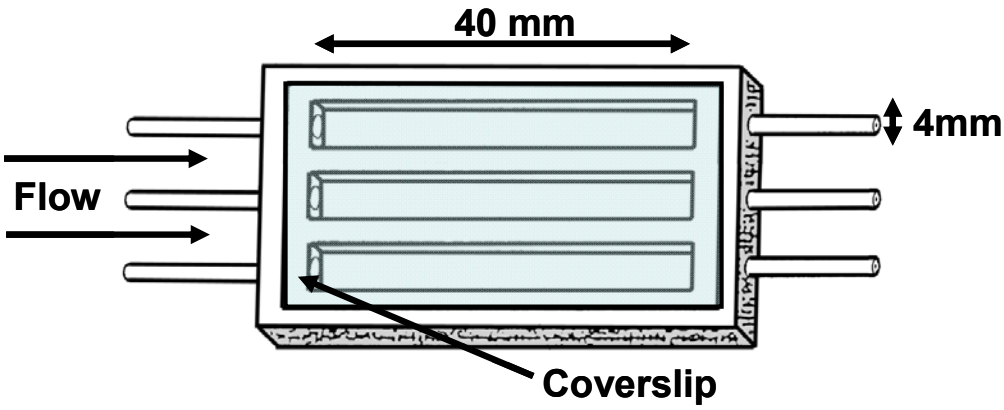

Figure 50. Flow chamber commonly used for biofilm analysis. Image taken from [43].

To seal the flow chambers and permit confocal microscopy observation of cell cultures, a thin glass cover slip is manually affixed to the flow chamber using silicone adhesives. Communications from the ENVIRO DTU group (Jose Seoane, PhD candidate) and personal experience (Biofilms Course, DTU Biosys, 2009) revealed that gluing of the cover slip is a tedious, irreproducible process with potentially low yields. Additionally, as flow chambers contain only 3 chambers, experiments which

require multiple conditions and observation of cultures necessitate multiple flow chambers (and gluing of cover slips) as well as manual switching and placement of flow cells on observation equipment.

To provide a more user friendly device, micromilled moulds were created that allowed creation of a PDMS gasket. The gasket contained 6 open structure chambers measuring approximately 18 mm (*l*) x 4 mm (*w*) x 1 mm (*h*) (Figure 51(b)). The casting process involved the use of fibre inserts as previously described (Section B, Chapter 2) to create integrated inlet and outlet channels leading to 6 open flow chambers. Thicker PDMS sections were found at inlet and outlet areas to provide support for press-fitting of needles used for chip-to-world connectivity. Following curing of the PDMS part, a hand-held corona treater [41] was used to bond glass cover slips to both sides of the gasket. A completed device is shown in Figure 51. Total thickness of the device in the viewing area, including top and bottom glass cover slips, is approximately 1.2 mm.

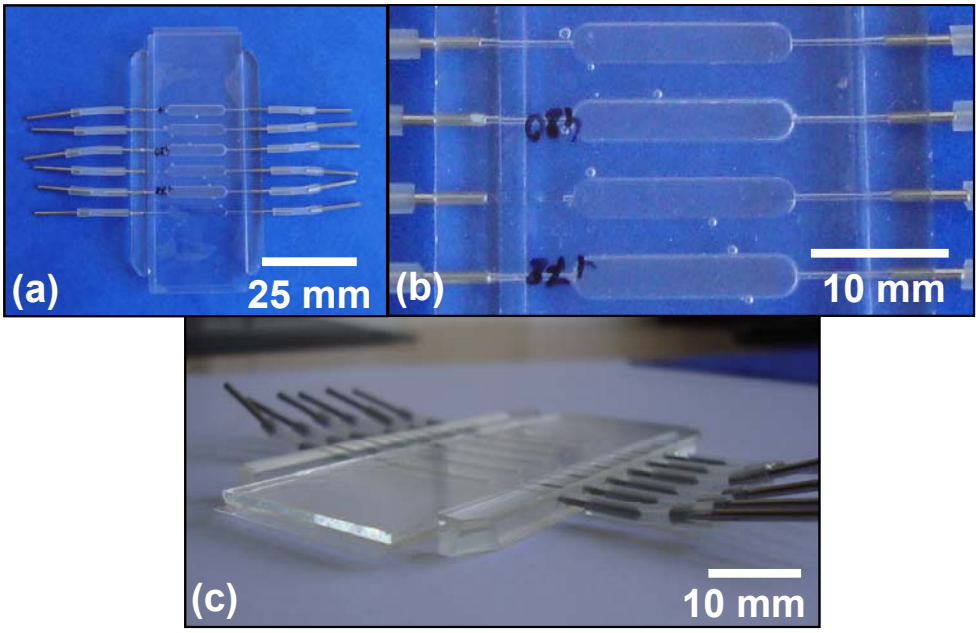

Figure 51. PDMS gasket based biofilm device. (a) Completed device. Blunted needles were press fit into integrated channels providing inlets and outlets to flow chambers (middle). Incomplete bonding, which did not affect usability of the piece shown, results from use of milled surfaces in moulds (see below). (b) Close-up of chambers within the device. Bubbles were formed during the PDMS curing process but did not affect performance. (c) Side profile of device. The thin profile and glass coverslips found on both top and bottom of the PDMS gasket provide good optical characteristics.

The use of cover slips on either side of the device lends very good optical characteristics to the final device. The device shown in Figure 51 has been used by the ENVIRO group for preliminary biofilm experiments using confocal microscopy. In these preliminary experiments biofilm growth was observed and monitored.

Hopefully collaborative efforts between *FAST* and DTU ENVIRO will continue as the device offers the advantages related to adhesive-free devices (Chapter 1) and increased channel numbers. The latter reduces manual intervention required for multi-condition experiments. Future efforts may introduce greater channel numbers

and seek to incorporate a similar device into a *SWAN* configuration. This would greatly reduce the burdensome experimental footprint of typical biofilm experiments. Prototyping of the device revealed that in order to ensure good bonding between the PDMS and the cover slips, mould components forming bonding surfaces should preferable be made of virgin/unmilled PMMA. In future, where this design requirement is difficult to circumvent the use of a chloroform treatment [44] may be used to smooth milled PMMA surfaces.

REFERENCES

1. Dufva, M. and D. Sabourin, *A biologist's guide to programmable cell culture, manuscript submitted.* Integrated Biology, 2010.
2. Nakanishi, J., et al., *Recent advances in cell micropatterning techniques for bioanalytical and biomedical sciences.* Analytical Sciences, 2008. **24**(1): p. 67-72.
3. Wu, M.H., S.B. Huang, and G.B. Lee, *Microfluidic cell culture systems for drug research.* Lab on a Chip, 2010. **10**(8): p. 939-956.
4. Falconnet, D., et al., *Surface engineering approaches to micropattern surfaces for cell-based assays.* Biomaterials, 2006. **27**(16): p. 3044-3063.
5. Stangegaard, M., *A biocompaticle micro cell culture chamber (uCCC) for culturing and on-line monitoring of Eukaryotic cells, Ph.D. Thesis.* MIC - Department of Micro- and Nanotechnology, Technical University of Denmark, 2005.
6. Xia, Y.N. and G.M. Whitesides, *Soft lithography.* Annual Review of Materials Science, 1998. **28**: p. 153-184.
7. Li, N., A. Tourovskaia, and A. Folch, *Biology on a Chip: Microfabrication for Studying the Behaviour of Cultured Cells.* Critical Reviews in Biomedical Engineering, 2003. **31**(5&6): p. 423-488.
8. Hung, P.J., et al., *A novel high aspect ratio microfluidic design to provide a stable and uniform microenvironment for cell growth in a high throughput mammalian cell culture array.* Lab on a Chip, 2005. **5**(1): p. 44-48.
9. Khabiry, M., et al., *Cell Docking in Double Grooves in a Microfluidic Channel.* Small, 2009. **5**(10): p. 1186-1194.
10. Cho, C.H., et al., *Layered patterning of hepatocytes in co-culture systems using microfabricated stencils.* Biotechniques, 2010. **48**(1): p. 47-52.
11. Hook, A.L., H. Thissen, and N.H. Voelcker, *Surface manilpulation of biomolecules for cell microarray applications.* Trends in Biotechnology, 2006. **24**(10): p. 471-477.
12. Torisawa, Y.S., et al., *Microfluidic hydrodynamic cellular patterning for systematic formation of co-culture spheroids.* Integrative Biology, 2009. **1**(11-12): p. 649-654.
13. Chandra, R.A., et al., *Programmable cell adhesion encoded by DNA hybridization.* Angewandte Chemie-International Edition, 2006. **45**(6): p. 896-901.
14. Douglas, E.S., et al., *Self-assembled cellular microarrays patterned using DNA barcodes.* Lab on a Chip, 2007. **7**(11): p. 1442-1448.

15. Cho, E.J., J.W. Lee, and A.D. Ellington, *Applications of Aptamers as Sensors.* Annual Review of Analytical Chemistry, 2009. **2**: p. 241-264.
16. Mairal, T., et al., *Aptamers: molecular tools for analytical applications.* Analytical and Bioanalytical Chemistry, 2008. **390**(4): p. 989-1007.
17. Rowe, W., M. Platt, and P.J.R. Day, *Advances and perspectives in aptamer arrays.* Integrative Biology, 2009. **1**(1): p. 53-58.
18. Dufva, M., et al., *Detection of mutations using microarrays of poly(C)10-poly(T)10 modified DNA probes immobilized on agarose films.* Anal Biochem, 2006. **352**(2): p. 188-97.
19. Gudnason, H., et al., *An inexpensive and simple method for thermally stable immobilization of DNA on an unmodified glass surface: UV linking of poly(T)10-poly(C)10-tagged DNA probes.* Biotechniques, 2008. **45**(3): p. 261-71.
20. Petersen, J., et al., *Microfluidic Device for Creating Ionic Strength Gradients over DNA Microarrays for Efficient DNA Melting Studies and Assay Development.* PLoS ONE, 2009. **4**(3): p. e4808.
21. Petersen, J., et al., *Detection of mutations in the beta-globin gene by colorimetric staining of DNA microarrays visualized by a flatbed scanner.* Anal Biochem, 2007. **360**(1): p. 169-71.
22. Dufva, M., et al., *Characterization of an inexpensive, nontoxic, and highly sensitive microarray substrate.* Biotechniques, 2004. **37**(2): p. 286-92, 294, 296.
23. Banuls, M.J., et al., *PMMA isocyanate-modified digital discs as a support for oligonucleotide-based assays.* Bioconjug Chem, 2007. **18**(5): p. 1408-14.
24. Diaz-Quijada, G.A., et al., *Surface modification of thermoplastics--towards the plastic biochip for high throughput screening devices.* Lab Chip, 2007. **7**(7): p. 856-62.
25. Fixe, F., et al., *One-step immobilization of aminated and thiolated DNA onto poly(methylmethacrylate) (PMMA) substrates.* Lab Chip, 2004. **4**(3): p. 191-5.
26. Fixe, F., et al., *Functionalization of poly(methyl methacrylate) (PMMA) as a substrate for DNA microarrays.* Nucleic Acids Res, 2004. **32**(1): p. e9.
27. Kimura, N., *One-step immobilization of poly(dT)-modified DNA onto non-modified plastic substrates by UV irradiation for microarrays.* Biochem Biophys Res Commun, 2006. **347**(2): p. 477-84.
28. Situma, C., et al., *Immobilized molecular beacons: a new strategy using UV-activated poly(methyl methacrylate) surfaces to provide large fluorescence sensitivities for reporting on molecular association events.* Anal Biochem, 2007. **363**(1): p. 35-45.
29. Situma, C., et al., *Fabrication of DNA microarrays onto poly(methyl methacrylate) with ultraviolet patterning and microfluidics for the detection of low-abundant point mutations.* Anal Biochem, 2005. **340**(1): p. 123-35.
30. Soper, S.A., et al., *Fabrication of DNA microarrays onto polymer substrates using UV modification protocols with integration into microfluidic platforms for the sensing of low-abundant DNA point mutations.* Methods, 2005. **37**(1): p. 103-13.

31. Wang, Y., et al., *Microarrays assembled in microfluidic chips fabricated from poly(methyl methacrylate) for the detection of low-abundant DNA mutations.* Anal Chem, 2003. **75**(5): p. 1130-40.
32. Zhao, Z., et al., *Plastic polymers for efficient DNA microarray hybridization: application to microbiological diagnostics.* J Clin Microbiol, 2008. **46**(11): p. 3752-8.
33. Situma, C., M. Hashimoto, and S.A. Soper, *Merging microfluidics with microarray-based bioassays.* Biomol Eng, 2006. **23**(5): p. 213-31.
34. Poulsen, L., et al., *Multi-stringency wash of partially hybridized 60-mer probes reveals that the stringency along the probe decreases with distance from the microarray surface.* Nucleic Acids Res, 2008. **36**(20): p. e132.
35. Stangegaard, M., et al., *A biocompatible micro cell culture chamber (microCCC) for the culturing and on-line monitoring of eukaryote cells.* Lab Chip, 2006. **6**(8): p. 1045-51.
36. Truckenmuller, R., et al., *Bonding of polymer microstructures by UV irradiation and subsequent welding at low temperatures.* Microsystem Technologies-Micro-and Nanosystems-Information Storage and Processing Systems, 2004. **10**(5): p. 372-374.
37. Bock, L.C., et al., *Selection of Single-Stranded-DNA Molecules That Bind and Inhibit Human Thrombin.* Nature, 1992. **355**(6360): p. 564-566.
38. Fialova, M., J. Kypr, and M. Vorlickova, *The thrombin binding aptamer GGTTGGTGTGGTTGG forms a bimolecular guanine tetraplex.* Biochemical and Biophysical Research Communications, 2006. **344**(1): p. 50-54.
39. Macaya, R.F., et al., *Thrombin-Binding DNA Aptamer Forms a Unimolecular Quadruplex Structure in Solution.* Proceedings of the National Academy of Sciences of the United States of America, 1993. **90**(8): p. 3745-3749.
40. Wang, C.L., et al., *Single-stranded DNA aptamers that bind differentiated but not parental cells: subtractive systematic evolution of ligands by exponential enrichment.* Journal of Biotechnology, 2003. **102**(1): p. 15-22.
41. Haubert, K., T. Drier, and D. Beebe, *PDMS bonding by means of a portable, low-cost corona system.* Lab on a Chip, 2006. **6**(12): p. 1548-1549.
42. Hirota, T., et al., *Distinct functions of condensin I and II in mitotic chromosome assembly.* Journal of Cell Science, 2004. **117**(26): p. 6435-6445.
43. Haagensen, J.A.J., K.B. Barken, and S.J. Johanna Pamp, *Protocol for work with the flow-chamber biofilm-system.* Center of Biomedical Microbiology, DTU, Denmark 2006.
44. Ogilvie, I.R.G., et al., *Reduction of surface roughness for optical quality microfluidic devices in PMMA and COC.* Journal of Micromechanics and Microengineering, 2010. **20**(6): p. 8.

CONCLUSION

Practical challenges encountered by users hinder adoption and implementation of microfluidic approaches. This project proposed solutions related to two of these practical issues: interconnections and pumping.

Methods for creating multiple, aligned, parallel and planar interconnections well suited to microscopy were described. Both reusable, non-integrated, and permanent, integrated interconnection solutions were presented. The construction of twelve and eight channel miniaturized, mechanically actuated peristaltic pumps was also described. The small footprint of the pumps allows their placement adjacent to microfluidic devices and on microscope stages.

These solutions were then combined into modular microfluidic systems. One of these systems, *SWAN*, provides high interconnection numbers/density and allows many possible configurations. Additionally, methods for control and actuation of microfluidic networks within *SWAN* configurations were described. DNA hybridizations and cell culture were demonstrated within *SWAN* configurations.

SWAN prototypes have begun to be distributed to external collaborators and researcher parties. These end-users will ultimately determine whether or not the approach was sound and whether the key motivation for development of such a system, providing a practical method for collection of relevant and novel biochemical and biological data from microfluidic devices, was reached.

APPENDIX A

PUBLICATION 1:

"*Interconnection blocks: a method for providing reusable, rapid, multiple, aligned and planar microfluidic interconnections*"

Interconnection blocks: a method for providing reusable, rapid, multiple, aligned and planar microfluidic interconnections

2009 J. Micromech. Microeng. 19 035021

(http://iopscience.iop.org/0960-1317/19/3/035021)

J. Micromech. Microeng. **19** (2009) 035021 (9pp) doi:10.1088/0960-1317/19/3/035021

Interconnection blocks: a method for providing reusable, rapid, multiple, aligned and planar microfluidic interconnections

D Sabourin, D Snakenborg and M Dufva

DTU Nanotech, Department of Micro- and Nanotechnology, Technical University of Denmark (DTU), Ørsteds Plads, Bygning 345Ø, DK-2800, Køngens Lyngby, Denmark

E-mail: martin.dufva@nanotech.dtu.dk

Received 5 December 2008, in final form 19 January 2009
Published 18 February 2009
Online at stacks.iop.org/JMM/19/035021

Abstract
In this paper a method is presented for creating 'interconnection blocks' that are re-usable and provide multiple, aligned and planar microfluidic interconnections. Interconnection blocks made from polydimethylsiloxane allow rapid testing of microfluidic chips and unobstructed microfluidic observation. The interconnection block method is scalable, flexible and supports high interconnection density. The average pressure limit of the interconnection block was near 5.5 bar and all individual results were well above the 2 bar threshold considered applicable to most microfluidic applications.

1. Introduction

Microfluidic and lab-on-a-chip applications offer many advantages to the chemical, biomedical and biological communities. Among these are decreased sample and reagent consumption, reaction time, analysis time and experimental footprints. For the biological community opportunities for parallelization and the ability to study whole or single cell populations under fine environmental control are also of great interest [1–3]. Though microfluidic approaches hold great promise, due to the lack of reliability and ease of use and integration they have not been adopted as widely as expected [4, 5].

Creating fluidic connections between microfluidic devices and the outside world represents a challenge. Contributing to this are a lack of standards for interconnecting components and a difference of scale [6]. Terms such as 'macro-to-micro' and 'world-to-chip' reflect the scale disparity between typical microfluidic channel dimensions, microns to hundreds of microns, and the tool and methods (often by hand) used to connect these to the outside world [7]. Additionally, the cost associated with packaging or interfacing devices can be prohibitive [8, 9].

Microfluidic devices can be fabricated from many different methods and materials, and each of the large number of applications for these devices can have unique requirements. A single interconnection solution addressing all possible criteria related to chemical and biological investigations including, but not limited to, bio and chemical compatibility, flow rates and pressure limits is not likely. Although commercial interconnection solutions are available and provide high pressure limits, these tend to limit device material choice, dimensions and/or the number and configuration of connections. A comprehensive review of interconnections is presented by Fredrickson and Fan [7]. Unless comparable to our approach, clean-room or high-temperature-dependent methods for creating connections to and within glass and/or silicon microfluidic devices are not discussed and the reader should consult other references for such methods [10–18]

Connections between microfluidic components and the devices which drive them, i.e. syringes and/or pumps, are generally classified as permanent or reversible (non-permanent). Permanent interconnection methods are often the easiest to implement and commonly involve directly attaching a needle, piece of tubing or fluidic reservoir to a corresponding inlet or outlet port of a microfluidic device with adhesives such as epoxy [7, 19]. The disadvantages associated with

Table 1. Reversible interconnection method summary.

General method	Description	Integrated	Planar	Number of interconnections	Maximum pressure (bar)	Reference
O-ring	O-rings heat annealed within the PMMA microfluidic chip	Y	N	4	7.5	[24]
	O-ring compressed on top of the microfluidic device/press-fit with tubing	N	Y[a]	3	15	[20]
Extended	Silicone tube compressed to the side of the microfluidic device	N	Y	1	12.3	[26]
Soft tubing	Silicone tube compressed to the top face of the microfluidic device	N	N	20	2	[8]
	Silicone tube compressed to the top face of the microfluidic device	N	N	10	2	[9]
Gasket	PDMS on smooth surface—no compression	Y	N/A	N/A	0.3	[28]
	PDMS microfluidic chip compressed between acrylic plates	Y	N	2	5.6	[19]
Press-fit	Cored PDMS bonded to the second PDMS layer via liquid PDMS	Y	N	2	4.9	[32]
	Cored PDMS O_2 bonded to PDMS and compressed	Y	N	1	7.0	[32]
	Cored PDMS O_2 bonded to PDMS	Y	N	1	5.1	[21]
	Cast PDMS compressed over matching surface relief silicon	N	N	3	2.2[b]	[22]
	Cast PDMS—minimal dead volume interconnection	Y	Y	1	10.3	[31]
	Cast PDMS	Y	Y	1	2.7	[25]

[a] Tubings were bent to become effectively planar.
[b] Maximum average value.

permanent methods include the increased risk of clogged channels and larger dead volumes resulting from the required manual alignment of features over small areas. Several methods have been proposed to prevent clogging when making permanent interconnections; however, not all are applicable to polymeric processing [13–15]. Permanent methods can also be laborious and time consuming for devices requiring multiple connections. With time and device use, loss of sealing capabilities is often observed as device handling places stress on the connection. Additionally, experience from our laboratory has demonstrated biocompatibility problems with epoxy use for creating permanent connections [3].

Reversible interconnections are described as ideally being reliable, both in terms of high seal/pressure performance and repeatability thereof, re-useable, easy to fabricate and assemble, easy to use and handle, flexible, having minimal pressure drops, having low dead volumes, operating over a range of flow rates, chemically and/or biologically compatible, of low cost and offering unobstructed observation [7, 20]. Commonly used methods to create reversible interconnections, not necessarily fulfilling all the criteria listed above, involve compression of an elastomeric microfluidic device [19], press-fit-type connections (placing an 'oversized' element into an 'undersized' recess) [20–25], the deformation of soft tubing [8, 9, 26], O-rings [20, 24, 27] or a combination thereof [20, 22, 24]. Reversible connections can be subdivided into integrated and non-integrated methods. Integrated methods contain an element which becomes part of the microfluidic component/device. Non-integrated connections can be wholly dissociated from the microfluidic device they address. Non-integrated approaches are favourable as they uncouple interconnection and microfluidic device yield, fabrication and design. Table 1 presents a summary of several reversible interconnection methods and their reported maximum leak pressures. In general, the maximum values are not representative of the expected performance of the method. The reader should consult the noted reference for a more complete description of test data collected.

Polydimethylsiloxane (PDMS) is a commonly used material in microfluidic devices [28] and has been used to create interconnections [19, 21–23, 25, 28–32]. PDMS can simultaneously function as a microfluidic device and gasket [19]. When moulded from smooth surfaces, PDMS can form reversible seals to other smooth surfaces that withstand pressures near 0.35 bar [28]. Additional compression can be used to increase seal pressures [19, 22, 32]. As PDMS is deformable and self-sealing, it has also been used in press-fit connections. Oversized needles/tubings can be repeatedly inserted and removed from PDMS holes to create connections; however, insertion and removal of needles/tubing may clog or damage the PDMS. The PDMS holes can be made by coring with a sharp tool or punch [21, 30, 32]. Often following coring,

the PDMS element is integrated in the microfluidic device via oxygen plasma-based bonding [25, 30, 32]. In general, the coring of PDMS is an irreproducible process which results in unpredictable seal performance [21, 32].

Casting of PDMS over mould inserts or sacrificial inserts has been used to create press-fit connections of better quality and reproducibility than those achieved via coring [22, 23, 25, 29, 31]. Quaglio *et al* [25] formed a press-fit PDMS element by casting PDMS and leak pressures were evaluated for PDMS elements of different thicknesses bonded to different substrates by treatments including oxygen plasma and a thin interlayer of PDMS. Chiou *et al* [31] used sacrificial fibre inserts to create an integrated minimal dead volume press-fit-type interconnection. A thin stainless steel wire was threaded through a fused-silica capillary placed into a side channel of a glass device. PDMS poured over the capillary wicked by capillary force into the channel area between the thin stainless steel wire and the channel wall resulting in a conical shaped entry which limited dead volume. Following PDMS curing, the metal wire was pulled through the capillary and removed. The silica capillary could be removed and reinserted. Saarela *et al* [22] used sacrificial fibres and an etched silicon master mould to create multi-inlet PDMS fluidic connectors. The completed PDMS connector was paired, aligned, and in some cases compressed against a silicon-based microfluidic device with identical surface relief as the PDMS connector. Insertion of either capillary or PEEK tubes into the PDMS connector piece established fluidic connections.

Protruding lengths of soft tubing have been used to create reversible, non-integrated fluidic interconnections [8, 9, 26]. When compressed against the face of a microfluidic device, the protruding tubing deforms and behaves as an O-ring. Snakenborg *et al* [26] provide a detailed theoretical review of this approach and compare it to experimental data obtained for silicone tubing. Yang and Maeda [8, 9] use this approach to establish fluidic connections to the top surface of the microfluidic devices in sockets designed for the rapid testing of microfluidic devices.

Perroziello *et al* [24] integrated O-rings into a heat-annealed multilayer polymethylmethacrylate (PMMA) device. Press-fit connections were established by inserting metal ferrules with an outer diameter (OD) greater than the inner diameter (ID) of O-rings. Bhagat *et al* [20] demonstrated a non-integrated interconnection system using O-rings and press-fit. Through-holes in a PMMA port clamp housed commercially available O-rings which created a press-fit connection with Teflon tubing. Tightening the port clamp into a holder via screws placed the port clamp O-rings against the top surface of the microfluidic device and formed a seal. The construction supported high pressures without leaking for PDMS-, glass- and COC-based test devices. In contrast to the method of Perroziello *et al* the use of Teflon tubing instead of a metal ferrule allowed the interconnections to become effectively planar and likely prevent damage to the O-rings.

This work introduces the concept of interconnection blocks (IBs). IBs are a practical and reliable solution for creating multiple reversible, aligned, non-integrated and planar interconnections. IBs were designed to facilitate the rapid testing of microfluidic devices and are manufactured using simple, low-cost methods. The described approach is flexible and scalable.

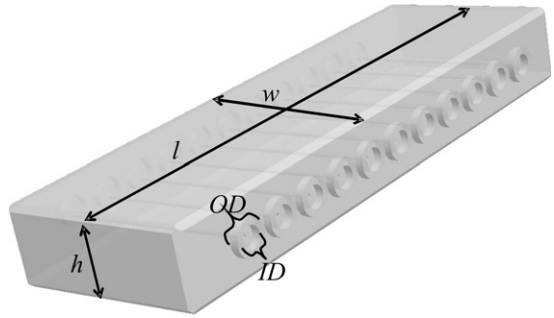

Figure 1. Schematic representation of the PDMS portion of the IB. The PDMS portion of the IB has a length (l) of 30 mm, a height (h) of 4 mm and a width (w) of 10 mm. O-ring-like structures are present on both sides of the IB. O-rings have inner diameters (ID) of 1.0 mm, outer diameters (OD) of 1.8 mm and protrude from the main PDMS body by 0.4 mm. In total the overall width of the IB is 10.8 mm.

2. Materials and methods

2.1. Interconnection design and fabrication

IBs are made from two materials/parts: a PMMA shell and a middle PDMS section. A schematic representation of the PDMS portion of an IB is shown in figure 1. The PDMS portion of the IB is designed to be 30 mm in length, 4 mm in height and contains twelve 240 μm diameter integrated channels. Integrated 240 μm diameter channels are spaced 2.25 mm centre-to-centre and are bookended by O-ring-like structures with an ID of 1.00 mm, OD of 1.80 mm and protrude from the sides of the IB by 0.40 mm. The total width of the IB inclusive of the protruding O-rings is 10.80 mm, and the total height and length including the PMMA shell are 6 and 40 mm, respectively.

IBs are cast in one piece with PDMS inside a PMMA (Nordisk Plast, Denmark) mould. All PMMA mould pieces were made by a CNC controlled micromilling machine (Folken, Glendale, CA). The IB fabrication process is depicted schematically in figure 2, and mould pieces and completed IB are shown in figure 3. PDMS (Sylgard 184, Dow Corning) was mixed in a 10:1 mass ratio of elastomer to curing agent and placed under vacuum to remove air bubbles. The IB mould contained four pieces. All mould pieces were aligned and held together by 2 mm screws in combination with 2 mm alignment pins. An assembled mould is depicted schematically in figure 2(a) and an actual mould is shown in figure 3(a). Two mould pieces have twelve 250 μm diameter through-holes around which the negative image of an O-ring was centred (figure 3(b)). Before injecting PDMS into the mould, 240 μm optical fibres (Polymicro Technologies, Phoenix, Arizona) were threaded through the 250 μm holes in each of the two pieces (figure 2(b)). These two mould pieces along with the optical fibres created the integrated channels and their terminal O-rings (figure 3(c)). Mould vents allowed PDMS to be

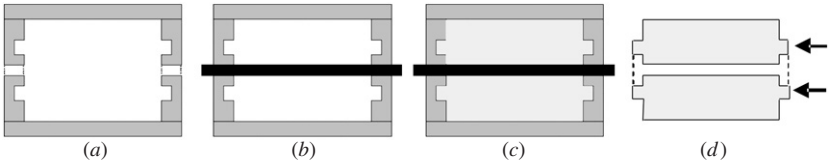

Figure 2. Schematic representation of IB fabrication. Drawings not to scale. (*a*) Cross-sectional view of the mould used for casting IBs. Mould shapes defining O-rings are seen on the left- and right-hand sides of the mould. Openings at the end represent through-holes through which fibre inserts are placed. (*b*) Fibre inserts resulting in integrated channels are placed through terminal mould pieces and are centred within structures forming O-rings. (*c*) PDMS is cast into the mould and subsequently cured. Following PDMS curing, fibre inserts are removed and the mould is disassembled. (*d*) Cross-section of completed IB. Arrows indicate the O-ring sealing surface.

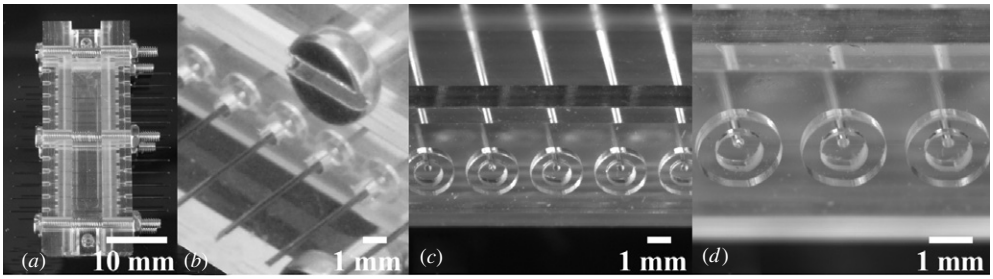

Figure 3. IB fabrication. (*a*) Mould used for casting IBs. Fibre inserts resulting in integrated channels pass through terminal mould pieces. (*b*) Close-up of terminal mould pieces which result in the formation of O-ring-like structures bookending integrated channels. (*c*) Section of the cast IB. The PMMA shell is visible on top of the PDMS portion. Channels and O-rings are spaced 2.25 mm centre-to-centre. (*d*) Close-up of O-rings on the completed IB.

injected by hand using a syringe and prevented air bubbles from being trapped within the finished part (figure 2(*c*)). The filled mould was then placed in an oven to cure at 80 °C for 1 h. Once the mould had cooled enough to be handled, the fibres were removed to form the integrated channels (figure 2(*d*)). The two mould pieces defining the O-rings were removed and the remaining pieces formed the aforementioned PMMA shell. A portion of a completed IB is shown in figure 3(*c*) and a close-up of the integrated O-rings is shown in figure 3(*d*). Prior to testing, IBs were inspected for damage, poorly formed O-rings and/or blocked channels.

2.2. Leak pressure testing

Leak pressures were determined by placing the IB between two needle assemblies on an aluminium base plate, made by micromilling, as shown in figure 4. The needle assemblies provided 12 fluidic inlets/outlets that aligned to the 12 IB channels. To construct needle assemblies, metal tubings were glued with epoxy (R&G GmbH, Waldenbuch, Germany) into pieces of PMMA containing through-holes with a 250 μm diameter at the PMMA surface that contacted the IB.

Alignment of the IB and needle assemblies was accomplished using 2 mm guide channels and alignment holes in the aluminium base. The IB was placed in the middle of the aluminium base plate using 2 mm alignment pins. The pins were inserted into the needle assemblies and these were slid horizontally towards the IB using the 2 mm guide channels. Once slid to the proper position, indicated by 2 mm alignment holes in the aluminium base plate, the aluminium pins were pushed through the alignment holes to secure the needle assembly position. The base plate alignment features compressed the 10.80 mm wide IB to a width of 9.60 mm.

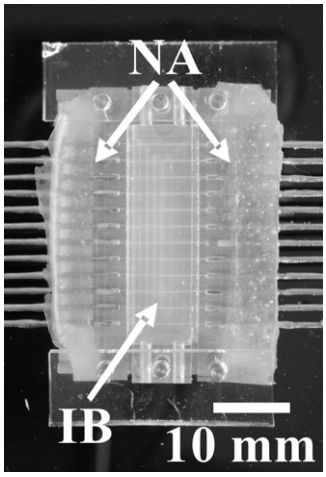

Figure 4. IB pressure test assembly. The IB was placed between PMMA two needle assemblies (NA) on an aluminium base plate. Needle assemblies contain blunted syringe tips which are glued into a pre-drilled PMMA piece. PMMA pieces horizontally placed above and below IB provide additional alignment and a surface with which to secure the assembly for microscopic observation. All pieces are aligned via 2 mm alignment pins.

The IB PMMA shell is centred and has a total width of 8 mm, and does not interfere with the compression of the PDMS portion of the IB. Two small PMMA pieces provided both additional alignment and a surface for which to secure the IB test assembly for microscopic observation.

The leak pressure of the O-rings bookending a channel was determined visually, under microscopic observation, and using a pressure sensor. To test the leak pressures of individual channels of the IB, a dye solution was pumped from a syringe

pump through the test system and a single channel of the IB. Once the dye solution had passed through the tubing of the outlet needle assembly the syringe pump was stopped. The outlet channel was blocked, the syringe pump started and the leak pressure recorded. A leak was defined as the point at which the dye solution breached the outer edge of either of the channel's terminal O-rings. This test was repeated for several but not all channels within the IB each time it was inserted into the test assembly described above. The group of tests conducted for each insertion of the IB is referred to as a test cycle.

In between test cycles the IB was rinsed with water, dried under a nitrogen stream and inspected for damages. Test pieces were marked so that during all test cycles the assembly was put together with the same orientation. This allowed investigation of systematic errors; for example, leaks occurring on a single side of the IB. Twelve test cycles were completed. The final two cycles were completed within an incubation chamber with a set point of 40 °C to verify the suitability of IBs for biological investigations. The temperature within the incubation chamber was monitored with an electronic thermometer and was found to vary between 39 °C and 41 °C. Sufficient time was allowed between test events to allow all liquids and components to come to temperature.

2.3. Interconnection block demonstration

The microfluidic chip used to demonstrate the IBs was made from two 3 mm PMMA layers. All channels had a square profile measuring 0.4 mm × 0.4 mm. To bond the PMMA layers, the bonding surfaces of the PMMA layers were placed facing a UV source lamp (DYMAX, Torrington, CT) and exposed for 75 s. Following UV exposure, the PMMA layers were aligned and placed in a bonding press (P/O/Weber, Remshalden, Germany). Bonding press heating plates were set at 85 °C and an initial pressure of 5.5×10^3 kN m^{-2} was applied. The microfluidic chip was bonded for a total of 80 min. Fine-grade sanding paper and fibre-polishing paper were used to obtain a smooth side surface on the PMMA microfluidic chip. Similar to leak pressure testing, the microfluidic chip and the IBs were mounted on an aluminium base plate between needle assemblies. In all cases, the IB was compressed from an initial width of 10.80 mm to a width of 9.6 mm.

3. Results

3.1. Pressure testing

The IB mould shown in figure 3(*a*) was easily assembled and the IB readily cast. The finished IB never showed blocked channels and/or poorly formed O-rings. An IB was tested through 12 insertion/removal cycles; the first ten cycles at room temperature and the final two cycles at 40 °C. 40 °C was chosen as it is above the 37 °C reference point required for most biological assays. For all test cycles, all 24 fluidic inlet and outlet connections to the needle assemblies were formed without any misalignments. Figure 5 shows a typical alignment of an IB channel to a needle assembly channel. The typical misalignment between these was estimated at 0.1 mm.

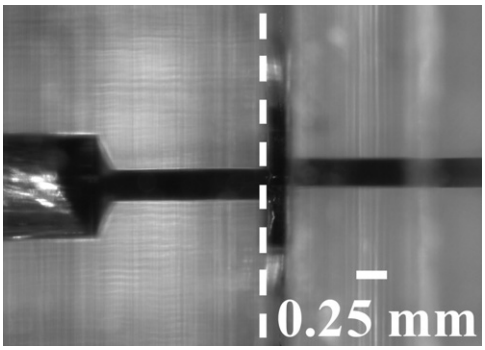

Figure 5. Typical alignment of the IB channel to the needle assembly (NA) channel in leak pressure test assembly. Channels filled with dye to facilitate visualization. The IB is on the right side of the dashed line and the NA on the left. The NA channel narrows from a diameter of 0.8 mm to 0.25 mm at the IB interface. The compressed O-ring is visible immediately to the right of the dashed line and dye can be seen filling the area created by its inner diameter.

Table 2. Interconnection block leak pressure test data.

Cycle	Average (bar)	Maximum (bar)	Minimum (bar)	Channels tested
1	5.85	6.70	3.35	6
2	6.03	6.44	5.57	4
3	6.08	6.31	5.80	6
4	5.95	6.05	5.80	4
5	6.03	6.05	5.93	6
6	5.96	6.05	5.64	6
7	5.68	6.05	5.41	6
8	5.78	6.05	5.49	6
9	5.88	6.05	5.41	6
10	5.73	6.05	5.23	6
11[a]	4.51	4.51	4.51	1
12[a]	5.54	6.05	3.94	6

[a] Testing completed at 40 °C.

Within each test cycle the pressure limit of several individual channels was tested. The number of channels/O-rings tested varied during a test cycle as the dye solution that leaked from an O-ring prevented determination of leakage from adjacent O-rings. During initial test cycles, it was observed that the pressure limit of the test set-up (e.g. the needle assemblies) was sometimes reached prior to observing leaks at the O-rings. To collect more data points within each test cycle by preventing unnecessary cleaning and disassembly, a cut-off pressure was set at 6.05 bar from cycle 3 onwards. Set-up leaks sometimes also occurred below 6.05 bar (e.g. cycle 11 in table 2). In these cases, the pressure at which the set-up leak occurred was recorded as the final test value. Maximum, minimum and average leak pressure results for each test cycle are summarized in table 2. As the O-ring-like structures and channels are all similarly formed in the milling/casting process, the normal sampling of 6 of the 12 IB channels yields a representative assessment of IB leak pressure performance.

All individual leak pressure values shown in figure 6 were well above the 2 bar limit considered applicable for

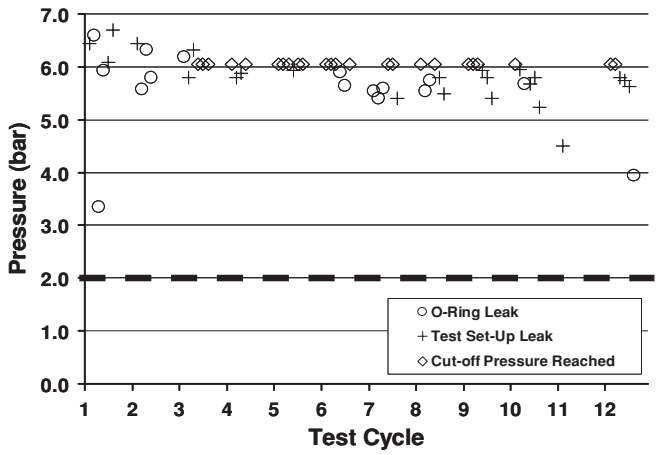

Figure 6. IB leak pressure run order data. All data points are shown. The imposed stop pressure of 6.05 bar is seen from the middle of cycle 3. The dashed line at 2 bar represents the pressure threshold considered applicable for most microfluidic applications.

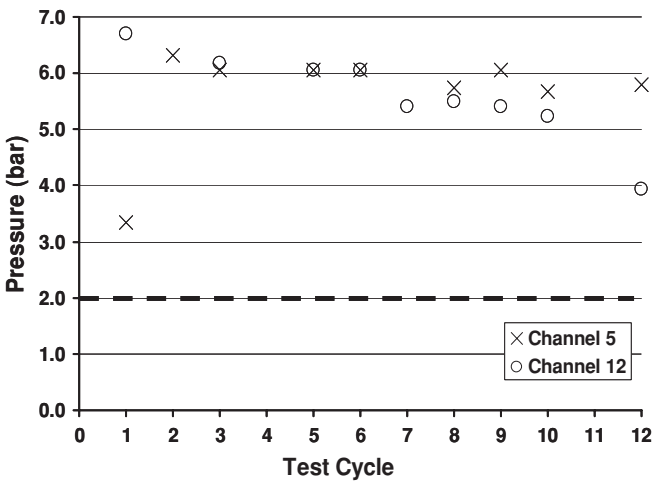

Figure 7. Leak pressure data for channels 5 and 12 of the IB. The dashed line at 2 bar represents the pressure threshold considered applicable for most microfluidic applications.

most microfluidic applications [20]. Of the 63 total test points collected 21 tests were stopped due to test set-up leaks occurring below 6.05 bar and 26 tests were stopped at the pressure limit of 6.05 bar. For the subset of 16 tests where O-ring leaks were observed prior to leaks in the test set-up, the average leak pressure was 5.6 bar with a standard deviation of 0.8 bar. Maximum and minimum values within this subset were 6.6 bar and 3.4 bar, respectively. Low, outlying values are noted in test cycles 1, 11 and 12. The low values from test cycles 1 and 12 were true O-ring leaks. The outlying, and only, value from cycle 11 resulted from a test set-up leak. This leak forced the set-up to be disassembled and cleaned.

Given the limitations of the leak pressure test set-up, it is difficult to quantify degradation of leak pressure of the IB through successive cycles. The IB appears to maintain its average capabilities through all insertions including the final test at 40 °C. From cycle 4 onwards the frequency of test points which reach the 6.05 bar limit is consistent (figure 6). The O-ring leaks near 5.5 bar in cycles 6 and 7 are within the same distribution as those from cycles 1 and 2. For test cycle 7, assembly related causes, such as uneven compression on different faces of the IB, are suspected as O-ring leaks were all from the same side of the IB. In contrast to the IB, it appears that the test set-up suffered fatigue from cycle 7 onwards as leaks in the set-up increasingly occur at lower values.

Leak pressure values from two representative channels, designated 5 and 12, of the IB are shown in figure 7. The low, outlying values obtained in test cycles 1 and 12 of 3.35 and 3.94 bar respectively, originate from O-ring leaks. Channels 5 and 12 were tested in the majority, 9 out of 12, of test cycles. Test data from channel 5 demonstrates recovery from a lower pressure value (3.35 bar). For all insertions after cycle 1, it consistently tests near 6 bars. This indicates that the observation of a single lower value, perhaps due to assembly or contamination issues, does not signify a permanent loss in sealing capability. Channel 12 demonstrates that it is possible for a channel to yield a lower value on a given insertion; however, this lower value of 3.94 bar is still well above the 2 bar threshold and, similarly to channel 5, recovery to previous values is expected.

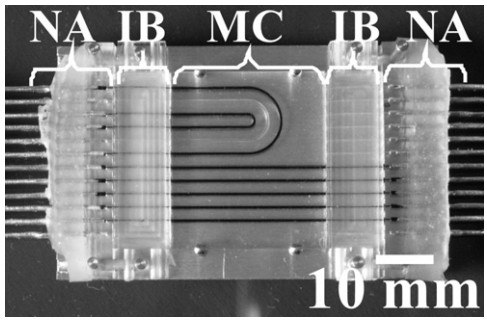

Figure 8. A PMMA microfluidic chip (MC) is placed between two IBs. Two needle assemblies (NA) are shown at the outer left and outer right. In the lower half of the chip fluid flows into the chip through one IB and out through a second IB. In the top half of the chip, fluid enters and leaves through the IB on the left-hand side of the image.

3.2. Interconnection characterization

IBs can be used in different configurations to interface with microfluidic devices. Figure 8 shows the realization of these two configurations using the same PMMA microfluidic chip. Assembly and disassembly of the system shown in figure 8 was performed in a few minutes. When assembled, all channels were aligned. Interconnections between IBs and test chips have been established for >100 h without leaks (unpublished results).

Dead volumes, V_D, for the interfaces shown in figure 8 between IB/needle assembly and IB/microfluidic chip are estimated according to

$$V_D = C_W\,(A_{\mathrm{OD}} - A_{\mathrm{CE}}) \qquad (1)$$

where C_W is the compressed IB O-ring width, A_{OD} is the cross-sectional area inside an IB O-ring and A_{CE} the cross-sectional area of a channel the IB is addressing. These terms are depicted

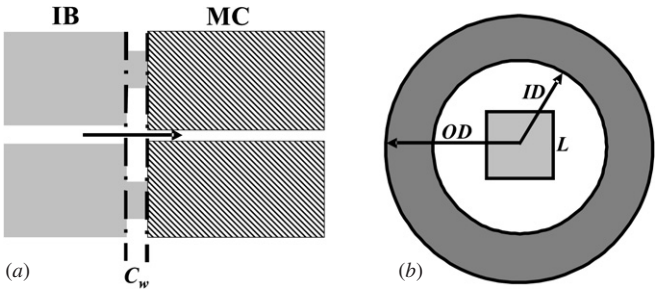

Figure 9. Schematic cross-sections of an IB (left) planar interconnection with a microfluidic chip (MC) with a square channel. Not drawn to scale. (*a*) Fluid flows in the direction shown by the arrow. When an IB is compressed against the MC to form a planar interconnection, the O-ring is compressed against the side face of the MC and to a width of C_W, the distance between the dashed lines. (*b*) Front view of the O-ring and microfluidic chip interface. Fluid flows into the page, through an IB with O-rings with outer diameter, *OD*, and inner diameter, *ID,* and into a square microfluidic channel with side length *L*. The area of no fluid flow is the unshaded area between *ID* and the outer perimeter of the microfluidic channel. The dead volume is obtained when this area is multiplied by C_W from above.

schematically in figure 9. The area given by $A_{\mathrm{OD}} - A_{\mathrm{CE}}$ is shown as the shaded hashed region in figure 9(*b*).

As can be seen from figure 5, IB O-rings compress from 0.4 mm to approximately 0.25 mm (C_W). Assuming that the ID of the O-ring remains at 1.0 mm, V_D is estimated to be 165 nL for the IB/chip interface and 185 nL for the IB/needle assembly interface.

4. Discussion

4.1. Fabrication

All materials and methods used to fabricate the IB are readily available and of low cost. Micromilling and casting were chosen as they are practical microfabrication methods. Micromilling affords lower start-up and running costs, a broader range of substrates and faster design changes than clean-room-based approaches. Although not as precise and/or able to create features of similar small dimension as clean-room processes, devices and channels of acceptable scale and precision for microfluidic investigations can be manufactured. The channel/O-ring spacing of 2.25 mm centre-to-centre is identical to the standard published by SBS/ANSI for 1536 well microtiter plates. This will facilitate the creation of systems using the IBs that are compatible with 1536 well microtiter plate assays and/or the automated fluidic handling systems built for this established platform.

4.2. Performance and design considerations

Leak pressure test data demonstrated that the IB provides reliable seal/pressure performance well above the 2 bar threshold considered applicable for most microfluidic applications [20]. Though the average leak pressure of the IB is well above the 2 bar threshold, as a single interconnection failure usually represents a lost experiment, it is more important that the lowest individual values are well above this threshold (table 2) in order to prevent yield loss and/or system downtime. As a result of the limitations of the pressure test set-up, the average and possibly the maximum leak pressure values in table 2 are underestimated. IB connections were robust to handling and demonstrated recovery: a low leak pressure value did not signify a permanent decrease in seal performance for a particular IB channel. Though some methods report higher maximum leak pressures, the IB performs equally, and provides maximum leak pressures better or equivalent to other methods (table 1).

The IB is re-usable and little degradation in overall performance occurred with repeated use. Reversible connections have shown decreases to a constant value in leak pressure following initial usages [31]; however, establishing degradation of the IB sealing capability is difficult as the test set-up showed signs of degradation during the test cycle. IB connections were more robust than the test set-up connections and, barring any damage to the IB, leak pressures near 5.5 bar and well above the 2 bar threshold are expected to be maintained.

During screening of IB designs, user related factors and not solely pressure performance were considered. Increased leak pressures would likely have been obtained if the IB were further compressed and/or the O-ring sealing surface area decreased. Both these changes should result in greater sealing force per unit area of the O-ring-like structures; however, these changes could decrease ease of use. With increased compression greater manual force would be required for IB insertion. Due to the tolerances of the materials and methods used, smaller O-rings could result in fewer successful alignments. Methods using alignment pins have reported tolerances of 50 μm [24] and with such alignment, O-ring IDs and ODs could be decreased to yield decreased dead volumes and increased interconnection packing density. The estimated dead volumes of 165 nL for the IB/chip interface and 185 nL for the IB/needle assembly interface (results) are specific for the dimensions used in the interfacing elements shown in figure 8. These dead volumes are not expected to be problematic for most biological applications but may be for other applications. In such cases, smaller O-ring dimensions, and/or matching the O-ring ID, IB channel diameter and interfacing channel diameters would decrease dead volume. The 24 connections provided by the IB are greater in number and packing density than most methods reported in table 1 and avoid the tedious handling of small O-rings and tubing. Additionally, to create reliable connections with soft tubing, the tubing must be cut very flat. The IB casting process eliminates and addresses handling and assembly issues by yielding 24 *in situ* O-rings, or alternatively, aligned banks of 12 extended tubing ends, with very consistent shape and dimensions (figure 3(*d*)). With increased alignment, packaging of one interconnection per mm^2 should be possible. Although PDMS is widely used in microfluidic research, in some cases it may be advantageous to consider the use of other elastomeric materials. Toepke *et al* [33] discuss the absorption and partitioning of small molecules in PDMS and Saarella *et al* [22] note that use of PDMS may be limited in sensitive

mass spectroscopy applications as it can generate background signals.

4.3. Comparison to other methods

In contrast to integrated solutions, IB and microfluidic chip design, manufacture and yield are separate. If an IB is damaged, mould pieces are re-usable and another part can be fabricated within a few hours. Perroziello *et al* [24] rely on the 'trapping' of O-rings within a heat-bonded multilayer PMMA structure. Design iterations, the inclusion of poorly formed O-rings and/or channel collapse caused during the heat bonding process [34] can lower yield and requires both O-rings and the microfluidic device to be made again. Additionally, IBs require no processing and are ready for use following PDMS casting and curing. Coring of PDMS results in irreproducible, unevenly spaced PDMS press-fit connections and poor yields for devices requiring multiple inlets/outlets [21, 34]. Saarela *et al* [22] avoided coring by using sacrificial fibres to create PDMS press-fit connections; however, following casting and demoulding, the fibres were pushed through the PDMS to ensure that through-holes and individual connector chips were diced with a scalpel. These additional processing steps increase the likelihood of damage and yield loss. The fibres used in IB fabrication pass completely through the mould ensuring unblocked channels. In some cases, a thin PDMS film formed around the outer edges of the IB, not near the O-rings. These were peeled away by hand. Furthermore, the IB PDMS does not require plasma treatment like many other methods (table 2).

Press-fit methods require the removal of a needle, ferrule or tubing from the device each time a separate device is tested or the test system disassembled. This risks damage to the interconnection and/or clogging the inserted element with interconnection material. The IB establishes self-aligning planar connections by compression between two planar elements and does not require needle, ferrule or tubing insertion. Horizontally sliding and guiding the elements together, as shown in figures 4 and 8, reduces the risk of damage. To interface with the IB microfluidic chips require a fairly smooth sidewall with height greater than the OD of the compressed IB O-ring. Polymeric and glass-based devices can be interfaced via the IB and PDMS should compensate for surface irregularities, the degree of which was not investigated. Planar connections offer several benefits: top-down compression methods, i.e. tightening of screws, are avoided. From experience, these can lead to uneven force distributions and collapsed or deformed elastomeric channels and/or damage to microfluidic devices, for example cracked slides. Planar connections do not require valuable microfluidic chip surface area used for, and permit, unobstructed microscopic observation.

IBs allow rapid testing of microfluidic chips. The chip test assembly shown in figure 8 took only a few minutes to assemble. IBs are not used alone, but are used alongside other system parts including the aluminium base plate and the needle assemblies. Further use and future work will lead to manufacturing and design changes focused on integrating the IB approach into pumping and reservoir components in order to yield an adhesive and needle-free microfluidic system which allows rapid chip testing.

5. Conclusion

A simple method and practical approach for creating re-usable, multiple, aligned and planar interconnection methods has been presented. IBs are easy to fabricate, easy to use, of low cost and the IB approach is both flexible and scalable, permitting a large number of interconnections and a wide variety of potential configurations. IBs support pressures well above the threshold considered applicable to most microfluidic applications (2 bar) and represent an interconnection solution allowing the rapid testing of microfluidic chips.

Acknowledgments

The authors acknowledge funding from a DTU PhD student grant and the Danish Strategic Research Council (NABIIT programme).

References

[1] Whitesides G M 2006 The origins and future of microfluidics *Nature* **442** 368–73
[2] Beebe D J, Mensing G A and Walker G M 2002 Physics and applications of microfluidics in biology *Annu. Rev. Biomed. Eng.* **4** 261–86
[3] Stangegaard M, Petronis S, Jorgensen A M, Christensen C B V and Dufva M 2006 A biocompatible micro cell culture chamber (uCCC) for the culturing and on-line monitoring of eukaryote cells *Lab. Chip* **6** 1045–51
[4] Blow N 2007 Microfluidics—in search of a killer application *Nature Methods* **4** 665–8
[5] Andersson H and ven den Berg A 2006 Where are the biologists *Lab. Chip* **6** 467–70
[6] Pepper M, Palsandram N S, Zhang P, Lee M and Cho H J 2007 Interconnecting fluidic packages and interfaces for micromachined sensors *Sensors Actuators* A **134** 278–85
[7] Fredrickson C K and Fan Z H 2004 Macro-to-micro interfaces for microfluidic devices *Lab. Chip* **4** 526–33
[8] Zhen Yang Z and Maeda R 2002 A world-to-chip socket for microfluidic prototype development *Electrophoresis* **23** 3474–8
[9] Zhen Yang Z and Maeda R 2003 Socket with built-in valves for the interconnection of microfluidic chips to macro constituents *J. Chromatogr.* **1013** 29–33
[10] Gonzalez C, Collins S D and Smith R L 1998 Fluidic interconnects for modular assembly of chemical microsystems *Sensors Actuators* **49** 40–5
[11] Gray B L, Jaeggi D, Mourlas N J, van Drieenhuizen B P, Williams K R, Maluf N I and Kovacs G T A 1999 Novel interconnection technologies for integrated microfluidic systems *Sensors Actuators* **77** 57–65
[12] Meng E, Wu S and Tai Y 2001 Silicon couplers for microfluidic applications *Fresenius J. Anal. Chem.* **371** 270–5
[13] Tsai J and Lin L 2001 Micro-to-macro fluidic interconnectors with an integrated polymer sealant *J. Micromech. Microeng.* **11** 577–81
[14] Puntambekar A and Ahn C H 2002 Self-aligning microfluidic interconnects for glass- and plastic-based microfluidic systems *J. Micromech. Microeng.* **12** 35–40

[15] Pattekar A V and Kothare M V 2003 Novel microfluidic interconnectors for high temperature and pressure applications *J. Micromech. Microeng.* **13** 337–45
[16] Lee E S, Howard D, Liang E, Collins S D and Smith R L 2004 Removable tubing interconnects for glass-based micro-fluidic systems made using ECDM *J. Micromech. Microeng.* **14** 535–41
[17] Gray B L, Collins S D and Smith R L 2004 Interlocking mechanical and fluidic interconnections for microfluidic circuit boards *Sensors Actuators* A **112** 18–24
[18] Pan T, Baldi A and Ziaie B 2006 A reworkable adhesive-free interconnection technology for microfluidic systems *J. Microelectromech. Syst.* **15** 267–72
[19] Korivi N S and Jiang L 2007 A generic chip-to-world fluidic interconnect system for microfluidic devices *IEEE 39th Southeastern Symp. on System Theory (Macon, GA, 4–6 March)* pp 176–80
[20] Bhagat A A S, Jothimuthu P, Pais A and Papautsky I 2007 Re-usable quick-release interconnect for characterization of microfluidic systems *J. Micromech. Microeng.* **17** 42–9
[21] Li S and Chen S 2003 Polydimethylsiloxane fluidic interconnects for microfluidic systems *IEEE Trans. Adv. Packag.* **26** 242–7
[22] Saarela V, Franssila S, Tuomikoski S, Marttila S, Ostman P, Sikanen T, Kotiaho T and Kostiainen R 2006 Re-usable multi-inlet PDMS fluidic connector *Sensors Actuators* B **114** 552–7
[23] Dalton C and Karan K V I S 2007 A cost effective, re-configurable electrokinetic microfluidic chip platform *Sensors Actuators* B **123** 628–35
[24] Geraldo Perozziello G, Frederik Bundgaard F and Oliver Geschke O 2008 Fluidic interconnections for microfluidic systems: a new integrated fluidic interconnection allowing plug 'n' play functionality *Sensors Actuators* B **130** 947–53
[25] Quaglio M, Canavese G, Guiri E, Marasso S L, Perrone D, Cocuzza M and Pirri C F 2008 Evaluation of different PDMS interconnection solutions for silicon, Pyrex and COC microfluidic chips *J. Micromech. Microeng.* **18** 1–10
[26] Snakenborg D, Perrozziello G, Geschke O and Kutter J P 2007 A fast and reliable way to establish fluidic connections to planar microchips *J. Micromech. Microeng.* **17** 98–103
[27] Yao T, Lee S, Fang W and Tai Y 2000 Micromachined rubber O-ring micro-fluidic interconnectors 0-7803-5273-4/00 ©IEEE pp 624–7
[28] McDonald J C and Whitesides G M 2002 Poly(dimethylsiloxane) as a material for fabricating microfluidic devices *Acc. Chem. Res.* **35** 491–9
[29] Armani D, Liu C and Aluru N 1999 Re-configurable fluid circuits by PDMS elastomer micromachining 0-7803-5194-0/99 ©IEEE pp 222–7
[30] Jo B, Linda M, van Lergerghe L M, Kathleen M, Motsegood K M and Beebe D J 2000 Three-dimensional micro-channel fabrication in polydimethylsiloxane (PDMS) elastomer *J. Microelectromech. Syst.* **9** 76–81
[31] Chiou C and Lee G 2004 Minimal dead-volume connectors for microfluidics using PDMS casting techniques *J. Micromech. Microeng.* **14** 1484–90
[32] Christensen A M, Cheng-Yen D A and Gale B K 2005 Characterization of interconnects used in PDMS microfluidic systems *J. Micromech. Microeng.* **15** 928–34
[33] Michael W, Toepke M W and Beebe D J 2006 PDMS absorption of small molecules and consequences in microfluidic applications *Lab. Chip* **6** 1484–6
[34] Tsao C W, Hromada L, Liu J, Kumar P and DeVoe D L 2007 Low temperature bonding of PMMA and COC microfluidic substrates using UV/ozone surface treatment *Lab. Chip* **7** 499–505

PUBLICATION 2:

"*Interconnection blocks with minimal dead volumes permitting planar interconnection to thin microfluidic devices*"

Microfluid Nanofluid (2010) 9:87–93
DOI 10.1007/s10404-009-0520-8

RESEARCH PAPER

Interconnection blocks with minimal dead volumes permitting planar interconnection to thin microfluidic devices

David Sabourin · Detlef Snakenborg · Martin Dufva

Received: 23 July 2009 / Accepted: 9 September 2009 / Published online: 12 November 2009

Abstract We have previously described 'Interconnection Blocks' which are re-usable, non-integrated PDMS blocks which allowing multiple, aligned and planar microfluidic interconnections. Here, we describe Interconnection Block versions with zero dead volumes that allow fluidic interfacing to flat or thin side-walled microfluidic devices. These designs increase the number of materials, types of devices and applications for which Interconnection Blocks can be used. Average leak pressures of 4.7 bar were recorded and all individual leak pressures recorded were above the 2-bar threshold for microfluidic applications. Additionally, the new Interconnection Block designs demonstrate that micromilling, a practical microfabrication method, can produce useful geometries not readily made through clean room-based approaches.

Keywords Interconnection · Dead volume · Planar · PDMS · Microfluidic

Abbreviation

IB:	Interconnection Block
BJIB:	Ball Joint Interconnection Block
BJIB-90:	Ball Joint Interconnection Block with integrated 90° turn
PDMS:	Polydimethylsiloxane
PMMA:	Poly (methyl methacrylate)

D. Sabourin · D. Snakenborg · M. Dufva (✉)
DTU Nanotech, Department of Micro-and Nanotechnology, Technical University of Denmark (DTU), Oersteds Plads, Bygning 345, 2800 Kongens Lyngby, Denmark
e-mail: martin.dufva@nanotech.dtu.dk

1 Introduction

Large difference of scale between microfluidic chips and devices which drive them such as pumps and a lack of standards for interconnecting components contribute to difficulties in establishing fluidic connections between microfluidic devices and the outside world (Pepper et al. 2007). Recently, we described so called Interconnection Blocks (IB) made from polydimethylsiloxane (PDMS) (Sabourin et al. 2009). IBs are a practical, flexible, scalable and reliable solution for creating multiple reversible, aligned, non-integrated and planar interconnections to microfluidic devices. IBs were designed to facilitate rapid connections to microfluidic chips and supported average pressures near 5.5 bar, well above the 2-bar threshold considered applicable for most microfluidic applications (Bhagat et al. 2007). Although IBs satisfy many 'ideal' criteria for reversible interconnections, including being reliable and re-useable (Bhagat et al. 2007; Fredrickson and Fan 2004) certain applications require interconnections that eliminate dead volumes (Saarela et al. 2006) and/or interface with flat, thin side-walled microfluidic devices such as chips made of glass or silicon.

Many solutions have been proposed for creating microfluidic interconnections (Fredrickson and Fan 2004). We previously discussed those most comparable to IBs (Sabourin et al. 2009) and for purposes of brevity, only those similar to the IB approach which afford near zero dead volumes and/or effectively planar connections to thin microfluidic devices are described.

Chiou and Lee (2004) created a near zero dead volume interconnection from PDMS. A stainless steel wire was passed through a fused silica capillary that was inserted into a side channel of a glass device. The wire protruded into the channel beyond the capillary. PDMS was poured over the

capillary and was wicked between channel and wire to form a conical shaped entry which limited dead volume. After the PDMS cured, the wire was removed. The resultant interconnection was reversible as fused silica capillaries could be removed and reinserted. The PMMA port clamp manufactured by Bhagat et al. (2007) allowed effectively planar interconnections. The clamp housed O-rings that created both a press-fit connection with Teflon tubing and a sealed connection to the top surface of the microfluidic device. Interconnections were considered planar as the teflon tubings could bend. Protruding lengths of soft tubing were used by Yang and Maeda (2002, 2003) to establish fluidic connections to the top of microfluidic devices held in sockets designed for rapid testing. As tubings were soft they were bent to yield effectively planar interconnections. In a similar approach, truly planar connections to microfluidic chips using soft tubings have been demonstrated (Snakenborg et al. 2007).

In this report, fabrication and leak pressure data for two new IB designs are presented. The first, the Ball Joint Interconnection Block (BJIB) creates planar interconnections with zero dead volume and the second, the BJIB-90, allows zero dead volume interconnections to flat or thin side-walled microfluidic devices.

2 Materials and methods

2.1 BJIB and BJIB-90 design and fabrication

The materials and methods used to make the new IB designs which identical to those previously described (Sabourin et al. 2009) with the exception of mould design. A schematic representation of the fabrication process, casting of PDMS inside poly (methyl methacrylate) (PMMA) moulds, is shown in Fig. 1.

PDMS (Sylgard 184, Dow Corning) was mixed in a 10:1 mass ratio of elastomer to curing agent and placed under vacuum to remove air bubbles. The BJIB mould contained four pieces. All mould pieces were aligned and held together by 2 mm screws in combination with 2 mm alignment pins. The balljoint features were made by two terminal mould pieces machined with a 2-mm flat end mill and a 1-mm ball end mill in which 250 μm diameter through holes were centered. Before injecting PDMS into the mould, 240 μm optical fibres (Polymicro Technologies, Phoenix, Arizona) were threaded through the 250-μm holes in each of the two pieces. These two mould pieces along with the optical fibres created the integrated channels and ball joint features. Mould vents allowed PDMS to be injected by hand using a syringe and prevented air bubbles from being trapped within the finished part. The filled mould was placed in an oven to cure at 80°C for 1 h. Once the mould had cooled enough to be handled, the fibres were removed to form the integrated channels (Fig. 2b, c). The two mould pieces defining the ball joints were removed and the remaining pieces formed the aforementioned PMMA shell (Fig. 2a). The total width of the BJIB, inclusive of the protruding ball joint features, is 11 mm and the total height and length including the PMMA shell are 6 and 40 mm, respectively.

A completed BJIB is shown in Fig. 2a. A PDMS insert with ball joint features (Fig. 2b, c) is housed in a PMMA shell for stability (Fig. 2a). The PDMS portion of the BJIB contains twelve 240 μm diameter integrated channels, spaced 2.25 mm centre-to-centre which are bookended and centred within ball joint features (Fig. 2b, c). The ball joint features have a cylindrical portion with outer diameters (OD) of 2 mm and width of 1 mm, and a semi-spherical feature with 0.5 mm radius and 0.5 mm height (Fig. 2b, c).

BJIB-90s (Fig. 3) were similarly manufactured. The BJIB-90 has eight 240 μm diameter integrated channels spaced 2.25 mm centre-to-centre which bend through 90° within the PDMS portion and end in a terminal ball joint feature on the bottom face (Fig. 3b). The BJIB-90 ball joint features are sized identically to those of the BJIB with the exception of the cylindrical feature which protrudes by 0.5 mm, as compared to 1 mm for the BJIB. The 90° turns were made by bending the fibres through the mould (Fig. 3a). The PDMS portion of the BJIB-90 measures 14 mm in length, 26 mm in width and 5 mm in height including the ball joint features. The total width, length and

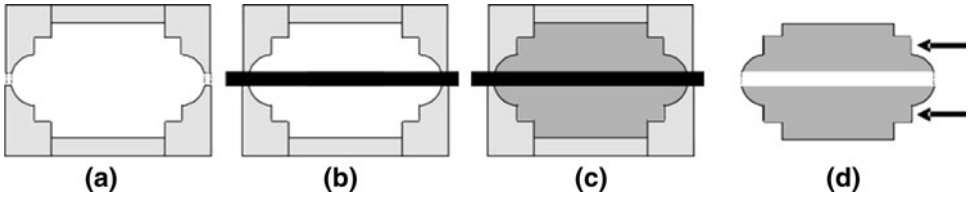

Fig. 1 Schematic representation of BJIB fabrication. **a** Cross-sectional view of a PMMA mould used to cast BJIB. Mould shapes defining the BJIB sealing features are shown on left- and right-hand side of mould. Openings at ends represent through holes in which fibres are placed. **b** 240 μm diameter fibre inserts resulting in integrated channels are placed through terminal mould pieces and are centred within structures forming ball joint features. **c** PDMS is cast into the mould and cured. Following curing, fibre inserts are removed and the mould disassembled. **d** Cross-section of completed PDMS portion of the BJIB. *Arrows* indicate the ball joint sealing surface areas

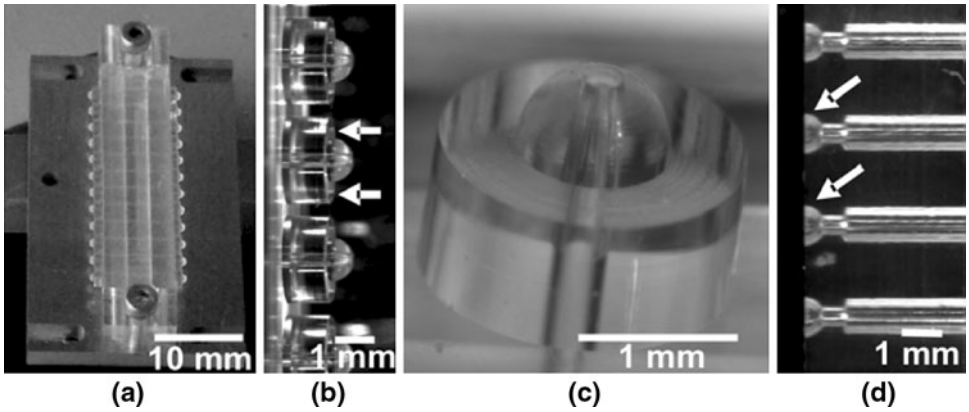

Fig. 2 BJIB design and fabrication. **a** Completed BJIB (PDMS portion housed in PMMA shell) mounted on aluminium base plate used for testing. Ball joint features protrude from both sides. **b** Close-up of ball joint features. The sealing surfaces are indicated with *arrows*. **c** Close-up of single ball joint interconnection feature. The integrated channel can be seen in the middle of the balljoint. **d** Top view of PMMA component of needle assembly used in pressure testing. *Arrows* indicate features complementary to ball joint features shown in **b** and **c**

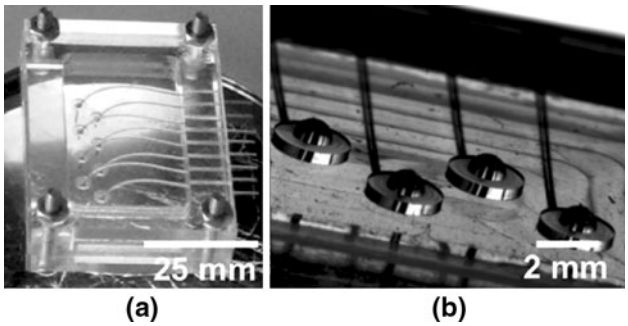

Fig. 3 BJIB-90 design and fabrication. **a** Mould used for BJIB-90 fabrication. Fibre inserts are bent through 90° within the mould. **b** Close-up of array of ball joint interconnection features on the interfacing BJIB-90 surface. Integrated channels bend and exit through the top of the semi-spherical features (not shown)

height of the BJIB-90 within its PMMA shell are 18, 36 and 6 mm, respectively. Prior to testing, both the BJIB and BJIB-90 were inspected for damage, poorly formed features and/or blocked channels.

2.2 Leak pressure testing

2.2.1 BJIB pressure testing

The pressure test assembly was similar to that previously described (Sabourin et al. 2009). The BJIB was aligned and compressed from a width of 11.0 to 9.5 mm between two needle assemblies (Fig. 4a) on an aluminium base plate. The degree of compression for BJIB testing, from a width of 11 to 9.5 mm, was selected to approximate the compression and forces acting on sealing elements in our previous report (Sabourin et al. 2009). Needle assemblies provide 12 fluidic inlets/outlets complementary in shape to the BJIB with 250 μm diameter througholes centred within a semi-spherical feature of radius 0.5 mm at the interfacing PMMA surface (Fig. 4a). These were manufactured by micromilling. Leak pressures were determined visually, under microscopic observation, and using a pressure sensor (Honeywell, Germany). A leak was defined as the point at which a dye solution breached the outer edge of the circular feature of the ball joint. In order to simulate wear, the BJIB was repeatedly placed into the test assembly. Pressure measurements were made every fifth insertion. For reasons previously described (Sabourin et al. 2009), tests were voluntarily stopped if the pressure reached 6.1 bar.

2.2.2 BJIB-90 pressure testing

In order to pressure test the BJIB-90, it was aligned and compressed over the top surface of a PMMA chip containing closed channel architectures. This was done using 2 mm screws until the PMMA shell was flush with the surface of the holder (Fig. 6b). This compresses the cylindrical feature of the BJIB-90 interconnections (Fig. 3b) against the top surface of the PMMA chip. Fluids were introduced by press-fitting 0.4 mm needles into the channels on the side of the BJIB-90. Prior to securing the BJIB-90 to the PMMA test chip, the channels of the BJIB-90 were filled with dye solution to limit the amount of air in the pressure test system. As above, leak pressures were determined visually, under microscopic observation, and using a pressure sensor (Honeywell, Germany). A leak was defined as the point at which a dye solution breached the outer edge of the circular feature of the ball joint. As a result of leaks observed at the pressure sensor interface for the BJIB-90 pressure measuring set-up during initial tests, tests were voluntarily aborted shortly after reaching

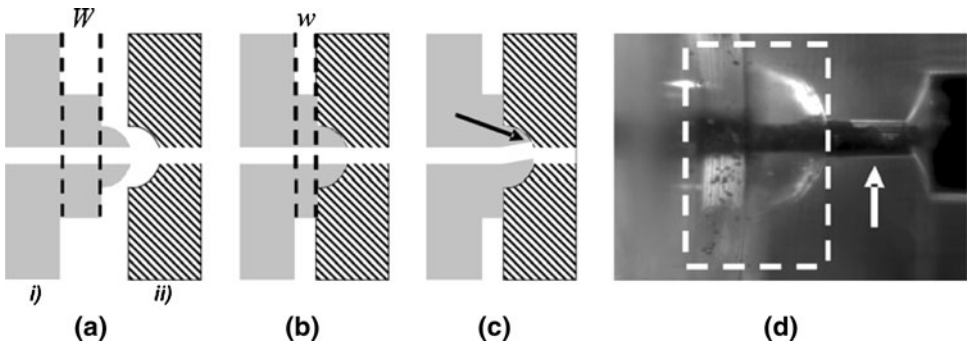

Fig. 4 BJIB interfacing. **a** PDMS BJIB (*i*) and complementary feature on microfluidic device (*ii*) when not compressed together. The cylindrical feature protrudes from the interconnection block by a length of *W*. **b** Ideal alignment. When compressed against the microfluidic device, the cylindrical feature is compressed to a width of *w*, where $w < W$. The semi-circular feature entering the microfluidic device is not compressed. Identical channel sizing in the BJIB and the microfluidic device results in zero dead volume interconnections. **c** Near-ideal alignment. The *arrow* indicates a slight internal misalignment between the BJIB's semi-circular feature integrated channel and the microfluidic device channel. **d** Close-up of the BJIB and needle assembly interface in pressure test assembly. Dye solution is used to facilitate visualisation. The BJIB interconnection feature is shown in the dashed white box. The *arrow* points to the inlet of the PMMA needle assembly component shown in Fig. 2d. The system results in effective zero dead volumes

pressures of approximately 4 bar. The BJIB-90 was put through four test cycles. In each test cycle, six of the eight interconnections (Fig. 3b) were tested.

2.3 BJIB-90 demonstration

In order to demonstrate the BJIB-90 interconnection, a test chip was made by micromilling eight channels measuring 1.0 mm in width and 0.5 mm in depth in 1.5 mm thick PMMA sheet. Channels were terminated with 1.0 mm diameter inlet and outlet holes. PCR tape (Abgene, United Kingdom) sealed the channels. The microfluidic chip was placed in an aluminium holder in which the top surfaces of the chip and aluminium holder were flush. The BJIB-90s were then aligned and compressed against the top of the microfluidic chip as described for pressure testing and fluids were introduced in a similar manner. In order to simulate exaggerated wear, the BJIB-90 was placed near the middle of the microfluidic chip and dragged across the top surface until it was properly aligned and was then pressed to the surface of the microfluidic chip. This was repeated over 40 times.

3 Results

3.1 Fabrication

BJIB and BJIB-90 moulds were easily assembled and parts were readily cast with PDMS. Moulds yielded reproducible ball joint features (Figs. 2b, c, 3b). Fibres were removed without demoulding agents to create unobstructed and wholly integrated, circular channels. The fibre's properties and the mould's precision resulted in part-to-part and channel-to-channel consistency for both the BJIB and BJIB-90, and similar channel curvatures for the latter.

3.2 Assembly of BJIBs for testing

The BJIB and BJIB-90 were designed to compress only the cylindrical portion of the ball joint feature (Fig. 2b, c). The semi-spherical portion mates with an identically dimensioned feature, in this case found on the needle assemblies used for testing, and should not be compressed (Fig. 4a, b) when the BJIB is placed against a complementary surface. Visual inspection indicated that this was the case. This yields near zero dead volume interconnections (Fig. 4d).

3.2.1 Pressure testing

For all BJIB test cycles, the BJIB aligned to the corresponding 24 fluidic inlet and outlet features of the needle assemblies. Ball joint features had self-aligning tendencies to the corresponding feature in the needle test assemblies. Pressure test results are shown in Fig. 5. The number of test points collected for each insertion tested varied as dye solution leaked from one interconnection site could hinder visual inspection of adjacent interconnections.

The average test pressure through all test cycles was 4.7 bar. All individual leak pressures were above the 2-bar threshold applicable to most microfluidic applications (Bhagat et al. 2007). All insertions established fluidic connections through the BJIB and needle assemblies. As structures and channels are similarly formed in the milling/casting process, sampling of 6–7 of the 12 BJIB channels yields a representative assessment of leak pressure.

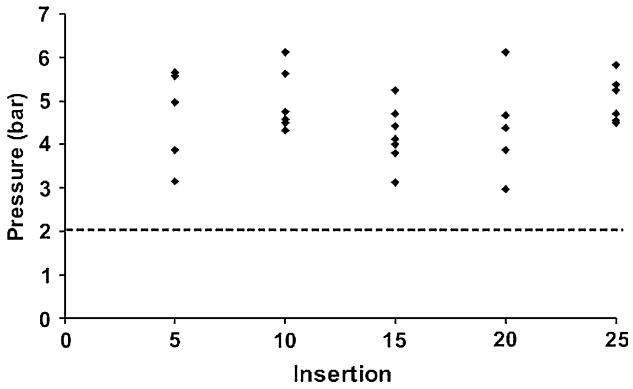

Fig. 5 Individual pressure test values for the BJIB. To simulate wear the BJIB was repeatedly inserted and removed from the pressure test assembly. Pressure test values were measured every 5th insertion starting at the 5th insertion

Lower test pressures for the BJIB were attributable to two causes. The first related to near-ideal alignments (Fig. 4c). In these, the semi-spherical portion of the interconnection feature (Fig. 2b, c) was globally aligned within the complementary feature in the needle assemblies but with slight misalignment of the integrated channel to the needle assembly channel (Fig. 4c). Although fluid still passed through the BJIB in these near-ideal alignments, pressure limits were lower as compared to cases with ideal alignment. The second cause was related to the configuration of the test assembly. Contrary to our previous report, the interconnection enters the microfluidic device (Fig. 4d). The semi-spherical portion enters the interfacing chip through the same horizontal forces which compress the cylindrical features (Fig. 4). Disassembly between insertions resulted in vertical forces and movements which damaged several of the semi-spherical features by the 20th insertion. By the 25th insertion some features had degraded to the point of not warranting further testing and testing was stopped.

During pressure testing the BJIB-90 also demonstrated self-aligning tendencies to the PMMA test chip. The BJIB-90 was tested through four insertion and removal cycles, with six of eight channels tested per insertion. No leaks were observed through all test cycles. As described (Sect. 2.2.2), a voluntary cut-off was set near 4 bar. This point was two-fold above the 2 bar threshold applicable to most microfluidic applications (Bhagat et al. 2007). Average pressure values for test cycle 1, 2, 3 and 4 were 4.6, 4.3, 4.3 and 4.3 bar, respectively. The minimum recorded pressure value was 4.0 bar. The greater average value for test cycle 1 does not indicate degradation of the BJIB-90 or its sealing capabilities. It results from initial tests in cycle 1 where pressures were allowed to run further above the 4-bar cut-off point.

3.3 BJIB-90 demonstration

Effectively planar interconnections to a flat, 1.5 mm thick PMMA chip, through two BJIB-90s were demonstrated (Fig. 6).

Interfacing a microfluidic chip to two BJIB-90s took only a few minutes (to tighten screws). As in pressure testing, during wearability testing the ball joint features provided alignment feedback to the user and would 'snap' into position on the top surface of the microfluidic chip. Following over 40 exaggerated insertion and removal cycles (see materials and methods), no visual signs of wear were noted. When attached to the aluminium housing, the BJIB-90's ball joints were fully compressed and made flush with the top surface of the device. Initial prototyping of the BJIB-90 showed that the curvature of the integrated channels must be set to avoid pinching and closing off of channel when the BJIB-90 is compressed against the microfluidic device.

4 Discussion

The new IB designs offer additional advantages compared to the O-ring based design previously reported (Sabourin et al. 2009). The BJIBs demonstrate self-aligning tendency which simplifies production of junctions between the chip

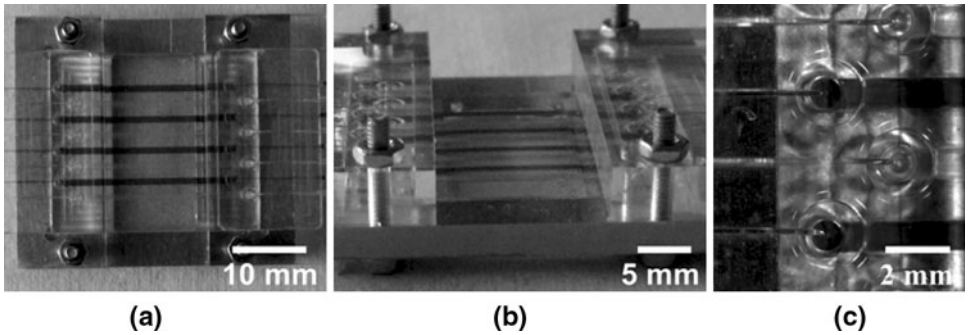

Fig. 6 BJIB-90 Interconnection. **a** *Top view* of two BJIB-90s interfacing with a thin, 1.5 mm thick PMMA chip. Alternating channels filled with dye solution. **b** *Side view* of demonstration chip. **c** Close-up of BJIB-90 interconnection

and the BJIB. In addition, the BJIB-90 made it possible to make connections to the top of the chips. For our previous IB report, dead volumes were estimated between 165 and 185 nL. As seen in Fig. 4, effective dead volumes for the BJIB are near zero even in the case of near-ideal alignments (Fig. 4d). It is very difficult to reproduce Fig. 4d for the BJIB-90, however, according to the analysis of Puntambekar and Ahn (2002) dead volumes are also expected to be near zero for the BJIB-90 when the vertical channel entry is properly manufactured in the interfacing chip.

One design issue to be addressed is degradation of the BJIB. Degradation was attributable to the design of the pressure measuring set-up. Disassembly resulted in vertical forces perpendicular to the horizontal compression forces. These forces damaged several of the semi-spherical features 'trapped' in the needle assemblies. Securing and interfacing BJIBs and chips in microfluidic systems are being reviewed to prevent damage but will likely involve a side by side slide in approach. As the IB fabrication method is suitable to other elastomers, harder, more durable elastomers and/or PDMS composition, i.e. the ratio of elastomer to curing agent, could also be used to avoid degradation.

All individual test pressures for the BJIB (Fig. 2) were above the 2-bar threshold, however, pressure limits were not as high as our previous report. The degree of compression for BJIB testing, from a width of 11 to 9.5 mm, was selected to approximate the compression and forces acting on sealing elements in our previous report. Higher test pressures would likely have been realised for the BJIB with further compression or if the sealing surface of the cylindrical features was decreased as both these changes should result in greater sealing force per unit area of the cylindrical feature. However, such changes would also decrease ease of use. Although many test points reach values similar to our previous report (Fig. 5), between 5 and 6 bar, lower test pressures result from degradation and non-ideal alignments (Fig. 4c). Non-ideal alignments could be reduced by using either harder elastomers to prevent twisting of the semi-spherical features within the complimentary and interfacing feature (Fig. 4c, d) or interfacing the BJIB to a channel that has a greater diameter than that of the integrated channel. The latter comes at the expense of increasing dead volume.

Individual test pressures for the BJIB-90 were all at least 2 fold greater than the 2-bar threshold suggesting that the BJIB-90 is suitable for a wide range of microfluidic applications. In addition, the BJIB-90 increases the number of microfluidic device materials and designs with which the interconnection block approach can be used because the BJIB-90 interfaces with top or bottom surfaces of chips instead of the sides. For instance, thin side-walled devices made from polymers, glass or silicon can be addressed by the BJIB-90, whereas they cannot be by the BJIB or the IB version previously reported (Sabourin et al. 2009). Although addressing the device from the top, the interconnections are effectively planar and allow unobstructed microscopic observation (Fig. 6). As compared to the BJIB and the O-ring based IB design (Sabourin et al. 2009), the BJIB-90 does not require that the side-wall of the microfluidic device to be polished (Sabourin et al. 2009) (as top surfaces are often very smooth) or machining of shapes complementary to the ball joints on the side face of the microfluidic device. The vertical interfacing and compression of the BJIB-90 to a microfluidic device provides sealing force in the same plane as the interface. This is in contrast to the BJIB, and as such the semi-spherical portion of the interconnection feature did not degrade.

5 Conclusion

Additional designs of Interconnection Blocks, a simple method and practical approach for creating re-usable, multiple, aligned and planar interconnection methods have been presented. These provide zero dead volumes and connections to flat or thin side-walled microfluidic devices and supported pressures above the threshold considered applicable to most microfluidic applications (2 bar). Easy to fabricate and use, of low-cost and made through a flexible and scalable approach, the new IB configurations presented increase the potential configurations, substrates and applications with which IBs can and will be used.

Acknowledgements The authors acknowledge funding from a DTU Ph. D. student grant, the Danish Strategic Research Council (NABIIT programme ProCell) and the FP7—EXCELL.

References

Bhagat AAS, Jothimuthu P, Pais A, Papautsky I (2007) Re-usable quick-release interconnect for characterization of microfluidic systems. J Micromech Microeng 17(1):42–49

Chiou CH, Lee GB (2004) Minimal dead-volume connectors for microfluidics using PDMS casting techniques. J Micromech Microeng 14(11):1484–1490

Fredrickson CK, Fan ZH (2004) Macro-to-micro interfaces for microfluidic devices. Lab Chip 4(6):526–533

Pepper M, Palsandram NS, Zhang P, Lee M, Cho HJ (2007) Interconnecting fluidic packages and interfaces for micromachined sensors. Sens Actuators A 134:278–285

Puntambekar A, Ahn CH (2002) Self-aligning microfluidic interconnects for glass- and plastic-based microfluidic systems. J Micromech Microeng 12(1):35–40

Saarela V, Franssila S, Tuomikoski S, Marttila S, Ostman P, Sikanen T et al (2006) Re-usable multi-inlet PDMS fluidic connector. Sens Actuators B Chem 114(1):552–557

Sabourin D, Snakenborg D, Dufva M (2009) Interconnection blocks: a method for providing reusable, rapid, multiple, aligned and

planar microfluidic interconnections. J Micromech Microeng 19(3):035021 (9pp). doi: 10.1088/0960-1317/19/3/035021

Snakenborg D, Perozziello G, Geschke O, Kutter JP (2007) A fast and reliable way to establish fluidic connections to planar microchips. J Micromech Microeng 17(1):98–103

Yang Z, Maeda R (2002) A world-to-chip socket for microfluidic prototype development. Electrophoresis 23(20):3474–3478

Yang Z, Maeda R (2003) Socket with built-in valves for the interconnection of microfluidic chips to macro constituents. J Chromatogr 1013:29–33

PUBLICATION 3:

"One-step fabrication of microfluidic chips with in-plane, adhesive-free interconnections"

One-step fabrication of microfluidic chips with in-plane, adhesive-free interconnections

2010 J. Micromech. Microeng. 20 037001

(http://iopscience.iop.org/0960-1317/20/3/037001)

J. Micromech. Microeng. **20** (2010) 037001 (7pp) doi:10.1088/0960-1317/20/3/037001

TECHNICAL NOTE

One-step fabrication of microfluidic chips with in-plane, adhesive-free interconnections

D Sabourin, M Dufva, T Jensen, J Kutter and D Snakenborg

DTU Nanotech, Department of Micro- and Nanotechnology, Technical University of Denmark (DTU), Ørsteds Plads, Bygning 345Ø, DK-2800, Kongens Lyngby, Denmark

E-mail: detlef.snakenborg@nanotech.dtu.dk

Received 27 August 2009, in final form 1 December 2009
Published 15 February 2010
Online at stacks.iop.org/JMM/20/037001

Abstract
A simple method for creating interconnections to a common microfluidic device material, poly(methyl methacrylate) (PMMA), is presented. A press-fit interconnection is created between oversized, deformable tubing and complementary, undersized semi-circular ports fabricated into PMMA bonding surfaces by direct micromilling. Upon UV-assisted bonding the tubing is trapped in the ports of the PMMA chip and forms an integrated, in-plane and adhesive-free interconnection. The interconnections support the average pressure of 6.1 bar and can be made with small dead volumes. A comparison is made to a similar interconnection approach which uses tubing to act as a gasket between a needle and port on the microfluidic chip.

S Online supplementary data available from stacks.iop.org/JMM/20/037001/mmedia

(Some figures in this article are in colour only in the electronic version)

1. Introduction

Increased adoption of microfluidic approaches can be encouraged by providing simple, low-cost, reliable and accessible fabrication methods and techniques. When beginning microfluidic work researchers often encounter difficulties establishing fluidic connections to devices. In this report a simple method for creating integrated interconnections to micromilled poly(methyl methacrylate) (PMMA) devices with deformable tubing is presented. PMMA is commonly used in microfluidic applications as it is highly amenable to fabrication by cost-effective and versatile methods such as micromilling, laser ablation, injection moulding and hot embossing. PMMA is of low cost, optically transparent and additionally it can readily be chemically modified or have biomolecules linked to its surface [1]. This report describes the creation of interconnections to PMMA microfluidic devices. Interconnections solutions for glass and silicon- [2–10] and PDMS- [11–18] based microdevices are described elsewhere and Fredrickson and Fan [19] provide a comprehensive review of interconnections.

Use of adhesives, such as epoxy, to create permanent and integrated interconnections by directly attaching needles and tubings to ports of microfluidic devices is usually regarded as the easiest method to create interconnections but suffers from drawbacks including risk of clogged channels, larger dead volumes resulting from manual alignment over small features. For multiple connections, this method can be time consuming and laborious. Methods to make permanent interconnections which prevent clogging have been proposed; however, not all are applicable to polymeric processing [8–10]. Solutions comparable to the method presented for creating interconnections to polymeric devices without adhesive use have been proposed.

Yang and Maeda [20, 21] used protruding silicone tubing to connect to the top surface of microfluidic devices placed in a socket. The protruding lengths of tubing act as O-rings when pressed against the face of a microlfluidic chip.

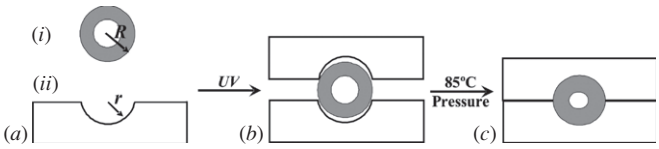

Figure 1. Schematic representation of the compressed tubing interconnection method. (*a*) (*i*) Cross-section of deformable tubing with outer radius R and (*ii*) cross-section of one of two PMMA layers milled with ball mill to yield nearly semi-circular half-ports with radius r. Note that $R > r$. (*b*) PMMA surfaces were UV exposed and aligned above and below the tubing. Parts were then placed in a bonding press under pressure and at 85 °C for 1 h. (*c*) Cross-section of completed interconnection. Due to compression, the ID of the tubing has decreased.

Snakenborg *et al* [22] demonstrate in-plane interconnections using protruding soft tubing and also provide a theoretical treatment of this approach. Bhagat *et al* [23] fabricated a port clamp that used both O-rings and Teflon tubings to connect to the top surface of microfluidic devices made from cyclic olefin copolymer (COC). The Teflon tubing could be bent to create effectively in-plane interconnections. Perroziello *et al* [24] used thermal bonding to integrate O-rings into PMMA microfluidic chips. The microfluidic chip was then interfaced to a housing which contained vertically oriented metal ferrules with outer diameters (OD) greater than the inner diameter (ID) of the integrated O-ring. The mating of the chip with the housing resulted in a press-fit interconnection. Multiple, in-plane interconnections to polymeric devices using PDMS interconnection blocks cast from micromilled moulds were proposed by Sabourin *et al* [25]. The interconnection blocks contained multiple integrated channels bookended by O-ring like features. When a polymeric chip was placed between two interconnection blocks, the O-ring features are compressed and create fluidic connections to the polymeric chip. Though the above described approaches provide interconnection solutions, their implementation is more involved as they necessitate creation of additional components and assemblies apart from the microfluidic chip; they address including holders, moulds and clamps.

This technical note presents the research community with two methods for creating interconnections to PMMA. The first interconnection method presented creates a press-fit between readily available tubing and a PMMA microfluidic device during UV-assisted bonding. This is referred to as the compressed tubing interconnection. Leak pressures for this interconnection method are compared to a second press-fit method we commonly use referred to as the needle-tubing press-fit. This second method inserts an oversize needle into tubing with undersized ID. The tubing is housed in a port with the same OD as the tubing and as such the tubing acts as a gasket between needle and chip.

2. Materials and methods

2.1. Interconnection design and fabrication

Schematic representations of the compressed tubing and needle-tubing press-fit interconnection methods are shown in figures 1 and 3 respectively.

For the compressed tubing interconnection method two bonding surfaces of a PMMA chip were micromilled with ball end mills to yield 'half-ports' with semi-circular profiles (figure 1(*a*)). Ball end mills with diameters slightly smaller than the tubing OD were used. For this report, 2 mm ball end mills were used for 2.1/0.7 mm OD/ID silicone tubing (Reichelt Chemietechnik GmbH, Germany). Additionally, when milling the half-port features in the PMMA, the feature depth is set at less than half the OD (i.e. radius) of the tubing. Half-port features in each half of the PMMA test chips were milled to depths of either 0.90 or 0.95 mm such that when two surfaces are aligned and placed together for bonding, nearly circular ports of 1.8 mm or 1.9 mm diameter result. Both port sizes are thus undersized compared to the OD of the tubing. To bond PMMA chips, bonding surfaces were placed underneath a UV light source (DYMAX EC 5000 with p/n 36970 bulb, Torrington, Connecticut) for 60 s at a distance of about 12 cm. As per the manufacturer's instructions, the light source was warmed up for 5 min prior to the exposure. After UV treatment (figure 1(*b*)), the tubings were aligned to the half-ports on one of the PMMA layers. The second PMMA layer was aligned bonding side down on top of the first layer and tubing (figure 1(*b*)). The entire bonding assembly was placed in a bonding press (P/O/Weber, Remshalden, Germany) with press heating plates set at 85 °C and an initial applied pressure of 1.0×10^5 kN m^{-2}. After 1 h the heating plates were turned off and the bonding assembly was allowed to cool to room temperature in the press.

A total of 6 PMMA chips were made for testing. Three of the six chips were made by compressing 2.1 mm tubing into 1.8 mm ports and the other three were made by compressing 2.1 mm tubing into 1.9 mm ports. Each chip had eight separate interconnections (figure 2(*a*)). For both 1.8 and 1.9 mm chips, four of the eight interconnections had 3 mm

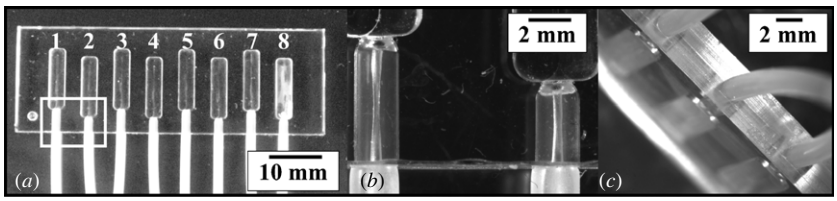

Figure 2. Compressed tubing interconnections. (*a*) PMMA chip used for pressure testing. Eight individual interconnections, assigned positions 1–8, were found on each chip. Tubing inserts of 5 mm were found in positions 1, 3, 5 and 7, and 3 mm tubing inserts were found in positions 2, 4, 6 and 8. A close-up of the area within the white box is shown in (*b*). (*b*) Top view of interconnection with 3 mm (left) and 5 mm (right) tubing inserts. (*c*) Side view of PMMA chip showing in-plane interconnections.

Table 1. Compressed tubing interconnection pressure data.

Port size diameter (mm)	Tubing insertion length (mm)	Pressure data: Average (bar)	SD (bar)	n	Individual values (bar)
1.8	3	4.4	2.0	12	6.1, 6.1, 3.1, 2.1, 0.9, 0.9, 0.6, 0.6, 6.1, 6.1, 6.1, 0.6
1.8	5	0.8	0.1	11[a]	5.1, 6.1, 6.1, 1.4, 1.1, 0.6, 0.8, 2.6, 1.4, 0.8, 0.6, 6.1
1.9	3	5.4	1.7	12	6.1, 6.1, 6.1, 0.6, 6.1, 6.1, 6.1, 3.6, 6.1, 6.1, 6.1, 5.6
1.9	5	6.1	0	11[a]	6.1, 6.1, 6.1, 6.1, 6.1, 6.1, 6.1, 6.1, 6.1, 6.1, 6.1

[a] Two data points were excluded. For the first a premature leak occurred in the pressure measuring setup. For the second improper handling of chip following bonding cracked the PMMA above one chamber.

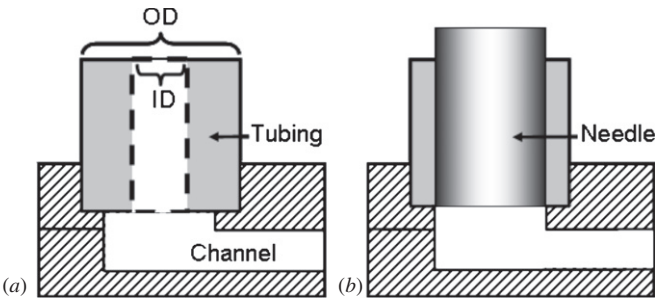

Figure 3. Needle-tubing press-fit interconnection. (*a*) Tubing with the same outer diameter (OD) as the circular port is inserted into the port directly above a microfluidic channel. (*b*) A needle with a larger OD than the tubing's ID is inserted into the tubing. The tubing is compressed against both the needle and sidewall of the device. If the microfluidic channels dimensions and needle diameters are properly selected and aligned, small dead volumes can result [9].

long tubing inserts and the remaining four interconnections had 5 mm long tubing inserts (figures 2(*a*) and (*b*)). The 3 and 5 mm tubing inserts were altered (figure 2(*a*)). To facilitate and allow systematic investigation of failure modes each interconnection was assigned a position: 5 mm tubing inserts were in positions 1, 3, 5 and 7, and 3 mm tubing inserts were in positions 2, 4, 6 and 8 (figure 2(*a*)).

For the needle-tubing press-fit approach (figure 3), tubing is placed in a port fabricated into the top surface of the microfluidic device. This port has the same OD as the tubing (figure 3(*a*)). A blunted syringe needle with larger OD than the tubing's ID is then inserted (figure 3(*b*)) into the tubing. Compression of the tubing against both the sidewall and the needle creates a seal. To demonstrate this method, the same 2.1 mm OD silicone tubing (Reichelt Chemietechnik GmbH, Germany) with 0.7 mm ID was cut to 7 mm lengths with an angular cut of 1 mm pitch at one end. The angled cut facilitates placement of the tubing in the port. The angled end was inserted manually into 2.1 mm diameter port holes with 3.75 mm depth. The port holes were made by drilling a 5 mm thick PMMA plate using a micromilling machine (Folken, Glendale, California). Syringe needles with OD of 0.7, 0.8 and 0.9 mm were blunted and inserted into tubing pre-mounted in the PMMA plate holes.

2.2. Leak pressure testing

Leak pressures were determined visually and using a pressure sensor (Honeywell, Germany). For the compressed tubing interconnections (figure 2), observation through a microscope was used. For the needle-tubing press-fit method, microscopic observation was not required as leaks were sudden and violent, whereas for the compressed tubing method they were not. For compressed tubing interconnections, leaks were defined as the point at which a dye solution breached the outside of the tubing at the edge of the PMMA chip (figure 2(*c*)). The dye solution was pumped from a syringe pump to the interconnection being tested. Steps were taken to limit the amount of air in the system as interconnections were tested in chips with closed channels. For the needle-tubing press-fit method (figure 3), a new piece of tubing and a new needle were used for each measurement. The needle-tubing press-fit method test values were collected first. As a result of observed leaks in the pressure measuring setup during testing of the needle-tubing press-fit method above 6.1 bar, tests for the compressed tubing method were voluntarily stopped at 6.1 bar. This value is three times greater than the 2 bar pressure limit described as applicable to most microfluidic applications [23]. For the needle-tubing press fit method, in cases where the test setup leaked the final pressure recorded was taken as the test value.

3. Results and discussion

3.1. Compressed tubing interconnections

The compressed tubing method simultaneously yields the finishing of the PMMA chip and the integration of in-plane interconnections during the bonding process. UV radiation reduces the glass transition temperature of polymer's surface layer, only several microns deep, without changing the glass transition temperature of the bulk polymer [26, 27]. Structures can then be bonded above the glass transition temperature of the surface layer but below that of the bulk PMMA layer. Sealing is thus permitted without a loss in structure quality.

Visual inspection of the compressed tubing interconnection test chips indicated that the bond quality of chips with 1.9 mm ports was superior to that when using 1.8 mm ports (figure 4). Areas where the two PMMA layers were not well bonded were seen adjacent to the interconnections on 1.8 mm port chips (figure 4(*b*)). For 1.8 mm port a physical limitation was reached where tubing could not consistently be compressed within the port opening during the bonding process. Bond quality suffered and, as a result, so did interconnection performance (table 1). The compression of the tubings affected the geometry of the channels inside the tubings. Tubing channels were more constricted for 1.8 mm port chips versus 1.9 mm port chips,

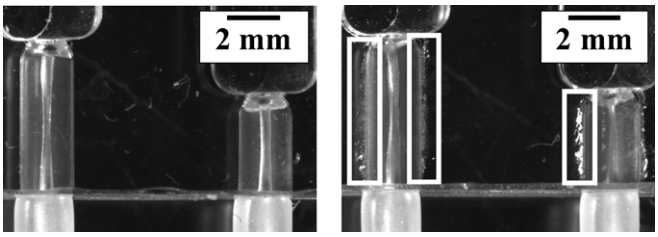

(*a*) (*b*)

Figure 4. Bond quality of compressed tubing interconnections. (*a*) 1.9 mm port interconnections for a 5 mm (left) and 3 mm (right) long tubing insert. 5 mm tubing inserts were more constricted than 3 mm tubing inserts. (*b*) 1.8 mm port interconnections for a 5 mm (left) and 3 mm (right) long tubing insert. Boxes indicate areas representative of poor bonding.

and for 5 versus 3 mm inserted tubing lengths (figure 4); however, no blocked channels were observed.

Table 1 presents results from a first test cycle of individual interconnections on chips with 1.8 or 1.9 mm ports and 3 or 5 mm tubing inserts. 1.9 mm port interconnections yielded higher and more consistent pressure performance as a result of better bond quality (table 1). For 1.8 mm ports, data scatter correlated to bonding quality (figure 4(*b*)).

For 1.9 mm ports, three values were recorded below the maximum 6.1 bar: 0.6, 3.6 and 5.6 bar. All three values came from position 8, a 3 mm long tubing insert, on the three separate 1.9 mm port sized chips. Inspection of position 8 for 1.9 mm port chips showed a clearly reduced bond quality. Position 8 also yielded the lowest pressure values for the three 1.8 mm port chips. A systematic failure in bonding, e.g. caused by an uneven distribution of bonding forces, is attributed as a cause and suggests that visual inspection of the bond quality prior to the usage is strongly advisable. Given the systematic failure at position 8, if these data points are removed, there is no difference in pressure limits for 1.9 mm ports with 3 or 5 mm long tubing insertions as both are tested with an average of 6.1 bar and SD of 0. However, a shorter tubing insert is probably preferable as the tubings were less constricted and less chip space was used (figure 4).

Test devices with multiple, as opposed to a single, interconnection were used to validate the pressure limits of the compressed tubing method. This is representative of microfluidic chips which need multiple reagents to be added to one reactor, or employ hydrodynamic focusing or in cases where a single chip contains many parallel but individually addressable fluidic networks. Importantly, as the failure of a single interconnection below a required design pressure threshold usually results in yield loss, system downtime and ultimately a lost experiment, it is important that the lowest expected pressure values are well above the threshold. Insertion of the 2.1 mm tubing 1.9 mm ports (table 1) consistently provided performance three times greater than the threshold of 2 bar applicable for most microfluidic applications. Owing to the pressure test setup limitations, it is likely that leak pressures for the 1.9 mm port size conditions are underestimated.

Re-usability and robustness to handling from repeated connection and removal from the test system was demonstrated by repetitive testing of a 1.9 mm port feature chip. Individual interconnections were tested up to four more additional times and all pressure readings reached 6.1 bar. Further insertion cycles could have been tested but due to PMMA's properties, including low cost, we consider this material most suitable for one-time use and/or rapid prototyping.

Table 2. Needle-tubing press-fit pressure data.

Tubing OD (mm)	Needle OD (mm)	Pressure data: Average (bar)	SD (bar)	*n*	Individual values (bar)
2.1	0.7	0	0	2	0, 0
	0.8	6.4	0.6	5	6.1, 5.7, 7.4, 6.1, 6.4
	0.9	7.4	0.6	4	6.3, 7.1, 7.8, 6.9

3.2. Needle-tubing press-fit

Tubing pieces and blunted needles were easily introduced into pre-fabricated holes and the tubing, respectively. Results for this method are shown in table 2. The reader may recall that these values were collected prior to values for the compressed tubing method and that following the observation of leaks in the measuring setup the voluntary stop limit of 6.1 bar was used for the compressed tubing method. Therefore, in some cases values reported in table 2 are above this point.

Leaks occurred immediately for 0.7 mm OD needle inserts. For 0.8 mm needle inserts, the average leak pressure was 6.4 bar with a maximum and minimum of 7.4 and 5.7 bar. For 0.9 mm needle inserts the average leak pressure was 7.0 bar with a maximum and minimum of 7.8 and 6.3 bar. Values for 0.9 mm needles are likely underestimated due to aforementioned leaks in the test setup. The needle-tubing press-fit method creates connections quickly and supports pressures well above the 2 bar pressure limit applicable to most microfluidic applications [23] and should work equally well with other polymers. Additionally, it performs equally well as a similar method reporting maximum pressure of 5.6 bar but which uses epoxy to affix syringe needles into polymeric ports [28].

3.3. Comparison of methods

Both interconnection methods are easily implemented, use readily available materials, are adhesive-free and yield seal performances well above 2 bar (tables 1 and 2) threshold. The tubing size used here was selected for ease of handling. In our experience, handling tubings less than 2 mm in diameter can be cumbersome. Both interconnection methods are applicable to other tubing sizes and initial experiments should quickly provide indication of suitable pairing of over- and undersized elements which provide suitable pressure performance and device yield.

The needle-tubing method ensures very consistent flow resistances from one interconnection to the next. As with other interconnection methods, especially those using glues, epoxies and/or adhesives, the compressed tubing method can introduce flow resistance variations within the interconnection

Table 3. Interconnection methods comparable to compressed tubing.

Method	General description	Pressure limits (bar)[a]	Number of interconnections	In-plane	Ref.
Protruding soft tubing	Silicone tubing compressed to top face	2	10	*y*[b]	[21]
	Silicone tubing compressed to top face	2	20	*y*[b]	[20]
	Silicone tube compressed to side face	12.3	1	*y*	[22]
O-ring	O-rings heat annealed within PMMA chip	7.5	4	*n*	[24]
	O-rings compressed to top face/press-fit with tubing	17	3	*y*[b]	[23]
	Chip placed between PDMS connecting blocks with integrated channels and O-ring features	5.5	24	*y*	[25]

[a] Due to differences in test methods and reporting of data, values reported are either average or maximum values. The reader should consult the appropriate reference for details concerning testing.
[b] Though the connection is made to the top face, tubings used with these methods could be bent to effectively become in-plane.

resulting from differences in the tubing constriction (figure 4). Whether or not this is problematic is both dependent on the application and the method used to drive the fluidic device. Devices driven by pressure sources can be affected by the difference in constriction; however, constant volume displacement pumps negate these differences as fluid velocities and volumetric displacements will be the same within equally sized microfluidic channels located after the interconnections.

Both interconnection methods can result in small dead volumes. The fabrication of high quality microfluidic chips from multiple layers requires proper alignment of layers which in turn reduces dead volumes. Two simple alignment strategies can be implemented: (i) machining aligned holes within the microfluidic chip layers capable of housing alignment pins, or (ii) to machining materials such as aluminium to create bonding assemblies. As used in this study, and in our general experience, it is easy to fabricate aluminium sheets containing holes which house alignment pins coincident with the periphery of the microfluidic chip to provide alignment. With proper chip layer alignment and features as shown in figure 3, and according to the analysis by Puntambekar *et al* [9], the needle-tubing press fit method can yield effectively zero dead volumes.

To minimize dead volumes in the compressed tubing method, tubing must be aligned next to the microfluidic channel entrance. The semi-spherical geometries shown in figures 2 and 4 do not allow such placement; however, these are not representative of channel architectures we would use for applications requiring small dead volumes. The semi-spherical geometries are present because the pressure test microfluidic chips were fabricated using minimum milling steps and tool changes. The semi-spherical geometries can be eliminated with further milling steps which can create geometries highly complementary to the tubing shape. Doing so will allow tubing to be brought next to the microfluidic channel and reduce dead volumes. For dimensions and materials used in this study, the estimated dead volume for tubing aligned to the edge of the semi-spherical geometry and where a 100 × 100 μm is used as the microfluidic channel following the interconnection channel is 1.9 μL (see supplementary information, available at stacks.iop.org/JMM/20/037001/mmedia). We consider this an estimate of maximum dead volume as (i) figures 2 and 4 show that tubing is compressed into this semi-spherical area, thereby reducing the dead volume, and (ii) a 100 × 100 μm channel is representative of the small end of channel dimensions created by micromilling. The compressed tubing procedure (section 2.1) provides feedback to the user with respect to placing tubing next to microfluidic channels. Following UV exposure, the bottom PMMA layer was placed on the bottom half of the aluminium bonding assembly which had alignment pins extending upwards. Tubing was then aligned to the half-ports on the bottom PMMA layer and the alignment pins ensured when the top PMMA layer was brought down on top of bottom layer, the features were aligned. When only lightly pressing the top PMMA layer to the bottom PMMA layer, and before placing the top aluminium layer on the assembly and into the bonding press, tubing could be slid towards the end of the interconnection channel. The user could then determine when tubing could not be further pushed towards the microfluidic channel. The transparent nature of PMMA also allows visual inspection. Therefore, for materials and dimensions used in this study, noting that (i) further milling steps can remove the semi-spherical geometries, (ii) a simple bonding assembly provides tubing alignment feedback to the user, (iii) as shown in figures 2 and 4, tubing is pressed towards the microfluidic channel during the bonding process, and (iv) if the IDs of the tubing and corresponding microfluidic channel are matched, we estimate that dead volumes of approximately 300 nL (see supplementary information, available at stacks.iop.org/JMM/20/037001/mmedia).

The compressed tubing method offers several advantages. Interconnections are formed while the chip is bonded allowing immediate testing and thus avoiding unnecessary downstream processing and/or machining steps. When assembling the PMMA devices following the UV exposure, the tubings provide self-alignment between layers. While the needle-tubing press fit requires additional post-fabrication handling of the microfluidic device, i.e. needle insertion, which could damage and place stress on the device, the compressed tubing method avoids this. When connecting devices using the compressed tubing approach, needles interface only to the tubing end not within the device (figure 2). The compressed tubing approach forms in-plane interconnections better suited to microscopic observation (figure 2) than the needle-tubing press-fit interconnections, which are usually oriented vertically (figure 3) to simplify device fabrication.

Methods comparable to the compressed tubing approach are presented in table 3. The pressure performance of the 1.9 mm ports is within the range of the methods found in table 3. Yang *et al* [20, 21] used 1 mm OD tubings to create interconnections to the top surface of microfluidic chip with interconnection pitches of 2.2 mm [21] or 2.5 mm [20] and Sabourin *et al* [25] report pitch of 2.25 mm using cast PDMS interconnection blocks. Had similar tubing sizes been used in this report, similar interconnection pitches to these methods are possible to achieve. The use of a holder or bonding assembly permitting placement and alignment of tubing is helpful when creating many interconnections or interconnections with similar pitch as those reported. Additionally, the compressed tubing method does not require side surfaces of microfluidic chips to be polished following bonding [22, 25] in order to obtain leak-free interconnections and accommodates slight misalignments between bonding layers. Methods that use holders or clamps [22–25] to create interconnections also dictate chip size and interconnection location. The compressed tubing method is flexible with respect to chip size and interconnection location. Though solutions using holders and clamps facilitate rapid chip testing, the compressed tubing method negates this advantage as interconnections are formed with the chip and tubing, to be hooked up to pumps, etc, is already present.

3.4. Example applications for the compressed tubing method

The compressed tubing method presented is a general method for creating in-plane, adhesive-free interconnections. Though presented for PMMA devices, for polymeric materials for which UV-assisted bonding is not possible, thermal or chemical bonding processes [27] could be used to implement the general approach.

A method which does not incorporate adhesive use to form interconnections is of great advantage as it avoids potential issues related to sensitivity and biocompatibility [29]. We will be using the 1.9 mm port compressed tubing interconnections for investigations related to parallel analysis of microarray hybridization and cell cultures within PMMA devices. The architecture of these devices will closely resemble the PMMA chips presented in figure 2, but with each chamber having both an inlet and an outlet. These applications require pressures much lower than the 6 bar reported. The compressed tubing is well suited to these applications. In particular the in-plane connections afford unobstructed microscopic observation.

4. Conclusions

Both interconnection methods presented are simple to implement. The compressed tubing methods eliminate additional processing steps while rapid, immediate testing is enabled resulting in in-plane interconnections better suited to microscopic observation. The achieved results indicate a strong correlation between bond quality and performance. The use of 0.7 mm/2.1 mm ID/OD tubing with a 1.9 mm port feature created by micromilling PMMA with a 2 mm ball mill yields interconnections which consistently show leak-free performance up to 6.1 bar, well above the 2 bar threshold considered applicable for most microfluidic applications.

Acknowledgments

The authors acknowledge funding from a DTU Ph D student grant, the Danish Strategic Research Council (NABIIT programme ProCell) and the FP7-EXCELL.

References

[1] Chen Y, Zhang L and Chen G 2008 Fabrication, modification and application of poly(methyl methacrylate) microfluidic chips *Electrophoresis* **29** 1801–14
[2] Gonzalez C, Collins SD and Smith RL 1998 Fluidic interconnects for modular assembly of chemical microsystems *Sensors Actuators* B **49** 40–5
[3] Gray BL, Collins SD and Smith RL 2004 Interlocking mechanical and fluidic interconnections for microfluidic circuit boards *Sensors Actuators* A **112** 18–24
[4] Gray BL *et al* 1999 Novel interconnection technologies for integrated microfluidic systems *Sensors Actuators* A **77** 57–65
[5] Lee ES, Howard D, Liang E, Collins SD and Smith RL 2004 Removable tubing interconnects for glass-based micro-fluidic systems made using ECDM *J. Micromech. Microeng.* **14** 535–41
[6] Meng E, Wu SY and Tai YC 2001 Silicon couplers for microfluidic applications *Fresenius' J. Anal. Chem.* **371** 270–5
[7] Pan T, Baldi A and Ziaie B 2006 A reworkable adhesive-free interconnection technology for microfluidic systems *J. Microelectromech. Syst.* **15** 267–72
[8] Pattekar AV and Kothare MV 2003 Novel microfluidic interconnectors for high temperature and pressure applications *J. Micromech. Microeng.* **13** 337–45
[9] Puntambekar A and Ahn CH 2002 Self-aligning microfluidic interconnects for glass- and plastic-based microfluidic systems *J. Micromech. Microeng.* **12** 35–40
[10] Tsai JH and Lin LW 2001 Micro-to-macro fluidic interconnectors with an integrated polymer sealant *J. Micromech. Microeng.* **11** 577–81
[11] Chiou CH and Lee GB 2004 Minimal dead-volume connectors for microfluidics using PDMS casting techniques *J. Micromech. Microeng* **14** 1484–90
[12] Christensen AM, Chang-Yen DA and Gale BK 2005 Characterization of interconnects used in PDMS microfluidic systems *J. Micromech. Microeng.* **15** 928–34
[13] Dalton C and Kaler K 2007 A cost effective, re-configurable electrokinetic microfluidic chip platform *Sensors Actuators* B **123** 628–35
[14] Jo B H, Van Lerberghe L M, Motsegood K M and Beebe D J 2000 Three-dimensional micro-channel fabrication in polydimethylsiloxane (PDMS) elastomer *J. Microelectromech. Syst.* **9** 76–81
[15] Li SF and Chen SC 2003 Polydimethylsioxane fluidic interconnects for microfluidic systems *IEEE Trans. Adv. Packag.* **26** 242–7
[16] McDonald J C and Whitesides G M 2002 Poly(dimethylsiloxane) as a material for fabricating microfluidic devices *Acc. Chem. Res.* **35** 491–9
[17] Quaglio M *et al* 2008 Evaluation of different PDMS interconnection solutions for silicon, Pyrex and COC microfluidic chips *J. Micromech. Microeng.* **18** 055012
[18] Saarela V *et al* 2006 Re-usable multi-inlet PDMS fluidic connector *Sensors Actuators* B **114** 552–7

[19] Fredrickson CK and Fan ZH 2004 Macro-to-micro interfaces for microfluidic devices *Lab Chip* **4** 526–33
[20] Yang Z and Maeda R 2002 A world-to-chip socket for microfluidic prototype development *Electrophoresis* **23** 3474–8
[21] Yang Z and Maeda R 2003 Socket with built-in valves for the interconnection of microfluidic chips to macro constituents *J. Chromatogr.* A 29–33
[22] Snakenborg D, Perozziello G, Geschke O and Kutter JP 2007 A fast and reliable way to establish fluidic connections to planar microchips *J. Micromech. Microeng.* **17** 98–103
[23] Bhagat A A S, Jothimuthu P, Pais A and Papautsky I 2007 Re-usable quick-release interconnect for characterization of microfluidic systems *J. Micromech. Microeng.* **17** 42–9
[24] Perozziello G, Bundgaard F and Geschke O 2008 Fluidic interconnections for microfluidic systems: a new integrated fluidic interconnection allowing plug 'n' play functionality *Sensors Actuators* B **130** 947–53
[25] Sabourin D, Snakenborg D and Dufva M 2009 Interconnection blocks: a method for providing reusable, rapid, multiple, aligned and planar microfluidic interconnections *J. Micromech. Microeng.* **19** 035021
[26] Truckenmüller R, HENZI P, Herrmann D, Saile V and Schomburg W K 2004 Bonding of polymer microstructures by UV irradiation and subsequent welding at low temperatures *Microsyst. Technol.* **10** 372–4
[27] Tsao C W and Devoe D L 2009 Bonding of thermoplastic polymer microfluidics *Microfluidics Nanofluidics* **6** 1–16
[28] Korivii NSaJ L 2007 A generic chip-to-world fluidic interconnect system for microfluidic devices *IEEE 39th Southeastern Symp. on System Theory (Macon, GA, 04–06 March)* 176–80
[29] Stangegaard M, Petronis S, Jorgensen A M, Christensen C B and Dufva M 2006 A biocompatible micro cell culture chamber (microCCC) for the culturing and on-line monitoring of eukaryote cells *Lab Chip* **6** 1045–51

Supplementary Information: Compression method dead volume estimates

A. Maximum dead volume estimate

This is the dead volume estimate for the case where the semi-spherical geometries (figures 2 and 4) and not removed with additional milling steps. As described in the Materials and Methods section, 2 mm ball end mills were used to mill half-port features in both layers of PMMA. The features depth of each half-port channel was set at 0.95 mm. When tubing is aligned to the edge of the semi-spherical geometry (figures 2 and 4) two quarter-sphere volumes, one in each layer of PMMA, remain. The volumes of the two quarter-spheres can be determined from the formula used for the volume of a partially filled sphere:

$$V = \left[\pi h^2 r\right] - \frac{\left[\pi h^3\right]}{3} \qquad \textbf{(1)}$$

where r is the radius of the sphere and h the height of fill. Using r = 1 mm, h = 0.95 mm the total volume of the semi-spherical feature is estimated as 1.94 L. This volume is not equivalent to true dead volume. As shown in figure S1 an element of fluid flows the tubing end into the microfluidic channel and is not considered dead volume.

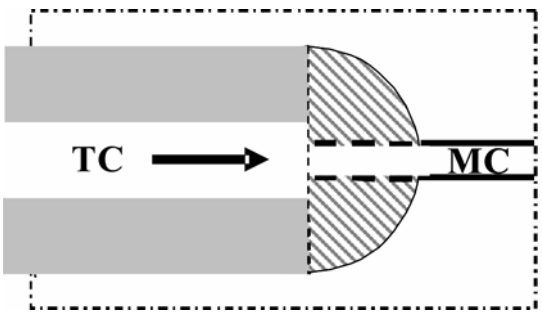

Figure S1. Schematic cross-sections of a compression method interconnection within a PMMA chip. Not drawn to scale. Fluid flows in the direction shown by the arrow from the tubing channel (TC) towards the microfluidic channel (MC) and through the semi-spherical geometry of the end of the interconnection channel. Hatched areas represent the dead volume.

For purposes of simplicity, the non-dead volume has been assumed to be equivalent in cross-sectional area to the microfluidic channel. For example microfluidic channel dimensions of 100 x 100 m and a flow length of 1 mm, the volume of this element is approximately 0.01 L. Given the approximations of this estimate, and again for simplicity, we provide 1.9 L as the estimate of maximum dead volume.

B. Dead volume estimate for removal of semi-spherical features by additional milling

With additional milling steps the semi-spherical geometries can be removed and a shape complimentary to the tubing created to the edge of the microfluidic channel. As such the tubing can be placed adjacent to the microfluidic channel. As shown in figures 2 and 4, tubing is pressed towards the microfluidic channel during the bonding process. The estimated dead volume is then based on the cylinder-like volume trapped between the tubing end and the microfluidic channel.

If one wished to minimize dead volume, a likely strategy is to match the microfluidic channel dimensions to this tubing outlet diameter. From figure 4, the tubing channel outlet is

approximately 0.4 mm when compressed. When i) approximating the cross-sectional area between the tubing and the microfluidic channel as a cylinder of diameter 1.9 mm, and ii) using a distance of 100 m between the end of the tubing and the PMMA wall in the compressed state a dead volume estimate of 283 nL , approximately 300 nL, results.

PUBLICATION 4:

"*Multi-channel peristaltic pump for microfluidic applications featuring monolithic PDMS inlay*"

Multi-channel peristaltic pump for microfluidic applications featuring monolithic PDMS inlay†

Peder Skafte-Pedersen,‡ David Sabourin,‡ Martin Dufva and Detlef Snakenborg*

Received 3rd April 2009, Accepted 6th July 2009
First published as an Advance Article on the web 17th July 2009
DOI: 10.1039/b906156h

The design, fabrication and characterization of a miniaturized, mechanically-actuated 12-channel peristaltic pump for microfluidic applications and built from simple, low-cost materials and fabrication methods is presented. Two pump configurations are tested, including one which reduces pulsating flow. Both use a monolithic PDMS pumping inlay featuring three-dimensional geometries favourable to pumping applications and 12 wholly integrated circular channels. Flow rates in the sub-μL min^{-1} to μL min^{-1} range were obtained. Channel-to-channel flow rate variability was comparable to a commercial pumping system at lower flow rates. The small footprint, 40 mm by 80 mm, of the micropump renders it portable, and allows its use on microscope stages adjacent to microfluidic devices, thus reducing system dead volumes. The micropump's design allows potential use in remote and resource-limited locations

Introduction

Lab-on-a-chip (LOC) and micro total analysis systems (μTAS) offer many advantages over conventional macroscale laboratory analysis methods and techniques,[1,2] however practical problems including pumping remain a challenge and barrier to the wide spread adoption of microfluidic solutions.[3] Many solutions to micropumping have been proposed and comprehensive reviews of these are available.[3–5] Pneumatic PDMS-based micropumps have been made *via* soft lithographic methods.[6] Though promising for highly multiplexed microfluidic applications due to scaling capabilities, construction and design is complicated by need of additional control channels and the clean room based methods normally used.[7] Mechanical approaches are often simple and well suited to established test platforms and assays which can benefit from fluidic activation.[8] Examples include moving ball bearings over single PDMS channels to drive flow[7,9] and the actuation of multiple PDMS channels *via* programmed Braille displays[10–12] or a motor driven screw.[13] In this report, we describe the design, fabrication and performance characteristics of a mechanically activated 12-channel peristaltic micropump.

Materials and methods

Micropump design and fabrication

The peristaltic micropump (Fig. 1) has three core components: a monolithic PDMS Pumping Inlay (PI), a Rotor Bed (RB), and a Multi-Roller (MR). The PI, containing 12 integrated channels raised above the plane (Fig. 2d), is placed in an RB complementary in shape to the MR. A stepper motor (p/n 415-8532, McLennan Servo Supplies Ltd, England) drives the pump.

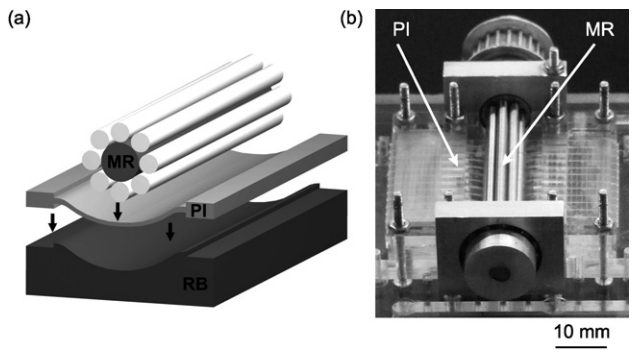

Fig. 1 PDMS based 12-channel micropump. (a) 3D schematic of core micropump components. (b) Assembled 12-channel micropump. The MR is mounted in ball bearings holders and the PI secured by PMMA brackets. The RB is not visible. Stepper motor (not shown) connects to the MR *via* belt-drive.

As the MR rotates, it contacts and compresses the PI's channels (Fig. 2) and pushes fluid in the direction of rotation. Two micropump configurations are presented. The first is referred to as the basic configuration. The second, designed to reduce flow pulsations, is referred to as the offset configuration. All core components were fabricated in-house by CNC micromilling (Folken, Glendale, California). The ESI contains comprehensive fabrication details.†

The monolithic PI (Fig. 1a, 2d) was cast from PDMS (Sylgard 184, Dow Corning) inside a PMMA (Nordisk Plast, Denmark) mould (ESI Fig. S2†) and using sacrificial fibre inserts *via* a process previously described.[14] Monolithic structures were chosen since they demonstrate better durability and strength than multi-layer structures.[6,15] One-step casting also eliminates additional bonding steps and alignment requirements. Micromilled moulds made with ball mills result in raised channels with dome shaped geometries (Fig. 2b, 2c, 2d and ESI Fig. S1†). These improve pump efficiency by reducing friction between the MR and the PI. The circular

Department of Micro- and Nanotechnology, Technical University of Denmark, DTU Nanotech, Building 345 East, DK-2800 Kongens, Lyngby, Denmark. E-mail: desn@nanotech.dtu.dk; Fax: +45 4588 7762; Tel: +45 4525 5785

† Electronic supplementary information (ESI) available: Micropump design and fabrication, Fig. S1 and Fig. S2. See DOI: 10.1039/b906156h
‡ Both authors contributed equally to this work.

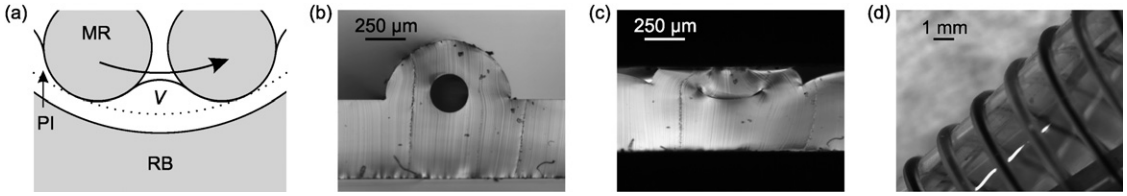

Fig. 2 Pump operation. (a) The PI is placed between the RB and the MR. Dashed line represents the PI's integrated channels. As the MR rolls over the PI, a fluid volume V is occluded between two pins of the MR. The RB provides rigid support to allow compression. Fluid flow occurs in the direction of MR travel, as indicated by the arrow. (b) Cross section of an uncompressed PI channel. (c) Cross section of the same channel when compressed the same amount as in pump. (d) Within the middle section of the PI, the integrated channels are raised above a supporting PDMS layer to facilitate compression and reduce friction between the PI and MR.

channels formed by the fibre inserts (ESI Fig. S2†) are more efficient at transferring in-plane strain to volumetric deflection as compared to standard flat-diaphragm chambers.[4] A PI for the offset configuration was similarly made, however following curing channel pairs were separated from one another by scalpel.

The PI rests on a RB made from PMMA. The RB provides the PI with rigid support complementary to the curvature of the MR (Fig. 1a). The RB contains grooves that accept the PI's cross-beam features and align and prevent the PI's advancement through the pump during operation. PMMA brackets secure the PI to the RB *via* the PI's bookending PDMS blocks (ESI Fig. S2†). In the basic configuration of the pump, the RB's curvature provides the same points of occlusion for all 12 channels. In the offset configuration, a different RB is used. The curvature of this RB occludes a pair of channels at different points to yield offset flow pulsations in each channel of the pair.

The MR assembly is made from eight 2 mm diameter brass rods placed equidistantly around a 4 mm brass drive shaft (Fig. 1). The 2 mm rods are mounted in aluminium disks with oversized 2.1 mm holes to allow free rotation and prevent mechanical damage to the PI. Aluminium disks are placed against ball bearings made from 2 mm stainless steel balls fit into aluminium ball bearing holders. The compression ratio of the pump is approximately 0.7 according to the method of calculation described by *Yobas et al.*[7]

Micropump characterization

Flow rates were measured with a flow sensor (Nano Flow Sensor, Upchurch Scientific) operating at a 2 Hz acquisition rate. For simultaneous measurement of multiple channels, time-lapse microscopy measured the advancement of a liquid front inside 12 channels of PMMA chip connected to the pump. Pressure capability was gauged with a pressure sensor (Honeywell 40PC150G) connected between pump outlet and a closed micrometering valve (P-446, Upchurch Scientific) with polytetrafluoroethylene (PTFE) tubing (S1810-09 Bohlender GmbH) and high-pressure fittings (Upchurch Scientific, Washington, USA). Pressure data was collected with a pressure sensor (40PC150G, Honeywell) and a LabView (National Instruments) interface.

Results

Flow rates and patterns

A representative flow pattern from a channel is shown in Fig. 3a. Measurements were collected at a rotational speed, v_r, of 0.19 min^{-1}. Sudden flow rate changes occur at the point of release of roller pins, indicated by arrows in Fig. 3a. These greatly exceed the resolution of the flow sensor.

The offset pump configuration is a simple approach to reducing pulsation (Fig. 3b). Two adjacent channels with out-of-phase pulse patterns are created. Combining these into a single stream significantly reduced pulsation and eliminated negative flows (Fig. 3c). Measurements were collected at the same v_r of 0.19 min^{-1}.

Flow rate estimates were based on the void volume, V, occluded within a channel between adjacent MR pins (Fig. 2a). V is estimated as 0.1 μL and with eight voids formed per revolution, the flow rate per channel per revolution, Q_{rev}, is estimated as 0.8 μL rev^{-1}. The expected linear relationship and close agreement with theoretical estimates between the rotational speed, v_r, and average flow rate, Q, was demonstrated over an order of magnitude increase in MR rotational speed (Fig. 4a).

Fig. 4b presents individual channel average flow rates. At flow rates of 0.17, 0.75, and 1.59 μL min^{-1} the channel-to-channel

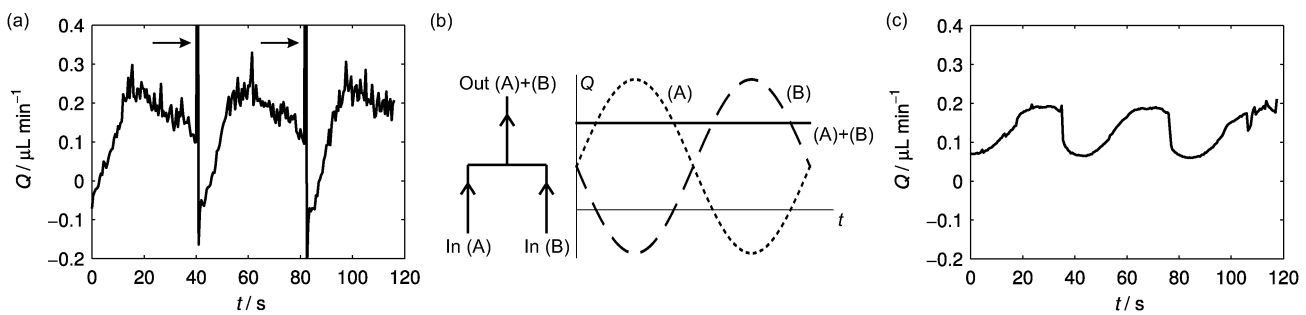

Fig. 3 Pulsation reduction in offset pump configuration. (a) Representative flow pattern for a single channel. Arrows indicate point of roller release. (b) Sketch of offset pump operation. Two out-of-phase flows, A (dotted) and B (dashed), are combined into a single channel, and a flow rate of A + B (solid line) results. (c) Representative flow pattern for channel with flow inputs from channel pair from offset pump configuration.

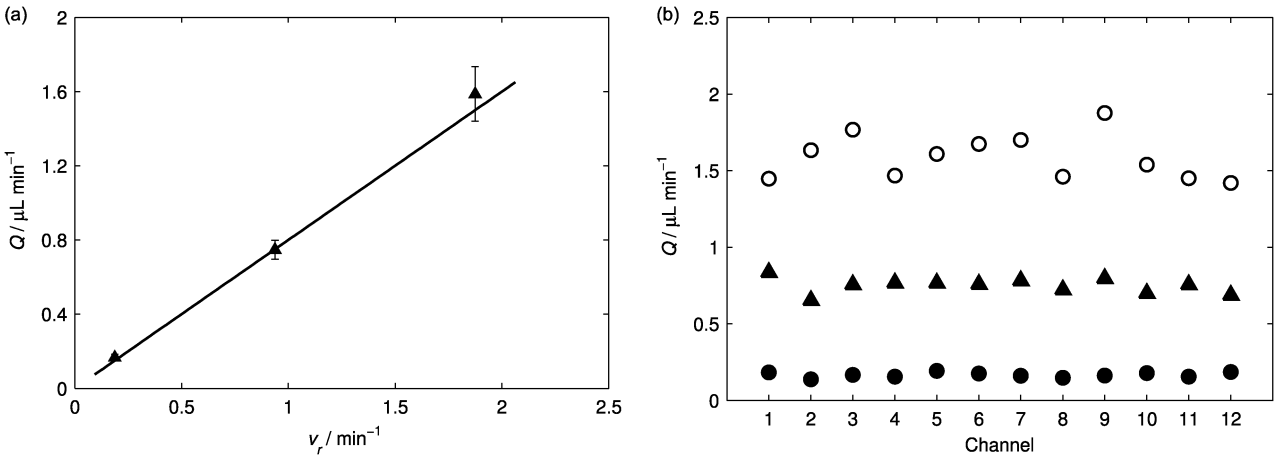

Fig. 4 (a) Theoretical (solid line) and average measured (triangles) individual channel flow rates, Q, at varying rotational speeds, v_r. Theoretical values are based on an estimate of the void volume between two roller pins. Measured flow rates are the average values from twelve individual channels in the offset configuration. Error bars represent the standard deviation of the average flow rate of the 12 individual channels. (b) Individual channel flow rate data. Flow sensor data at v_r values of 0.19, 0.94 and 1.88 min^{-1} corresponding to average flow rates of 0.17, 0.75, and 1.59 μL min^{-1}.

coefficient of variance (%CV) were 10, 7, and 9% respectively. In comparison, channel-to-channel %CV using a stepper pump (CMA 400, CMA Microdialysis AB) with four syringes (2 mL Luer Solo, B.Braun) at flow rates of 0.24, 0.56, and 2.06 μL min^{-1} were 12, 6.9, and 0.6% respectively. At a set v_r due to the pumping mechanism, the micropump should be indifferent to solution viscosity. This was confirmed by pumping glycerol solutions with viscosities approximately 2.5 (30% glycerol), 6.0 (50% glycerol), and 23 (70% glycerol) times that of water.[16] A $v_r = 3.57$ min^{-1} flow rates of 2.43 (water), 2.37 (30% glycerol), 2.38 (50% glycerol) and 2.42 (70% glycerol) μL min^{-1} with corresponding SDs of 0.11, 0.16, 0.14 and 0.12 μL min^{-1} were observed. To verify suitability to microfluidic systems, the pressure capability of the pump was measured. When outlet channels were blocked, the maximum pressure capability of the pump was 370 kPa. To verify use in cell culture applications, cells were passed through the pump without any cell lysis being observed.

Individual channels withstood over 1875 MR revolutions, or 15000 individual compressions.

Discussion

The micropump is suitable for many microfluidic applications. Flow rates were typical of microfluidic studies and in the lower range the flow rate variability was comparable to a commercial syringe pump. The maximum measured pressure of the pump, 370 kPa, is well above the 200 kPa threshold described as sufficient for most microfluidic applications.[16] The micropump is most useful for multiplexed assays which benefit and/or require fluidic activation from a number of fluidic inputs and in this manner differentiates itself from previous PDMS based mechanically actuated micropumps.[7,9,17] Examples of such assays include but are not limited to microfluidic perfused cell culture[18] and multi-stringency array hybridizations.[19] The approach presented to simultaneously pump multiple streams is more flexible than Braille display based methods, which must adhere to spacing and channel dimensions commensurate with the Braille device and flow rates dependent on Braille pin refresh rates.[10–12]

Although flow characteristics are not superior to commercially available syringe pumps, the micropump design provides many advantages. As the pump approaches dimensions of microfluidic devices, interfacing liquids to and from the pump can be completed without requiring excessive tubing and *via* simple methods such as press-fitting oversized needles into the PDMS channel inlet and outlets. This reduces both pump dead volumes and likely compliance as compared to typical pump setups. The micropump fits on a microscope stage and the planar orientation of channel inlet and outlets helps provide unobstructed microscopic observation. Recent reports have addressed the need to create microfluidic devices and components suitable for remote and/or resource-limited locations.[20] The micropump can be rendered suitable for such locations with simple modifications, *e.g.* a crank attached to the MR. In such locations, the micropump could deliver fluids to multiple assays and, for example, permit simultaneous detection across multiple patients or multiple pathogens or disease agents.

Work is in progress to build a modular system which connects the pump to microfluidic chips, designed for parallel processing of cell cultures and DNA microarrays, *via* interconnection blocks.[14] The durability of the PI is also being addressed to meet long-term cell culture requirements.

Conclusions

A low-cost, stand-alone multi-channel peristaltic micropump capable of pumping fluids at sub-μL min^{-1} to μL min^{-1} rates has been presented. The pump's flow and pressure characteristics make it suitable to many microfluidic applications. For applications where pulsation reduction is desired, a simple approach to reduce pulstation was demonstrated. The micropump's dimensions and the flexible and scalable methods used to build it, render it a viable pumping solution for microfluidic applications.

Acknowledgements

This work was supported by Grant No. 2106-08-0018 "ProCell" and Grant No. 2106-05-0047 "BioXTAS", under the Programme

Commission on Strategic Growth Technologies, the Danish Agency for Science, Technology and Innovation, and Grant agreement no. NMP4-SL-2008-214706 "EXCELL" under the European Community Framework Programme 7.

References

1 D. J. Beebe, G. A. Mensing and G. M. Walker, *Annual review of biomedical engineering*, 2002, **4**, 261–286.
2 G. M. Whitesides, *Nature*, 2006, **442**, 368–373.
3 D. J. Laser and J. G. Santiago, *Journal of Micromechanics and Microengineering*, 2004, **14**, R35–R64.
4 B. D. Iverson and S. V. Garimella, *Microfluidics and Nanofluidics*, 2008, **5**, 145–174.
5 N. T. Nguyen, X. Y. Huang and T. K. Chuan, *Journal of Fluids Engineering-Transactions of the Asme*, 2002, **124**, 384–392.
6 M. A. Unger, H. P. Chou, T. Thorsen, A. Scherer and S. R. Quake, *Science*, 2000, **288**, 113–116.
7 L. Yobas, K. C. Tang, S. E. Yong and E. K. Z. Ong, *Lab on a chip*, 2008, **8**, 660–662.
8 C. Situma, M. Hashimoto and S. A. Soper, *Biomolecular engineering*, 2006, **23**, 213–231.
9 K. Lim, S. Kim and J. H. Hahn, *Sensors and Actuators B-Chemical*, 2003, **92**, 208–214.
10 N. Futai, W. Gu, J. W. Song and S. Takayama, *Lab on a chip*, 2006, **6**, 149–154.
11 W. Gu, X. Y. Zhu, N. Futai, B. S. Cho and S. Takayama, *Proceedings of the National Academy of Sciences of the United States of America*, 2004, **101**, 15861–15866.
12 Y. C. Tung, Y. S. Torisawa, N. Futai and S. Takayama, *Lab on a chip*, 2007, **7**, 1497–1503.
13 W. Rhie and T. Higuchi, in *The 12th International Conference on Miniaturized Systems for Chemistry and Life Sciences (microTAS 2008)*, 2008, p. 3.
14 D. Sabourin, D. Snakenborg and M. Dufva, *Journal of Micromechanics and Microengineering*, 2009, **19**.
15 M. A. Eddings, M. A. Johnson and B. K. Gale, *Journal of Micromechanics and Microengineering*, 2008, **18**, 067001 (4pp).
16 A. A. S. Bhagat, P. Jothimuthu, A. Pais and I. Papautsky, *Journal of Micromechanics and Microengineering*, 2007, **17**, 42–49.
17 C. Koch, V. Remcho and J. Ingle, *Sensors and Actuators B-Chemical*, 2009, **135**, 664–670.
18 M. Stangegaard, S. Petronis, A. M. Jorgensen, C. B. Christensen and M. Dufva, *Lab on a chip*, 2006, **6**, 1045–1051.
19 L. Poulsen, M. J. Soe, D. Snakenborg, L. B. Moller and M. Dufva, *Nucleic acids research*, 2008, **36**, e132.
20 P. Yager, G. J. Domingo and J. Gerdes, *Annual review of biomedical engineering*, 2008, **10**, 107–144.

Multi-channel peristaltic pump for microfluidic applications featuring monolithic PDMS inlay: Supplementary information

Peder Skafte-Pedersen†, David Sabourin†, Martin Dufva and Detlef Snakenborg*

Received (in XXX, XXX) Xth XXXXXXXXX 200X, Accepted Xth XXXXXXXXX 200X
First published on the web Xth XXXXXXXXX 200X
DOI: 10.1039/b000000x

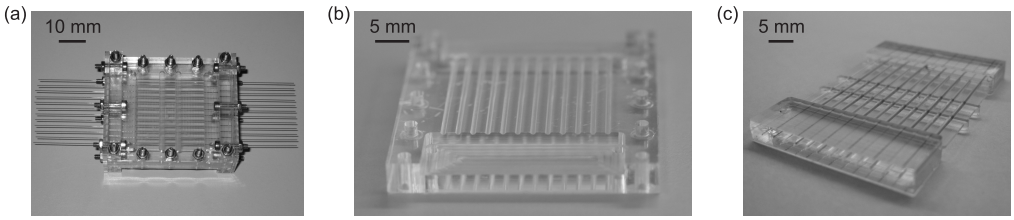

Fig. S2 PI fabrication. (a) Mould used to cast PI. Fibre inserts can be seen passing through the mould (b) Bottom part of mould showing the semi-circular grooves which result in raised channels. (c) Completed PI. Integrated channels loaded with dye to facilitate visualisation. Within the middle section of the PI, the integrated channels are raised above a supporting PDMS layer to facilitate compression and reduce friction between the PI and multi-roller (MR).

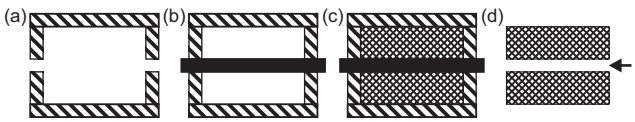

Fig. S1 Schematic representation of PI fabrication. Drawings not to scale. (a) Cross-sectional view of mould used for casting PIs. Openings at end represent through holes through which fibre inserts are placed. (b) Fibre inserts resulting in integrated channels are placed through terminal mould pieces. (c) PDMS is cast into mould and subsequently cured. Following PDMS curing, fibre inserts are removed and mould is disassembled. (d) Cross section of completed PI. Arrow indicates integrated channel.

Micropump Design and Fabrication

Pumping Inlay (PI)

The monolithic PI is cast from PDMS (Sylgard 184, Dow Corning) inside a PMMA (Nordisk Plast, Denmark) mould in a process depicted schematically in S1.
Mould pieces were aligned by 2 mm screws. An assembled PI mould is shown in S2a. Before injecting PDMS into the mould, 240 µm optical fibres (Polymicro Technologies, Phoenix, Arizona) were threaded through 250 µm holes in the end pieces (S1b). PDMS was mixed in a 10:1 mass ratio of elastomer to curing agent and placed under vacuum to remove air bubbles. Mould vents allowed PDMS injection via syringe and prevented air from being trapped in the finished part (S1c). The filled mould was placed in an oven at 80ºC for two hours to cure. Once the mould had cooled enough to be handled, fibres were removed to yield integrated channels and the mould disassembled (S1d).
A completed PI is shown in S2c. The PI is 30 mm in width and 45 mm in length. Two PDMS blocks bookend the middle section of the PI and facilitate handling, alignment and securing of the PI. The middle section of the PI measures 30 mm in width by 25 mm in length. Centred across its width are 12 half-tube structures. These are raised above a 0.5 mm thick support layer (2b, S2bc) and are spaced 2.25 mm apart, equivalent to the standard published by SBS/ANSI for 1536 well microtiter plates. The half-tubes have a radius and height of 0.4 mm and were created by using a 0.8 mm ball mill to form a mould piece (S2b). The 12 integrated 240 µm channels are centred at the intersection of the support bed and half-tubing planes (2b). The middle portion of the PI also contains crossbeam structures which hold the PI in place in the RB when the pump is in use.
For the offset configuration of the pump, another version of the PI was made. The offset PI version was manufactured as above, however following casting/curing channel pairs were separated from one another by scalpel. Prior to testing, all PIs were inspected for damage and/or blocked channels.

Rotor Bed (RB)

The PI rests on a RB (2a) made of PMMA sections held together by 2 mm alignment pins. The RB provides the PI with rigid support complementary to the curvature of the MR.

Multi-roller (MR)

The MR assembly is made from eight 2 mm diameter brass rods placed equidistantly around a 4 mm brass drive shaft (1b). The rods are mounted in aluminium disks with oversized 2.1 mm holes. These allow rods to freely rotate and prevent mechanical damage to the PI. The aluminium disks are secured to the drive shaft by pointed screws and are placed against ball bearings made from 2 mm stainless steel balls fit into 5 mm aluminium ball bearing holders with an outer footprint of 20 mm by 25 mm. At one end of the MR a 16 mm diameter toothed wheel (Synchroflex 16T2.5/20-2) is secured to the drive shaft by a pointed screw A toothed belt (Synchroflex 6/T2.5/145) provides a mechanical connection to the stepper motor. The MR is centred over the PI and RB and has a total width of 77 mm. The MR was lubricated with graphite powder.

Stepper Motor

The MR is driven by a geared stepper motor (p/n 415-8532, McLennan Servo Supplies Ltd, England) with a gear ratio of 250:3 controlled by an in-house built stepper circuit using 1/8th microstepping. This provides 32,000 steps per revolution and smooth rotation. The control is triggered by a function generator (digimess FG 100) or a clock built in-house and powered by a DC power supply (ISO-TECH IPS2303D).

Notes and references

Department of Micro- and Nanotechnology, Technical University of Denmark, DTU Nanotech, Building 345 East, DK-2800 Kongens Lyngby, Denmark. Fax: +45 4588 7762; Tel: +45 4525 5785; E-mail: desn@nanotech.dtu.dk

† Both authors contributed equally to this work.

PUBLICATION 5:

"Microfluidic DNA microarrays in PMMA chips: streamlined fabrication via simultaneous DNA immobilization and bonding activation by brief UV exposure"

Biomed Microdevices
DOI 10.1007/s10544-010-9420-7

Microfluidic DNA microarrays in PMMA chips: streamlined fabrication *via* simultaneous DNA immobilization and bonding activation by brief UV exposure

David Sabourin · Jesper Petersen · Detlef Snakenborg · Monica Brivio · Haukur Gudnadson · Anders Wolff · Martin Dufva

Abstract This report presents and describes a simple and scalable method for producing functional DNA microarrays within enclosed polymeric, PMMA, microfluidic devices. Brief (30 s) exposure to UV simultaneously immobilized poly(T)poly(C)-tagged DNA probes to the surface of unmodified PMMA and activated the surface for bonding below the glass transition temperature of the bulk PMMA. Functionality and validation of the enclosed PMMA microarrays was demonstrated as 18 patients were correctly genotyped for all eight mutation sites in the HBB gene interrogated. The fabrication process therefore produced probes with desired hybridization properties and sufficient bonding between PMMA layers to allow construction of microfluidic devices. The streamlined fabrication method is suited to the production of low-cost microfluidic microarray-based diagnostic devices and, as such, is equally applicable to the development of diagnostics for both resource rich and resource limited settings.

Keywords Microarray · Microfluidic · PMMA · UV-bonding · Beta-globin · Genotyping

David Sabourin and Jesper Petersen contributed equally to this work.

Electronic supplementary material The online version of this article (doi:10.1007/s10544-010-9420-7) contains supplementary material, which is available to authorized users.

D. Sabourin · J. Petersen · D. Snakenborg · M. Brivio · H. Gudnadson · A. Wolff · M. Dufva (✉)
DTU Nanotech, Department of Micro- and Nanotechnology, Technical University of Denmark (DTU), Ørsteds Plads, Bygning 345Ø, DK-2800 Køngens Lyngby, Denmark
e-mail: martin.dufva@nanotech.dtu.dk

1 Introduction

Within the last decade microfluidic and lab-on-a-chip (LOC) applications and approaches have received significant attention. The advantages of these approaches include, but are not limited to, reduced sample and reagent consumption, reaction time, analysis time, experimental footprint and increased assay parallelization, automation and portability (Whitesides 2006; Crevillen et al. 2007). During this same period microarray technology also underwent rapid development. Microarrays enable parallel analysis of biological variation, *via* DNA, RNA or protein that are spotted and attached to a solid support. Initially containing 45 probes on a glass microscope slide, microarrays now containing more than 2 million probes per slide are available (Dufva 2005). Microarrays hold great promise for, and can significantly impact, global health as they can be used for biosafety, diagnostic and preventative care applications. Microarray and microfluidic approaches can be readily combined as materials, glass or polymeric, used to build microfluidic structures can also be used as the solid support in microarrays. Importantly, there is similarity in scale between miniaturized probe spots and microfluidic channel dimensions. In addition to the general advantages for microfluidic approaches listed above, specific advantages of merging microarrays with microfluidics include the possibility of creating closed architectures. The latter is significant as it increases the ease-of-use of arrays by negating handling issues, thereby reducing the risk of contamination and/or probe damage. This can potentially yield false and/or inconclusive results (Wang et al. 2003; Situma et al. 2006).

To achieve wide-spread use and have greater impact, microfluidic devices should be simple to manufacture by

Published online: 25 March 2010

mass production methods (Situma et al. 2006; Yager et al. 2008). Though combining microfluidics and microarrays affords a reduction in sample and reagent cost, the glass-based supports used for microarray manufacturing are not suited to high volume/low cost manufacturing and represent a barrier to use. Polymers are of relatively low cost and are suitable to mass production methods including injection molding, hot embossing, and laser ablation. As such, these materials are of interest to microfluidic device manufacture (Becker and Locascio 2002).

Poly(methyl mehtacrylate) PMMA is a commonly used polymer for microfluidic device fabrication. Chen et al. provide a review of PMMA fabrication and modification methods for microfluidic device manufacture (Chen et al. 2008). Advantages of PMMA include its low cost, optical transparency, amenability to fabrication and modification, and biocompatibility (Stangegaard et al. 2006; Chen et al. 2008) The suitability of PMMA as a microarray support has been investigated by several groups (Wang et al. 2003; Fixe et al. 2004a, b; Situma et al. 2005; Soper et al. 2005; Kimura 2006; Banuls et al. 2007; Diaz-Quijada et al. 2007; Situma et al. 2007; Zhao et al. 2008). Chemical modification (Wang et al. 2003; Fixe et al. 2004a, b; Banuls et al. 2007; Diaz-Quijada et al. 2007; Zhao et al. 2008) and UV exposure (Situma et al. 2005; Soper et al. 2005; Kimura 2006; Situma et al. 2007) have been used to attach nucleic acids to the surface of PMMA. Fixe et al. treated PMMA with either isopropanol or ethanol allowing DNA probes to be covalently attached via a terminal thiol or amine group to the C-terminal ester of the PMMA (Fixe et al. 2004a). This same group also reported the reaction of PMMA with hexamethylene diamine to yield primary amines at the PMMA surface and with which DNA probes were attached (Fixe et al. 2004b). Waddell et al. demonstrated that aminated PMMA formed by reaction with *N*-lithioethylenediamine allows immobilization and hybridization of DNA (Waddell et al. 2000) and Wang et al. used this same process to create microarrays within an enclosed PMMA microfluidic chip(Wang et al. 2003). Isocyanate modification of PMMA was used by Bañuls et al. in order to covalently immobilize DNA to PMMA (Banuls et al. 2007). Diaz-Quijada et al. and Zhao et al. treated commercially available PMMA, PMMA-VSUVT, sequentially with sodium hydroxide, 1-ethyl-3-(3-dimethylaminopropyl) (EDC) and *N*-hydroxysuccinimide to produce arrayed oligonucleodies on a PMMA surface (Diaz-Quijada et al. 2007; Zhao et al. 2008). UV exposure has been used to create a skeleton on PMMA to which oligonucleotides in an EDC spotting solution were then attached. (Situma et al. 2005, 2007; Soper et al. 2005). UV exposure has also been used to directly attach oligonucleotides to surfaces including unmodified PMMA. Dufva et al. and Gunadson et al. have demonstrated the use of poly(T)10-poly(C)10–tagged DNA probes to unmodified and agarose-coated glass surfaces as well as PMMA (Dufva et al. 2006; Gudnason et al. 2008) and Kimura used oligonucleodtides incorporating a 5'-end poly(dT) tail and and an undisclosed spacer group (Kimura 2006) for attachment to unmodified PMMA.

Though, as previously discussed, there are many advantages of merging microarrays with microfluidic approaches and polymeric processes present an opportunity to do so, there are limited reports describing arrays integrated within fluidically addressable channels of entirely polymeric devices. Reports have described the use of UV exposure to enable bonding below the bulk glass-transition temperature (T_g) of PMMA (Truckenmüller et al. 2004; Tsao and Devoe 2009). Since UV exposure was also used to immobilize TC-tagged probes to PMMA (Gudnason et al. 2008) we hypothised that it may be possible to combine the immobilization of TC-tagged probes onto unmodified PMMA and simultaneously activate the surface of unmodified PMMA for bonding below the bulk T_g of PMMA. If so, enclosed, microfluidically addressable microarrays constructed from entirely unmodified PMMA, without use of chemical or adhesive treatments, could result. As probe immobilization alone does not validate probe functionality post-UV treatment, the functionality and selectivity of the resultant microarrays were tested via an allele specific hybridization (ASH) to segments of the human beta-globin gene (HBB) containing mutations. For the ASH assay, patient samples were used.

2 Materials and methods

2.1 Microarray design, preparation and fabrication

The enclosed microarrays were made from two 0.5 mm thick PMMA layers (Nordiskplast, Denmark). PMMA layers were patterned by computer controlled micromilling (Folken, Glendale, California). Both layers had overall dimensions of 76×26 mm, matching that of standard microscope slides. One of the layers was further machined to contain eight 20 mm×2 mm channels with depth of 250 μm. Each channel was bookended by 1.0 mm through holes (Fig. 1(a)). The eight channels were grouped into two sets of four channels 27 mm apart from each other. Within each group of four channels, spacing was set at 4.5 mm. Following milling, both layers were briefly wiped with 70% ethanol to remove any debris. DNA probes were spotted and immobilized on the PMMA layer without channels (see below).

Allele-specific DNA probes were designed for genotyping small genetic variations in the HBB gene. The probes had the variant base/bases positioned as close to the center of the probe as possible, and they contained a poly(T)10-poly(C)10

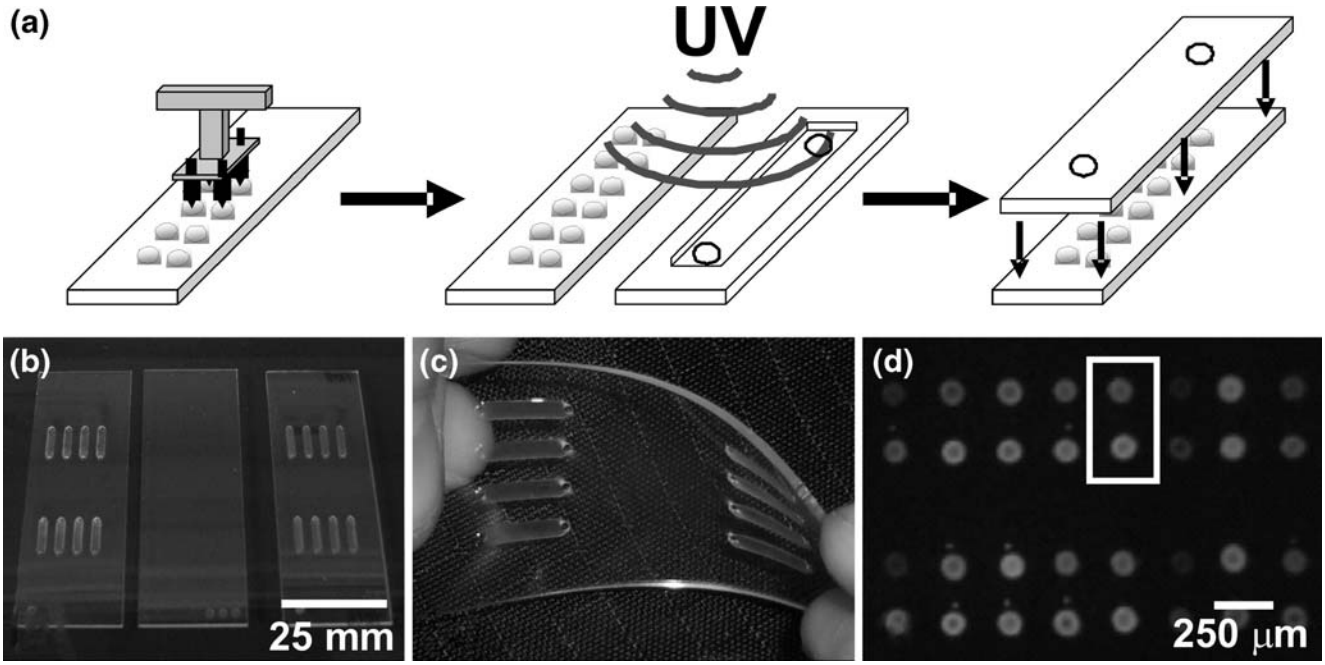

Fig. 1 PMMA microfluidic microarray construction (**a**) Schematic representation of PMMA microfluidic array manufacture. A featureless 0.5 mm PMMA layer is spotted with poly(T)-poly(C)-tagged DNA probes. The spotted layer and a second 0.5 mm PMMA layer, containing channels and throughholes for sample processing, are then placed with bonding surfaces facing a UV source. Both layers are exposed to UV for 30 s. and are subsequently bonded in a bonding press at 85°C for 1 h (**b**) The two 0.5 mm PMMA layers used to create the enclosed microarray device are shown on the left and in the centre. A bonded and completed enclosed PMMA microarray structure is shown to the right. (**c**) Twisting of the completed device did not result in delamination. (**d**) Two of four replicate subarrays found within each channel of the fluidic array made in PMMA. MT probes are found in the 1st and 3rd rows from the top, WT in the 2nd and 4th. Probe pairs for each mutagenic site were grouped as shown by the example *rectangle*

tag (TC tag) in the 5' end (Dufva et al. 2006) (Petersen et al. 2007). The TC tag increases hybridization signal by unknown mechanisms that may include increasing the probe immobilization efficiency during UV cross-linking (Dufva et al. 2004, 2006; Gudnason et al. 2008). A melting temperature (T_m)-matched probe set was designed based on criteria previously described (Petersen, Poulsen et al. 2008). For each of the 8 HBB mutagenic sites investigated, the probe set contains a wild-type (WT) and a mutant (MT) probe. WT refers to the non-disease causing nucleic acid sequence present in the majority of the population. Probe sequences and information concerning specific mutations at each site are found in supplementary information insert 1.

DNA oligonucleotide probes were diluted in 75 mM phosphate buffer containing 0.01% Triton X to a final concentration of 50 μM. Probes were arrayed on the PMMA slides using non-contact depositing (Nanoplotter, GeSim, Germany). Eight arrays were created in the areas corresponding to the eight channels. Within each area corresponding to a channel, four replicates of each probe were spotted. An example of two of the four subarrays is found in Fig. 1(d).

To immobilize the spotted DNA to the PMMA surface and prepare both PMMA layers for bonding, the substrates were placed bonding side up 12 cm below the light source (DYMAX EC 5000 with p/n 36970 bulb, Torrington, Connecticut) for 30 s. The light intensity is 225 mW/cm^2 according to the manufacturer's literature. Prior to this exposure, and as per manufacturer's instructions, the light source was warmed up for 5 min. Following UV exposure, the PMMA layers were placed between glass microscope slides and aligned on aluminum bonding blocks made by micromilling. The bonding assembly was placed in a bonding press (P/O/Weber, Remshalden, Germany) with press heating plates set at 85°C and an initial approximate applied pressure of 1.0×10^5 kN/m^2. After 1 h the heating plates were turned off and the bonding assembly was allowed to cool to room temperature in the press. A completed enclosed PMMA microarray slide is shown in Fig. 1(b) and (c).

To verify if channels within completed devices could withstand high flow rates, dye was passed through a minimum of four channels on three completed devices at approximately of 100 μL per second. Inspection of leaks was performed via microscope. Devices which had already been used to genotype patients were used for this test.

2.2 Microarray processing and analysis

All channels within the PMMA microarray devices were washed for 10 min with one channel volume, approximately

5 μL, of 0.1 × saline-sodium citrate (SSC) supplemented with 0.5% sodium dodecyl sulfate (SDS). The fluid was removed by capillary force by blotting with a paper towel and another 5 μL of 0.1 × SSC supplemented with 0.5% SDS was introduced into the channels to remove unbound probes. After 10 min, the channels were dried by capillary force, as above, and aspiration.

The 18 DNA samples used in this study originated from individuals that were heterozygous (n=13) or homozygous (n=4) for a mutation in HBB and from a control subject with no HBB mutations. A 300 base pair portion of the HBB gene, containing exon I and the first part of intron I, was amplified by PCR as previously described in (Petersen et al. 2008) (PCR primers listed in supplementary information Table 1). The PCR products were used directly (without purification steps) as a template for T7 *in vitro* transcription (IVT). Single-stranded RNA target was produced by T7 IVT in a 60 μl reaction mixture containing 2 μl of template DNA, 500 mM of each NTP, 12.5 mM (2.5%) Cy3-CTP (PerkinElmer Life and Analytical Sciences, Boston, MA, USA), 1 U/μl T7 RNA Polymerase-PlusTM (Ambion, Huntingdon, Cambridgeshire, UK) and 1 × transcription buffer provided with the enzyme. Prior to hybridization, the IVT products were diluted 1:1 in 10 × SSC supplemented with 1% SDS.

For each patient, four chambers on the PMMA microarray were filled with approximately 5 μL of diluted IVT product. As there are eight chambers on one PMMA microarray slide, two patients were analyzed per PMMA microarray slide. Hybridization was performed at 37°C in a dark humid chamber for 2 h. The hybridization solution was then removed from the chambers by capillary force, as above, to prepare for multi-salinity gradient washing.

Multi-salinity gradient washing allows genotyping via parallel analysis of identical arrays treated with different stringency wash buffers (Poulsen et al. 2008). In this case, each of the four chambers used to genotype a single patient was filled with one of the following four washing buffers: 2.0 × SSC, 0.55 × SSC, 0.10 × SSC and 0.035 × SSC, all supplemented with 0.1% SDS. These buffers correspond to 331.0, 91.6, 17.3 and 6.6 mM Na^+ respectively. The use of one equivalent chamber volume (approx. 5 μL) was introduced into each chamber for 1 min at room temperature to remove excess and unbound target. Following this initial wash another equivalent chamber volume of the same washing buffer was introduced into each chamber for 30 min. at 41°C. The chambers were then dried by capillary force and aspiration.

The surface of the slide was wiped to remove particles that may have interfered with imaging. A Cy3 imaging system consisting of a Leica MZFLIII microscope (Leica, Herlev, Denmark), camera (Sony DFW X710, Japan) and software (Fire-i V3, Unibrain, San Ramon, California, USA) was used to collect images of the microarrays. Identical focal and camera setting were used for all images collected. All signals were analyzed using GenePix Pro 6.1 (Molecular Devices, Sunnyvale, CA, USA). For each chamber/stringency used to genotype a patient, a normalized ratio for each probe pair was calculated as the signal from the wild-type probe (S_{WT}) divided by the sum of the signals from the wild-type and mutant probes (S_{MT}).

$$RATIO = \frac{S_{WT}}{[S_{WT} + S_{MT}]} \quad (1)$$

For an individual with no mutation, homozygous wild-type (WT) at a given mutagenic site, at an appropriate stringency during the post-hybridization washing step the normalized ratio should approach an ideal value of 1.0. Likewise, the ideal ratio for an individual who is heterozygote (HZ) at a given mutagenic site, with one wild-type and one mutant allele, should approach 0.5. Finally, the ideal ratio of a homozygous mutated (MT) individual should approach zero.

3 Results

3.1 Fabrication

The two PMMA layers and a completed microfluidically-addressable enclosed PMMA microarray are shown in Fig. 1(a). The UV-assisted immobilization and bonding process resulted in devices, which were of high quality in terms of optics, usability and durability. The enclosed channels in the completed devices were never blocked and were easily filled by capillary force. The devices were robust to handling and, as seen in Fig. 1(b), twisting did not delaminate the layers. Spotting probes on the PMMA surface prior to bonding was not problematic and the resultant arrays within each channel were highly ordered. Spot sizes were consistently near 80 μm. Spot morphology, though acceptable, had a tendency towards coffee spot patterns despite the addition of a small concentration of surfactant to the spotting solution (Fig. 1(d)). The spots in the completed devices were easily visualized by microscopy. To verify applicability to polymerase chain reaction (PCR) applications and covalent attachment of probes to PMMA, TC tagged DNA probes attached to the PMMA surface were hybridized with complementary target and imaged. Following immersion in 97°C water for 20 min and rehybridization, a 33% reduction in signal was observed. As such the materials and methods used are applicable to PCR-based assays. At flow rates of approximately 100 μL per second no leaks in chambers of the device were observed.

3.2 Melting of DNA immobilized in the microfluidics devices

Low resolution melting curves of the immobilized probes were made by washing hybridized arrays with eight washing buffer solutions (Fig. 2). Application of different stringencies resulted in DNA melting (Fig. 2). The melting curves obtained are similar to those previously described (Petersen et al. 2008, 2009). For more comprehensive discussion of the curves associated with the multi-salinity gradient approach the reader is encouraged to consult other references (Poulsen et al. 2008; Petersen et al. 2009; Dufva et al. 2009). Melting of perfect matched hybrids (WT) was observed at a lower buffer concentration than mismatch hybrids (MT). The ratio between perfect match and mismatched hybrids had a maximum at 0.55 × SSC and 0.25 × SSC. This demonstrates that the immobilized probes retain their ability of discriminating between matched and mismatched targets as a function of applied stringency. After inspection of melting curves and ratio curves from all sites, we could reduce the number of buffers used in the gradient to four (2.0 × SSC, 0.55 × SSC, 0.10 × SSC and 0.035 × SSC). The reduction in the number of required buffer solutions allowed two patients to be tested per PMMA microarray device: four channels for each patient in an eight channel device.

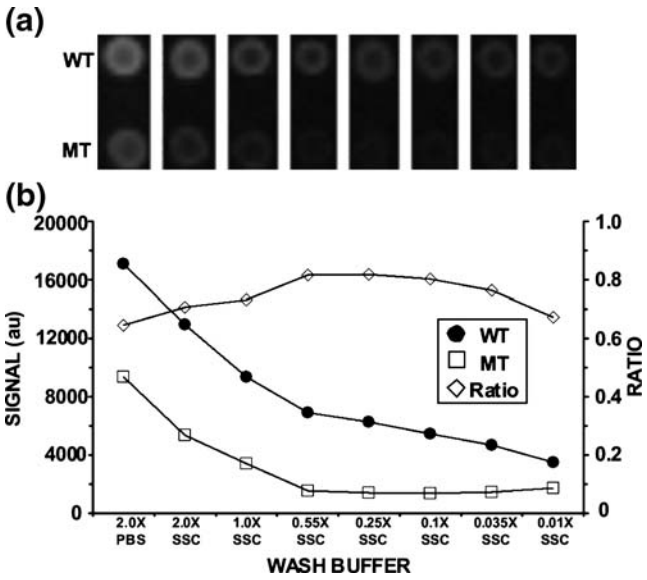

Fig. 2 Multi-salinity gradient method results for IVS I + 6 mutagenic site. (**a**) Image of quantified spots for wild-type (WT) and mutant (MT) probe at eight different wash buffer/stringency conditions after hybridization and processing of a IVS I + 6 wild-type sample. Stringency increases from left to right. (**b**) Graphical representation of the quantified spots found in (**a**) for the IVS I + 6. The primary axis represents the quantified signal from WT (●), and MT (□) probes. The secondary axis represents the ratio (◊) between WT and MT signals according to Eq. 1

3.3 Genotyping

Eighteen patients were genotyped for mutations within HBB using the PMMA microarray devices and the multi-salinity gradient method with the four selected buffers (see above). The multi-salinity gradient method collects differential stringency hybridization data simultaneously *via* the use of different washing buffers over independent yet identical microarrays (Petersen et al. 2008, 2009; Poulsen et al. 2008). Data collected from the mutagenic site referred to as CD 8/9 is used for demonstrating the application of the multi-salinity gradient approach.

For each of the 18 patients tested and for each of the four wash buffers used, the signal intensities (corrected for background) for the WT and MT hybridizations were used to calculate the ratio described by Eq. 1. The average ratio values for all WT, HZ and MT patients for the CD 8/9 site are shown in Fig. 3 as a representative example of how increasing stringency can affect classification.

The ratio obtained for the CD8/9 site showed increased separation between WT, HZ, and MT types was observed with increasing stringency washing conditions. Greater separation between min and max values of different genotypes is desired as it results in increased confidence when classifying individuals. The 0.035 × and 0.10 × SSC washing buffers provide similar ratio values for each genotype and adequate separation between these. The 0.10 × SSC condition was selected as it provided greater signal strengths (data not shown). This same analysis was completed for the seven remaining mutagenic sites investigated. The 0.55 × SSC buffer was best for genotyping three of the eight mutagenic sites and the 0.10 × SSC was best for the other five mutagenic sites (Fig. 4). The ratio

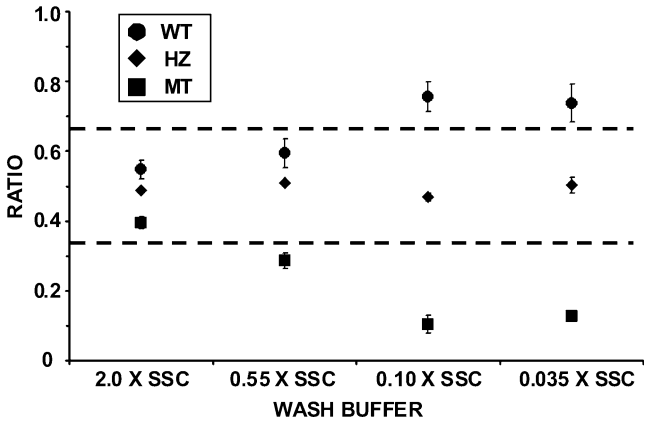

Fig. 3 Average ratio values for each genotype of the CD 8/9 mutagenic site at four different wash buffer/stringency conditions. Eighteen patients were tested of which n=16 for WT (●), n=2 for HZ (♦) and n=2 for MT (■). Error bars represent the maximum and minimum observed values of the ratio values for each genotype in each wash buffer

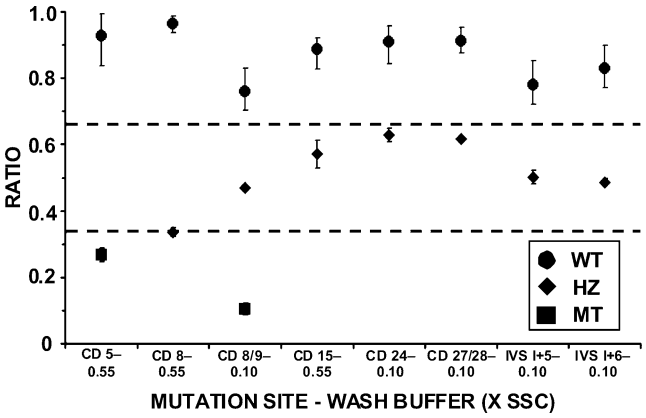

Fig. 4 Average ratio values for each genotype at each mutagenic site at the indicated SSC washing buffer concentration. Eighteen patients were tested of which 13 were HZ (♦) and 4 MT (□) for the eight mutagenic HBB sites tested. One patient was WT (●) at all sites. Error bars represent maximum and minimum ratio values for each genotype at each mutagenic site

values for all 18 patients at each mutagenic site for the wash buffer selected for genotyping of each mutagenic site are shown in Fig. 4. The original diagnosis of the patients used in the study was made by measuring the level of HbA2 by high-performance liquid chromatography (HPLC) and genotyping by automated DNA sequencing. For the eight mutagenic sites investigated, the use of a PMMA array and the multi-salinity gradient method correctly identified the genotypes of all 18 patients for each mutagenic site.

4 Discussion

This report describes the streamlined fabrication of an entirely unmodified PMMA-based diagnostic device containing microarrays within fluidically-addressable channels. The functionality of the microarrays was validated by an ASH assay for mutations in the HBB gene that used test samples derived from real patient samples. All 18 patients were correctly genotyped for all eight mutation sites interrogated.

4.1 Device fabrication

As UV treatment results in DNA damage, our central concern at the onset of the investigation was whether a UV exposure could be found which would facilitate low temperature bonding without rendering the DNA unselective and non-functional. Using the UV source previously reported for TC-tag immobilization on PMMA, UV exposure beyond points known to irreversibly damage DNA (Dufva et al 2004, Gudnason, unpublished data) did not sufficiently activate PMMA to permit bonding at settings similar to those used (unpublished results). The results indicate that the process using the stronger but shorter UV exposure than previously reported yielded 1) immobilized probes that could capture target specifically (Figs. 2, 3 and 4), indicating essential probe function was conserved (see Section 4.2 below), and 2) sufficient activation of the PMMA surface to allow PMMA to PMMA bonding (Fig. 1) at temperatures below the bulk T_g.

The specific mechanism of activation for the poly(T) poly(C) tag is unknown, however the TC site is required and increases immobilization efficiency as compared to a poly(T) or poly(C) sequence (Dufva et al. 2006; Petersen et al. 2007; Gudnason et al. 2008). As compared to chemical methods(Wang et al. 2003; Fixe et al. 2004a, b; Banuls et al. 2007; Diaz-Quijada et al. 2007; Zhao et al. 2008), the use of UV to directly immobilize TC tagged probes to unmodified PMMA surface is more rapid and streamlined method as it removes the processing step(s) required to prepare the PMMA surface for subsequent probe immobilization. Potentially harsh and/or toxic chemicals are avoided. *Kimura* and *Soper* et al. previously reported the use of UV exposure to immobilize DNA arrays on PMMA (Soper et al. 2005; Kimura 2006). Soper et al. used an initial UV treatment of 5–30 min to carboxylate PMMA (Soper et al. 2005). This UV treatment is longer and, in contrast to our method whereby UV treatment directly immobilizes DNA to unmodified surface, is used to create a scaffold onto which probes in an EDC solution are spotted. *Kimura* attached DNA probes containing a poly(T) and undisclosed spacer molecule to the surface of unmodified PMMA (Kimura 2006) while we use a known, fully described and easily incorporated probe tag.

With respect to PMMA layer bonding and construction of PMMA microfluidic devices, UV-assisted bonding has advantages over both solvent and thermal bonding of PMMA. Solvents can be absorbed by the polymer and can lead to polymer flow and deformation during bonding (Tsao et al. 2007). As compared to thermal bonding, a UV-assisted method permits bonding well below the bulk T_g of PMMA as UV radiation reduces the T_g of only a few microns of the polymer's surface layer without altering the T_g of the bulk polymer [26, 27]. Structures can then be bonded above the T_g of the surface layer but below that of the bulk PMMA layer. Even at temperatures 10°C below the T_g of PMMA, channel collapse/distortion occurs (Tsao et al. 2007). This allows sealing without loss in structure quality. The manufacture of arrays within very small channels, potentially required due to small sample volume requirements, is enabled while minimizing device yield loss. As Fig. 1(c) demonstrates, the PMMA devices could withstand severe handling (twisting by hand) without delaminating. This report does not claim to have shortened bonding times of UV-activated PMMA as compared to

other reports (Shinohara et al. 2007; Tsao et al. 2007). The focus was the manufacture of functioning microarrays within structures made entirely of PMMA. Future work will examine cycle time reductions for the production of the described enclosed microarrays via shortened bonding times. Initial investigations indicate this is possible (unpublished results).

4.2 Immobilized probe behavior and applicability to genotyping

We have previously demonstrated that genotyping performance can increase if DNA microarrays are processed at several different conditions at once (Petersen et al. 2008, 2009). The methods are based on creating spatial gradients of temperature or ionic strength buffers over a slide containing many identical subarrays of probes. This genotyping approach is suitable for demonstration of the PMMA device as it can detect selective dehybridization as a function of stringency. Therefore, the assays demonstrated provided both information about probe melting on the PMMA surface and usability of the device for clinical-like genetic assays. This was not proven in previous work (Gudnason et al. 2008).

Melting of DNA as a function of applied stringency occurred in the device (Fig. 2) and the resultant melting curves are similar to those previously observed (Petersen et al. 2008, 2009). The flat shape of the curve is typical for immobilized probes (Kajiyama et al. 2003; Vainrub and Pettitt 2003; Petersen et al. 2008, 2009; Poulsen et al. 2008). Increased assay specificity as a function of applied stringencies was also observed and corroborates past observations using other devices, solid supports and genetic systems (Poulsen et al. 2008; Petersen et al. 2009). As expected and previously observed, wild type and mutant probe were selectively melted off with increasing stringency (Fig. 3) resulting in better discrimination between WT, MT and HZ genetic states at increased stringency (Fig. 3). A suitable stringency for CD 8/9 genotyping, 0.10 × SSC buffer, was identified and similarly, the best conditions for the remaining seven mutagenic sites were selected according to the same analysis as Fig. 3. When the results of this genotyping study are compared to the results for a similar study investigating the same mutagenic sites on agarose support (Petersen et al. 2009), very similar patterns are observed for each respective mutation site. This study differentiates itself from previous studies (Petersen et al. 2008, 2009) as the number of stringency conditions (*i.e.* wash buffers) has been decreased from 7 or 8 to 4. Furthermore, as Fig. 4 indicates it would have been possible to select two, instead of four, different conditions for running genetic tests confidently. Reducing to two buffer conditions would make it possible to analyse four patients per slide for the device layout shown in Fig. 1(b). Chamber densities could have easily been doubled across the surface of the PMMA slide and as a result eight patients could be analysed for an assay covering about 50 to 150 different mutations.

This report addressed array fabrication. Sample preparation, labeling and detection were not its focus. Cy3-labelled target was used for convenience. Previous work has demonstrated use of low-cost colorimetric detection methods (Petersen et al. 2007) can be employed in genotyping and preliminary results indicate these methods function on PMMA as well (unpublished results).

4.3 Applicability to diagnostics

Production and processing methods which result in more user-friendly, cost-effective and robust assays will increase use of diagnostic microarrays. The fabrication and processing methods presented can address these points.

The enclosed microarrays produced have significant advantages with respect to handling and prevention of contamination and/or damage (Wang et al. 2003; Situma et al. 2006). The fragility of glass-based microarrays and their associated handling procedures prevent their adoption in environments outside of clean and controlled environments. Admittedly, the handling of the PMMA-based microarray shown in Fig. 1(c) is very harsh and outside of expected handling thereof. Unlike the microarrays on glass slides, the closed architecture of the device presented prevents contamination or destruction of microarray spots by handling. Furthermore, samples are directly loaded into the individual lanes of the device, a feature which avoids cross-contamination of samples. Glass slides can also be used as solid support in microfluidics devices but this requires gluing the glass slide to the polymeric microfluidic cover piece (Keramas et al. 2004) using a multistep fabrication process. In contrast we demonstrate the incorporation of microarrays into multiple microfluidic networks by a two-step process. Both Wang et al. and Soper et al. report microarrays enclosed within PMMA microfluidic devices, however the devices were bonded by a high temperature thermal bonding process (Wang et al. 2003; Soper et al. 2005). This could result in channel collapse (Tsao et al. 2007), dimensional distortions and, ultimately, lead to lower device yield and/or differential hybridization conditions (Adey et al. 2002). Glues and/or adhesive films (*e.g.* double-sided tape) could also have been used to assemble the enclosed microarray. As with chemical treatments, these add steps, materials and/or labour to the fabrication process and their use can lead to manufacturing defects resulting from, for example, tape ooze. Additionally, the composition of these materials may not be well defined and may result in sensitivity and detection

problems by either absorption of reacting species and/or general biocompatibility (Stangegaard et al. 2006). In the case of reactions carried out at more elevated temperature, the release of volatiles from such materials may be especially problematic. The use of ÚV-assisted bonding avoids these potential issues and a streamlined, scalable process for the mass production of functional microarrays enclosed within PMMA microstructures results.

The production of enclosed, PMMA supported microarrays via the described method and high-speed thin-film processes incorporating probe spotting operations upstream from PMMA layer UV exposure and in-line thermal and pressure bonding is possible. Assuming an approximate cost of 0.05 EURO for PMMA pieces, the total device manufacture at volume, including arrayed probes and instrumentation should be near 1 EURO. Given that commercial glass slides typically cost 10–20 EURO significant decreases in array fabrication costs are possible. Within high volume and low margin applications such as food safety, or for use in resource poor locations, the process described would likely address cost issues related to broader adoption of wholly disposable diagnostic assays (Yager et al. 2008).

Though low-cost production is often associated with implementation in resource-poor areas, the devices produced and approach used can be integrated into modern diagnostic laboratories. As the enclosed PMMA microarray device has the same overall dimensions as a microscope slide it can be interfaced with standard microscope slide scanning equipment. Spacing on the PMMA devices was identical to 384-well plates and as such they can be paired with automated fluidic handling. This could result in increased throughput *via* reduced assay times and increased samples processed per gradient generating device. Robotic fluid handling systems could prepare DNA, PCR and targets in tubes and directly pipetting these into the closed microstructure lanes as required (Meyvantsson et al. 2008). Following hybridization, washing buffers could also be introduced and removed by such robotic systems since fluid exchange in the channels could be made by a pipette. The ability of the chambers in completed devices to sustain flows of 100 μL/sec. without leaks (Section 3.1) demonstrates that the PMMA devices are equally well suited to applications using active rather than the passive (capillary) driven flows used in this study.

The overall dimensions and spacing of channels was selected to interface to standard laboratory equipment. Given the ease with which polymers such as PMMA can be shaped, it is a simple matter to scale the approach to larger PMMA chips capable of housing greater probe numbers and/or alternate channel dimensions and patterns as dictated by the requirements of the particular assay. Visualization of the TC tagged probes was little affected by using PMMA layers that were 1.0 mm and 3.0 mm thick (unpublished results). The probes as well as the bonded structure withstood PCR denaturing conditions indicating that PCR could be performed directly on chip, thereby minimizing sample handling (Section 3.1). However, device design must consider heat transfer parameters as thermal cycling steps in PCR approach the T_g of PMMA. Where this may be problematic (*e.g.* due to channel collapse), rolling circle and other isothermal amplification methods may be used or, alternatively, robotic systems as discussed above.

The conservation of probe function following immobilization opens interesting possibilities for future work including, but not limited to, the production of enclosed antibody arrays or other heat sensitive materials by bar coding the antibodies or heat sensitive material with oligonucleotides (Kattah et al. 2008). Production of oligonucleotide arrays in enclosed PMMA devices could subsequently lead to immobilized and spatially controlled antibody arrays within the same enclosed and microfluidically-addressable device. Generation of antibody arrays in this manner would avoid issues associated with thermal, chemical or UV compatibility with biomaterials. Microarray detection was not investigated as it is affected by factors such as detection systems, detection strategy and chip structure. Such studies may form the basis for exploration of other applications where detection limits are a more important design consideration, *e.g.*, bacterial and viral diagnostics, antibody arrays, *etc*. and can be overcome with practical approaches such as PCR optimization.

5 Conclusion

The PMMA microfluidic devices containing enclosed microarrays were made *via* a UV exposure step which simultaneously attached poly(T)poly(C)-tagged oligonucleotide probes to and activated an unmodified PMMA surface for bonding below the bulk's glass transition temperature. This fabrication method is simpler than previous reports as it involves fewer production steps and avoids preparatory modifications of the PMMA. The greatest advantage of the method is its suitability to the mass production of microfluidic, polymeric and wholly disposable diagnostic microarrays. It can therefore address the low-cost requirement of microfluidic solutions in the global health care context. Eighteen patients were successfully genotyped for eight mutations in HBB within PMMA microfluidic devices containing an enclosed microarray. The produced devices withstood exposure to typical peak PCR thermal cycling temperatures and, as such, the method is also applicable to PCR based assays and devices.

Acknowledgements The authors acknowledge funding from a DTU Ph. D. student grant and from the Copenhagen County Research Foundation, grant application Nr. 803.

References

N.B. Adey, M. Lei et al., Gains in sensitivity with a device that mixes microarray hybridization solution in a 25-mu m-thick chamber. Anal. Chem. **74**(24), 6413–6417 (2002)

M.J. Banuls, V. Gonzalez-Pedro et al., PMMA isocyanate-modified digital discs as a support for oligonucleotide-based assays. Bioconjug. Chem. **18**(5), 1408–1414 (2007)

H. Becker, L.E. Locascio, Polymer microfluidic devices. Talanta. **56**(2), 267–287 (2002)

Y. Chen, L. Zhang et al., Fabrication, modification, and application of poly(methyl methacrylate) microfluidic chips. Electrophoresis. **29**(9), 1801–1814 (2008)

A.G. Crevillen, M. Hervas et al., Real sample analysis on microfluidic devices. Talanta. **74**(3), 342–357 (2007)

G.A. Diaz-Quijada, R. Peytavi et al., Surface modification of thermoplastics–towards the plastic biochip for high throughput screening devices. Lab. Chip. **7**(7), 856–862 (2007)

M. Dufva, Fabrication of high quality microarrays. Biomol. Eng. **22**(5–6), 173–184 (2005)

M. Dufva, S. Petronis et al., Characterization of an inexpensive, nontoxic, and highly sensitive microarray substrate. Biotechniques **37**(2), 286–292 (2004). 294, 296

M. Dufva, J. Petersen et al., Detection of mutations using microarrays of poly(C)10-poly(T)10 modified DNA probes immobilized on agarose films. Anal. Biochem. **352**(2), 188–197 (2006)

M. Dufva, J. Petersen et al., Increasing the specificity and function of DNA microarrays by processing arrays at different stringencies. Anal. Bioanal. Chem. **395**(3), 669–677 (2009)

F. Fixe, M. Dufva et al., One-step immobilization of aminated and thiolated DNA onto poly(methylmethacrylate) (PMMA) substrates. Lab. Chip. **4**(3), 191–195 (2004a)

F. Fixe, M. Dufva et al., Functionalization of poly(methyl methacrylate) (PMMA) as a substrate for DNA microarrays. Nucleic Acids Res. **32**(1), e9 (2004b)

H. Gudnason, M. Dufva et al., An inexpensive and simple method for thermally stable immobilization of DNA on an unmodified glass surface: UV linking of poly(T)10-poly(C)10-tagged DNA probes. Biotechniques. **45**(3), 261–271 (2008)

T. Kajiyama, Y. Miyahara et al., Genotyping on a thermal gradient DNA chip. Genome. Res. **13**(3), 467–475 (2003)

M.G. Kattah, J. Coller et al., HIT: a versatile proteomics platform for multianalyte phenotyping of cytokines, intracellular proteins and surface molecules. Nat. Med. **14**(11), 1284–1289 (2008)

G. Keramas, G. Perozziello et al., Development of a multiplex microarray microsystem. Lab. Chip. **4**(2), 152–158 (2004)

N. Kimura, One-step immobilization of poly(dT)-modified DNA onto non-modified plastic substrates by UV irradiation for microarrays. Biochem. Biophys. Res. Commun. **347**(2), 477–484 (2006)

I. Meyvantsson, J.W. Warrick et al., Automated cell culture in high density tubeless microfluidic device arrays. Lab. Chip. **8**(5), 717–724 (2008)

J. Petersen, M. Stangegaard et al., Detection of mutations in the beta-globin gene by colorimetric staining of DNA microarrays visualized by a flatbed scanner. Anal. Biochem. **360**(1), 169–171 (2007)

J. Petersen, L. Poulsen et al., Use of a multi-thermal washer for DNA microarrays simplifies probe design and gives robust genotyping assays. Nucleic Acids Res. **36**(2), e10 (2008)

J. Petersen, L. Poulsen et al., Microfluidic Device for Creating Ionic Strength Gradients over DNA Microarrays for Efficient DNA Melting Studies and Assay Development. PLoS ONE. **4**(3), e4808 (2009)

L. Poulsen, M.J. Soe et al., Multi-stringency wash of partially hybridized 60-mer probes reveals that the stringency along the probe decreases with distance from the microarray surface. Nucleic Acids Res. **36**(20), e132 (2008)

H. Shinohara, J. Mizuno et al., Low-temperature direct bonding of poly(methyl methacrylate) for polymer microchips. Ieej Transactions on Electrical and Electronic Engineering. **2**(3), 301–306 (2007)

C. Situma, Y. Wang et al., Fabrication of DNA microarrays onto poly (methyl methacrylate) with ultraviolet patterning and microfluidics for the detection of low-abundant point mutations. Anal. Biochem. **340**(1), 123–135 (2005)

C. Situma, M. Hashimoto et al., Merging microfluidics with microarray-based bioassays. Biomol. Eng. **23**(5), 213–231 (2006)

C. Situma, A.J. Moehring et al., Immobilized molecular beacons: a new strategy using UV-activated poly(methyl methacrylate) surfaces to provide large fluorescence sensitivities for reporting on molecular association events. Anal. Biochem. **363**(1), 35–45 (2007)

S.A. Soper, M. Hashimoto et al., Fabrication of DNA microarrays onto polymer substrates using UV modification protocols with integration into microfluidic platforms for the sensing of low-abundant DNA point mutations. Methods. **37**(1), 103–113 (2005)

M. Stangegaard, S. Petronis et al., A biocompatible micro cell culture chamber (microCCC) for the culturing and on-line monitoring of eukaryote cells. Lab. Chip. **6**(8), 1045–1051 (2006)

R. Truckenmüller, P. Henzi et al., Bonding of polymer microstructures by UV irradiation and subsequent welding at low temperatures. Microsyst. Technol. **10**, 372–374 (2004). doi:10.1007/s00542-004-0422-3

C.W. Tsao, D. Devoe, Bonding of thermoplastic polymer microfluidics. Microfluid. Nanofluid. **6**, 1–16 (2009). doi:10.1007/s10404-008-0361-x

C.W. Tsao, L. Hromada et al., Low temperature bonding of PMMA and COC microfluidic substrates using UV/ozone surface treatment. Lab. Chip. **7**(4), 499–505 (2007)

A. Vainrub, B.M. Pettitt, Surface electrostatic effects in oligonucleotide microarrays: Control and optimization of binding thermodynamics. Biopolymers **68**(2), 265–270 (2003)

E. Waddell, Y. Wang et al., High-resolution near-infrared imaging of DNA microarrays with time-resolved acquisition of fluorescence lifetimes. Anal. Chem. **72**(24), 5907–5917 (2000)

Y. Wang, B. Vaidya et al., Microarrays assembled in microfluidic chips fabricated from poly(methyl methacrylate) for the detection of low-abundant DNA mutations. Anal. Chem. **75**(5), 1130–1140 (2003)

G.M. Whitesides, The origins and the future of microfluidics. Nature. **442**(7101), 368–373 (2006)

P. Yager, G.J. Domingo et al., Point-of-care diagnostics for global health. Annu. Rev. Biomed. Eng. **10**, 107–144 (2008)

Z. Zhao, R. Peytavi et al., Plastic polymers for efficient DNA microarray hybridization: application to microbiological diagnostics. J. Clin. Microbiol. **46**(11), 3752–3758 (2008)

Supplementary Insert 1

Table 1: DNA probes and PCR primers used for HBB genotyping

Probe name	Sequence	Type of Mutation
CD5 MT	TTTTTTTTTTCCCCCCCCCCGCACCTGACTCGAGGAGAAGT	-CT
CD5 WT	TTTTTTTTTTCCCCCCCCCCGCACCTGACTC**CT**GAGGAGAA	-CT
CD8 MT	TTTTTTTTTTCCCCCCCCCCCCTGAGGAGGTCTGCCG	-AA
CD8 WT	TTTTTTTTTTCCCCCCCCCCCCTGAGGAG**AA**GTCTGCCG	-AA
CD8/9 MT	TTTTTTTTTTCCCCCCCCCCGAGGAGAAG**G**TCTGCCGTTAC	+G
CD8/9 WT	TTTTTTTTTTCCCCCCCCCCGAGGAGAAGTCTGCCGTTACTG	+G
CD15 MT	TTTTTTTTTTCCCCCCCCCCACTGCCCTGT**A**GGGCAAGGT	G > A
CD15 WT	TTTTTTTTTTCCCCCCCCCCTGCCCTGT**G**GGGCAAGG	G > A
CD24 MT	TTTTTTTTTTCCCCCCCCCCAAGTTGG**A**GGTGAGGCCCT	T > A
CD24 WT	TTTTTTTTTTCCCCCCCCCCGAAGTTGG**T**GGTGAGGCCC	T > A
CD27/28 MT	TTTTTTTTTTCCCCCCCCCCGTGAGGCCC**C**TGGGC	+C
CD27/28 WT	TTTTTTTTTTCCCCCCCCCCGTGAGGCCCTGGGCAG	+C
IVS I+5 MT	TTTTTTTTTTCCCCCCCCCCGGCAGGTTG**C**TATCAAGGTTACA	G > C
IVS I+5 WT	TTTTTTTTTTCCCCCCCCCCGGCAGGTTG**G**TATCAAGGTTACA	G > C
IVS I+6 MT	TTTTTTTTTTCCCCCCCCCCGGCAGGTTGG**C**ATCAAGG	T > C
IVS I+6 WT	TTTTTTTTTTCCCCCCCCCCGGCAGGTTGG**T**ATCAAGGTTACA	T > C

PCR primers	
BCF	AGCAGGGAGGGCAGGAGCCA
T7-BCR	GAAATTAATACGACTCACTATAGGGAGAAGAGTCAGTGCCTATCAGAAACCC

APPENDIX B

PEER-REVIEWED CONFERENCE PROCEEDING 1:

"*Modular Microfluidic System with a Cast PDMS Pumping Bed and Planar PDMS Interconnection Blocks*"

MODULAR MICROFLUIDIC SYSTEM WITH A CAST PDMS PUMPING BED AND PLANAR PDMS INTERCONNECTION BLOCKS

D. Sabourin, D. Snakenborg, P. Skafte-Pedersen, J.P. Kutter and M. Dufva

Dept. of Micro- and Nanotechnology, Technical University of Denmark, DENMARK

ABSTRACT

A modular microfluidic system using re-useable PDMS components and featuring multiple planar interconnections, a multi-channel peristaltic pump, a small footprint, unobstructed microscopic observation, and allowing rapid testing of microfluidic chips is described. Data on interconnection and pump performance is presented.

KEYWORDS: Interconnection, Pump, Modular, Testing

INTRODUCTION

The peripheral equipment and interfacing components required to drive microfluidic devices are often costly and bulky, resulting in serious limitations and restrictions in the operation of these devices, such as microscopic observation. The described approach addresses these issues and supports rapid testing.

DESIGN AND FABRICATION

The system shown in Figure 1 consists of a re-useable 12-channel polydimethylsiloxane (PDMS) interconnection block (IB) and pumping bed (PB), both containing integrated o-rings. A multi-roller peristaltic pump made from 2mm brass rods driven by a stepper motor simultaneously pumps all channels by mechanically squeezing the PDMS. A sample reservoir, microfluidic chip and sample outlet complete the system.

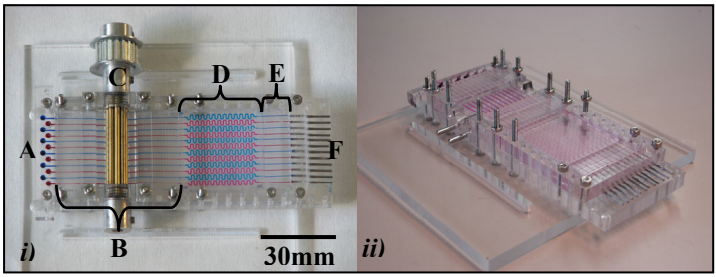

Figure 1. Assembled system. i) A) Sample reservoirs, B) PDMS 12-channel PB, C) multi-roller, D) PMMA microfluidic chip, E) PDMS IB, and F) sample outlet. Stepper motor not shown. Dye visible in chip corners results from incomplete bonding of chip. ii) System side profile with multi-roller removed. Planar features including microfluidic chip and IB are 4mm in height.

The IB and PB shown in Figure 2 were cast from micromilled poly(methyl methacrylate) (PMMA) moulds. The 240µm inner diameter channels in each were formed by removing sacrificial fibre inserts following PDMS curing. Channels are spaced 2.25 mm centre-to-centre and are bookended by o-rings with 0.6mm inner diameter, 1.4mm outer diameter and 0.4mm height. To improve pump efficiency and reduce friction between the PDMS and the roller, PB channels are raised above the PB plane.

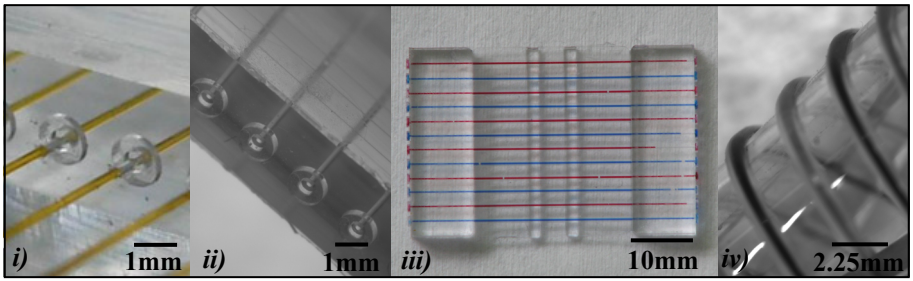

Figure 2. PDMS IB and PB features. i) Mould features and sacrifical fibre inserts yielding integrated o-rings. ii) Close-up of o-rings bookending PB and IB iii) PB with dye solution in channels iv) Close-up of raised fluidic channels in mid-portion of PB. PB folded over and channels filled with dye solution to show raised and integrated channels.

Manually clicking in "oversized" and complimentary chips between the IB and PB compresses the o-rings resulting in 24 aligned and planar interconnections. Microfluidic chips are rapidly inserted and removed from the system and tested.

EXPERIMENTAL

The leak pressure of the o-rings bookending a channel was determined visually and using a pressure sensor. An IB was placed between two PMMA faces providing inlet and outlet, and filled with dye solution. The outlet channel was blocked, a syringe pump started and the leak pressure noted.

A PMMA chip was inserted into the system to characterize the pump. The roller was set at rotational speeds of either 0.71 and 3.05 revolutions/min and time-lapse micrsoscopy measured the advance of a liquid front within the chip. Repeated measurements were collected for different chip orientations to calculate both mean flow rate and to separate chip volume variation from pump variation.

RESULTS AND DISCUSSION

The average pressure limit from 20 measurements and repeated insertions of the IB was determined to be 430kPa with a standard deviation (SD) of 60kPa. The maximum and minimum values were 540kPa and 320kPa, respectively. All readings were above the 200 kPa limit considered suitable for most microfluidic applications [1]. Previously, re-usable o-ring based connections with a maximum pressure limit of 1700 kPa were reported in [1] and re-usable PDMS interconnects

from [2] sustained 220 kPa. However, neither form planar connections nor demonstrate an equivalent number of interconnects. Planar connections supporting 1230kPa were described in [3]; however, auxiliary/non-integrated tubing is required. The use of integrated o-rings within the components of the system eliminates the need for permanent bonding methods, which in turn facilitates rapid chip interchange and testing.

At the higher roller rotational speed the average flow rate was 1.92µL/min with a SD of 0.17µL/min between channels and a within channel SD of 0.08µL/min. At the lower rotational speed, the average flow rate was 0.43µL/min with a SD of 0.036µL/min between channels and a within channel SD of 0.02µL/min. The rotational roller speed could be further reduced to lower flow rates. Additionally, differing flow rates between channels or pumping beds can be produced by varying the sacrifical fibre diameter when casting the PDMS. The PB design eliminates the need for further tubing and limits compliance, set-up time and pump dead volume (approx. 2.4µL per channel).

Comparable integrated devices using Braille-display drives have been described [4,5]; however, this approach is applicable only to elastomeric materials, whereas the approach presented here is applicable to rigid polymeric, glass and elastomeric materials. The described system will be used for cell culture as it offers unobstructed microscopic observation, lacks cytotoxic adhesives and uses biocompatible materials. Other uses include gene expression based biocompatibility studies, biofilm analysis, and spotted array investigations.

CONCLUSIONS

A modular microfluidic system has been designed and characterized. Among the system's features, its small footprint, modularity, integration and planar interconnections make it well suited to the rapid testing of microfluidic chips and for applications where unobstructued microscopic observation is required.

REFERENCES

[1] A. Bhagat and I. Papautsky, *Re-useable quick-release interconnect for characterization of microfluidic systems*, J. Micromech. Microeng., (17) , pp. 42-49, (2007).

[2] V. Saarela and R. Kostiainen, *Re-useable multi-inlet PDMS fluidic connector*, Sensors and Actuators, (114), pp. 552-557, (2006).

[3] D. Snakenborg and J.P. Kutter, *A fast and reliable way to establish fluidic connections to planar microchips*, J. Micromech. Microeng., (17), pp. 98-103, (2007).

[4] W. Gu and S. Takayama, *Computerized microfluidic cell culture using elastomeric channels and Braille displays*, PNAS, (101), pp. 15861-15866, (2004).

[5] Y. Chi-Tung and S. Takayama, *Small volume low mechanical stress cytometry using computer-controlled Braille display microfluidics*, Lab on a Chip (7) pp. 1497-1503, (2007).

PEER-REVIEWED CONFERENCE PROCEEDING 2:

"Fast and Simple: Reconfigurable Elements and Solutions for Creating and Driving Fluidic Networks"

Topic No. 6.2, 4.2, 6.3 Paper ID No: 1064
Oral or Poster

FAST AND SIMPLE: RECONFIGURABLE ELEMENTS AND SOLUTIONS FOR CREATING AND DRIVING FLUIDIC NETWORKS

David Sabourin*, Peder Skafte-Pedersen*, Vasile Coman*, Mette Hemmingsen*, Jesper Petersen**, Jörg P. Kutter*, Jenny Emneus*, Detlef Snakenborg* and Martin Dufva*
*DTU Nanotech, Department of Micro- and Nanotechnology, Technical University of Denmark, Kongens Lyngby, DENMARK
**Herlev University Hospital, Department of Hematology, Herlev, DENMARK

Ease of use, reliability and accessibility remain barriers to the adoption of microfluidic approaches [1, 2]. Practical issues including interconnections, pump capacity and control, and suitability to microscopic observation often complicate microfluidic setups. We present modular interconnection and pump components which provide simple, reliable and multiple parallel chip-to-world and chip-to-chip interconnectivity and pump capacity. Motorized and unmotorized control of fluidic actuation needed for perfusion cell culturing and multistep genotyping assays respectively demonstrates the wide applicability of the modular system.

Cast PDMS-based microfluidic ribbons (MR) (Figure 1), containing eight integrated channels with 240 µm inner diameters spaced 2.25 mm centre-to-centre (1536 well plate standard) and bookended with ball joint features provide self-aligning, minimal dead volume interconnections which support pressures greater than 200 kPa [3], the threshold applicable to most microfluidic applications [4]. Two MR configurations eliminate further tubing requirements. The first permits direct chip-to-chip or chip-to-reservoir connectivity and the second connects microfluidic components through a further miniaturized and improved version of an 8-channel miniaturized peristaltic pump (Figure 1) we previously described [5]. Pump dimensions, excluding motor, measure only 20 mm (h) x 20 mm (w) x 40 mm (l). The pump's small footprint and proximity to microfluidic chips reduces compliance and pump dead volume to 2.25 µL. System modularity permits many configurations (Figure 2) with higher interconnection numbers than previous reports [4], i.e. up to 32 interconnections on a 30 mm x 30 mm chip. Multiple pumps can be connected to the same device without extensively increasing system footprint permitting highly multiplexed assays.

For simple microfluidic analyses, or use in resource poor and remote locations, hand cranks are attached to pumps to deliver fluids. A hand crank system (Figure 2) was used to genotype a patient for mutations in the β-globin gene (Figure 3) within a disposable microfluidic microarray-containing PMMA device [6].

For non-experts developing microfluidic investigations requiring higher degrees of automation there is also a lack of accessible and easily implementable control solutions. We resolve this issue by using the commercially available LEGO® Mindstorms™ kit to program and control our pumps. The low-cost product includes motors, a controller and a "child friendly" graphical interface. As motor rotation can be controlled to 1°, multiple pumps can be accurately activated to time, meter and flow fluids through chips. Large flow rate ranges are possible; we have used between 0.033 and 60 µL min^{-1}. The coefficient of variation (% CV) for channel to channel fluid delivery volumes through the pumps was evaluated to approximately 3% (Figure 3). Cell culture of HeLa cells within a PMMA chip and associated processing steps including, sterilization and loading, were performed with this approach (Figure 3).

We believe this approach to be more accessible than similar solutions, including Braille displays [7]. The system's modular components and compact design allows construction of setups that fit on microscope stages or similar life science instruments, thus making it suitable for experiments involving kinetic studies of molecular interactions (e.g. DNA hybridization) and cells (e.g. growth, migration, gene expression).

Word count: 496

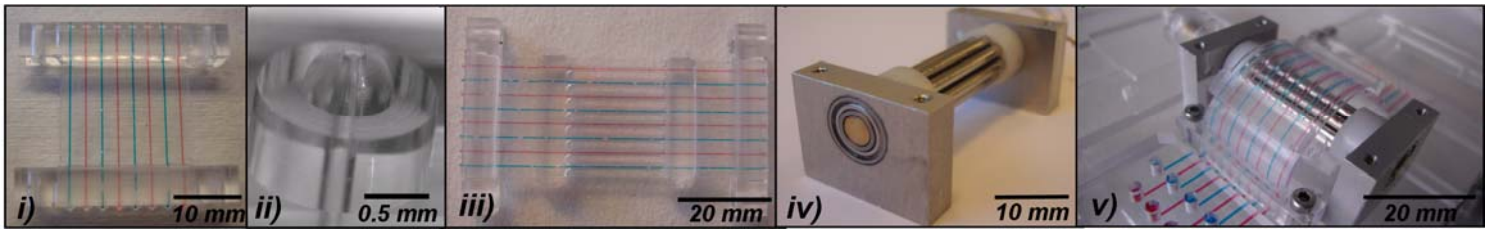

Figure 1. Modular components of microfluidic system. i) TYPE 1 microfluidic ribbon (MR) containing 8 integrated 240 um inner diameter channels. Channels filled with dye to facilitate visualization. All channels are bookended by Ball Joint interconnection features. ii) Ball Joint interconnection feature. iii) Type 2 MR used for connecting microfluidic chips through a miniaturized peristaltic pump. Channel dimensions and interconnection features are identical to Type 1MR. iv) The peristaltic pump is made from eight free-rolling 2 mm stainless steel rods. v) A Type 2 MR is placed across the pump's multi-roller to deliver fluids. A covering piece compresses the Type 2 MR against the multi-roller to pump fluids (not shown).

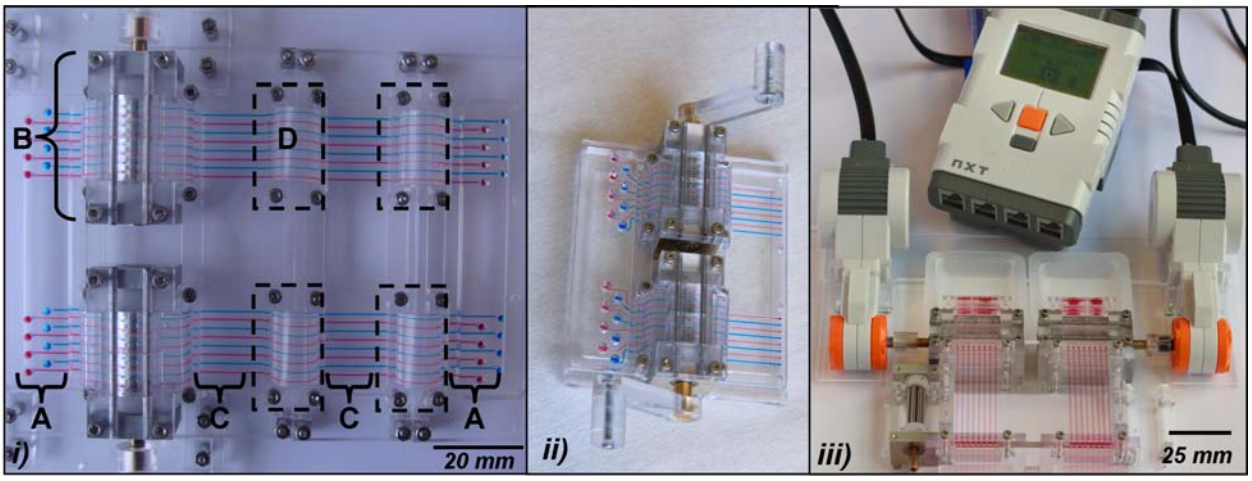

Figure 2. Assembled systems in assorted configurations. i) Two pump configuration with 96 interconnections - motors not shown. A) Sample reservoirs and outlet chips, B) miniaturized 8 channel peristaltic pump with Type 2 MR inside, C) PMMA microfluidic chips, D) Type 1 MR (dashed boxes). ii) Two pump system powered by hand cranks. iii) Two pump system showing LEGO motors and controller.

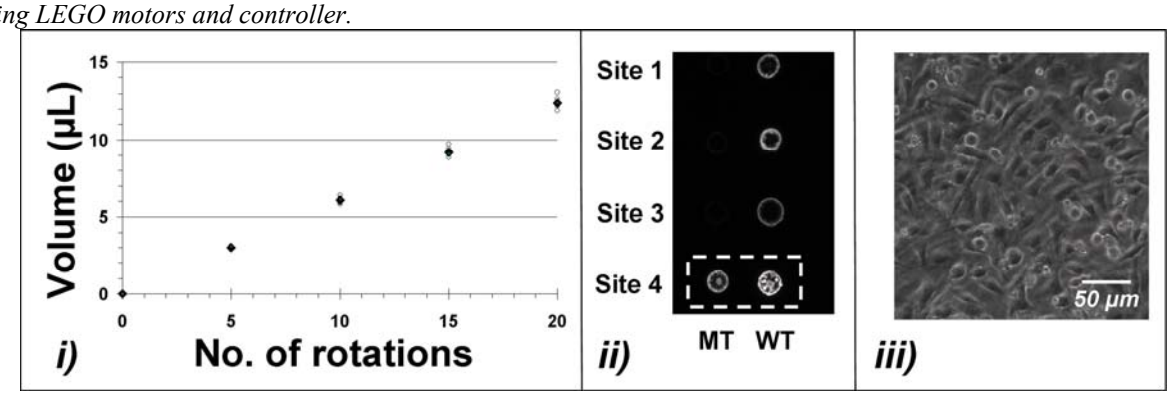

Figure 3. i) Flow test data. Volume displaced as a function of number of rotations for each of 8 channels is shown (o) as is the average (♦) for all 8 channels. % CVs are approximately 3 % at each rotation count. ii) Image of fluorescently-detected allele-specific hybridization (ASH) assay used to genotype a patient for mutations in the β-globin gene. A PMMA microfluidic chip containing ASH microarrays and the hand crank system shown in Figure 2(iv) were used to process patient material. The patient shown was wild-type (WT) for all interrogated sites with the exception of site 4, for which they were heterozygous mutant type (MT), and therefore carry a mutation associated with a β–globin deficiency. Spot sizes are approximately 250 µm. iii) Image of HeLa cells cultured using a PMMA chip and a system configuration similar to that shown in Figure 2(iii). Fluidic control and assorted operations including sterilization and cell seeding were achieved by LEGO® Mindstorms™ motors and control.

REFERENCES:

[1] Andersen, H. et al. "Where are the biologists?", Lab on a Chip, 6, 467-470 (2006).
[2] Young, E.W. et al. "Macro- and microscale fluid flow systems for endothelial cell biology", Lab on a Chip, 10, 143-160 (2009)
[3] Sabourin, D. et al. "Interconnection blocks with minimal dead volumes permitting planar interconnection to thin microfluidic devices", Microfluidics and Nanofluidics, DOI: 10.1007/s10404-009-0520-8 (2009)
[4] Bhagat, A. et al, "Re-useable quick-release interconnect for characterization of microfluidic systems", J. Micromech. Microeng., (17), 42-49, 2007.
[5] Skafte-Pedersen, P. et al. "Multi-channel peristaltic pump for microfluidic applications featuring monolithic PDMS inlay", Lab on a Chip, 9, 3003-3006 (2009)
[6] Sabourin, D. et al. "Microfluidic DNA microarrays in PMMA chips: streamlined fabrication via simultaneous DNA immobilization and bonding activation by brief UV exposure", Biomedical Microdevices, DOI 10.1007/s10544-010-9420-7, 2010.
[7] Gu, W. et al, "Computerized microfluidic cell culture using elastomeric channels and Braille displays", PNAS, (101), 15861-15866, 2004.

PEER-REVIEWED CONFERENCE PROCEEDING 3:

"A user-friendly, self-contained, programmable microfluidic cell culture system for high quality microscopy"

Topic No. 1.5, 1.7, 4.2 Paper ID No: 0869
Oral or Poster

A user-friendly, self-contained, programmable microfluidic cell culture system for high quality microscopy

Peder Skafte-Pedersen*, David Sabourin*, Mette Hemmingsen*, Peter Friis Østergaard*, Felician Stefan Blaga**, and Martin Dufva*

*Department of Micro- and Nanotechnology, Technical University of Denmark, DTU Nanotech, Building 345 East, DK-2800 Kongens Lyngby, DENMARK
**Department of Informatics and Mathematical Modelling, Technical University of Denmark, DTU Informatics, Building 321, DK-2800 Kongens Lyngby, DENMARK

The use of microfluidic tools in cell culture is often limited by the complexity and need for peripheral components in typical research setups incompatible with standard, sterile cell biology work flows and microscopy [1,2]. We present a self-contained, automated system including pumps, reservoirs and interconnections for programmable long-term cell culture. The system is especially designed for use in cell labs and to fit into standard motorized stages in inverted life science microscopes. Except the power supply and electrical controller, every component for driving the microfluidic chip is on the system. It can therefore easily be moved from cell culture labs for cell loading to microscopes for observation just by connecting one single electrical cable (Fig. 1).

The system distinguishes itself from other integrated systems [3,4] by having more fluidic inputs/outputs, accepting polymeric and silicon/glass based chips, not relying of pneumatics for fluidic control and being compatible with unobstructed, high quality real-time transmission and fluorescence microscopy observation. We demonstrate how the system can be used to switch between different liquid inputs, which is necessary for programming purposes, and that cells can be seeded and cultured on-chip in a microscope for several days.

The platform (Fig. 1), consists of three miniaturized 8-channel peristaltic pumps [5], up to 30 reservoirs and a chip holder allowing the exchangeable chip to be readily snapped on to 32 self-aligning fluidic interconnections [6]. The exchangeable microfluidic chip of poly(methyl methacrylate) (PMMA) contains passive microfluidic networks and has microscope slide foot print for ease of use and compatibility with standard life science equipment.

The pump control is obtained through a single electrical interconnection to a custom-made controller. A VBA script in Zeiss AxioVision was developed to simultaneously control the pumps and Zeiss Axio Observer microscope for automated imaging/analysis.

The cells where loaded by pipetting cell suspension into integrated 90 μL wells at the outlet side. A uniform cell seeding is readily achieved upon reversing the flow. Due to the design of wells and channel system no agitation between pipetting steps is required making it easy to load different cell lines in each well. When sterilized and assembled the system is fully enclosed and can be transferred between equipment without risk of contamination.

Fig. 2 shows a time-lapse series of HeLa Tet-On cells cultured using the platform in a microscope equipped with CO_2 controlled incubator. The proliferation and adhesion proves the seeding and perfusion method suitable for the application.

Fig. 3 demonstrates how two pumps are used to switch between a fluorescent and nonfluorescent liquid in a T-junction with a downstream leakage only limited by diffusion. The fluorescent signal is changed approximately two orders of magnitude within 3 minutes at a flow rate of 250 nL/min in channels with 400x150 μm^2 cross section. The result is in fair agreement with finite element (FEM) simulations thus verifying the system's switching properties. Switch characteristics can be tailored by changing geometry and flow rate, which has been experimentally verified, and proves the system suitable for cell studies with temporally varied exposure profiles.

Word Count: 500

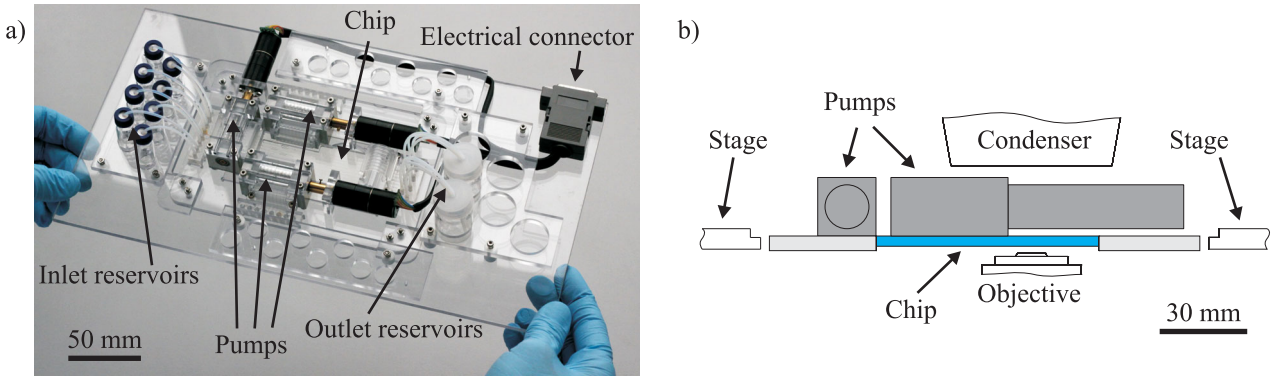

Figure 1. a) The complete platform mounted with chip, eight inlet reservoirs and two outlet reservoirs. Miniaturisation of pumps and connections allows these and the observation area to fit between life science objectives and a 26 mm working distance (WD) condenser in an inverted microscope. b) Side view showing fit of central parts between 26 mm WD condenser and 2.9 mm WD objective.

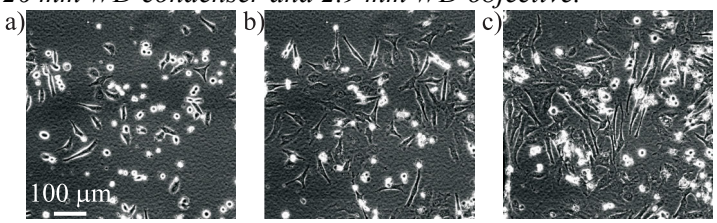

Figure 2. HeLa Tet-On cells (Clonetech) cultured in a PMMA chip containing 8 chambers with a height of 200 µm and 3.2 µL volume perfused with an average flow rate of 250 nL/min. Time lapse images acquired at a) 5 hours, b) 24 hours and c) 48 hours after cell seeding show cell adhesion and proliferation.

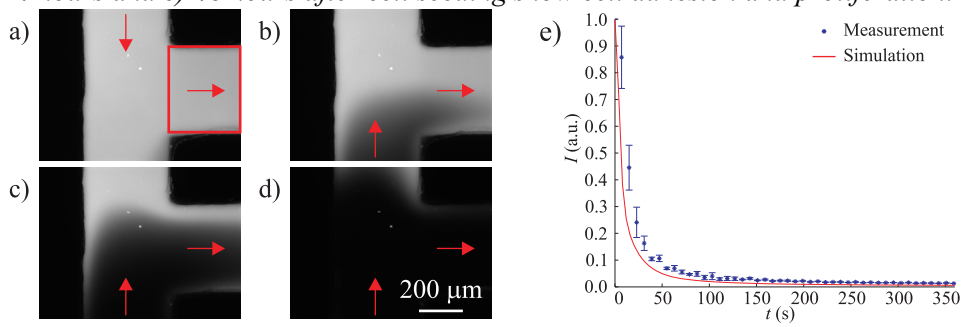

Figure 3. Switching sequence between buffer and fluorescent Cy3-streptavidin conjugate in a T-junction with channel cross section of 400x150 μm^2 at a flow rate of 250 nL/min. Arrows indicate flow settings under a) initial condition and b) 8 s, c) 16 s and d) 112 s after switching. Quantification by background corrected, relative pixel intensity over three repetitions and theoretical data based on a 2D convection-diffusion FEM simulation in COMSOL 3.4 is given in e). The box annotation in a) indicates the analysis region.

REFERENCES:

[1] "Macro- and microscale fluid flow systems for endothelial cell biology", E.W. Young & C.A. Simmons, Lab on a Chip, 10, 143-160 (2009)

[2] "Fundamentals of microfluidic cell culture in controlled microenvironments", E.W.K. Young & D.J. Beebe, Chemical Society Reviews,39, 1036-1048 (2010)

[3] "Handheld recirculation system and customized media for microfluidic cell culture", N. Futai, W. Gu, J.W. Song & S. Takayama, Lab on a Chip, 6, 149-154 (2006)

[4] "A cell culturing system that integrates the cell loading function on a single platform and evaluation of the pulsatile pumping effect on cells", J.Y. Kim, H. Park, K.H. Kwon, J.Y. Park, J.Y. Baek, T.S. Lee, H.R. Song, Y.D. Park, & S.H. Lee, Biomedical Microdevices, 10, 11-20 (2008)

[5] "Multi-channel peristaltic pump for microfluidic applications featuring monolithic PDMS inlay", P. Skafte-Pedersen, D. Sabourin, M. Dufva & D. Snakenborg, , Lab on a Chip, 9, 3003-3006 (2009)

[6] "Interconnection blocks with minimal dead volumes permitting planar interconnection to thin microfluidic devices", D. Sabourin, D. Snakenborg & M. Dufva, Microfluidics and Nanofluidics, DOI: 10.1007/s10404-009-0520-8 (2009)

APPENDIX C

CONFERENCE PROCEEDING 1:

"*Re-useable PDMS interconnect blocks allowing multiple rapid planar interconnections*"

Re-useable PDMS interconnect blocks allowing multiple rapid planar interconnections

David Sabourin, Detlef Snakenborg, Jörg P. Kutter and Martin Dufva

DTU Nanotech, Department of Micro- and Nanotechnology, Technical University of Denmark, Ørsteds Plads 345Ø, DK-2800, Kgs Lyngby

Introduction

Interfacing microfluidic devices to fluids is often tedious, laborious and time consuming. A method to rapidly connect, prototype and characterize microfluidic chips is desired. Re-useable PDMS interconnect blocks allowing rapid formation of 24 planar connections to a microfluidic chip without permanent bonding methods and rapid prototyping are presented.

Materials

PDMS interconnect blocks (Figure 1) were cast from micromilled PMMA molds. Each interconnect block contains twelve channels spaced 2.25mm centre to centre. Channels are formed via sacrificial fibre inserts and are bookended by integrated o-rings.

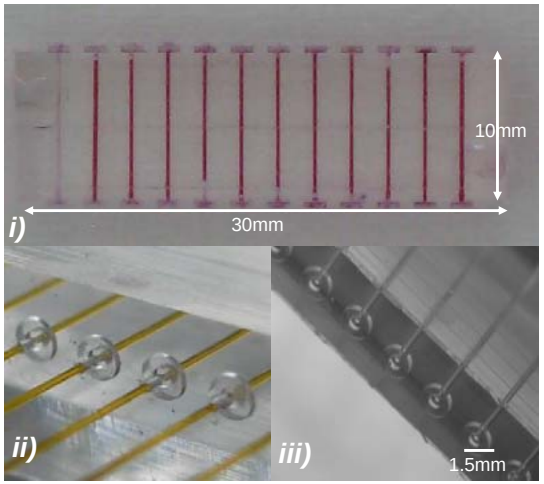

Figure 1: ***i)*** PDMS interconnect block - top view ***ii)*** Micromilled PMMA mold showing O-ring mold elements and sacrificial fibres, and ***iii)*** side view of interconnect block and o-ring elements

Methods

To prototype and/or test a microfluidic chip/design, a complimentary chip is inserted by hand between two interconnect blocks within an undersized frame (Figure 2). This compresses, seals and aligns the integrated o-rings to the fluidic channels along opposite sides of the microfluidic chip. In this manner, the o-ring structures behave similarly to excess tubing lengths described in [1].

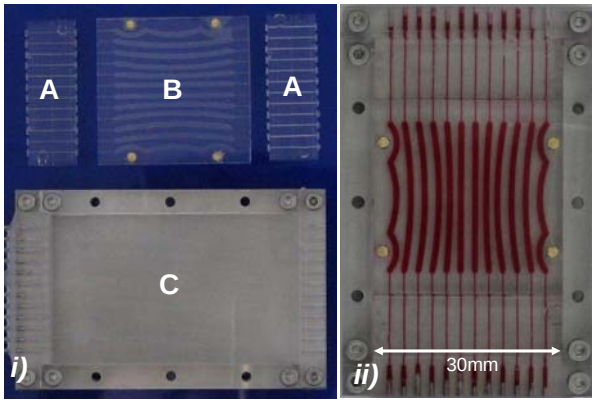

Figure 2: ***i)*** PDMS interconnect blocks (A), PMMA microfluidic chip (B), and undersized frame (C) ***ii)*** Assembled system filled with dye solution

The pressure leak test set-up is depicted in Figure 3.

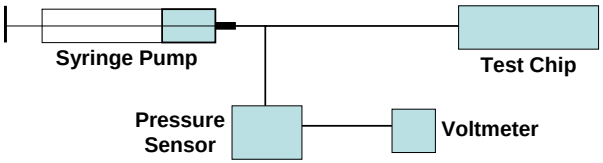

Figure 3: PDMS interconnect block channels were filled with dye solution, compressed between two PMMA faces and observed under a microscope. A syringe pump was started and the pressure at which either of the two o-rings bookending a channel leaked was recorded via a pressure sensor and voltmeter.

Results

Pressure test data, in bar, is summarized below.

AVG	SD	Max	Min	n
4.3	0.6	5.4	3.2	20

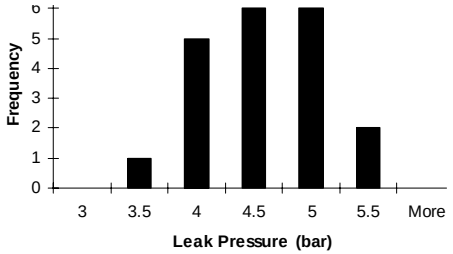

Data was collected over several insertions of the PDMS interconnect block. No decrease in the average leak pressure was noted. The average and lowest observed leak pressure are well above the 2 bar threshold described as suitable for most microfluidic applications [2]. Microfluidic chips have been rapidly tested via this approach.

Conclusions

Re-useable PDMS interconnect blocks yielding 24 inputs/outputs with good seal quality were manufactured. Advantages include:

- practicality
- suitability to rapid prototyping/testing of microfluidic devices
- compatibility with microfluidic chips with rigid side surfaces, and
- planar connections allowing unobstructed observation via microscope

In future the PDMS interconnect blocks can be used as part of a modular microfluidic system.

References

1. Snakenborg, D. et al, *A fast and reliable way to establish fluidic connections to planar microchips*, J. Micromech. Microeng., (17), 98-103, 2007.
2. Bhagat, A. et al, *Re-useable quick-release interconnect for characterization of microfluidic systems*, J. Micromech. Microeng., (17), 42-49, 2007.

DTU Nanotech
Department of Micro- and Nanotechnology

CONFERENCE PROCEEDING 2:

"*Genotyping of Human β-Globin Mutations using capillary driven flows in PMMA microfluidic chips containing fully enclosed allele specific hybridization microarrays*"

Genotyping of Human β-Globin Mutations using capillary driven flows in PMMA microfluidic chips containing fully enclosed allele specific hybridization microarrays

David Sabourin, Jesper Petersen, Detlef Snakenborg, Monica Brivio, Haukur Gudnadson, Anders Wolff and Martin Dufva

DTU Nanotech, Department of Micro- and Nanotechnology, Technical University of Denmark, Ørsteds Plads 345Ø, DK-2800, Kgs Lyngby

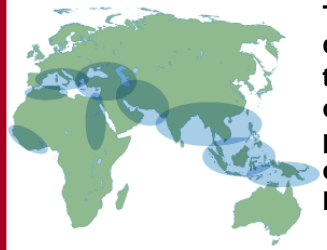

Thalassaemia syndromes result from synthesis deficiencies of α- or β−chains caused by mutations in the human globin genes. These mutations are the most common human monogenic disorder and are highly prevalent in resource limited regions[1]. In such regions, cost remains a barrier to wider diagnostic test adoption. Polymer-based diagnostics may help address this[2].

PMMA chips containing allele specific hybridization (ASH) microarrays for β−thalassaemia mutations enclosed in individual microfluidic chambers were manufactured by a simple and scalable UV-based process.

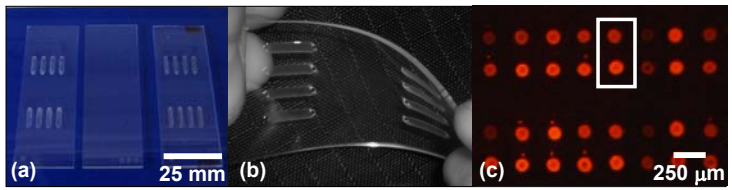

(a) Left to right: PMMA lid with chambers, PMMA with spotted arrays, bonded PMMA chip (b) PMMA chip robust to handling and twisting (c) Microarray found in each channel of device. Square indicates ASH wild-type (WT) and mutant (MT) probe pair

Genotyping was completing using the PMMA-based diagnostic microarray chips and multi-salinity gradients[3]. For each chamber/stringency used to genotype a patient, a normalized ratio for each ASH probe pair is calculated as:

$$RATIO = [S_{WT} / (S_{WT} + S_{MT})]$$

where S_{WT} and S_{MT} are signal from wild-type (WT) and mutant (MT) probes. Ideally RATIO = 1 for WT, 0 for MT and 0.5 for heterozygotes (HZ).

DNA dissociation curves obtained by multi-salinity gradients are comparable and as useful in genotyping and assay optimization as those obtained by temperature changes. Furthermore, the multi-salinity gradient method is simple to implement.

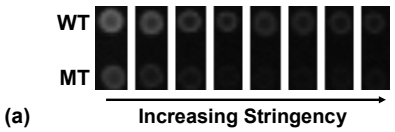

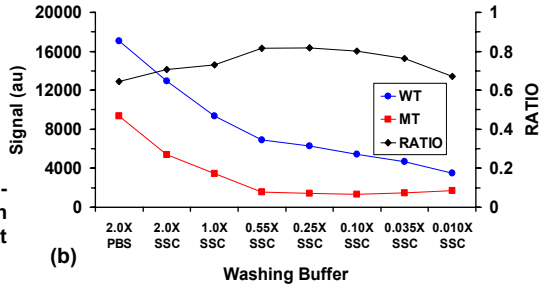

(a) WT and MT signals following multi-salinity gradient washing for a HBB mutation (b) Signal for WT and MT probes from (a) at each stringency and calculated RATIO value

PCR product of an HBB fragment was used as T7 *in vitro* transcription (IVT) template to yield cy3-labelled ssRNA target. 5 µL of diluted IVT product was placed in 4 microarray chambers for 2 hours @ 37°C. Each chamber was flushed with 5 µL of either 2.0X, 0.55X, 0.10X or 0.035X SSC and washed with another 5 µL of the same for 30 minutes at 41°C.

Average RATIO values for each genotype at a HBB mutagenic site (CD 8/9). 18 patients were tested for which n=16 were WT (•), n=2 were HZ (♦) and n=2 were MT (■). Error bars represent min/max RATIO values. The figure demonstrates potential pitfalls associated with running microarrays at a single stringency. Even though probe pairs were melting temperature matched, false confidence in assay results if the proper wash buffers are not selected.

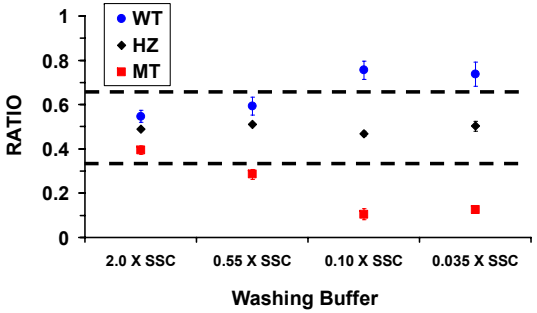

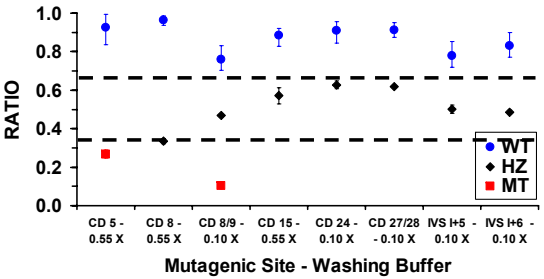

Average RATIO values for each genotype at each mutagenic site at the indicated SSC washing buffer concentration. 18 patients were tested of which 13 were HZ (♦) and 4 MT (■) for the 8 mutagenic HBB sites tested. One patient was WT (•) at all sites. Error bars represent min/max RATIO values for each genotype at each mutagenic site

High assay specificity was obtained *via* parallel multi-stringency washes in individual chambers. 18 patients were correctly genotyped for 8 HBB mutations (original diagnosis performed by HLPC and DNA sequencing).

Perspectives:

Solutions introduced into the 5 µL chambers by capillary force, suitable for remote locations. Chamber spacing equivalent to 384-well plates allows potential integration into centralized laboratory testing with automated fluidic handling systems and increase in microarray assay throughput

References:

1. Birgens H, Ljung R. The thalassaemia syndromes. Scand J Clin Lab Invest 2007; 67: 1-15.
2. P. Yager, G. J. Domingo and J. Gerdes, *Annual review of biomedical engineering*, 2008, 10, 107-144.
3. J. Petersen, L. Poulsen, H. Birgens and M. Dufva, *PLoS ONE*, 2009, 4, e4808.

DTU Nanotech
Department of Micro- and Nanotechnology

CONFERENCE PROCEEDING 3:

"*Peristaltic Micropump for microfluidic applications*"

Peristatlic Micropump for Microfluidic Applications

Sabourin, David; Peder Skafte-Pedersen; Snakenborg, Detlef; Dufva, Martin
DTU Nanotech: Department of Micro- and Nanotechnology,
Technical University of Denmark, Kongens Lyngby, Denmark
Ph: + 45 4525 6333
Fx: + 45 4588 7762
Em: david.sabourin@nanotech.dtu.dk

Abstract
A mechanically actuated multichannel peristaltic micropump is presented. The pump is constructed using simple materials and fabrication methods. The pump's small footprint and portability easily allow it's placement on microscope stages and as such it is suited to integration with standard assay and test platforms that can benefit from fluidic activation.

1.0 Introduction

Pumping remains a practical problem which poses a challenge to wide adoption of microfluidics approaches[1]. Though pneumatic PDMS-based micropumps have demonstrated promise for highly multiplexed microfluidic applications, their construction and design can be complicated[2]. For platforms and assays which can benefit from fluidic activation, simple mechanical approaches are well suited.[3]

2.0 Pump Design and Construction

The micropump (Figure 1) has three main components, all fabricated by CNC micromilling. These are a monolithic PDMS Pumping Inlay (PI), and a Rotor Bed (RB) and a Multi-Roller (MR). The PI contains up to 12 integrated channels raised above the plane (Figure 2). The PI (Figure 2) was cast from PDMS (Sylgard 184, Dow Corning) inside a PMMA (Nordisk Plast, Denmark) mould *via* previously described methods[4]. The PI is placed in a RB complementary in shape to the MR. As the MR, made with eight 2 mm brass pins, is rotated by a motor, it contacts and compresses the PI's channels (Figure 2) and fluid is driven in the direction of rotation.

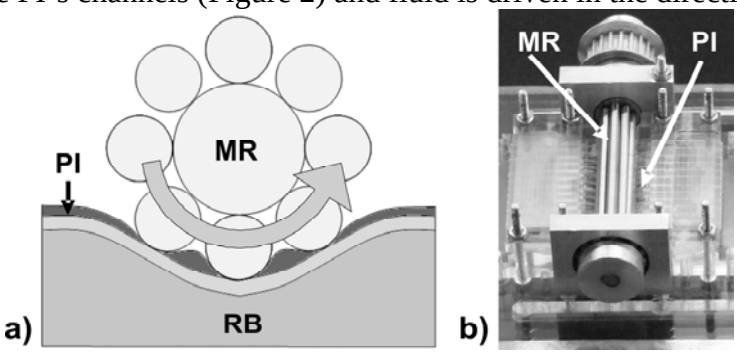

Figure 1: Peristaltic PDMS-based micropump. a) Cross-section showing operating principal and core micropump components: multiroller (MR), pump inlay (PI) and rotor bed (RB). As the MR rolls over the PI fluid is trapped between MR pins and pushed in the direction of rotation. b) Assembled micropump – motor not shown.

---

[1] D. J. Laser and J. G. Santiago, *Journal of Micromechanics and Microengineering*, 2004, **14**, R35-R64.
[2] L. Yobas, K. C. Tang, S. E. Yong and E. K. Z. Ong, *Lab on a chip*, 2008, **8**, 660-662
[3] C. Situma, M. Hashimoto and S. A. Soper, *Biomolecular engineering*, 2006, **23**, 213-231
[4] D. Sabourin, D. Snakenborg and M. Dufva, *Journal of Micromechanics and Microengineering*, 2009, **19** and P. Skafte-Pedersen, D. Sabourin, M. Dufva and D. Snakenborg, *Lab-on-a-Chip*, 2009.

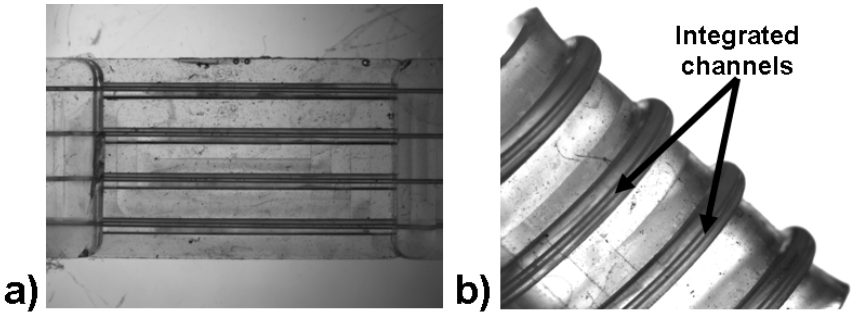

Figure 2: Pumping Inlay (PI). a) Top view of 4-channel. PI b) The integrated channels of the PI are raised above a supporting PDMS layer to reduce friction with the MR and facilitate compression and pumping.

3.0 Results

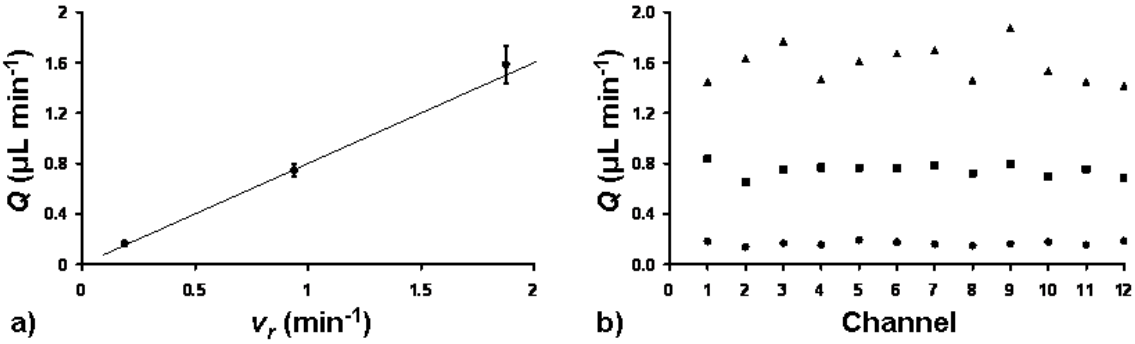

Figure 3: a) Theoretical (line) and average (•) of individual channel flow rates at varying MR rotational speeds (v_r) for a 12-channel micropump. Theoretical values based on void volume between MR pins. Error bars represent standard deviation of individual channel average flow rate. b) Individual channel flow rates at average flow rates of 0.17, 0.75, and 1.59 µL min^{-1}.

At average flow rates of 0.17, 0.75, and 1.59 µL min^{-1} a 12-channel micropump demonstrated % CVs of 10, 7, and 9% respectively (Figure 3). At a set MR rotational speed, water and gycerol solutions with viscosities of 2.5, 6.0, and 23 times that of water had flow rates of 2.43, 2.37, 2.38, and 2.42 µL min^{-1} respectively with corresponding SDs of 0.11, 0.16, 0.14 and 0.12 µL min^{-1}, thus demonstrating indifference to viscosity. The passage of cells through the pump without observed cell lysis confirmed micropump applicability to cell culture work. Individual channels have withstood over 15000 individual compressions.

4.0 Discussion and Conclusions

The micropump is suitable for microfluidic applications. When compared to typical setups the small size of the pump limits tubing requirements thereby reducing pump dead volumes and likely compliance. The micropump is easily placed on microscope stages and unobstructed microscopic observation is possible as channel inlets and outlets are oriented in-plane. The multichannel micropump is most useful for multiplexed assays which benefit from or require fluidic activation from multiple inputs such as perfused cell culture[5] and multi-stringency array hybridizations[6].

---

[5] M. Stangegaard, S. Petronis, A. M. Jorgensen, C. B. Christensen and M. Dufva, *Lab on a chip*, 2006, **6**, 1045-1051

[6] L. Poulsen, M. J. Soe, D. Snakenborg, L. B. Moller and M. Dufva, *Nucleic acids research*, 2008, **36**, e132

CONFERENCE PROCEEDING 4:

"*Modular system for connecting and actuating parallel microfluidic networks*"

MODULAR SYSTEM FOR CONNECTING AND ACTUATING PARALLEL MICROFLUIDIC NETWORKS

D. Sabourin, P. Skafte-Pedersen, D. Snakenborg, J.P. Kutter and M. Dufva

DTU Nanotech, Dept. of Micro- and Nanotechnology, Technical University of Denmark, DENMARK

Creating reliable interconnections to and between microfluidic components can be problematic. A prototype modular system featuring multi-channel MINIATURIZED PERISTALTIC PUMPS and MICROFLUIDIC RIBBONS, re-usable, PDMS-based components providing simple, reliable and multiple parallel chip-to-chip and chip-to-world interconnectivity is presented.

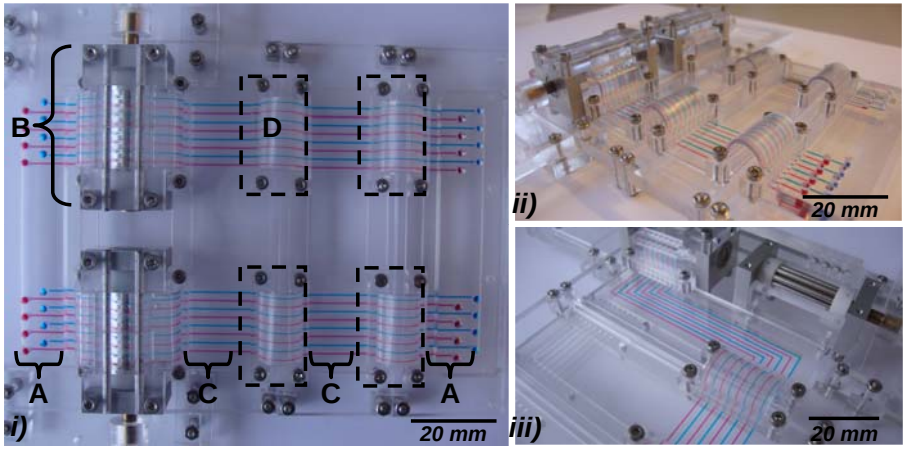

Figure 1 *Assembled systems. i) Two-pump configuration with 96 interconnections A) Sample reservoirs and outlet chips, B) miniaturized 8 channel peristaltic pumps, C) PMMA microfluidic chips, D) Type I Microfluidic Ribbons (dashed boxes). Motors not shown. ii) System side profile. iii) System components can be combined to generate many configurations and flow schemes.*

MINIATURIZED PERISTALTIC PUMP[1]

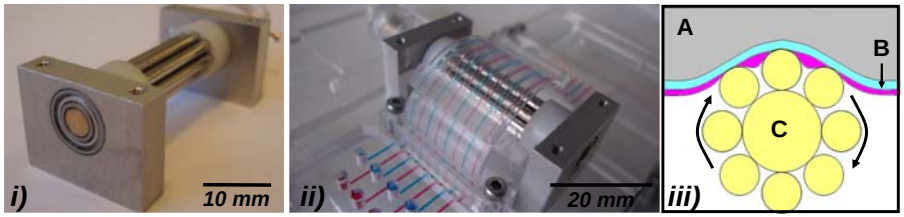

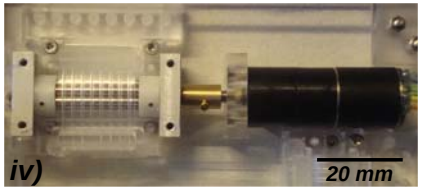

Figure 2 *i) The peristaltic multi-roller is made from eight free-rolling 2 mm stainless steel rods. ii) A Type 2 Microfluidic Ribbon is placed across the multi-roller to pump fluids. iii) Principle of operation. A rotor bed (A) compresses the raised tubing of a Type 2 Microfluidic Ribbon (B) (see Figure 4) over a multi-roller (C). iv) Pump driven by stepper motor.*

- **Small footprint: 20 mm (h) x 20 mm (w) x 40 mm (l), excluding motor**
- **Pumps up to 8 channels with Type 2 Microfluidic Ribbon**
- **Small pump dead volume ~ 2.25 µL**
- **Flow rates between 0.1 and 30 µL/min**

MICROFLUIDIC RIBBONS

TYPE 1: CHIP-TO-CHIP CONNECTIVITY

- **Monolithically cast from PDMS**
- **8 integrated 240µm diameter channels spaced to 1536 plate standard**
- **Ball Joint interconnections[2]: multiple, aligned, reversible and zero dead volume interconnections with seal pressures > 2 bar threshold[3]**

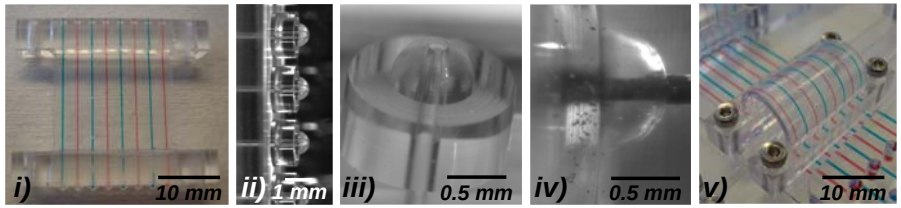

Figure 3 *i) TYPE 1 Microfluidic Ribbon. A flexible PDMS central portion containing 8 integrated channels is held between two fastening supports. All channels are bookended by Ball Joint interconnection features. ii) Ball Joint interconnection features. iii) Single Ball Joint Interconnection feature. iv) Zero-dead volume interconnection. v) Type 1 Microfluidic Ribbon connecting chips to each other within modular system.*

TYPE 2: CHIP-TO-WORLD CONNECTIVITY

- **Similar to Type 1 but with raised channels to increase pump efficiency**

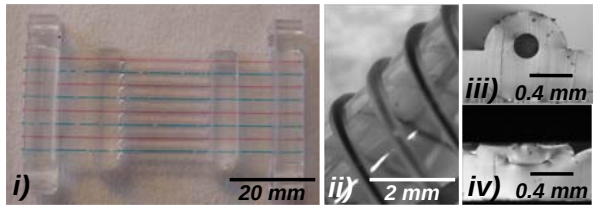

Figure 4 *i) TYPE 2 Microfluidic Ribbon. ii) Raised channels found in the middle of the TYPE 2 Microfluidic Ribbon. Cross-sections of uncompressed (iii) and compressed (iv) TYPE 2 integrated and raised channels*

SYSTEM BENEFITS

- **Small footprint: fits on stage, unobstructed observation**
- **Reusable components**
- **Small pump and system dead volumes, little compliance**
- **Limits tubing handling and requirements**
- **Flexibility of chip substrate**
- **Rapid or long term testing**
- **Possibility to interface to automated liquid handling**

APPLICATIONS

- **Kinetic Studies**
- **Cell culture**
- **Biofilms**
- **Biocompatibility Assays**
- **Gene Expression Profiling**
- **Microarray processing**

Acknowledgements:
Otto Mønsteds Fond Grant and DTU Stipend

References:
[1] Skafte-Pedersen et al. *Lab Chip* (9) p.3003-3006, 2009.
[2] Sabourin et al. *Micro. Nanofluidics*. DOI 10.1007/s10404-009-0520-8, 2009.
[3] Bhagat et al. *J. Micromech. Microeng.* (17) p.42-49, 2007.

APPENDIX D

APTAMERIC OLIGONUCLEOTIDE SEQUENCES

Class	Oligo	Recognition	Spacer	Tag	Total Length (bases)
Aptamer	1	GGTTGGTGTGGTTGG	-(T)16-	CCCCCCCCCCTTTTTTTTTT	51
	2	GGTTGGTGTGGTTGG	-(T)16-	CCCCCTTTTTCCCCCTTTTT	51
	3	GGTTGGTGTGGTTGG	-(T)16-	CAGTTCGAATATTGGTTACGTCTGC	56
	4	GGTTGGTGTGGTTGG	-(T)30-	CCCCCCCCCCTTTTTTTTTT	65
	5	GGTTGGTGTGGTTGG	-(T)30-	CCCCCTTTTTCCCCCTTTTT	65
	6	GGTTGGTGTGGTTGG	-(T)30-	CAGTTCGAATATTGGTTACGTCTGC	70
Scrambled	7	GGTGGTTGTTGTGGT	-(T)16-	CCCCCCCCCCTTTTTTTTTT	51
	8	GGTGGTTGTTGTGGT	-(T)16-	CCCCCTTTTTCCCCCTTTTT	51
	9	GGTGGTTGTTGTGGT	-(T)16-	CAGTTCGAATATTGGTTACGTCTGC	56
	10	GGTGGTTGTTGTGGT	-(T)30-	CCCCCCCCCCTTTTTTTTTT	65
	11	GGTGGTTGTTGTGGT	-(T)30-	CCCCCTTTTTCCCCCTTTTT	65
	12	GGTGGTTGTTGTGGT	-(T)30-	CAGTTCGAATATTGGTTACGTCTGC	70

The highlighted portions of the scrambled sequence indicate points of difference from the aptamer sequence.